

ABSTRACT

This thesis discusses the preliminary development of a microfluidic system for low concentration vapour analysis incorporating a novel analyte preconcentration method to extend vapour detection limits. The topicality of this subject is evidenced by the urgent requirement to detect vapours released by explosives or their manufacturing byproducts, allied to recent reports of gas phase detection of pathogen-related chemical markers.

Commercially available, non-microfluidic, sensitive, delayed response, broadly specific, gas-phase analysis methods have been developed recently. However *microfluidic* analysis offers the prospect of both the improved *specificity* of liquid phase analytical methods and increased *sensitivity* with fast response times. The necessary conditions to achieve a viable microfluidic vapour analysis system are discussed from collection, sampling, assay and measurement perspectives.

Efficient, rapid, vapour collection into a liquid phase is predicated by large surface area to volume ratio phase-interfaces, as occur within microfluidic devices. Accordingly, research has focussed on stable, segmented gas and liquid microflows. The literature has concentrated on fixed structures and precise flow rate control to produce such segmented flow. In contrast, we have investigated pressure driven flow and small active valves in combination with precision patterned passive valves to provide deterministic control over flow and thus define gas and liquid segment sizes. This has allowed introduction of larger, precise gas volumes and hence gas/liquid ratios while still maintaining more stable flow patterns than those previously reported in the literature.

Ethanol was employed as a completely soluble, volatile, 'model' analyte to assess collection efficiency. Research into detection focussed on a number of optical methods utilising either 'wet' or enzymatic chemistries. The *Phase-to-Phase Extraction via a Chemical Reaction to give Lower Limits of Chemical Detection* hypothesis (for the purpose of brevity this is shortened to 'Chemical Amplification' within this dissertation) was proposed. Thorough testing of the hypothesis using an enzyme catalysed reaction scheme has demonstrated its validity, and potential value if applied to 'real world' systems, particularly those for detecting low solubility analytes such as the explosive 2,4,6-trinitrotoluene (TNT) or its byproduct 2,4-dinitrotoluene (2,4-DNT).

ACKNOWLEDGEMENTS

Arriving at UH with no real understanding of what I was letting myself in for and even less about the actual processes I was expected to adopt and adapt, Mark, Ian, John, Christabel and Gordon somehow managed to put up with me and, I hope, turn me into a competent researcher. Although I think England winning the Rugby world cup and the Ashes may have helped their morale for a while at least.

To Judith, who always met my, initially constant, requests for reagents and chemistry lab space with a smile and a great conversation. Thankyou so much, you were a life-saver.

My thanks to QinetiQ and the EPSRC for the financial support, throughout my PhD, via the iCASE scholarship.

Special thanks also to Dr Tim Cox of QinetiQ for his valuable advice and insightful comments about some of the directions my research took.

Despite my constant, inane, background chatter, Christabel and John somehow managed to survive the last 4 years without reaching for a pair of earplugs every time I came in the door. The microfab crash-course and black-art help Christabel gave was invaluable. These, along with the odd PhD and university survival tips she gave would make a great self-help manual for any future student joining the group. Although dreading the times when I *really* had to ask John for something, because it meant I really was up the creek without a paddle, his manner and help always reassured.

For the reminders that Australia can be beaten by the English (at least occasionally) and the (almost) constant discussion about file conversion programs and new pieces of hardware, oh and even some great, if occasionally sarcastic, technical advice now and again, Thankyou Ian.

Not cracking me one despite the last year with all the ups and downs, watching me go for sleepless night after sleepless night, and then still going to the gym after, must have been an exercise in will power. You didn't exactly stop me going insane, but at least with you around it was a fun, if occasionally painful insanity. Thanks Alice.

But my greatest thanks must still go to Mark, Helena and my parents.

Since the initial conversation where I spent the first minute desperately trying to remember which PhD application he was calling about, I have grown to respect and admire Dr Mark Tracey. His persistent jibes about my 'aussie' fashion sense (although few Australians would be caught dead wearing what I did), the common belief that bureaucracy is there to

be used then fought against, the wish that he'd stop saying sorry quite so much and the (finally realised) blunt honesty approach to communication made him more approachable and my time at UH much more entertaining. Even if the humour was occasionally black. His constant intellectual curiosity, persistent anger at the waste inherent in the paper work required to maintain even a group as small as ours and obvious delight in seeing something new work as intended have reassured me that its possible to be an angry, but young man at heart for as long as I have the energy.

Helena helped me survive and even prosper for the majority of the three years of experimental work. Despite the frustration it caused Mark, without Helena's dragging me off here, there and everywhere I don't believe I would have come out the insanely well-balanced person I am. For her putting up with my early starts, late evenings and occasional weekends and sometimes not seeing me for more than a few hours during the week I owe her more than she could imagine. She was my rock for that entire period.

Finally

Words cannot express how much I owe my parents for turning me into the person who believed, at least for that crazy period before I realised what I'd let myself in for, that I could finish this. The background education and curiosity engendered by just being around you has stood me in greater stead than any formal education ever could.

CONTENTS

Abstract	i
Acknowledgments	ii
Contents	iv
Abbreviations	viii
Chemical Formulae	ix
Glossary	x
Table of Equations	xii
1. INTRODUCTION	1
1.1. Olfaction	3
1.1.1. Insecta	3
1.1.2. Mammalian	5
1.1.3. Artificial Olfactory Developments	7
1.2. Microfluidics	11
1.2.1. Principles	11
1.2.2. Components	16
1.3. Vapour Analysis	17
1.3.1. Sampling	17
1.3.2. Analysis	18
1.4. Plan of Work	20
1.5. Introduction to Further Chapters	21
2. INTRODUCTION TO MICROFABRICATION	23
2.1. Introduction	23
2.2. Rapid Prototyping – Introduction	24
2.2.1. Basic PDMS Device Microfabrication Process	24
2.2.2. Material Properties	25
2.2.3. Microfluidic Assembly Related Properties	27
2.3. Rapid Prototyping – Manufacture	31
2.3.1. Computer Assisted Design (CAD)	31
2.3.2. Mould Manufacture (SU-8 Processing)	32
2.3.3. Device Assembly	34

3. INTEGRATED MICROVALVE DEVELOPMENT	36
3.1. Introduction	36
3.2. Burst Valves	39
3.2.1. Experimental, Results and Discussion	39
3.3. Check Valves	42
3.3.1. Experimental, Results and Discussion	43
3.4. Seal valves	54
3.4.1. Experimental, Results and Discussion	55
4. INTRODUCTION TO VAPOUR COLLECTION	57
4.1. Diffusion	57
4.2. Microfluidics	60
4.2.1. Solid Sorbent Vapour Collection	60
4.2.2. Liquid Sorbent Vapour Collection	62
4.3. Microfluidics for Vapour Analysis	65
4.4. Experimental Parameters	69
5. VAPOUR COLLECTION	71
5.1. Experimental	73
5.1.1. NR Valve Controlled Devices	74
5.1.2. Non-PDMS Devices	74
5.1.3. Lee Valve Controlled PDMS Devices	76
5.1.4. Generic Set-up Detail	77
5.2. Summary	81
5.2.1. Major Fluid Flow Artefacts	82
5.2.2. NR Valve Controlled PDMS Devices	84
5.2.3. Non-PDMS Devices	85
5.2.4. Lee Valve Controlled PDMS Devices	85
5.2.5. Segmented Flow Device	86
5.3. NR valve Controlled PDMS Devices	87
5.3.1. Device 1	87
5.3.2. Device 2	88
5.3.3. Device 3	90
5.3.4. Device 4	91
5.3.5. Device 5	92
5.4. Non-PDMS Devices	95
5.4.1. Modular Device	95
5.4.2. PMMA Micro-junctions	98

5.5. Lee Valve Controlled PDMS Devices	101
5.5.1. Device 10	101
5.5.2. Device 11	103
5.6. Segmented Flow Devices	107
6. VAPOUR ANALYSIS	112
6.1. Introduction	113
6.1.1. Microfluidic Methods	113
6.1.2. Ethanol Analysis	114
6.2. Experimental	116
6.2.1. Chemiluminescence	117
6.2.2. Fluorescence	118
6.2.3. Absorbance – Tetramethylbenzidine	120
6.2.4. Absorbance - 4-Aminoantipyrine	122
6.3. Results and Discussion	124
6.3.1. Chemiluminescence	124
6.3.2. Fluorescence	126
6.3.3. Absorbance – Tetramethylbenzidine	128
6.3.4. Absorbance – 4-Aminoantipyrine	132
7. PHASE-TO-PHASE EXTRACTION VIA A CHEMICAL REACTION TO GIVE LOWER LIMITS OF CHEMICAL DETECTION	136
7.1. Introduction	136
7.2. Experimental	141
7.2.1. Tetramethylbenzidine	141
7.2.2. 4 – Aminoantipyrine	145
7.3. Results and Discussion	148
7.3.1. Tetramethylbenzidine	149
7.3.2. 4 – Aminoantipyrine	153
8. CONCLUSION	161
8.1. Vapour Collection	161
8.2. Chemical Amplification	162
8.3. Microfabrication Experiments	163

9. FUTURE WORK		164
10. REFERENCES		165
Appendix 1 :	Rapid Prototyping	178
1.1	Computer Aided Design (CAD)	178
1.2	SU-8 Processing	178
1.3	Soft Lithography	180
1.4	Device Assembly	182
1.4.1	Standard Assembly	182
1.4.2	Push-fit Fluid Connection Devices	183
1.4.3	Check Valve	183
1.4.4	Seal Valve	184
1.4.5	PMMA	185
Appendix 2 :	Electronic Control	187
2.1	Example Script 1 – Sequential	187
2.2	Example Script 2 – Loop	188
Appendix 3 :	Detail of Selected Microfluidic Experimental Conditions	190
3.1	Design 2	190
3.2	Design 4	190
3.3	Design 5a	191
3.4	Modular Device	192
3.5	PMMA Micro-junctions	192
3.6	Design 10	193
3.7	Design 12	194

Abbreviations

4-AAP	<i>p</i> – Aminoantipyrine
ABTS	2,2'-Azino-bis(3-ethylbenzothiazoline-6-sulfonate)
ADH	Alcohol Dehydrogenase
AOD	Alcohol Oxidase
BRENDA	An enzyme information database found on the internet.
CAD	Computer Aided Design
CO	Carbon Monoxide
DARPA	Defense Advanced Research Projects Agency
D.I.	Deionised
DMSO	Dimethylsulfoxide
DNT	2,4 - Dinitrotoluene
DOAS	Differential Optical Absorption Spectroscopy
ECD	Electron Capture Device
EDTA	Ethylenediaminetetraacetic acid
FEP	Fluoroethylene polymer
FFMR	Falling Film Microreactor
FID	Flame Ionisation Detector
GC	Gas Chromatography
4-HPAA	<i>p</i> – Hydroxyphenylacetic acid
HPLC	High Performance Liquid Chromatography
HRP	Horseradish peroxidase
IC	Integrated circuit
ID	Internal diameter
IMS	Ion Mobility Spectroscopy
IPA	<i>i</i> – Propanol
IR	Infra Red
IT-MS	Ion Trap Mass Spectroscopy
LOC	Laboratory on a Chip
MBC	Microbubble Column
MEMS	Micro-Electro-Mechanical Systems
MOS	Metal Oxide Semiconductors
MS	Mass Spectrometry
MS-MS	Mass Spectroscopy – Mass Spectroscopy
NAD	Nicotinamide Adenine Dinucleotide
NR	Neptune Research Inc.
OBP	Odorant binding protein
OD	Outer diameter

ORN	Odorant receptor neuron
PAL	Phase Alternating Line. A TV encoding system operating at 25 frames per second.
PDMS	Polydimethyl Siloxane
PE	Polyethylene
PEEK	Polyetherether Ketones
PMMA	Polymethyl methacrylate
PTC	Phase Transfer Catalyst
PU	Polyurethane
PVC	Polyvinyl Chloride
PVP	Polyvinyl pyrrolidone
PZT	Piezoelectric
QCM	Quartz Crystal Microbalance
QMS	Quadrupole Mass Spectroscopy
SAW	Surface Active Wave
SHM	Staggered Herringbone Mixer
SVOC	Semi-volatile Organic Compound
TMB	Tetramethyl benzidine
TNT	2,4,6 - Trinitrotoluene
TOF-MS	Time of Flight Mass Spectroscopy
U	Units (measurement of amount of enzyme)
UV/Vis.	UltraViolet / Visible Spectroscopy
VOC	Volatile Organic Compound

Chemical Formulae

NH_4Cl	Ammonium chloride
H_3BO_3	Boric acid
$\text{Cr}_2(\text{SO}_4)_3$	Chromium sulphate
$\text{CH}_3\text{CH}_2\text{OH}$	Ethanol
H_2O_2	Hydrogen peroxide
$\text{K}_2\text{Cr}_2\text{O}_7$	Potassium dichromate
KH_2PO_4	Potassium dihydrogen phosphate
KOH	Potassium hydroxide
SiO_2	Silicon dioxide
AgNO_3	Silver nitrate
Na_2CO_3	Sodium carbonate
NaOH	Sodium hydroxide
H_2SO_4	Sulfuric acid

Glossary

Absorption	Absorption is a physical or chemical phenomenon or a process in which atoms, molecules, or ions enter some bulk phase - gas, liquid or solid material
Adsorption	The surface retention of solid, liquid, or gas molecules, atoms, or ions by a solid or liquid. It is a purely physical process which occurs without chemical reaction.
Amplification	The act of increasing in size, magnitude or significance
Analysis	The division of a physical or abstract whole into its constituent parts to examine or determine their relationship or value.
Boundary Layer	The layer of reduced velocity in fluids that is immediately adjacent to the surface of a solid past which the fluid is moving.
Chemical Amplification	The increasing of analyte, or an analyte-derived compound, concentration using purely chemical means, i.e. by utilising a particular chemical system that produces more of the component being detected. The polymerase chain reaction is a classic example.
Convection	Transfer of energy or mass by the directed movement of large numbers of molecules having similar velocity.
Detection	The act of discovering or the fact of being discovered.
Diffusion	A process by which substances, heat, or other properties of a medium are transferred from regions of higher concentration to regions of lower concentration.
Electronic Amplification	The act of increasing the amplitude of the output signal of a device, relative to the input signal, by using power drawn from an external power source
Electronic Nose	An electronic nose is an instrument which comprises an array of electronic chemical sensors with partial specificity and an appropriate pattern recognition system, capable of recognising simple or complex odours.
Gas	Any substance that is gaseous at room temperature and atmospheric pressure
Hydrostatic Head	Pressure resulting from the flow of liquid from a source raised above the device.
Laminar	(flow) Nonturbulent motion of a fluid in which parallel layers have different velocities relative to each other.
Number - Peclet	The dimensionless ratio of the product of the mass transfer coefficient and a representative length to the diffusion coefficient.
Number – Reynold's	Quantification of relative importance of inertial to viscous forces.
Physical Amplification	Increasing the instantaneous signal power by decreasing the time period over which the component being detected passes through the detector.
Signal Amplification	The increasing of signal, voltage or current expressed as a ratio of output to input.
Sorb	To either adsorb or absorb, or both.

Sorbent	The substrate into which or onto which a substance is sorbed.
Spectrometer	Any instrument for producing a spectrum, esp. one in which wavelength, energy, intensity, etc, can be measured.
Spectroscope	Any of a number of instruments for dispersing electromagnetic radiation and thus forming or recording a spectrum.
Spectroscopy	The science and practice of using spectrometers and spectroscopes and of analysing spectra, the methods employed depending on the radiation being examined.
Surface Free Energy	see Surface Tension
Surface Tension	The property of liquids caused by intermolecular forces near the surface leading to an apparent presence of a surface film. The measure of this, expressed as the force acting normal to one side of a line of unit length on the surface.
Turbulent	(flow) Flow of a fluid in which its velocity at any point varies rapidly in an irregular manner.
Vapour	A gaseous substance at a temperature below its critical point

Table of Equations

	Title	Section	Page
1	Reynold's number	1.2.1	11
2	Hydraulic diameter	1.2.1	11
3	Volume flow rate	1.2.1	12
4	Fluidic resistance	1.2.1	13
5	Peclet number	1.2.1	14
6	Fick's First law of diffusion	1.2.1	15
7	Fick's Second law of diffusion	1.2.1	15
8	Henry's Law	4.1	58
9	Integrated solution to Fick's Second law	4.1	58
10	Recirculating flow	4.3	67
11	Vorticity	4.3	68
12	Young LaPlace Equation	5.2.2	87
13	Lambert Beer Equation	6.1.2	114
14	Partition Coefficient	7.1	137
15	Dependency of Henry's Constant of SO ₂ on pH and Reaction Constants	7.1	138
16	Expanded Equation for Henry's Constant	7.3.2	158
17	Equivalence of Henry's Constant for adjacent aliquots.	7.3.2	158
18	Solving Equation 18 simultaneously	7.3.2	158
19	Degree of Chemical Amplification	7.3.2	159

1. INTRODUCTION

Vapour, as defined by The Collins English Dictionary [1] is “, A gaseous substance at a temperature below its critical point.” The majority of vapours are organic in nature and have boiling points above normal atmospheric temperatures. Michulec and Wardencki [2] review the variation between a range of organic vapours (see Figure 1.1) and the methods used to sample them.

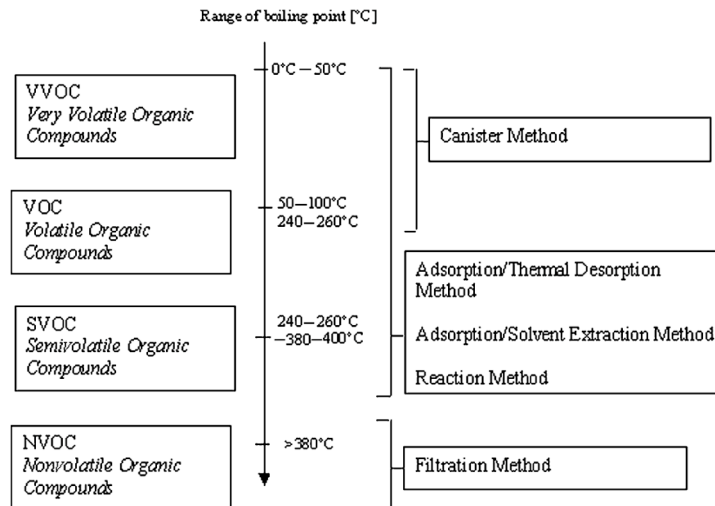


Figure 1.1 : Michulec and Wardencki's [2] classification of vapours based on boiling point and the associated collection methods.

The primary aims of vapour analysis, as with most branches of analytical chemistry, have long been to lower detection limits and widen the concentration range over which analytes could be detected. Partially as a result of terrorist events, significant reductions in both the time required to complete the analysis and the physical size of vapour analysis systems have recently become almost as important.

Developments in electronics and microengineering have provided the means to reduce system size or analysis time or detection limit. However, until recently, simultaneous reduction of the physical dimensions and either the analysis time or detection limit was problematic. Whilst analysis systems have begun to appear commercially in which the active component is microengineered, system design still limits the overall physical size and analysis time.

Microfluidics, a significant subset of research into MicroElectroMechanical Systems (MEMS), *permits both size and analysis time reduction without raising the detection limit.* Microfluidics has yet to be fully investigated for vapour analysis applications [3]. Many standard and biological vapour analysis methods have the potential for implementation in simple form using microfluidic techniques.

Olfactory systems, whether biological or artificial must overcome basic problems associated with capturing extremely diffuse and dilute sample streams. Biological olfactory systems appear to be best differentiated by Linnaean taxonomic classification. Literature coverage of biological olfaction is therefore divided into piscine, mammalian and insecta systems.

As biological olfaction, with minor caveats, appears to be the best known example of a vapour analysis system, the ideal synthetic equivalents are called artificial noses [4-6]. However recreating any biological olfactory system exactly is an almost impossible task. The piscine, mammalian and insecta olfactory senses are amazingly complex [7-10] with extensive and evolving compound recognition and high, if variable, sensitivity. Biological olfactory systems are capable of recognising volatile organic compounds (VOCs), semi-volatile organic compounds (SVOCs) and gases with a wide range of chemical and physical properties and, with a single prior exposure, are able to identify a vapour again.

The complexity of the biological olfactory system and the current methods of attempting to reproduce it are encompassed separately in Section 1.1. Section 1.2 covers the theory behind and practical application of microfluidics and the equations governing gas and liquid flow and interaction. Then, Section 1.3 summarises two of the major problems associated with vapour detection, which are sampling and analysis. Section 1.4 presents the research plan followed throughout the course of the project. Finally, Section 1.5 outlines the contents of the theoretical and practical chapters following this.

1.1. Olfaction

Mammalian, insecta and piscine olfaction follow the same basic two-phase gas collection system. However the piscine olfactory system will not be discussed further in this thesis as the analyte and collection phase are both liquids. As the manner in which the mammalian and insecta systems operate differs slightly, but significantly, they will be covered separately. Finally, the development of artificial olfactory systems will be discussed to demonstrate the current state of miniaturised, multi-compound detection systems.

1.1.1. Insecta

It is possible, to a degree, to consider the insect olfactory system as a modular system. The analyte capture, transport and detection modules of the insect olfactory system are generally located on the flagellomeres (the fine hairs) attached to the antennae [8], although some species also have flagellomere located on the legs [11]. Finally, the brain remotely processes electrical signals, generated and then transmitted to it by chemosensory neurons located within the flagellomeres [12].

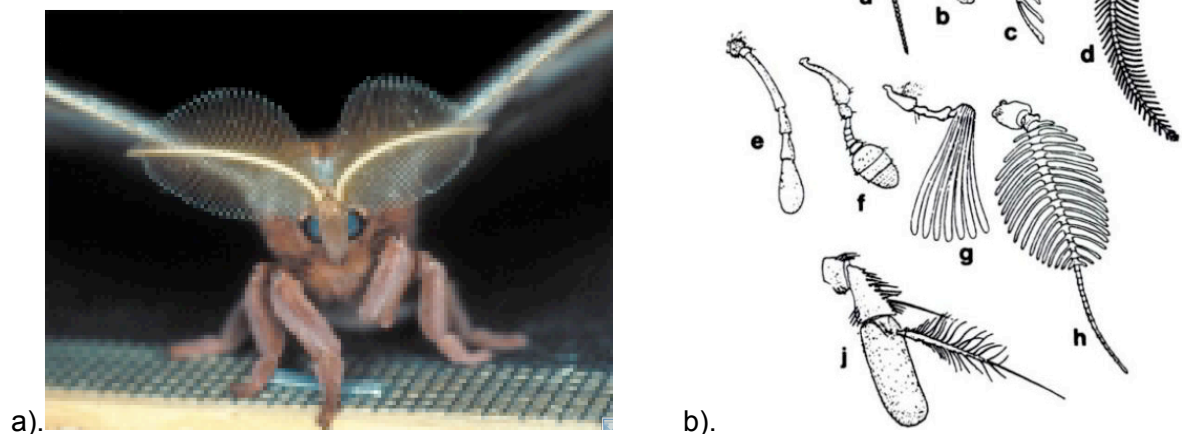


Figure 1.2 : a). A male *Antheraea Polyphemus* moth (from Hansson [8]). b). A gallery of insect antennae. (from Keil [13]).

The primary element, vapour collection, is influenced by the morphology of the antennae and the attached flagellomeres. Figure 1.2 demonstrates the range of antennae structures that insects exhibit. As stated by Schneider, Price, et al [14] “, Antennae morphology plays a critical role in modifying the flow patterns.” Changing the morphology affects the volume

of atmosphere sampled and the thickness of the boundary layer (see Section 4.1 for explanation). These two aspects between them control the quality, intensity and temporal distribution of any analyte plume being detected by the insect.

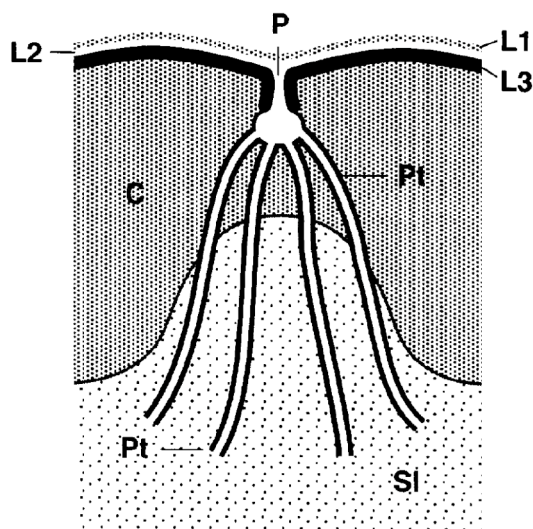


Figure 1.3 : Structure of insect sensilla. Shown are the epicuticular analyte capture and transport layers (L1, L2 and L3), outer pore (P), pore tubules (Pt), cuticle body (C) and sensillum lymph (SI) (from Steinbrecht [7]).

Actual vapour collection occurs by impact of the analyte molecule on a lipid coated cuticle. The lipid coating appears to be composed of several layers. The middle layer (L2 from Figure 1.3), a non-chemically homogeneous wax mixture, is responsible for analyte capture and transport [7] from the point of collection to the entrance of the sensory pore. Non-lipid soluble compounds are dissolved within layer 2 despite there being no chemically observable, solubility enhancing component present within layer 2 [7].

Transport of analyte molecules appears to occur primarily by diffusive processes. From the surface of the cuticle, to the pore entrance and thence, via the pore tubules to the sensillum lymph, calculated diffusion times were found to be up to 100 times faster than the receptor response times (up to 500 ms) [7]. The fast diffusion is purely a result of the minute distances involved. Whilst there are not any solubility enhancers within layer 2 at the surface, once within the pore, two types are present, although apparently not simultaneously. The first enhancers are the epicuticular filaments, fine hair like structures within the pore and pore tubules [7]. As the analyte passes into the sensillum lymph, a non-homogeneous aqueous based mixture, they are replaced by the second enhancers, odorant-binding proteins (OBPs) [15, 16].

A separate feature of the OBPs is their apparent dual function as both analyte transportation and compound selection mechanisms. These secondary and ternary roles, as a compound

distinction [16] and chromatography mobile phase, enable insects to have a wide analyte discrimination despite the limited number of olfactory receptor neurons (ORNs) [12, 16].

Binding of the unified OBP-analyte complex with the cilia of the ORN initiates a signal cascade that opens a cation channel [7, 12]. The transport of ions induces an electrical signal that is transmitted to the brain for signal processing. Each analyte produces a pattern of signal strengths and arrival times received from each ORN. Compound discrimination and recognition results from the pattern recognition ability of the insect brain. Hansson [8] and Huotari [17] indicate that, although adaptive to a point, the restricted capacity of the olfactory processing centre in the brain of insects limits the effective number of compounds differentiated.

Insect olfaction is however a highly sensitive vapour detection system, for the vapours it is capable of detecting. Multiple vapours, present at widely different concentrations can be detected and identified simultaneously. The range of vapour detection limits, between the insects species, is partially a result of differences in the antennae structure and the concentration of pores on the antennae [7].

1.1.2. Mammalian

The mammalian olfactory system is remarkably similar to that of the insecta. As with insecta olfaction, mammalian olfaction can be considered a modular system. Vapour collection, transportation, detection and signal processing are, while contiguous, handled separately. Deeper similarities, down to the presence of OBPs in both systems, also exist. However there are also significant differences between mammalian and insecta olfactory systems that are worth noting.

Vapour collection in mammals, unlike that of insects, initially utilises the same structures involved in respiration. The nasal passages through which air passes to the lungs, also humidify and warm the air [10]. Structures, also contained within the nose, but adjacent to the main respiratory pathway contain the main mammalian olfactory elements. While it is possible for gases and vapours to be detected during the normal course of breathing, the act of sniffing diverts the air-flow over the surface of the mucosal layer responsible for the harvesting of gas and vapour molecules [18].

Diffusion, while rapid within gases, is still too slow for the majority of vapour molecules to impact upon the olfactory mucosa. Therefore once the air stream enters the olfactory structures it is further perturbed, by the turbinate bones (see Figure 1.4), to allow convection, as well as diffusion to occur [10, 18]. The disturbance of the air-flow also reduces the thickness of the gas boundary layer present over the surface of the mucous.

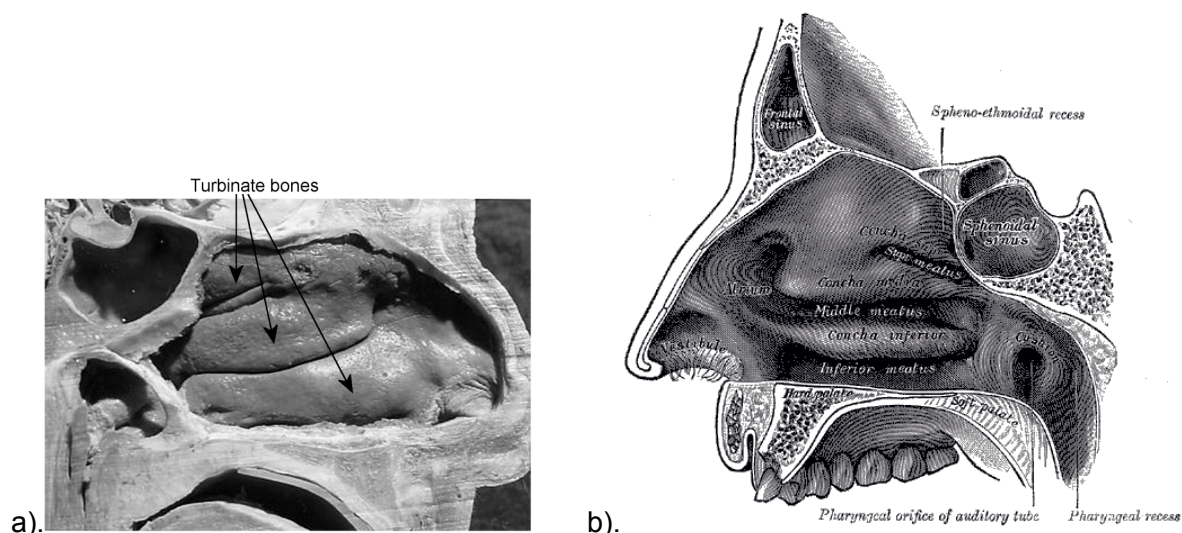


Figure 1.4 : a). Photograph showing human turbinate bones, mucous membranes and nasal passages (from Jones [10]) and b). the associated anatomical drawings (from Gray [19]).

The olfactory mucosa, in contrast to the insect olfactory system, fulfils the role of both the lipid layer covering the cuticle and the sensillum lymph. It captures the analyte and, being primarily an aqueous layer, also contains the cilia of the ORNs [20]. As with the sensillum lymph it also contains a mixture of lipids, OBPs and enzymes [10]. The OBPs and lipids are also contained within the aqueous solution and moreover function in compound discrimination and chromatographic mobile phase roles [21].

There is some debate as to the mechanism by which the transport of the analyte molecules to the ORNs occurs. Mucous is produced by the Bowman's gland and spreads from the gland over the surface of the membrane. Movement of the mucous layer, independent of spreading from the Bowman's gland, has been documented and implicated in analyte transport [22]. Pelosi [18] discusses the current conflicting beliefs that the cilia terminating the neurons either actively move the mucous by a 'stroking' motion or are moved by the mucous. While apparently unimportant, active cilia may imply a possible convective as well as diffusive transport mechanism for analytes traversing the mucous layer to the ORNs.

Reception of the analyte-OBP complex by an ORN as per the insect olfactory system initiates a signalling cascade that results in an electrical signal passing from the ORN to the brain. Unlike insects, the variety of ORNs and OBPs found in mammals [5, 21] allow the detection of up to 10 000 different analytes [10]. However signal processing and pattern recognition, although complex, remains rapid and adaptive.

Despite interspecies diversity in sensitivity, mammalian olfactory systems do not exhibit significant structural differences. Lovett [23] explains that a dog's olfactory epithelium covers about 100 cm² while a human's covers ~3 cm². This difference, combined with the increased sensitivity resulting from weaker eyesight, may in part account for the inter-

species detection limit divergence. A dog for instance can detect α -ionone at 4×10^9 molecules/mL while human's detection limit is 4×10^5 molecules/mL, a factor of 10 000 difference [24].

Unfortunately, as with most biological systems, environmental factors, the aging process, tiredness and accidents can irreversibly degrade the sensitivity and adaptability of the mammalian olfactory system. Inter-species differences lead to these occurring at different rates. Explosives detection 'sniffer' dogs, requiring extensive and rigorous training, still become tired and lose concentration after between 30 and 120 minutes [25].

While able to differentiate between several different analytes, dogs are incapable of accurately indicating concentration or the composition of the vapour they are detecting [25]. Artificial olfactory systems are being developed to address these problems with biological olfaction.

1.1.3. Artificial Olfactory Developments

Traditionally vapour analysis has been performed by absorption into, and detection of, analytes in a liquid phase [26]. However as gas phase analysis technology has improved, vapour analyses developed to utilise this technology.

Laboratory gas detection systems tend to follow the same broad pattern. Generally a passive method is used to gather the sample, followed by using a gas chromatography (GC) unit attached to appropriate detectors. A number of passive sampling modules have been developed that can be integrated with a variety of chromatographic techniques. Other vapour analysis systems, generally employing optical detection techniques and capable of being operated remotely have been developed, although they are not in widespread use [27]. Aragon, Atienza, et al [28] provide a thorough review of the current state of laboratory, organic vapour, analytical techniques.

However most of the systems discussed by Aragon, Atienza, et al [28] are not considered olfactory mimics. Although the concept of artificial olfactory systems, or 'Electronic Noses', have been introduced by earlier authors, Gardener & Bartlett [6] provide a good definition: "*An electronic nose is an instrument which comprises an array of electronic chemical sensors with partial specificity and an appropriate pattern recognition system, capable of recognising simple or complex odours.*"

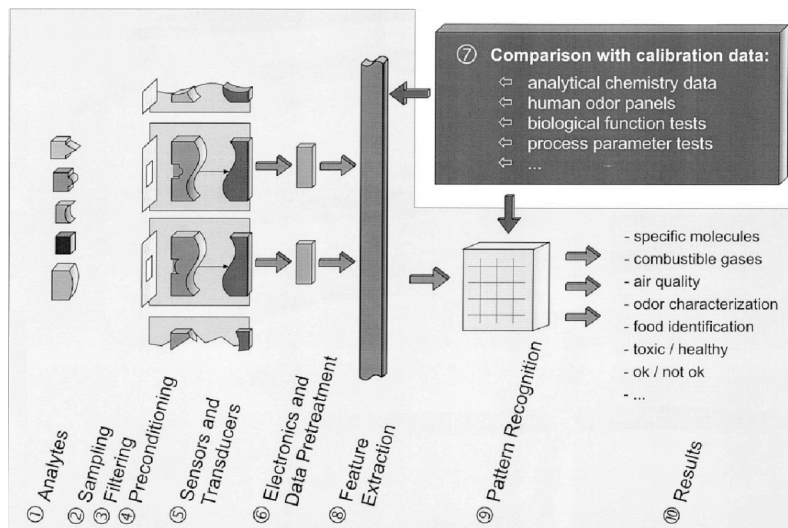


Figure 1.5 : Biological olfactory vapour and gas analysis modules as applied to electronic nose system arrangement. Taken from Gopel (1998) [29].

The vast majority of electronic noses use detection or capture technology that is only capable of operating completely in the gas phase. Many, the quartz crystal microbalance (QCM), surface acoustic wave (SAW) and polymer coated fibre-optic bundles being some of the most common examples [30], function by absorbing the analyte or analyte mixture into a coating applied over a sensor [28, 31-33] and detecting the change in response to an applied signal. The coatings used tend to absorb a wide range of vapours and as a result the individual sensors are non-specific.

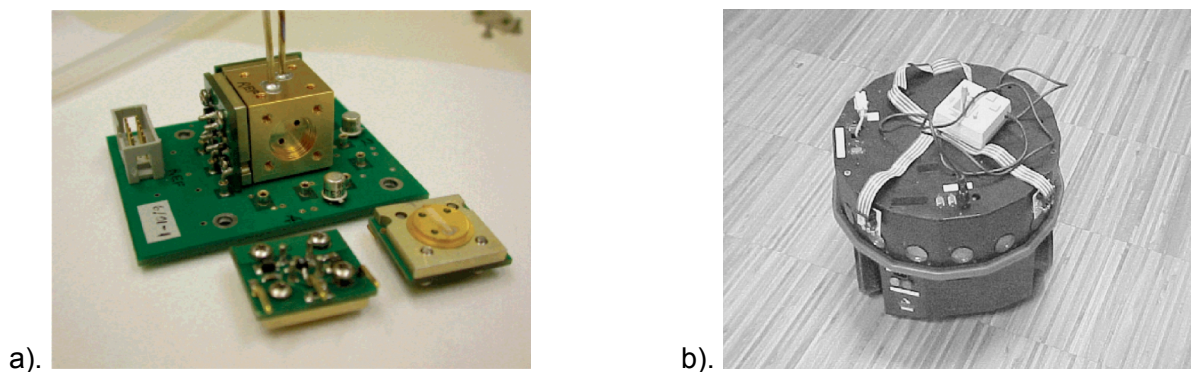


Figure 1.6 : a). Four packaged SAW detectors with flow system and circuitry attached, from Stubbs, Lee, et al [34] and b). Robot with two sets of four MOS sensor packages attached, from Marques, Nunes, et al [35].

Initial research focused on pattern recognition to differentiate vapours. By applying a separate coating to the surface of every sensor, the response of each sensor is discrete [20]. The detector thus operates by recognising the pattern of responses from the sensor cluster, either as a raw signal or after the application of multivariate pattern analyses. However, despite the need for multiple sensors as exemplified by the two different sensor systems (shown in Figure 1.6), the systems remain compact.

Sensor Type	Coating	Analyte	Concentration Limit	Reference
SAW	Polymer	2,4-DNT	<100 ppt	[36]
QCM	Antibodies	Cocaine	≈ 50 ng	[37]
MOS	-- None --	CO	<50 ppm	[38]
Fibre-optic Bundle	Polymer	2,4-DNT	ppb	[39, 40]
Molecular Wire	Fluorescent Polymer	TNT	Femtogram	[41]

Table 1.1 : Detection limits of a variety of sensors, used in arrays, to specific analytes.

Recent advances in sensor design and manufacture have resulted in several small proprietary devices being developed and commercialised. Two modern examples are those produced by Seacoast Science Inc. (San Diego, USA) and Nomadics Inc. (OK, USA). Seacoast Science, utilising MEMS, manufactures capacitive sensors coated with polymers specifically applied to optimise detection of particular compounds (<http://www.seacoastscience.com>). ICx Nomadics, (<http://www.nomadics.com>), in conjunction with DARPA (Defense Advanced Research Projects Agency), have developed Fido, an explosives detection system employing fluorescent polymers specifically developed by The Massachusetts Institute of Technology to detect TNT and related compounds [42].

Despite the ability of such detection systems to detect multiple compounds, it is not possible to truly compare them to biological olfactory systems. As stated by White, Kauer, et al [33] biological olfactory systems are capable of identifying and roughly determining the concentration of individual vapours, even within simple mixtures. The majority of systems developed so far are incapable of repeating this feat. Of the few attempts that have been made [33, 43], each required a number of data processors, increasing the size, cost and system complexity, with specific processor software developed for the task, further increasing the cost.

In contrast, novel developments in mass spectrometry (MS) technology and manufacturing processes have led to several systems being produced that can more closely be called 'electronic noses'. Mass spectrometry operates by fragmenting and ionising molecules and then separating the fragments using variable electric and magnetic fields. Each molecule produces a unique spectrum of fragment sizes dependant on the mass to charge ratio (m/z) [44]. Many different variants (hyphenations) of MS exist: time of flight MS (TOF-MS); quadrupole (Q-MS); ion trap (IT-MS); and MS-MS being only a fraction of all the possible types developed or used. The use of hyphenated modifications to standard MS technology provides greater separation capabilities [44].

Increasing the separation and definition capabilities of the basic MS allows the identification of multiple, simultaneously applied compounds. QinetiQ, Barringer Research Ltd and Graseby Dynamics Ltd, amongst others utilise Ion Mobility Spectrometry (IMS) for explosives detection systems. While not exactly the same as standard MS, IMS still relies on ionising compounds and separating the ions, albeit at atmospheric pressure [45]. The systems can be compact, low power and, as the pattern is a distinct spectrum for each compound, much easier to analyse than the indistinct and abbreviated patterns resulting from the limited sensor numbers present in the majority of electronic noses. Microsaic Systems Ltd, using technology developed by Imperial College and Liverpool University, produce QMS based gas and vapour detection systems. The individual MEMS manufactured QMS modules are designed to be 'plug-and-play' and the entire system is small enough to fit into a large briefcase. As with standard MS systems, an m/z spectrum, with distinct peaks, is produced. Likewise with the IMS, this facilitates simpler analysis of a spectrum resulting from a mixture of compounds.

Therefore, thus far, these systems are, despite the difference to the standard electronic nose idea, the closest mimics of the most important aspects of biological olfactory systems. Consider the Microsaic Systems' ionChip® containing systems as an example: a mixture of compounds is separated into its original components by gas chromatography; each component produces a spectrum; the system is adaptive (addition of standard spectra to the library increases the range of identifiable compounds). However as detailed later (Section 1.3) the need for a chromatographic module to separate the analytes is a major weakness of MS based analysis systems.

The field of electronic noses is constantly evolving, however a more detailed review is not within the scope of this project, the reader is referred to several review articles. Gopel (1998) [29], Craven and Gardner [20] and more recently Garcia-Gonzalez and Aparicio [46] and James, Scott, et al [30] have reviewed the origins, some of the developments and possible future innovations in the field of electronic noses.

1.2. Microfluidics

Originally an offshoot of the integrated circuit (IC) production industry, microfluidics initially, and in many cases continues to, utilise the precision patterning and etching capabilities of the IC industry to allow the production of devices with microscopic channels and chambers [47]. Early microfluidic devices were almost uniformly produced by etching channels into silicon wafers. After associated packaging, that is sealing the top of the channel by bonding it to another material and then connecting fluid supply and removal tubes, fluid could then be pumped through these channels.

Following initial research into applying the new technology, effort simultaneously flowed into development of substrates other than silicon and new fluid control methods. Unlike the IC industry, until recently, the demonstration of new functionalities was paramount: whilst potential applications were identified rapidly, subsequent progress in system development has been slow.

1.2.1. Principles

Fluid, meaning both gas and liquid, flow behaviour is governed by a number of equations and can, ideally, be described by certain parameters. These parameters, independent of the physical properties of the fluid, are determined by channel geometry, surface characteristics of the channel and flow rate.

One parameter, used to characterise the degree of turbulence of fluid flow is Reynolds number, Re . Reynolds number is a dimensionless parameter calculated using Equation 1 [48] (symbol definitions on following page):

$$Re = \frac{\rho \cdot D_h \cdot v}{\eta} \quad \text{Equation 1}$$

where

$$D_h = 4 \cdot \frac{A}{P_{wet}} \quad \text{Equation 2}$$

Symbol	Definition	Units
ρ	Fluid density	kg/m ³
D_h	Hydraulic diameter	M
A	Cross sectional area	m ²
P_{wet}	Wetted perimeter	M
v	Average fluid velocity	m/s
η	Fluid viscosity	kg/m.s

Table 1.2 : Symbol definitions for Equations 1 and 2.

Generally, if Re is greater than 3000 then flow is certainly turbulent, but if Re is less than 2000 then fluid flow tends to be laminar. The transitional flow region, in which Re is between 2000 and 3000 possesses no clearly defined characteristic, but is rather dependant upon the specific flow conditions for the device in question [48]. Laminar flow, as defined by Collins English Dictionary [1], is “, The non-turbulent motion of a fluid in which parallel layers have different velocities relative to each other.” Microfluidic channels are generally considered to have cross-sections with linear dimensions of 1 mm or less. As will be shown below, liquid flow in microfluidic channels is generally laminar, however gas flow, due to the low density, can still exhibit turbulence even at low fluid velocity. Table 1.3 demonstrates the pressures required to force fluid (liquid and gas are both shown) through a 500 μm x 100 μm x 30 cm channel at a high enough velocity to create turbulent flow at a Reynold’s number of 2000. The pressures presented in Table 1.3 (133 kPa for gas and 497 kPa for liquid) are far greater than the pressures normally applied to fluids within microfluidic devices used for research purposes.

	Pressure	Velocity
Gas (air)	133 kPa	180 m/s
Liquid (water)	497 kPa	12 m/s

Table 1.3 : The pressure required to force fluid through a 500 μm x 100 μm x 30 cm channel at sufficient velocity for Reynold’s number to equal 2000. Density and viscosity values are presented in Table 1.4.

Volume flow rate, Q, related to the fluid velocity and the cross-sectional area of the channel, is determined from the applied pressure differential, ΔP , and the fluidic resistance, R, of a channel by Equation 3 [48]:

$$Q = \Delta P / R$$

Equation 3

The fluidic resistance ($\text{kg/m}^4\cdot\text{s}$) is in turn either measured directly or calculated using Equation 4 if a rectangular cross-section channel is being used [49, 50]:

$$R = \frac{(a+b)^2 \cdot K \cdot \eta \cdot \ell}{8a^3b^3} \quad \text{Equation 4}$$

in which

a and b represent the height and width of the channel (m),

K is a dimensionless correction factor determined by the ratio of a and b , and

ℓ is the channel length (m).

Further equations for the calculation of the fluid resistance, dependent upon the channel cross-sectional morphology, have been derived [48].

The relationship between the fluid flow rate and the flow resistance affects the flow of fluids through microchannels directly. As shown by the units for R , the fluidic resistance is inversely proportional to the channel cross-sectional dimension, to the fourth power. At microchannel dimensions, the flow rate is normally very low (in the order of $\mu\text{L}/\text{min}$) and therefore the Reynolds Number is, significantly, within the laminar flow region.

	Water	Air	Units
Density	998	1.2	kg/m^3
Viscosity	0.001002	0.000018	$\text{kg/m}\cdot\text{s}$
Reynold's Number	324	1206	Dimensionless

Table 1.4 : Comparison of physical constants, taken from Geschke, Klank, et al [48]. Reynold's number values are calculated assuming an applied pressure of 25 kPa to a 30 cm long circular tube of radius 250 μm .

Gases and liquids, despite being governed by the same rules, can exhibit significantly different behaviour. The fluidic resistance of gases in channels tends to be much lower than that of liquids as a result of gas' much lower viscosity (see Table 1.4) and therefore the flow rate is proportionately higher for the same applied pressure. A higher gas flow rate and lower viscosity compensate for the higher density of liquid, hence gases may exhibit turbulent flow while liquids, in the same channel and under the same applied pressure, exhibit laminar flow.

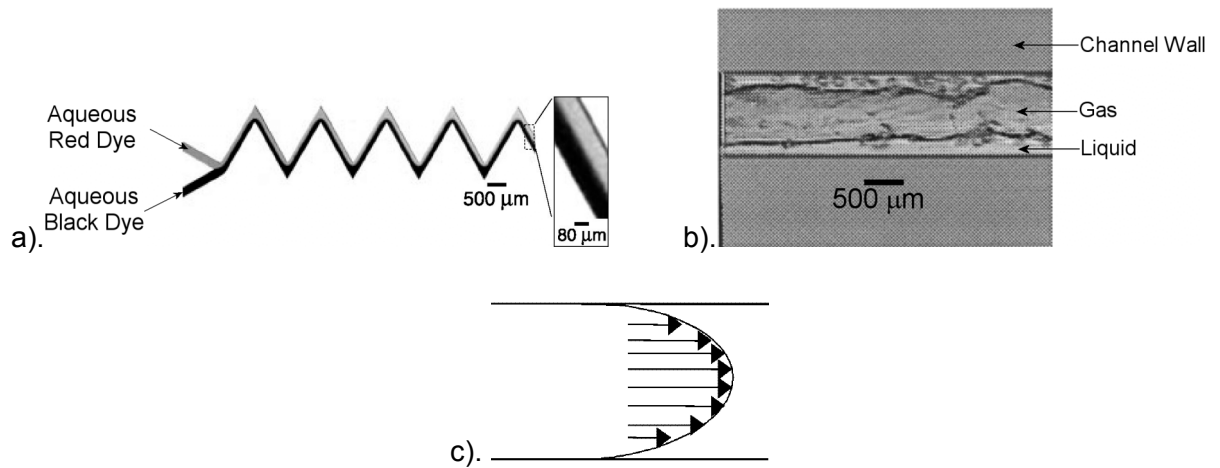


Figure 1.7 : a). Optical micrograph of laminar flow of two aqueous dye streams in a 200 μm wide channel (taken from Kenis, Ismagilov, et al [51]), b). turbulent gas and liquid flow (from Triplett, Ghiaasiaan, et al [52]) and c). the velocity profile of laminar fluid flow within a microchannel (from Greenwood and Greenway[53]).

As a result of laminar flow being the predominant flow regime in microchannels, fluid is presumed to conform to the 'no-slip condition', though a recent article disputes this [54]. The no-slip condition is a theoretical condition in which the fluid is assumed to be 'pinned' (that is stationary) to the channel wall at the boundary between the solid and fluid [54, 55]. This creates a parabolic flow pattern down the length of the channel as shown in Figure 1.7 c).

The majority of microfluidic processes require fluids to be mixed at some point in a system of channels. The Peclet number (Pe), calculated using Equation 5 [48], is a measure of the relative rate of mixing of fluid flow under laminar flow conditions:

$$Pe = \frac{v \cdot d}{D} \quad \text{Equation 5}$$

where

d is a characteristic length (m) and

D is the diffusion constant of liquid 1 in liquid 2.

If Pe is greater than unity, mixing is controlled by the fluid flow, while if less than unity, diffusion is the principal mass transport method. Flow controlled fluid spreading results from the continued development of the parabolic flow pattern without diffusion spreading the molecules (Figure 1.8) [48].



Figure 1.8 : Photograph of parabolic fluid front between two liquids spreading as flow develops (From Tabeing [56]).

Assuming a single fluid is present, laminar flow is the predominant fluid flow regime in microfluidic devices, although localised turbulent flow can occur due to localised flow structures such as ‘pinch points’. Hence diffusion is the major mode of mixing. Two separate laws of diffusion cover fluid flow, Fick’s First Law of Diffusion and Fick’s Second Law of Diffusion. Diffusion of a compound through a carrier gas follows Fick’s First Law of Diffusion (Equation 6 [57]).

$$J = -\frac{1}{2}\bar{c}\lambda\left(\frac{dC}{dz}\right) \quad \text{Equation 6}$$

J , the mass flux of each gas ($\text{mol}/\text{m}^2.\text{s}$) is a function of
 \bar{c} , the average speed of the gas molecules,
 λ , the average distance a molecule travels before colliding with another molecule,
 C , concentration, and
 z , the axis normal to the change in concentration.

The negative symbol indicates that the movement of matter is from high to low concentration regions.

Fick’s Second Law of Diffusion (Equation 7 [57])

$$\frac{\partial C}{\partial t} = D \frac{\partial^2 C}{\partial z^2} \quad \text{Equation 7}$$

concerns diffusion of molecules into liquids. D , the diffusion coefficient (m^2/s) is itself a function of the viscosity of the medium, the temperature and the molecular radius. Molecular diffusion through liquids is much slower than through gases. Mixing in microfluidic devices can therefore be much slower than in larger devices. For instance, diffusion controlled mixing of small molecules across a $100 \mu\text{m}$ wide channel can take several minutes, which increases rapidly as the size of the molecules increases [56].

Further discussion of gas & liquid flow in microchannels follows in Chapter 3.

1.2.2. Components

A review of the literature reveals that applications in fields as diverse as microbiology, microprocessor design, forensics and synthetic organic chemistry have been proposed for microfluidics. The principal requirement for the development of a microfluidic device for each application is a desire to control small volumes of fluid. To that end, microfluidics research can be considered to have followed two paths. The development of either subsystems, commonly termed 'Lab on a Chip' (LOC), or individual components. Commercially released LOC devices are limited in number and despite the name, are generally not complete subsystems. Although a number of complete LOC instruments have been designed or proposed [58, 59] little or no evidence of true commercialisation of these devices has been discovered.

Knowledge of the extent of individual component design is therefore more practical for the production of a microfluidic system. Integral components are generally limited to those requiring direct fluid interaction, such as pumps, valves, mixers and separators. Microfluidic valves, determined to be integral to consistent vapour collection device operation, are discussed further in Chapter 3 and 5. No other microfluidic component is covered in this dissertation. Recent reviews on micropumps [60, 61], micromixers [62] and unconventional microfluidic detection methods [63, 64] are provided. Although microfluidic analytical devices are discussed further, it is more likely that microfluidic devices will be integrated into an analytical system, rather than an analytical device integrated into a microfluidic platform.

1.3. Vapour Analysis

1.3.1. Sampling

Two fundamental problems face analytical chemists. Firstly, ensuring that the sample obtained is representative of the environment from which it is being taken. Secondly, determining the sample phase the analyte is found in, whether it is adsorbed onto dust or soil, etc, or even the chemical nature of the analyte (for example whether ligands are bound to the native compound). While the chemical nature of an analyte can be difficult to account for, gas and vapour detection systems have attempted to account for the physical aspects of the second problem. Many detection systems collect both gas and particles. Adsorbed vapours are then thermally desorbed or solvent extracted from particulates [2, 65] to ensure a representative sample has been taken. While this does not ensure that a completely representative sample is taken it guarantees the sample is complete for the environment in which it is taken.

The detection of low concentration vapours not only requires a sensitive detector, but also efficient vapour collection and the representative sampling methods discussed below. Increasing the sensitivity of vapour detection systems has also been accomplished by incorporating inline preconcentration methods [66]. Combinations of vapour collection and preconcentration [67] or even vapour collection, preconcentration and detection [68] are increasingly being used.

Gas phase systems for low concentration vapour detection tend to incorporate preconcentration and separation modules. The vast majority of these utilise a solid or liquid absorbent. Aragon, Atienza, et al [28] list 145 analysis methods for volatile organic compounds (VOCs). Of these, 127 entail the VOC dissolving in a polymer or liquid either in the course of sampling, separation or detection.

The inclusion of sorbent based, or even cryogenic, sampling of VOCs, while effective, introduces dilemmas. Sorbents, for the purposes of this introduction, include any material in which vapour or liquid is adsorbed or absorbed (see glossary). Cryogenic and non-packed sorbent samplers do not allow the sampling of analyte adsorbed onto particulate material. Moreover separate sampling units (as supposed to sampling directly into a gas chromatograph (GC)), utilising sorbents or cryogenics require that a batch sampling method is used as a result of the collection period. Finally, every sampling method that includes the absorption of analyte introduces an added delay, resulting from analyte transportation being limited by diffusion. This occurs even if the sorbent is purely a membrane between the analyte and the detector carrier flow. As demonstrated by the relative proportion of sorbent

to non-sorbent based sampling methods listed by Aragon, Atienza, et al [28], sorbent based sampling is the most effective sampling method for low concentration VOCs.

1.3.2. Analysis

Vapour analysis can be performed in either the vapour phase or by collection and later detection in a liquid. Liquid and vapour phase analysis are both covered by a wide range of methods as summarised briefly in Table 1.5.

	Method	Abbreviation	Reference
Vapour	Mass Spectrometry (plus many variants)	MS	[69]
	Electron Capture Device	ECD	[42]
	Flame Ionisation Detector	FID	[70]
	Thermal Conductivity Detector	TCD	[70]
	Metal Oxide Semiconductor	MOS	[35]
	Quartz Crystal Microbalance	QCM	[43]
	Surface Acoustic Wave	SAW	[34]
	Ultraviolet/Visible Absorbance Spectroscopy	UV/Vis.	[71]
	Infrared Spectroscopy	IR	[70]
	Fluorescent Polymer Coated Optical Fibres		[33, 42]
	Differential Optical Absorption Spectroscopy	DOAS	[70]
Liquid	Fluorescence		[72]
	Chemiluminescence		[73]
	Ultraviolet/Visible Absorbance Spectroscopy		[74]
	Conductimetric		[75]
	Electrochemical		[76]

Table 1.5 : Detection techniques, both standard and emerging, used to detect vapour while in vapour phase or dissolved in liquid. Due to the vast number of techniques and variations used the list is, by necessity, incomplete.

Whilst vapour phase analysis of VOCs is more widespread and has a greater variety of methods, liquid phase analysis nonetheless possess some distinct advantages. Many of the vapour phase detectors listed in Table 1.5 produce non-specific responses. They therefore require the incorporation of either a chromatographic module or an array of detectors, with attached signal processing and pattern recognition, to identify vapours. Other, spectrum producing detectors, such as some optical detection methods [71] or MS and IMS [77] operate under similar constraints as detector arrays. MS and IMS are capable of being tailored to respond well to specific vapours.

Many liquid phase analysis methods may operate under similar constraints to gas based methods, but sample pre-treatment is more easily performed. Some analytical methods for vapour and many for liquid require a transformation of the analyte, either at the time of detection (for example flame ionisation detection and electrochemical detection) or to produce a compound that is more easily analysed (chemiluminescence and fluorescence are prime examples) [78]. Biological materials (cells, enzymes and proteins) are becoming more popular as efficient and specific catalysts for the latter analyte transformations discussed above [63, 79-81]. Despite the recent rapid increase in vapour phase, biologically enhanced reactions, the use of cells, enzymes or proteins in liquid phase reactions remains much more common. As many systems utilising biological material generate more specific responses than their non-biological equivalent, detection systems and associated electronics can be made simpler [72, 75, 82-84]. If efficient sampling techniques are used, liquid phase capture and detection of VOCs is therefore capable of providing a simple, but elegant vapour analysis system.

1.4. Plan of Work

Development of a microfluidic vapour analysis system was determined to be best accomplished by research into each module separately. The vapour collection and fluid analysis modules were determined to be the most important to the complete system. However literature reviews of other modules potentially enabling the sensitivity and dynamic range to be increased, such as a gas removal system, were performed to make available sufficient information if research into these modules was possible given the time restrictions.

Following review of current vapour collection methods and determination of the desired properties of the final analytical system, pressure driven segmented flow was selected as the chosen vapour collection method.

Therefore research into a pressure driven segmented flow device will be undertaken. Following observation of relevant details in current and prior research performed at the University of Hertfordshire (much of it unpublished), the gas and liquid junction and balanced fluid supply paths are determined to be vital. Understanding of the fluid flow properties will be gained by using low resolution rapid prototyping to manufacture simple devices. Device evolution will continue as comprehension of the major fluid flow artefacts becomes more complete.

It is believed that the fluid flow will require finer control than that provided by external pressure sources and valves. Integrated fluid regulating methods will also be investigated as the desired properties of the control methodologies are determined. Finally, high resolution structures will replace the original low resolution structures within microfluidic devices as the designs of both the integrated fluid control methods and the pressure driven segmented flow devices become more complex.

Following development of the vapour collection module, practical investigation of analytical methodologies will be undertaken. A compound will be selected for use as an analyte to measure the effectiveness of the vapour collection system. Wet chemical, including standard and biochemical, reactions will be investigated as a result of the literature review. A full study of the analytical method will also be performed to account for sensitivities to external physical and chemical effects. This study will also be extended to an investigation of the modifications to the vapour collection device or the fluid flow regimes required for the chosen method to be effective.

1.5. Introduction to Further Chapters

Chapter 2 is primarily an experimental chapter. PDMS and the various physical and chemical properties that make it a useful, but occasionally frustrating material is introduced as the primary substrate. Similar, but slightly less detailed introductions are provided for SU-8, as the compound used to manufacture the microfluidic moulds, and PMMA as an alternative substrate for microfabrication. Section 2.3, demonstrates the manufacture of a representative device. Following the procedure from design to mould manufacture to device assembly provides the reader with the opportunity to visualise the complete process.

Chapter 3 describes the development and testing of several permutations of valves to be integrated into later vapour collection modules. Microfluidic valves (microvalves) are first introduced, with the compelling rationale behind integrating microvalves into the vapour collection module following. The subsequent rationale behind developing novel valves is then discussed. The evolution of valves from the initial Burst valves to Check valves, then finally to Seal valves is shown.

The behaviour and development of each valve type are discussed in detail. Rapid prototyping combined with an abbreviated testing regime are demonstrated to result in fast evolution of either device manufacture or design. Experimental results and the implications for further microvalve development are discussed fully. Finally, the experimental results that led to the decision to halt research into integrated valving, original to this work, are surveyed. Conclusions include the observation that time was the main limiting factor in the valve development, leading to the use of external valves as satisfactory replacements that would allow broader progress to be maintained.

Chapter 4 expounds on the vapour sampling issues discussed in Chapter 1, reviews microfluidic gas collection methods and *describes the rationale behind choosing the segmented flow vapour collection method*. Firstly the common gas and vapour collection techniques are reviewed. This leads to the theory behind sorbent based sampling being elaborated upon, firstly for solid, then fluid, sorbents. Microfluidic gas and vapour collection methods are then described and some operational detail provided of those determined to be most relevant to this project. Finally, the experimental parameters, defined by the previous work of other groups and by the available materials and equipment, are stipulated.

Chapter 5 details the development and gradual evolution of the vapour collection device and further specific experimental methodology used in assembling and testing these devices. Segmented, that is interleaved, gas and liquid flow device evolution is first summarised, then expanded upon and explained in the results and discussion. The, apparently separate and sequential, evolutionary progressions of the vapour collection device and microvalve

are finally unified. Few positive conclusions are drawn as to the future of segmented flow for vapour collection for analytical purposes.

Chapters 6 and 7 describe the method proposed for the analysis of the vapour suggested as a representative analyte by the industrial sponsors of this research project, that is ethanol, and the subsequent research into a novel effect of this and similar reactions.

Chapter 6 presents an introduction to liquid phase analysis followed by the development and testing of a specific methodology for ethanol analysis. Several of the liquid phase analytical methods tabled in Section 1.3.2 are discussed in greater detail and examined specifically with respect to analysis within a microfluidic device. Following the conclusion that analysis of a solution's optical properties is much more rapidly and reliably implemented. Chemiluminescent, fluorescent and absorbance methods are examined in turn. A novel two-stage reaction producing a chemiluminescent product is developed, tested and found not to react as anticipated. The subsequent testing of a fluorescence analysis method, based on an enzyme catalysed oxidation of ethanol followed by a separate enzyme catalysed reaction to produce a fluorophore, is believed to have been successful. However an absorbance method was finally adopted due to the difficulty in implementing fluorescence analytical instrumentation. Two methods, utilising similar reactions to the fluorescence method, but different final substrates, are examined before an analysis method, appropriate to the conditions required for the experiments discussed in Chapter 7, is found.

Chapter 7 describes the hypothesis that a two phase system incorporating an irreversible reaction in one phase could be used to lower the detection limit of an analyte originating in the other phase and its subsequent testing and discussion of the results. Similar hypotheses have been discussed previously, but not in the field of analytical chemistry. The chemical methodology, previously developed for ethanol vapour analysis, is refined for this application. Additional experimental development, related to maintaining quantities of vapour over extended periods of time while taking and adding solution aliquots, is also reported. The final experimental methodology used to test the hypothesis results from step-by-step refinements designed to increase the sensitivity of the experiment, while simultaneously reducing the possibility of operator error. Final examination of the results lead, despite using a difficult analyte, to the conclusion that chemical amplification does occur.

The concluding chapter contains the final deductions from each major piece of experimental work, specifically: research into microfluidic vapour collection; integrated valving; and chemical amplification. Also included are the conclusions drawn from several small, but interesting, experiments conducted during the period of experimental research.

2. INTRODUCTION TO MICROFABRICATION

2.1. Introduction

Control of single phase fluid flow in microfluidic devices has been the subject of extensive research since the late 1980's [85]. However the theoretical bases governing the flow of, and movement of molecules within liquid and gases were established far earlier. For instance Adolph Fick published both his first and second laws (Equations 6 and 7 respectively) in 1855 [57], while Osborne Reynolds devised the equation governing the relationship between channel dimensions, fluid velocity and fluid properties (Equation 1) around 1889 [86].

Multiphase flow is governed by the same equations that describe single phase flow combined with further equations that describe the effect of the interphase fluid boundaries. Ideally, theoretical calculations of the fluid flow and properties for multiphase systems would allow the production of systems without experimental development. However in reality, as dimensions decrease and the effect of small variations in manufacturing technique become proportionately large in relation to the device, the first order theoretical calculations bear diminishing resemblance to observed fluid flow patterns. Experimental testing of ideas by rapid manufacture of test devices can frequently be more *accurate* than first order calculations and *faster* than more intricate computer modelling. Accordingly, an experimentally based development route is common in microfluidics research.

Several different manufacturing methods and substrates were potentially available to the author for the production of microfluidic devices. Silicon, glass, polydimethyl siloxane (PDMS) and polymethyl methacrylate (PMMA) were commonly available, but available processing expertise combined with other factors meant the latter two offered advantages over the former. Importantly, all four substrates are inert to the reagents used during all experiments. PDMS and PMMA were able to be rapidly prototyped, with device turnaround from design to testing being as rapid as 2 days provided the channel width exceeds 20-30 μm . In contrast silicon and glass assembly times are dependant on relative channel dimensions [47, 87]. PDMS, SU-8 (used to manufacture the moulds upon which the PDMS is cast) and PMMA are therefore discussed in greater detail in the following sections.

2.2. Rapid Prototyping – Introduction

2.2.1. Basic PDMS Device Microfabrication Process

While a more detailed description of the steps involved in the design, mould manufacture, casting and assembly of a slightly complex, but representative PDMS device is presented later, a very basic description is provided here.

A design of the device is produced such that the fluid paths and design perimeters are shown. This design, produced using a computer aided design (CAD) program, is converted to a format accepted by specialist printing companies. The printing company supplies a printed polyethylene terephthalate film (overhead projector film) photomask. The photomask is printed almost entirely black, with only the designs produced using the CAD program being transparent: this is a so-called 'dark field' photomask.

SU-8, a photosensitive, epoxy resin, after being poured over the surface of a silicon wafer and spun to achieve the required thickness, is selectively cross-linked by exposure to ultraviolet light passing through the photomask. The wafer is then washed with solvent. The SU-8 below the transparent regions of the photomask is cross-linked and insoluble in the particular solvent used, while the remainder of the SU-8 is removed. The resulting mould consists of structures, raised above the level of the wafer, that are of the same pattern as the transparent regions of the photomask.

Liquid PDMS, a 2-part silicone elastomer is poured over the mould and allowed to cure. When removed, the PDMS casting is flat, but with small indentations in the pattern of the mould. Following drilling, of the PDMS or the substrate to which it will be bonded, and cleaning, the PDMS is treated with UV and O₃ to activate the surface. The PDMS is then bonded to the substrate and fluid connections attached.

The device is then ready for testing.

2.2.2. Material Properties

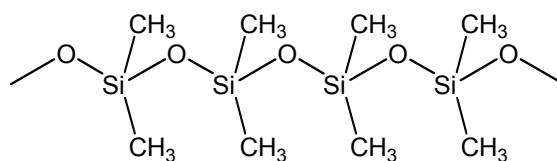


Figure 2.1 : Chemical structure of PDMS as described in the following paragraph.

Polydimethyl siloxane (PDMS) is used almost exclusively as the substrate for the majority of microfluidic devices in this thesis. A backbone of alternating silicon and oxygen atoms (Figure 2.1) confers greater torsional flexibility in PDMS than is normally found in the carbon to carbon bonds of most polymers. The two methyl groups attached to each silicon atom exhibit low intermolecular forces, thereby producing a low surface free energy (γ_{sv}) [88]. The torsional flexibility is partly responsible for the high gas permeability ($325 \text{ cm}^3 \text{ gas (RTP).cm/s.cm}^2 \text{.cmHg.}\Delta P$ [89]) of PDMS [90].

A low glass temperature ($T_g \approx -125^\circ\text{C}$) also confers PDMS with mechanically useful properties [91]. High degrees of flexibility ($E \approx 250 \text{ kPa}$), compressibility and a low loss tangent ($\tan \delta \ll 0.001$) [91], provide a substrate that is capable of being used in a wide range of mechanically active devices. Solid PDMS also exhibits remarkable conformity to contacted materials. A number of theories have been proposed, but van der Waals forces are most likely to provide the high degree of stiction observed between PDMS and flat surfaces [91].

PDMS is a chemically stable polymer, relative to many carbon based polymers. Although it is reactive towards compounds that other silicon based materials, such as glass, react to, the methyl groups are less prone to attack than structurally equivalent carbon back-boned polymers. While the C-Si and C-C dissociation energy are roughly equal ($\approx 325 \text{ kJ/mol}$ and $\approx 330 \text{ kJ/mol}$ respectively [92, 93]), PDMS is more resistant to oxidative attack.

PDMS also exhibits considerable molecular permeability. The polymer backbone mobility is again responsible for the high diffusivity of low molecular weight compounds [94]. Concomitant with the exposure and subsequent diffusion of many organic compounds into PDMS is a noted swelling [95]. Determination of the compatibility of PDMS with solvents or reactive compounds must therefore include the diffusivity of the compound through PDMS and the swelling ratio (S) [95].

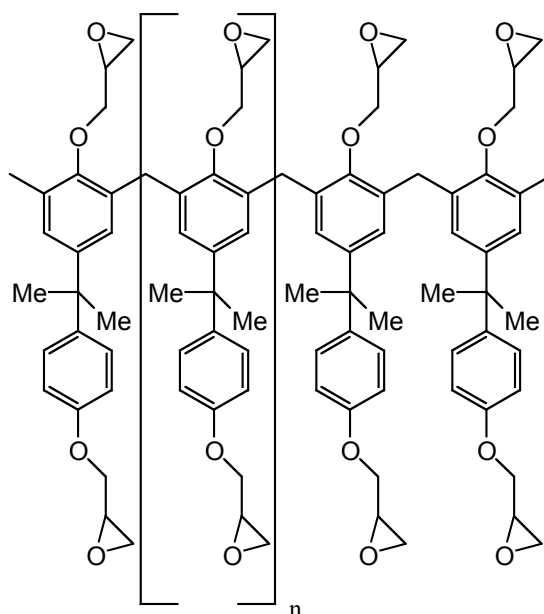


Figure 2.2 : Chemical structure of SU-8 [96].

SU-8 (Microchem Inc., USA), a glycidyl ether derivative of bisphenol-A novolac combined with a photosensitive acid in an organic solvent, is a negative photoresist originally manufactured by IBM [97]. Mechanically robust ($E = 4.02$ GPa [98]) and with low absorbance in the UV spectrum [96], SU-8 is thus able to be patterned with high aspect ratio features. The thermal stability of the cured and cross-linked SU-8 ($T_g = 240^\circ\text{C}$ and $T_d = 380^\circ\text{C}$ [96]) also makes it ideal for use as a mould for heat formed or heat cured polymers. SU-8's low molecular weight increases the range of solvents in which SU-8 is soluble and the concentrations that can be achieved [96]. For instance the current solvent in which SU-8 is provided by Microchem Corp is cyclopentanone (the SU-8 2000 range of products) while originally it was γ -butyrolactone (the SU-8 0000 range). Finally, SU-8 is near UV cross-linked by a reaction in which a Lewis acid generated by exposure to deep UV initiates cross-linking via a ring opening reaction of the 1,2-epoxy (Figure 2.3) [99]. The viscosity of the baked SU-8, before exposure to UV, is such that the photogenerated acid does not diffuse from the region in which the exposure to UV takes place, localising the cross-linking reaction.

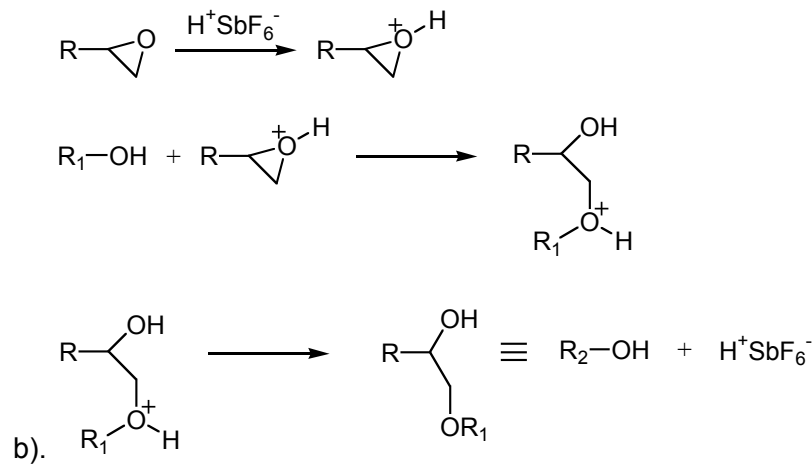
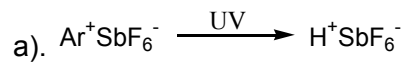


Figure 2.3 : a). Generation of the Lewis acid under exposure to UV and b). the series of reactions, initiated by the Lewis acid, that lead to the cross-linking of the bi-epoxy SU-8 chains. Taken from [99].

Utilising PMMA as a substitute substrate provided opportunities to observe the fluid behaviour when in contact with a substrate other than PDMS. Some desirable properties exhibited by PMMA or resulting from the manufacturing process allowed PMMA to be utilised in a number of devices.

PMMA, while not possessing the wide ranging chemical resistance of PDMS, is sufficiently inert for the purposes of this project.

Design and manufacture of PMMA devices could be completed rapidly 'in house'.

PMMA (Young's Modulus = 3.3 GPa [100]) is considerably more rigid than PDMS (Young's Modulus = 360 to 870 kPa [101]), allowing it to form both a support for microstructured PDMS or the sole substrate for microfluidic devices.

2.2.3. Microfluidic Assembly Related Properties

Surface oxidation of PDMS is used to create a chemically reactive layer for bonding PDMS to other substrates [102] and has been employed extensively in the work reported here. As chemical oxidation is ineffective, short term exposure to plasma, UV, or, as reported here, UV and ozone (UV/O₃) is used instead [103] (see Figure 2.4). The torsional flexibility of PDMS requires that bonding must occur within a brief period of time following oxidative treatment. It is believed that, to reduce the surface energy of the PDMS, the oxidised

surface polymer chains are replaced by unoxidised polymer chains, thereby recovering the surface properties [104].

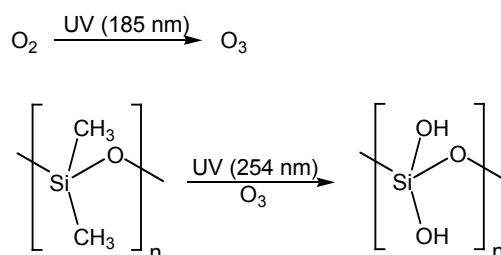


Figure 2.4 : Dual frequency UV/O₃ oxidation of the surface of PDMS (adapted from [104]).

In a similar manner, the surfaces of PDMS channels in contact with polar liquids for extended periods of time were observed by the author to become more hydrophilic. The changing chemical nature of PDMS surfaces in response to external stimuli can be useful when required by certain applications [95, 105]. However when external conditions are constantly varying and yet it is necessary that the chemical surface properties remain constant there is little that can be done.

However despite these disadvantages, PDMS' central property, the ease with which rapid prototyping of high aspect ratio channels can be performed [102], ensured that PDMS was selected as the primary substrate. As previously stated, rapid prototyping provides advantages over both basic theoretical calculations and computer modelling. The interaction between the gas/liquid menisci and the rough surface of the channel walls, as will be discussed in Chapter 5, was observed to significantly influence the behaviour of the fluid flow. Applying fundamental fluid dynamics equations to the segmented flow of gas and liquid assumes that channel walls are perfectly smooth and therefore does not account for these interactions. Sufficiently complex computer modelling is capable of including the basic surface details, supposedly making possible a prediction as to the behaviour of more complex fluid flow within a device. However the modelling of more than two or three segmented injections of gas and liquid is prohibitive due to the degree of modelling complexity required to accurately predict the interaction between multiple gas and liquid menisci and the channel surface [106].

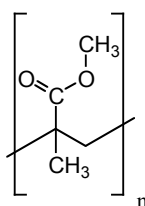


Figure 2.5 : Chemical structure of the PMMA monomer.

Devices that were manufactured in PMMA were restricted by both the manufacturing process and PMMA's intrinsic properties. The chemical structure of the PMMA monomer (Figure 2.5) increases the difficulty in bonding PMMA to either PDMS or PMMA components (as discussed below). While the channels in the PMMA devices contained smoother channel walls than the initial PDMS devices (discussed in greater detail in Chapter 5), only 'step' changes in the channel width of the PMMA devices were possible.

Bonding PMMA to PMMA or to PDMS required different surface activation methods. As discussed in Appendix 1, bonding PMMA to PMMA was accomplished by first polishing the two pieces of PMMA with ultra-fine abrasive polish, pressing the two polished pieces together, then heating the unified device above the glass temperature (T_g) while applying a uniform pressure. Polishing the PMMA with ultra-fine particulate polish is believed to break the polymer chains at the surface. Heating the PMMA sheets above their glass temperature ($T_g \approx 108^\circ\text{C}$) while applying pressure then bonds the PMMA, by forcing the surface polymer chains to interdiffuse [107].

PDMS to PMMA bonding had been considered impossible following Duffy, McDonald, et al's article [102] as a result of the lack of polar surface moieties on PMMA. However, an attempt was made by the author to modify the surface of PMMA by hydrolysing the methacrylate to methacrylic acid moieties with concentrated (1 M to 10 M) sodium hydroxide and dilute hydrochloric acid (see Figure 2.6). While partially successful, the conditions and treatment time required modified the PMMA adversely in other respects. PDMS to PMMA bonding, as discussed in Section 3.4.1, was finally achieved by coating the PMMA with a 100 nm thick SiO_2 layer.

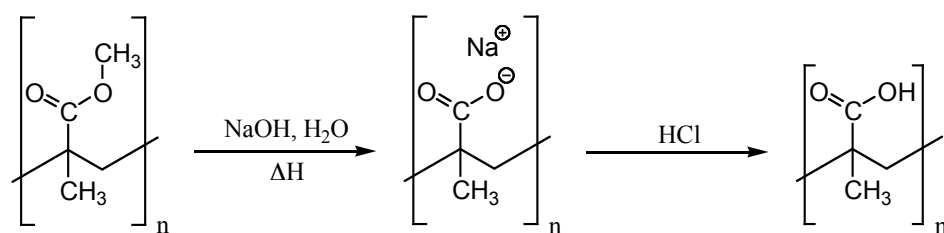


Figure 2.6 : Reaction scheme for attempted hydrolysis of PMMA surface polymer chains.

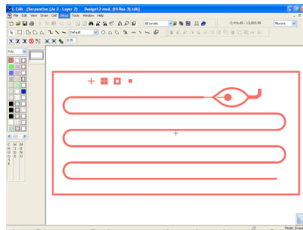
Microfabrication of PMMA devices was accomplished by milling channels into flat ($\pm 100 \mu\text{m/m}$ height variation/length) cast Clarex (a commercial PMMA). Utilising a small PCB prototyping machine (Protomat 91s/vs, LPKF Laser and Electronics, Garbsen, Germany) and assorted drills, routers (cutting tools) and cutters, structures were milled, and connecting holes drilled, into PMMA. While channels have also previously been created in PMMA by hot-embossing with either wire or a metallised mould [108, 109], milling channels allowed faster production times of typically 2-3 days from design to testing.

It was observed that due to the defined width of the cutting tools, increasing the channel width would have required multiple passes of the tool along the channel as the channel widened. However, each pass would have resulted in a step change in the width, rather than a smooth widening. As discussed in Chapter 4, smooth channel walls were determined to be essential for the development of regular gas and liquid flow in microfluidic devices. Therefore microfabricated devices incorporating PMMA were limited to those in which PMMA served as a support, to which other microstructured pieces were bonded, or in which the channel width was constant throughout.

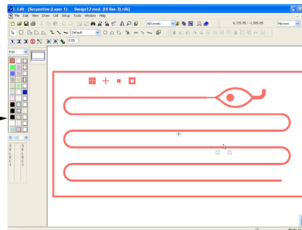
2.3. Rapid Prototyping – Manufacture

2.3.1. Computer Aided Design (CAD)

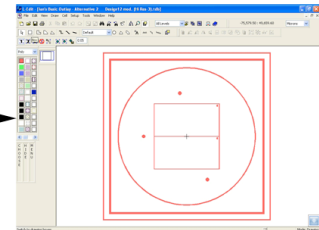
A step-by-step introduction to the process scheme used to design the photomasks used in the SU-8 mould manufacturing process.



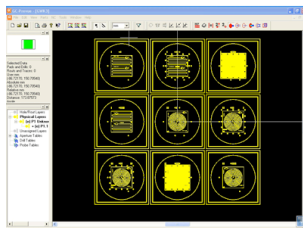
1. One of the main designs for the device created in L-Edit. Also shown are the alignment marks (see step 9 of the SU-8 processing summary).



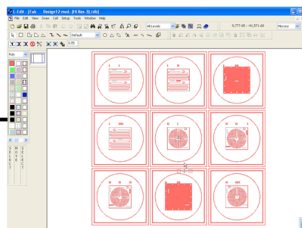
2. As the one mould has two layers (double depth), a design for the 2nd layer, to be placed on a separate wafer, is also completed.



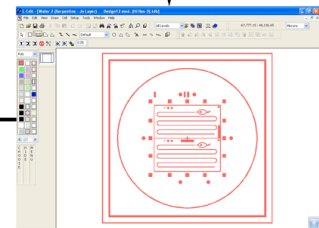
3. A frame for the designs is composed for the precise placement on the wafers.



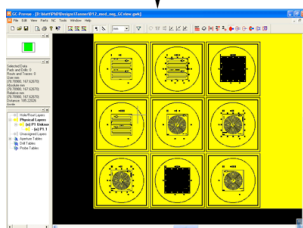
6. The photomask production company accepts .gbr (gerber) file format. The original .tdb L-Edit file is converted using LinkCAD.



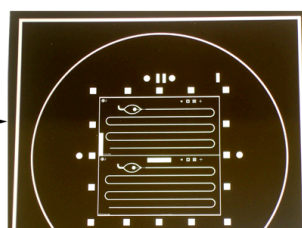
5. Each full photomask design is comprised of several wafer designs. This photomask incorporates designs for several different devices.



4. The microfluidic designs are placed within the frame.



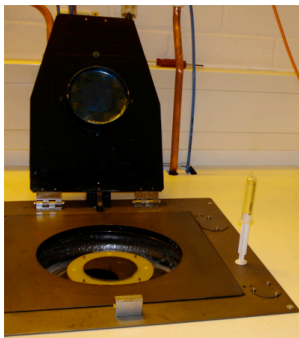
7. Finally the polarity of the .gbr file is reversed (from positive to negative) before emailing the .gbr file to, for this design, JD Photo Tools for printing.



8. The photomask received by special delivery is printed on PET film. The photomask is cut, using a razor blade, into the separate wafer designs

2.3.2. Mould Manufacture (SU-8 Processing)

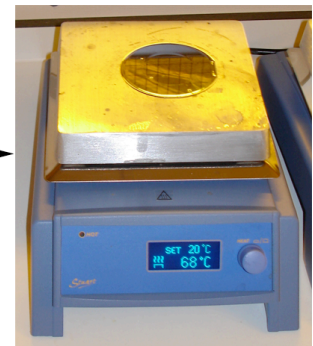
This section details the steps followed in the production of an SU-8 mould.



1. Preparation of SU-8 before pouring onto a silicon wafer. Wafer is already placed in the Gyrset resist spinner.



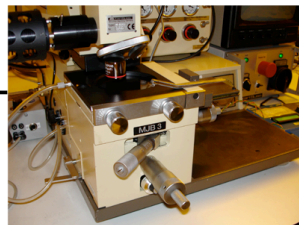
2. Pouring SU-8 onto a silicon wafer.



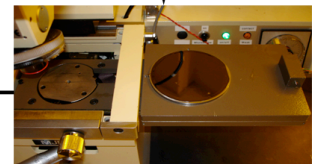
3. Soft baking freshly spun SU-8. Removes the solvent from the SU-8 to harden the photo-patternable polymer.



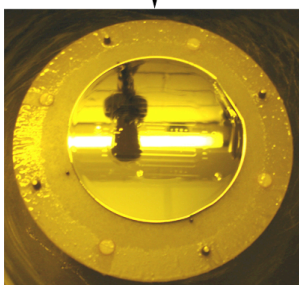
6. Hard baking SU-8 following exposure to UV. Baking propogates the cross-linking initiated by the UV created free radicals.



5. Setting the wafer height in the aligner and UV exposure equipment.



4. Wafer placed in the aligner and UV exposure wafer platform.



7. Wafer after spinning a 2nd layer of SU-8 over the exposed and hard-baked 1st SU-8 layer.



8. The device being demonstrated is composed of 3 levels: 2 within one layer

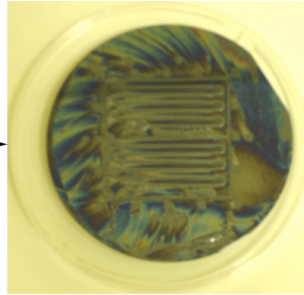


9. Having a double depth mould requires that the photomask, through which the top layer of SU-8 is to be exposed, is precisely aligned to the bottom layer. A microscope is used to view the faint lines of the exposed SU-8 through the photomask. The wafer is then moved laterally or rotated until the designs are aligned. Alignment marks placed on both photomasks enable more precise alignment.

10. Hard baking the 2nd layer of SU-8 is performed as per step 6 above.



11. The uncross-linked SU-8 is removed by immersing within previously used developer (EC Solvent).



12. After the 1st rinse using 'old' developer, impurities remain on the wafer.



13. The wafer is inspected to ensure the structures are correct.



15. The depth of the 2 layers of SU-8 is then measured using a Starrett dial gauge.



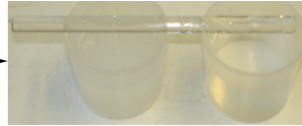
14. If the structures are correctly designed and aligned, the wafer is immersed in fresh developer (left), then dried and inspected again. Once the structures appear fully developed (all un-exposed SU-8 removed) the wafer is immersed in i-propanol (IPA) to confirm this (fine white precipitate indicates remaining undeveloped SU-8), dried and finally inspected again.

2.3.3. Device Assembly

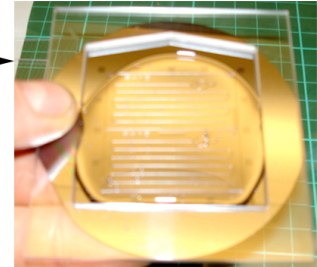
Section 2.3.3 demonstrates, in some detail, the steps followed in the casting, preparation and subsequent assembly of a PDMS device .



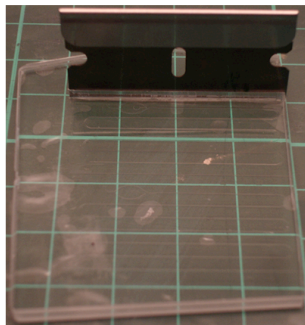
1. Dow Corning Sylgard 184 2-part silicone elastomer mix. Adding the catalyst (right hand container) to the silicone base (left) 'cures' the mixture.



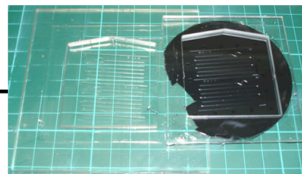
2. Mixing the 2 liquids thoroughly (left container) includes bubbles which need to be removed under vacuum (right). Also shown is the glass mixing rod.



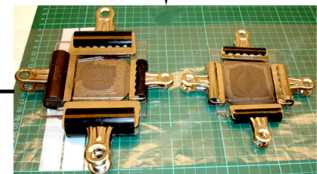
3. Following mixing, the silicone catalyst mixture is poured onto the mould with a PMMA frame used to contain the liquid within the mould boundaries.



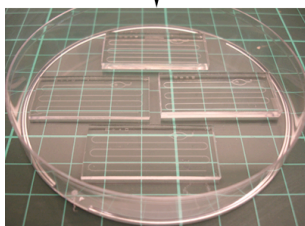
6. Cutting the cured PDMS into separate devices. The surrounding lines are used as guides to position the razor blade.



5. Showing before and after removal of the wafer from the frame. The wafer was partly broken after cracking by 1 of the clamps before placing into the oven.



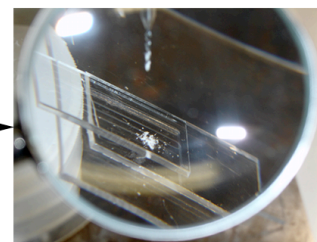
4. The 2 wafers containing the microstructured designs after baking at 65 degC for 4 hours to completely cure the PDMS mix.



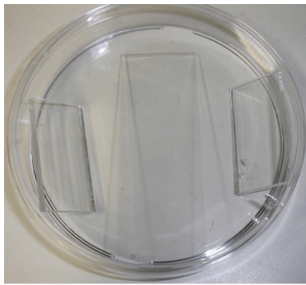
7. Following cutting of the 2 mould designs into the 4 separate pieces.



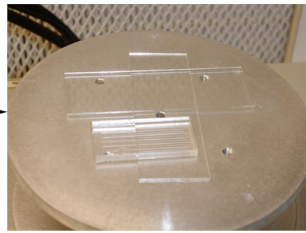
8. Set-up for drilling the holes for the fluid supplies into one of the pieces of PDMS. The holes are drilled at an angle by hand.



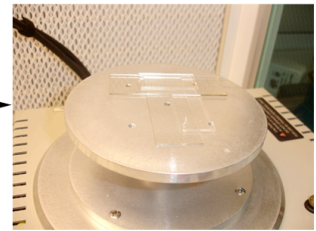
9. After drilling, PDMS swarf coats the surface of the PDMS piece.



10. All pieces for the device, the 2 PDMS pieces and the microscope slide acting as the support, are cleaned under water with a neutral detergent, then desiccated under vacuum.



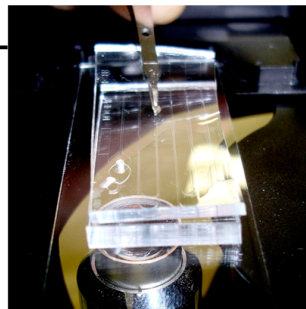
11. The 1st 2 pieces, for the device are placed onto a platform within the UV/ozone cleaner to treat the surfaces for bonding. They are rested on a clean slide to prevent contamination.



12. After bonding the 1st layer, the 2 layers of PDMS are then UV/ozone treated to complete the bonding of the device.



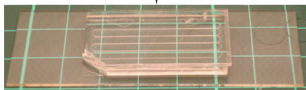
15. The device after baking to ensure a complete bond throughout.



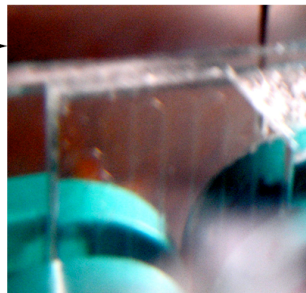
14. Bonding occurs immediately after the 2 pieces contact. Care must therefore be taken to ensure that alignment is complete across the entire device.



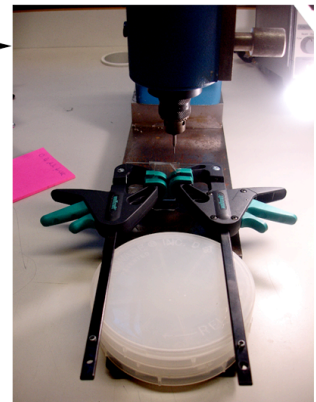
13. Very careful aligning of the microstructured designs on the 2 pieces of PDMS is performed under a microscope to a strict time limit of 2 minutes.



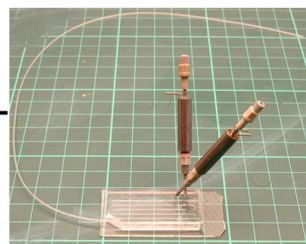
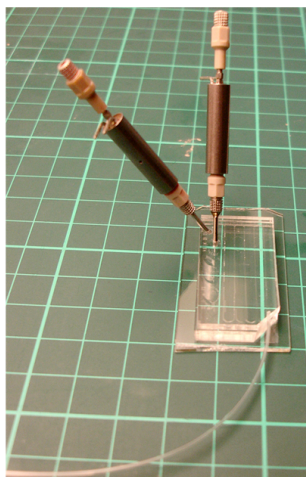
16. The corner, at which the channel ends, is then cut from the device.



17. The exposed channel end is then widened (initially with a 300 micron drill bit, then with a 700 micron bit) to accommodate tubing used to lengthen the channel without direction change.



18. Set-up for drilling the channel end.



19. To the left- 2 views of the completed device, with the external valves and channel extension in place. All holes were drilled slightly smaller than the connections. The PDMS thus forms a hermetic seal.

3. INTEGRATED MICROVALVE DEVELOPMENT

3.1. Introduction

Following preliminary attempts to produce segmented flow using external active valves, research was redirected towards developing integrated valving. Fluid, both liquid and gas, flow into microfluidic devices was initially controlled by solenoid valves (Neptune Research, NJ, USA). These valves, as detailed in Section 5.2.2, were unable to provide the volume flow control necessary for the increasingly fine structures present at the gas and liquid junctions. Valves able to completely prevent flow of one fluid into the supply channel for the alternate fluid during flow switching were determined to be essential for the development of actively produced segmented flow.

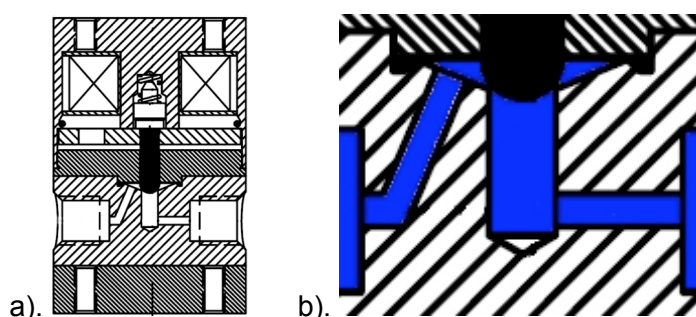


Figure 3.1 : a). Schematic of 2-way solenoid controlled isolation valve and b). Close-up of Fluid Path with plunger in solid black showing at top (from Neptune Research, NJ, USA).

Initial attempts to produce segmented flow, as detailed in Section 5.2.1, were visibly affected by the opening and closing of the gas and liquid control valves that created a slight pumping effect. Following numerous attempts to design a microfluidic device to compensate for the secondary effects on fluid flow associated with valve opening and closing, the Neptune Research 2-way solenoid controlled isolation valves were examined in greater detail. As shown in Figure 3.1 b). (a close up of the fluid path within the solenoid valve shown in Figure 3.1 a.) the valve inlet and outlet channels lead to a chamber into which fluid will be drawn as the plunger (in black) is raised. Likewise, as the plunger is depressed the fluid is pushed out. The plunger displaces about $13.5 \mu\text{L}$, a significant volume considering the microfluidic device channel volumes (a $300 \mu\text{m} \times 300 \mu\text{m}$ channel would be filled to a length of about 150 m by $13.5 \mu\text{L}$). Fluid displaced from or sucked into the chamber produces an asymmetric pumping action due to the imbalanced placement of the channels on the chamber. However the degree of asymmetry between pumping and sucking is unequal, preventing equilibrium being established by altering the inlet and outlet channels. Therefore an overall net pumping effect is produced by the valves.

A number of alternate valves, also manufactured by Neptune Research, were considered, but assessment indicated that integrated valves proffered better flow control. Replacing external valving was motivated by the large internal volume and pumping effect of the original solenoid valves. Integrating valves in the flow structures dramatically reduces the valve's internal volume and hence associated pumping effects as the volumes of fluid moved by the valve opening and closing were, by design, smaller. Many different microfluidic valves (microvalves) have been reported. However most are manufactured as separate structures. Oh and Ahn [110] provide a comprehensive review of the current state of research and development of microvalves, although a brief summary follows.

Microvalves are generally defined as either passive or active. Passive microvalves operate in response to the direction and pressure of the applied fluid flow (see Figure 3.2), while active microvalves require external actuation. Passive valves are subdivided according to whether they contain moving parts or whether the fluid control is intrinsic to the basic structure. They also tend to be integrated within the device within which they are controlling the fluid supply. Active valves can be further subdivided depending upon whether the valve seal is directly or indirectly actuated or whether the valve is a completely separate module. Lack of drive circuitry or necessity for fluidic connections, thereby reducing internal volume between the valve and the vapour/liquid junction, indicated that passive valves best fulfilled the fluid control requirements of this project.

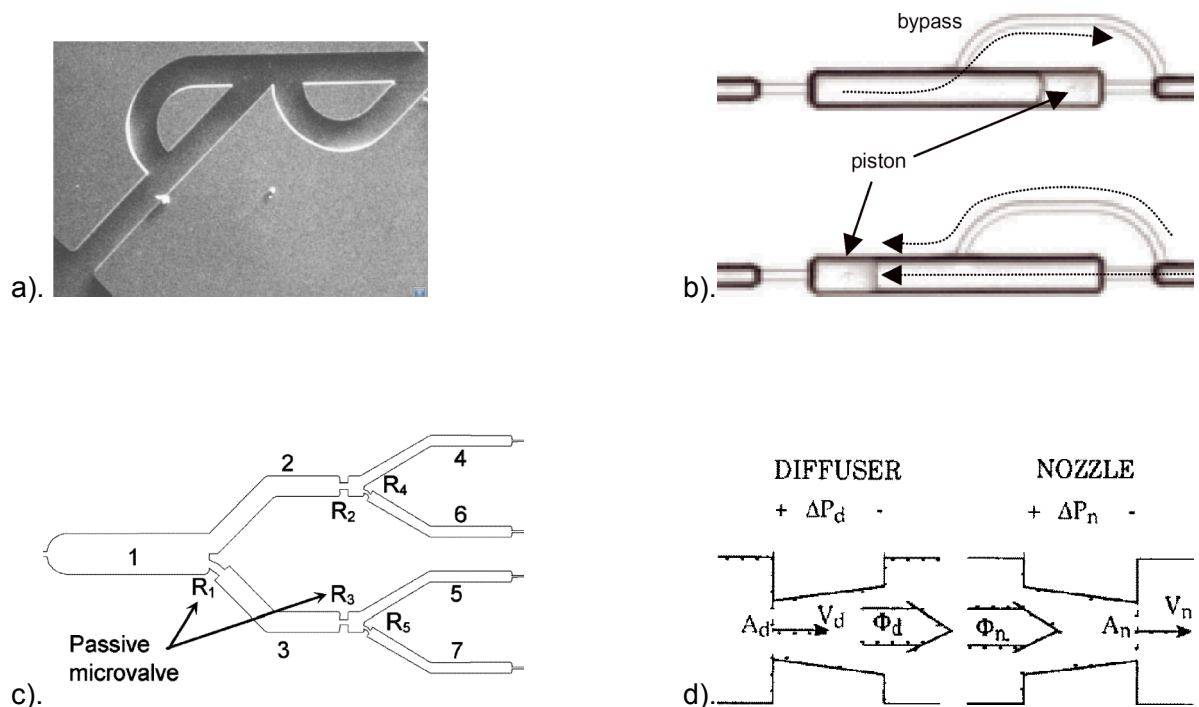


Figure 3.2 : a). The T45-R geometry based non-moving-part valvular microchannel (from Feldt and Chew [111]), b). Unidirectional Piston valve (from Rehm, Sheppard, et al [112]), c). Passive microvalves used to define preferred fluid flow direction (from Ahn, Choi, et al [59]) and d). a comparison of the diffuser and nozzle passive microvalves (from Stemme and Stemme [113]).

For passive microvalves to be effective at high flow rates and pressures requires unidirectional flow control. Diffuser and nozzle [113] microvalves and associated equivalent designs, such as those produced by Ahn, Choi, et al [59], employ complex fluid dynamic effects to operate as unidirectional valves until a finite pressure, determined by the substrate and geometry of the device and the liquid being used, is reached. Mechanical passive valves have been designed that only permit flow in one direction [114-116]. However, as detailed by Oh and Ahn [110] many mechanical passive valve designs utilise substrates that are incompatible with PDMS devices.

All passive valves investigated (in the context of this work) exhibited either complicated device manufacture, incompatible substrates or long actuation times. Novel mechanical passive valves were therefore investigated. Three separate classes of valve were researched: Burst valves; Check valves; and Seal valves. Burst valves are formed of a single seal across a channel which has been previously cut so as to open when pressure is applied from one direction. Check valves use applied fluid pressure to push the valve seal away from the valve seat, opening a fluid path. Seal valves are active valves in which the fluid flow is stopped by a piezoelectric disc 'sealing' a glass membrane to a PDMS valve seat.

The remainder of the chapter discusses in considerable detail the experimental evolution of the valve types. To aid the reader, a very brief summary of the sequence and aims of the work follows.

Burst valve manufacture was investigated initially. Based on a simple 'flap' valve design, they were found to be extremely difficult to construct due to the method of bonding PDMS to PDMS.

Check valves were also studied following the development of a design that was simpler to prototype. Check valves, a broad class of unidirectional valves, in this case utilise a membrane around which fluid flows in the forward direction, but which seals when a reverse pressure is applied.

Irregular valve opening and closing times by Check valves led to the investigation of Seal valves, a class of active valve. The Seal valve explored here was a piezoelectrically actuated valve membrane that depresses against a raised (from the body of the channel) seal to close the fluid flow path. While Seal valves almost operated as required, the uncertain length of time (in the context of this work) required to develop them to full effectiveness led to their research ultimately being halted as well.

3.2. Burst Valves

Burst valves were designed to operate by the application of pressure opening a fine cut in a cross channel PDMS membrane that would then completely close to stop the fluid flow once the pressure was released. They presented a number of potential advantages over other designs considered. Namely the lack of alignment to other structured PDMS during assembly, complete sealing of the valve and, theoretically, the ability to set the valve opening pressure by varying the depth of the channel during manufacture. A hysteresis pressure (here known as the *burst pressure*), the pressure at which the force applied to the valve was sufficient to overcome the PDMS to PDMS adhesive force, was also expected to be present. A burst pressure was believed to be of advantage for valves controlling gas and liquid injection into a junction.

3.2.1. Experimental, Results and Discussion

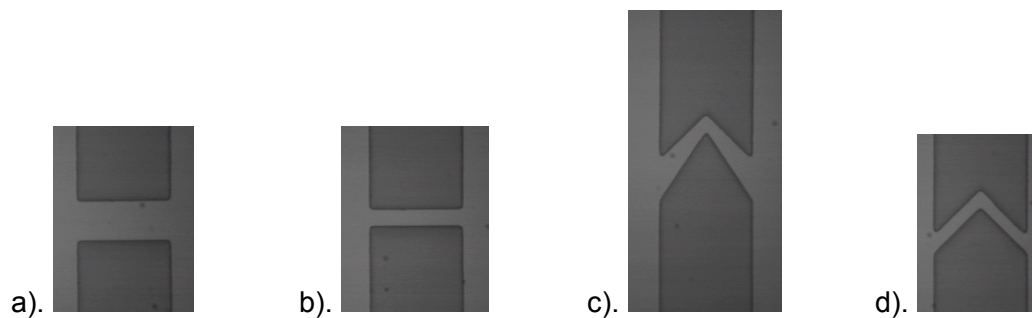


Figure 3.3: The four original Burst valve designs implemented in PDMS. All channels are 500 μm wide.

Photomask 6 (extracts shown in Figure 3.3) was the first to include Burst valve designs. Four different straight channel valves, designed to be tested using a single phase, and two junction valves, for two phase flow, were included in the initial design. All designs were printed at a resolution of 4040 dpi.

Following the method described in Section 2.3 and in greater detail in Appendix 1, two SU-8 moulds were fabricated with feature depths of 75 μm and 130 μm .

Originally PDMS was cast as per Appendix 1.3 and each device assembled as per Appendix 1.4.1 with the following modification. Before treatment with UV/O₃ the PDMS membrane forming the valve seal was cut by placing the structured PDMS under a microscope and carefully slicing through the membrane using a razor blade. The top of the membrane was masked with PE tape during UV/O₃ treatment to prevent bonding to the flat PDMS.

Initial tests were performed by applying a gradually increasing pressure, to a maximum of 200 kPa, to the inlet tube. Three of the valve membranes opened in the 130 μm structure. A series of pressure pulses, of magnitude 100 kPa, were then applied to the unbroken membrane. All valve membranes of the 75 μm deep structured PDMS remained unopen following burst attempts. Details of the 130 μm deep structure results are shown in Table 3.1.

Valve Seal Design	Max. Test Pressure (kPa)	Subsequent Opening Pressure (kPa)
A	≈ 150	13
B	≈ 200	20
C	≈ 200	---Did not burst---
D	≈ 150	3.5

Table 3.1 : Opening pressure tests of 130 μm PDMS device, design 6.3. Where a valve bursts, the maximum test pressure is the applied pressure required to open it.

Initial membrane burst pressures, when compared to the subsequent opening pressures, indicate that the valve seal changed after being forcibly opened. The valve membrane, due to stiction, was expected to require a burst pressure slightly higher than the normal opening pressure. Repetitive opening of the valve, after initial bursting, showed no increase in required pressure, even following drying and retesting. Stiction alone is therefore not responsible for the initial high burst pressures.

Further PDMS castings, using the original Burst valve moulds, were made and assembled in almost the same manner as mentioned above. Accordingly an alternative method of masking the membranes from UV/ozone was evaluated. The cut in the valve seal was made slightly deeper and a fine, soluble spacer (Wrigley's Ultra Thin Ice™, Wrigley's, USA. Here referred to as Wrigley's) was placed within the cut. Wrigley's, a 10 μm thick membrane composed primarily of sodium alginate and maltodextrin (i.e. a breath freshener), was cut into fine slices before being positioned. The PDMS was then treated and bonded as before. During attempts at bonding the structured PDMS to the flat PDMS the spacer was displaced from the cut in the membrane. No attempt to rupture the PDMS membranes was successful.

All repetitions of the above attempts were also unsuccessful.

Finally we attempted to fabricate membranes with the break already formed by design, as per Figure 3.4. Several repeats of each design were included within the photomask. The low resolution of the photomasks used resulted in all membranes containing wide breaks. This occurred in spite of the understanding that the ink spot size of the printing method of

Phillips Digital should result in a very slight overlap of the two membrane flaps. As a result of the breaches in continuity no initial seal was possible.

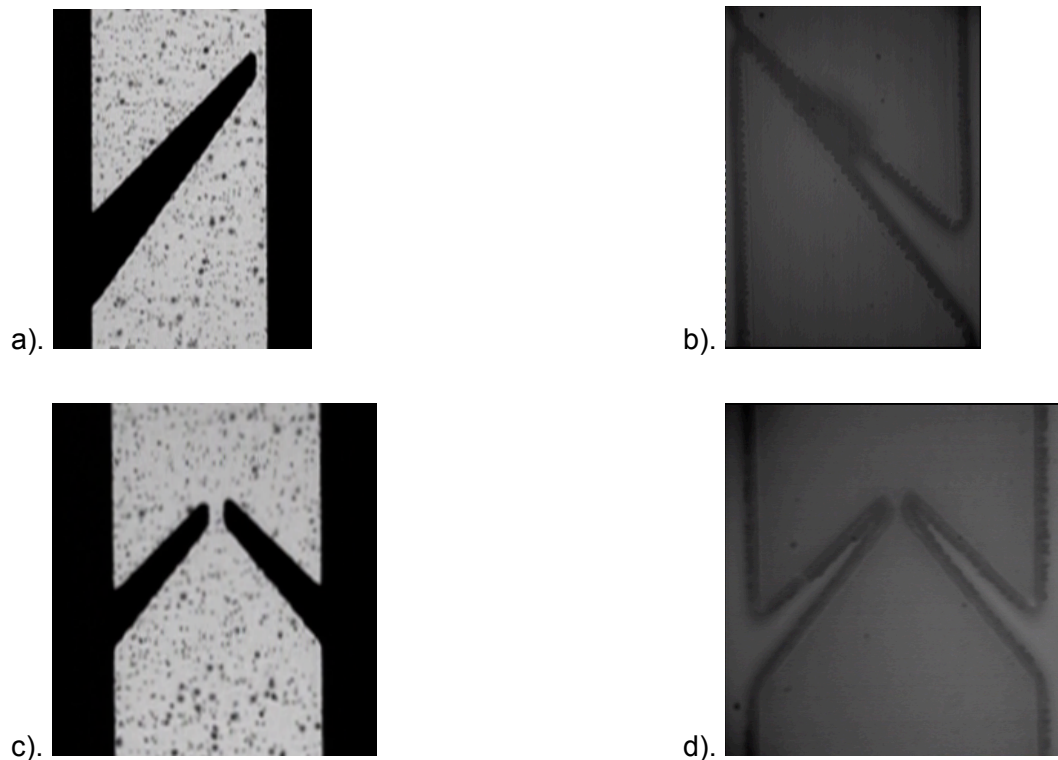


Figure 3.4 : Design of Burst valve membranes incorporating structured breaks. a). and b). Design 7.1.c photomask and mould respectively and c). and d). Design 7.2.b photomask and mould.

It is believed that the high valve seal initial burst pressure results from the re-bonding of the cut in the membrane. The bonding of PDMS to another substrate is believed to occur, as shown in Figure 3.4, via the formation of ozone from oxygen and the subsequent UV driven reaction of ozone with the surface of PDMS. No information regarding the UV opacity of the PE tape, initially used to mask the membrane, was available. Diffusion of the ozone around the PE tape to the surface of PDMS would create the correct conditions for bonding of the surface layer of the PDMS membrane and is currently believed to be the most likely explanation

No advancement had been made in the development of Burst valves despite a significant investment of time. Check valves were therefore considered as a replacement passive valve design.

3.3. Check Valves

Check valves operate by using two aligned pieces of structured PDMS to form the valve seat and the valve seal, also called the valve membrane. Both pieces have the same channel depth and width. However the piece forming the valve inlet is thicker, with the body of the PDMS thus forming the valve seat. The structured PDMS forming the outlet is thinner, with the PDMS being cast to a specific thickness, and operates as the valve seal. The basic structure is shown in Figure 3.5 a).

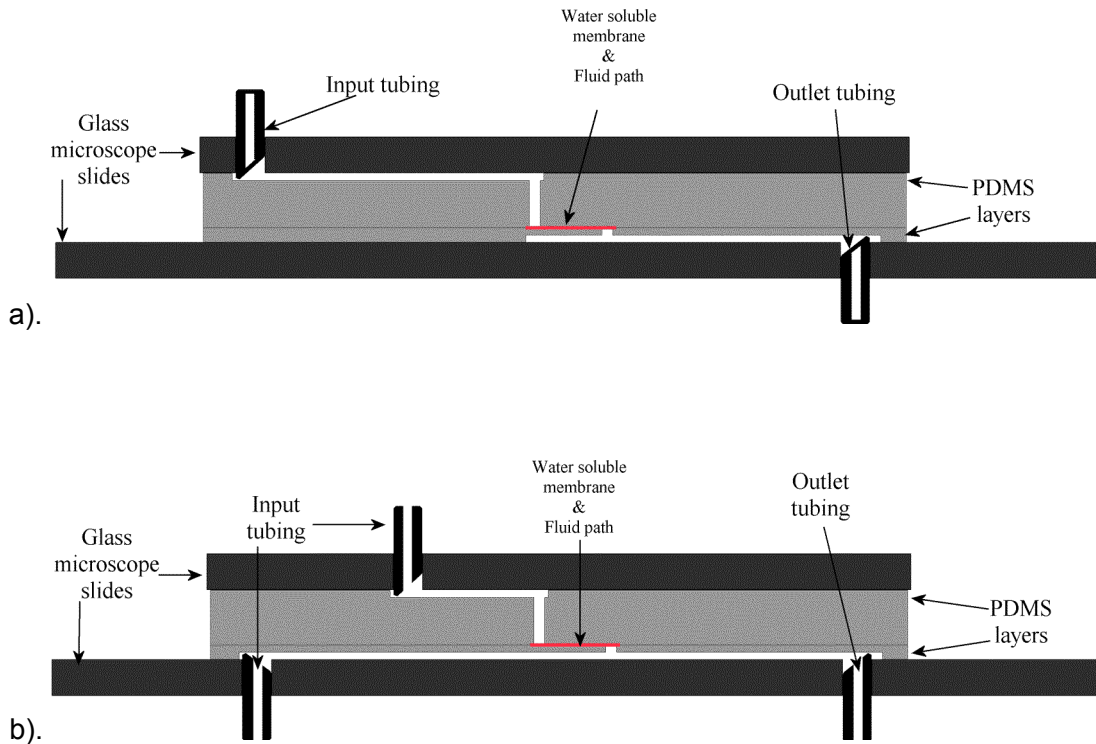


Figure 3.5 : Schematic of devices manufactured from a). Design 7.4 (for initial testing of check valve design) and b). Design 8.1 (for testing injection of one fluid into another, as would occur using intended vapour collection method). The fluid path between the valve seat and the valve membrane is initially held open by the water soluble membrane. The valve closes after the water soluble membrane is removed by flushing the device with water (see below).

The Check valve, despite being more intricate and requiring more precise alignment, was potentially a better design than the Burst valves. Masking of the valve membrane and seat with PE tape was more likely to be effective, the valve could be post-integrated into other fluidic designs and the flow resistance of the valves could be changed more easily. As the surface to be masked was flat and the diffusion distance of O_3 into the PDMS would therefore be less, parasitic bonding of the masked surface should logically be less likely.

Incorporating Check valves within previously designed microfluidic structures is possible. Re-casting the main microfluidic structure to a controlled thickness and drilling a hole at the desired fluid input results in the Check valve membrane layer. Bonding a predrilled piece of

structured PDMS to the main structure, as per the methodology in Appendix 1, results in a complete flow path from the input, via the valve and through the fluid structure of the main microfluidic layer. Finally, changing the flow resistance and opening pressure in Burst valves requires redesign of the microfluidic structure. In contrast, varying the casting thickness and inter-hole distance of Check valves, rather than the original structure provides similar effect.

It should be noted that following cessation of research into Check valves an article incorporating similar structures into fluid structures was discovered [117]. Further discussion follows the examination of issues associated with the journal article towards the end of Section 3.3.1.

3.3.1. Experimental, Results and Discussion

Original Check valve assembly methods were refined several times before the final, tested, devices were manufactured. Techniques of hole formation and masking the valve seat and valve membrane were changed and various thicknesses of valve seal were tried. These refinements are described below.

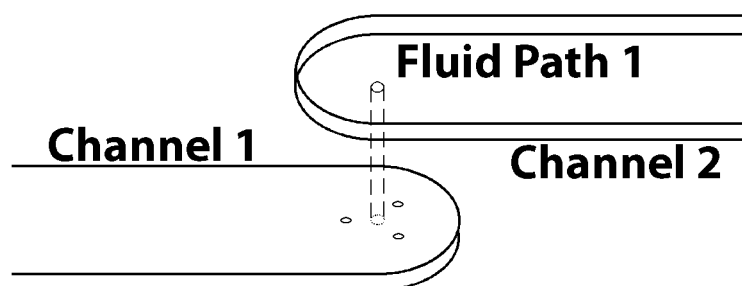


Figure 3.6 : Expanded schematic of the original proposed Check valve. In the forward direction, fluid would flow along channel 2, down the fluid path 1, through the three holes and along channel 1. Fluid flowing in the reverse direction flows along channel 1, up the 3 holes and is then blocked by the body of the substrate containing fluid path 1 and channel 2.

Initial design and assembly ideas, as shown in Figure 3.6, had a central hole in the valve seat feeding fluid to three surrounding holes in the valve membrane. This was only possible to achieve if the valve membrane holes were created by fine pins. Unfortunately these bonded closed in all attempts. The valve seat hole to valve membrane hole arrangement was therefore changed to that shown in Figure 3.5. Holes were thereafter drilled using a 300 μ m diameter spiral drill, the smallest, supplied by LPKF Laser and Electronics, mechanically robust enough to be used with PDMS.

Various methods were used to try and prevent the valve seat and membrane bonding. Despite theory indicating masking of only one valve surface was necessary, both were masked to ensure any bonding was definitely a failure of the masking method. Both PE and PDMS were assessed as masking materials. Neither material was effective, as detailed later. Following detailed testing of both masking materials, membrane thicknesses and hole arrangements, alternative methods to prevent valve surfaces bonding were deemed necessary. Sacrificial membranes (used to mask a selected region, before dissolving under liquid flow), placed between the valve surfaces before permanent bonding, were subsequently tested as described in the next paragraph. The resulting valves ultimately demonstrated low bursting pressures and repeatable (to within 500 Pa) behaviour.

Removable, contiguous masking layers applied prior to UV/ O₃ treatment did not, as previously stated in Section 3.2.1, prevent the valve seat and membrane permanently bonding. As previously stated, two wavelengths of UV are required to modify the PDMS surface to allow it to bond (see Figure 2.4). While PE and PDMS are relatively transparent to UV at 254 nm (emitted by the UV/ozone lamp), neither are transparent at 185 nm (also emitted by the UV/ozone lamp). Therefore O₃ cannot form in situ from oxygen present within the PDMS. Thirty seconds (UV treatment time) is also insufficient time for O₃ to diffuse around the masking layer and into the bulk PDMS. Accordingly it would seem that parasitic bonding is doubly unlikely. No explanation has therefore been forthcoming regarding the parasitic bonding.

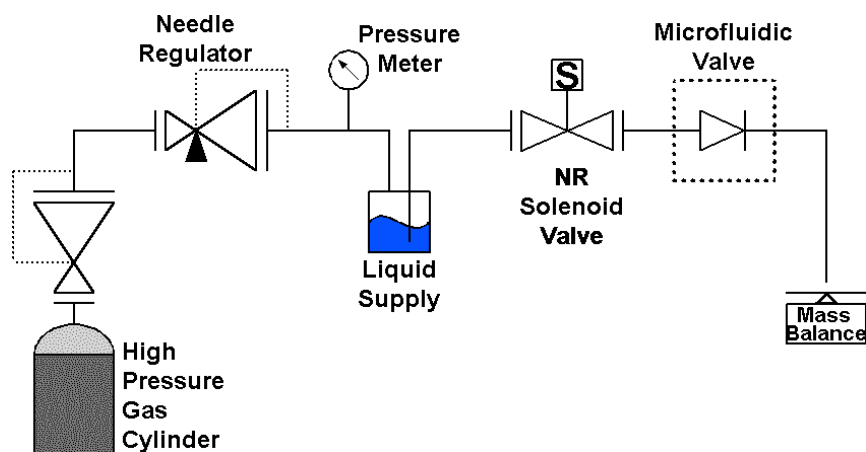


Figure 3.7 : Schematic of the set-up for testing Check valve design 7.4.

During testing to determine if parasitic bonding had occurred, one Check valve device burst. Believed to be due to tearing of the valve membrane, it occurred at a pressure of approximately 180 kPa after slowly increasing the liquid pressure. Despite the burst method not being truly an opening of the valve, the decision was made to pursue the full testing regime to gain insight into valve behaviour. Therefore following bursting the valve flow rate test arrangement, shown in Figure 3.7, was filled with degassed, de-ionised water. The flow

rate as a function of pressure was then measured as pressure was increased steadily and then as the pressure was decreased to ensure the valves behaved regularly. After reversing the direction of flow through the valve, the measurement was repeated to determine the unidirectional nature of the valve. Flow rate was determined using a program custom written in Labview (Austin, USA) that reads data from a mass balance (Sartorius AG, Goettingen, Germany).

The device behaved as expected, as shown in Figure 3.8. Of particular note is the hysteresis pressure shown upon opening, but not closing of the valve. Despite tearing of the valve membrane effectively rendering the valve bidirectional, the design still requires a much greater pressure to open in the reverse direction and has lower flow rates than those shown when operating in the forward direction. This result indicated that the valve operated as expected and, provided the device could be manufactured with an unbonded valve membrane, was capable of being utilised within microfluidic devices at much lower pressures. Therefore effort was continued into manufacturing Check valves with valve membranes unbonded to valve seats.

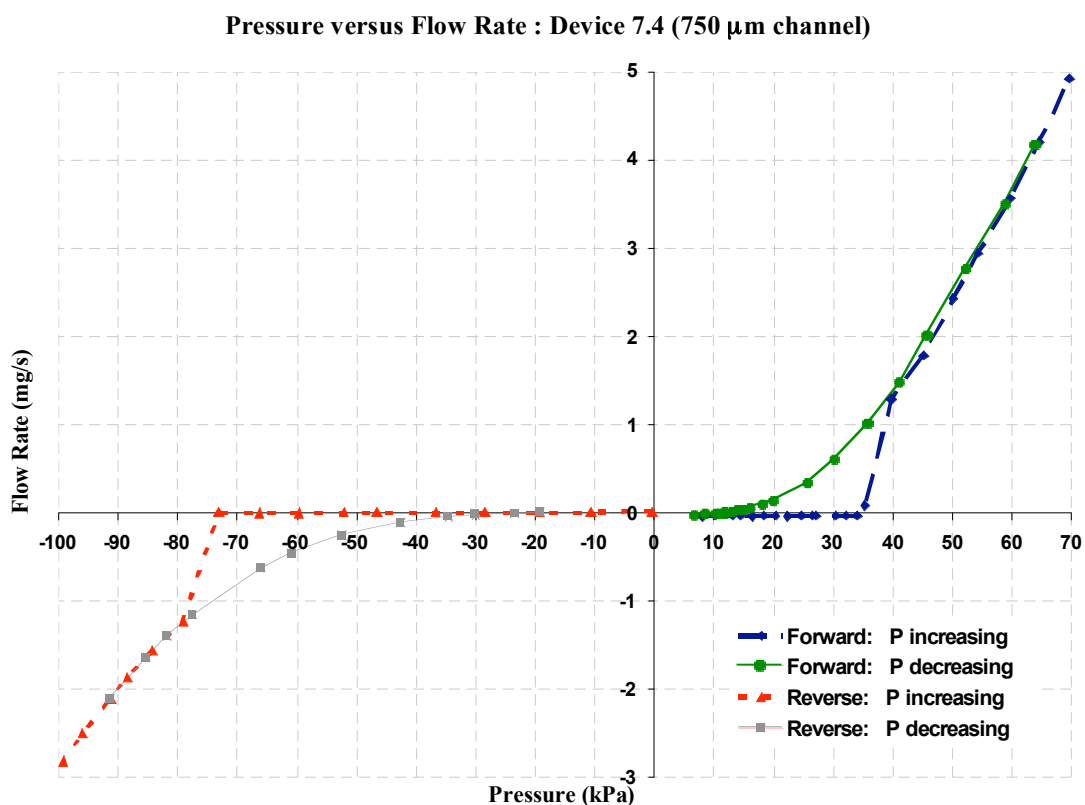


Figure 3.8 : Plot of the pressure vs flow rate for a check valve on device 7.4. Assembled using PDMS as the masking membrane. Valve seal thickness = 225 μm , Inter-hole distance = 1.54 mm.

Two different materials were tested for use as sacrificial layers to prevent bonding of the valve seat and valve membrane. These were polyvinyl pyrrolidone (PVP) and Wrigley's. A

droplet of PVP, a water soluble polymer, solution, was applied to a controlled area of the valve seal and membrane, then allowed to dry, forming one test sacrificial layer. The PVP solution consisted of 350 mg of PVP dissolved in 10 mL of deionised water. A piece of Wrigley's, cut to approximately 80% of the channel width and to the inter-hole distance, measured from hole centre to hole centre, formed a second sacrificial layer to test on another device. Wrigley's was placed on the valve seal following treatment under UV/O₃ and before placement of the valve membrane. Both soluble materials dissolved upon flowing water through the device, however an undissolved Section of the PVP layer remained along the edges of the water flow path. Wrigley's demonstrated similar behaviour, although to a lesser and more reproducible extent, and was therefore selected as the preferred sacrificial material for check valve fabrication.

Check valves, of Design 7.4, and fabricated using Wrigley's, were tested in a similar manner to that previously performed on the PDMS masked check valves. Similar plots were obtained, however the bursting pressure, forward hysteresis and reverse hysteresis pressure were much lower, at 20.5 kPa, 5 kPa and 10.5 kPa respectively for the 500 μm wide channel. This indicated that the valve membrane opened without tearing. Design 7.4 Check Valves were repeatably fabricated and continued to show low hysteresis pressure. Design 8.1, an extension of Design 7.4 incorporating a Check Valve onto a pre-existing fluid channel (compare Figure 3.5.b with Figure 3.5.a) was therefore used for further testing.

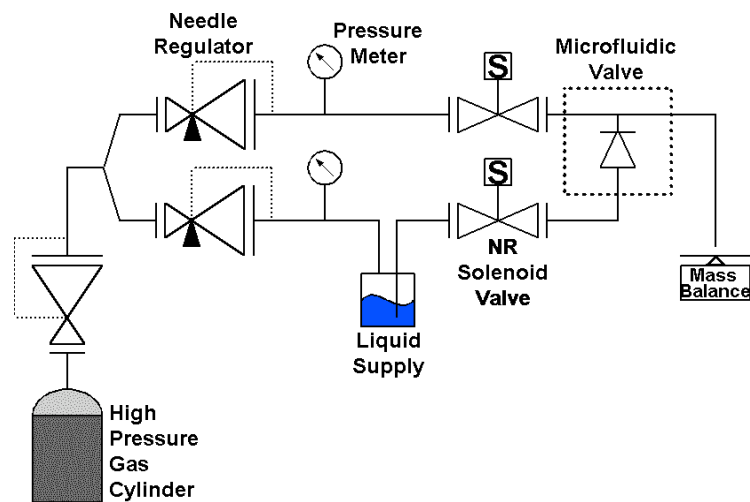


Figure 3.9 : Schematic of the set-up for the original testing of Check valve Design 8.1.

Several moulds and castings were made before the correct dimensions and assembly techniques were determined for the manufacture of Design 8.1 Check Valves. Dimensions and some measured test parameters of the final device used for testing are shown in Table 3.2. Hysteresis pressure, valve opening times and the behaviour of Design 8.1 Check

Valves under an applied closing pressure were all measured. However hysteresis pressure was the only definable quantity, as will be explained later.

Channel Height		260 μm
Membrane Thickness		240 μm
Inter-Hole Distance –	500 μm	0.727 mm
	1 mm	0.725 mm
	2 mm	0.911 mm
Hysteresis Pressures -	500 μm	415 Pa
	1 mm	500 Pa
	2 mm	≈ 260 Pa

Table 3.2 : Dimensions and some measured test parameters of Design 8.1 Check Valves.

The graphs, of hysteresis pressure and flow rate as a function of applied pressure, of Design 8.1 Check Valves (Figure 3.10) were obtained in a similar manner to that previously used for both tested Check valve devices. No burst pressure was measured for any of the valves tested as no initial parasitic seal, between the valve seat and membrane, formed. Prior to all measurements the secondary flow channel and the waste channel was filled with water. Valve 3 was then closed and the measurements proceeded as for Design 7.4.

Pressure versus Flow Rate : Device 8.1

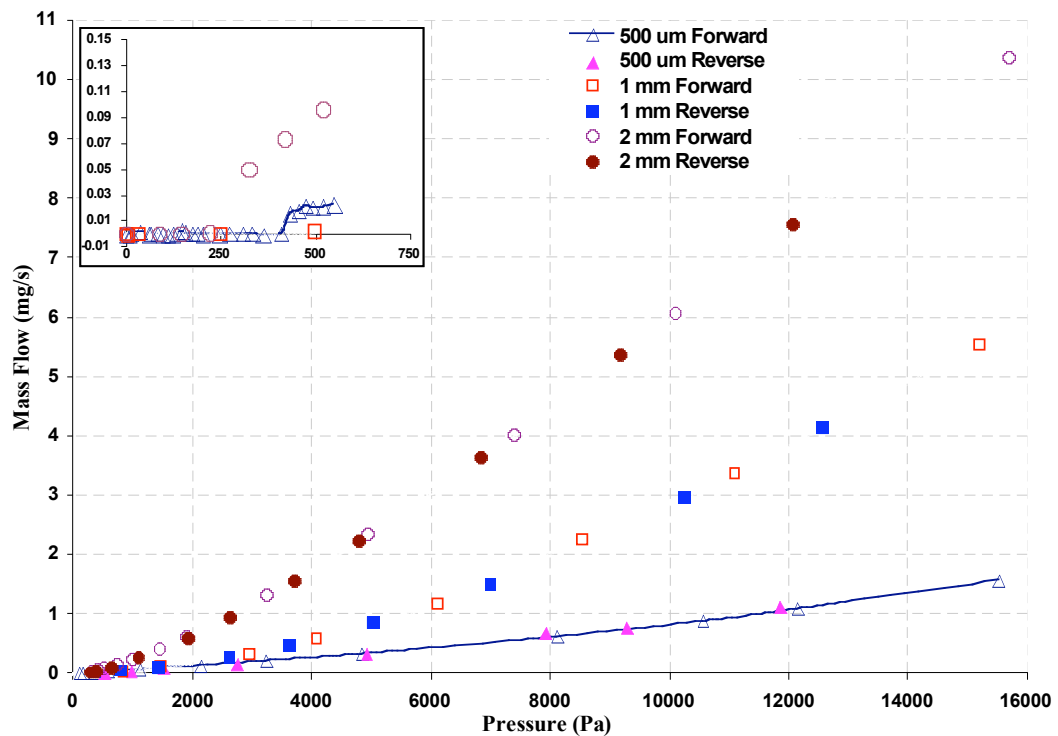


Figure 3.10 : Plot of pressure vs flow rate for all Check valves on Design 8.1 Check Valve. Inset plot shows close-up of the valve opening pressures.

Attempts were made to measure the opening and closing actuation times, of Design 8.1 Check valves, under two different conditions. Both conditions involved actuating the Check valve for predetermined periods of time, by opening and closing NR Valve 1 (Figure 3.11) to which a set pressure was applied. NR pinch valves (operated by applying pressure orthogonally to special silicone tubing through which the fluid flows) were used rather than the original NR valves possessing an internal volume (see Figure 3.1) to prevent the opening of the NR valves providing a pressure pulse to the Check valve being tested. Each relaxation time, when NR valve 1 is closed, followed by an actuation time, when NR valve 1 is open, is referred to as a cycle. The first test condition, referred to as the ‘basic’ condition (Figure 3.11 a.), was performed as per the initial flow rate versus pressure tests. The second test condition, the ‘advanced’ condition (Figure 3.11 b.), differed from the first by flowing water through the secondary flow channel at a set pressure and using pressurised air as the Check valve test fluid.

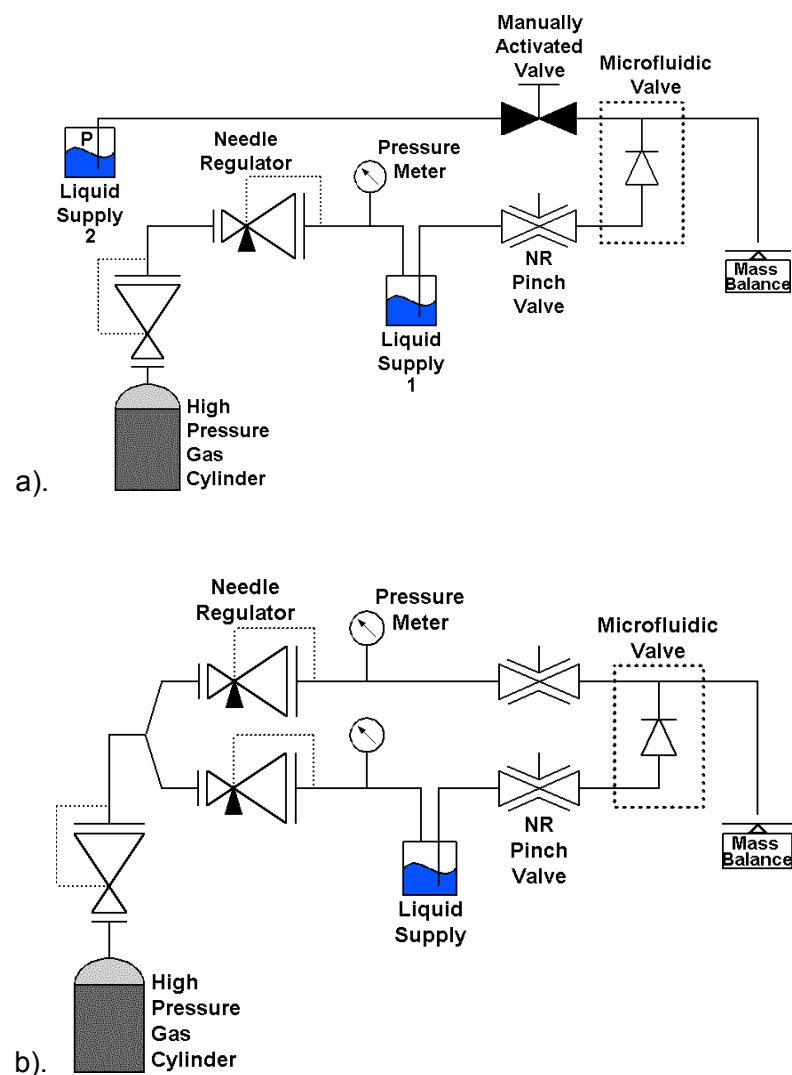


Figure 3.11 : a). Basic and b). Advanced test conditions for Check valve Design 8.1. The manually actuated valve in the basic test condition is open initially to allow the systems to fill with liquid, but closed during the experiments.

Basic condition tests were performed to determine the ability of the valve to close against a fluid present in the space between the valve seat and valve seal. Figure 3.12 is a plot of the liquid volume flowing through the 500 μm wide channel on device 8.1 with cycles of 20 s and 500 ms (relaxation and actuation time respectively). Measurements of the Check valve behaviour under varying cycle timings and a number of pressures demonstrated that a much higher pressure, than the hysteresis pressure, was required to open the valve when a pressure ‘pulse’ was applied. The valve behaviour was also observed to be unreliable under the conditions tested.

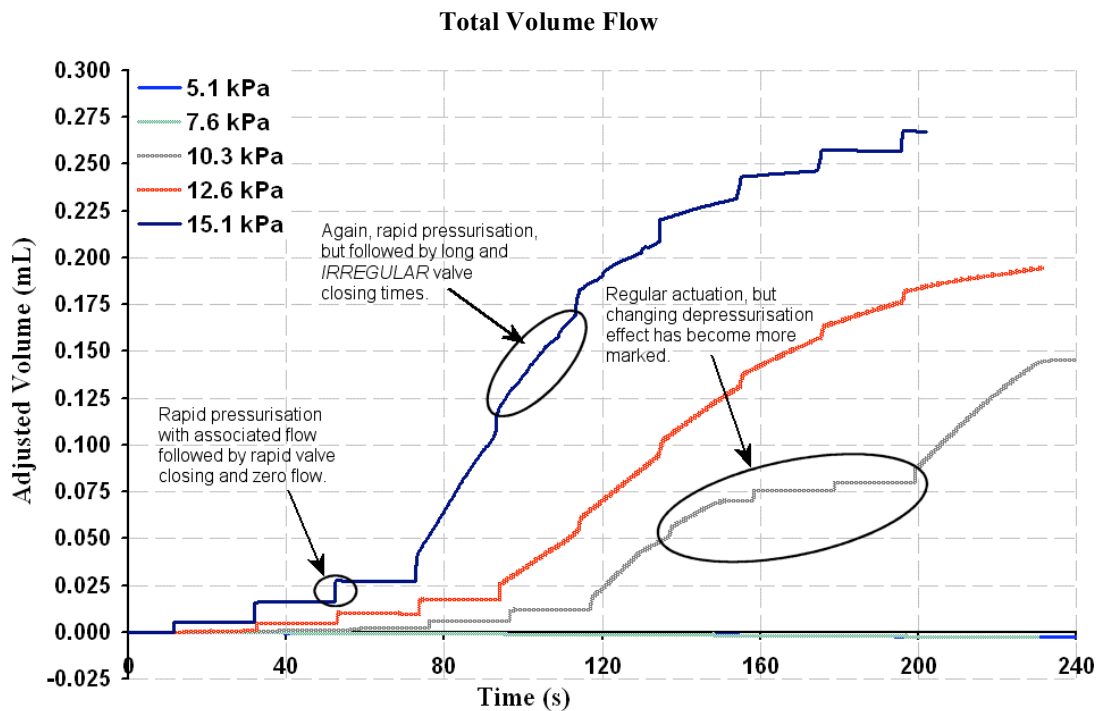


Figure 3.12 : Plot of Volume (Adjusted from the measured mass) vs Time for the 500 μm wide channel. Pressure is applied for 500 ms (actuation time) with a following 20 s pressure dump (relaxation time). That is, a cycle time of 20.5 seconds.

The PDMS membrane flexibility is believed to be partly responsible for both behaviours. Stiction between the valve seat and membrane combined with the high flexibility of thin PDMS membranes are believed to be responsible for the higher opening pressures. A low shear modulus also implies that recovery of the membrane is slower if any fluid is present between the membrane and valve seat. The pressure exerted by recovering PDMS decreases as the strain decreases. Therefore as the volume of liquid contained between the membrane and valve seat decreases, the pressure does likewise. This effect is demonstrated in Figure 3.13 by observation of the flow rate, in which the check valve remained open, decreasing within each cycle.

Volume Flow per Cycle : Device 8.1 (500 μm channel)

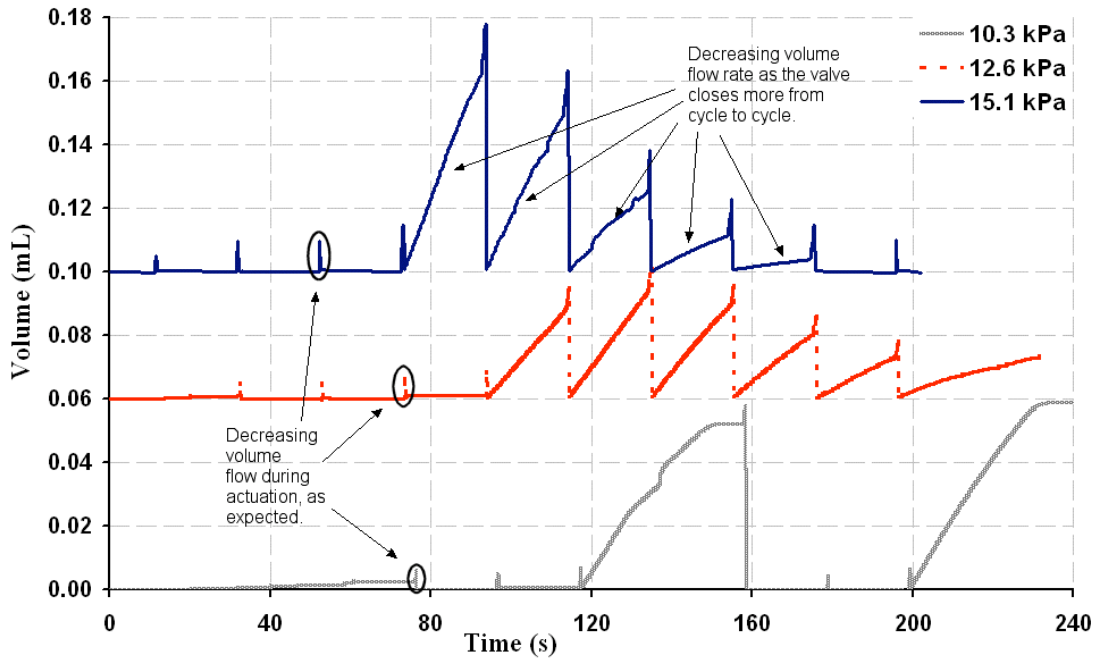


Figure 3.13 : As per plot 3.11, adjusted to illustrate the volume flow per cycle.

As a result of the irregular behaviour exhibited by Device 8.1, as shown in Figure 3.13, the ‘advanced’ test condition was adopted. By applying pressure to the membrane, via the secondary channel (closing pressure), it was expected that there should be no decrease in the rate that the Check valve closed as the strain decreased. The Check valve should therefore close faster as the closing pressure increases or as the actuating pressure decreases. Figure 3.14, the open test condition equivalent plot to Figure 3.13, demonstrates that this did not occur and further, that no pattern was observed across the full range of closing or opening pressures. The datasets shown were taken from a series of experiments performed over a range of opening and closing pressures as presented in Table 3.3 (shown on page 52). Figure 3.15 presents the ideal volume flow per cycle to allow comparison to the plots in Figure 3.14. The dataset used to produce Figure 3.15 was manufactured by taking the data representing a single cycle from each of the datasets presented in Figure 3.14. This data was chosen based upon the expected variation in flow rate and resulting from the two different applied pressures. It was then replicated multiple times to represent a series of cycles.

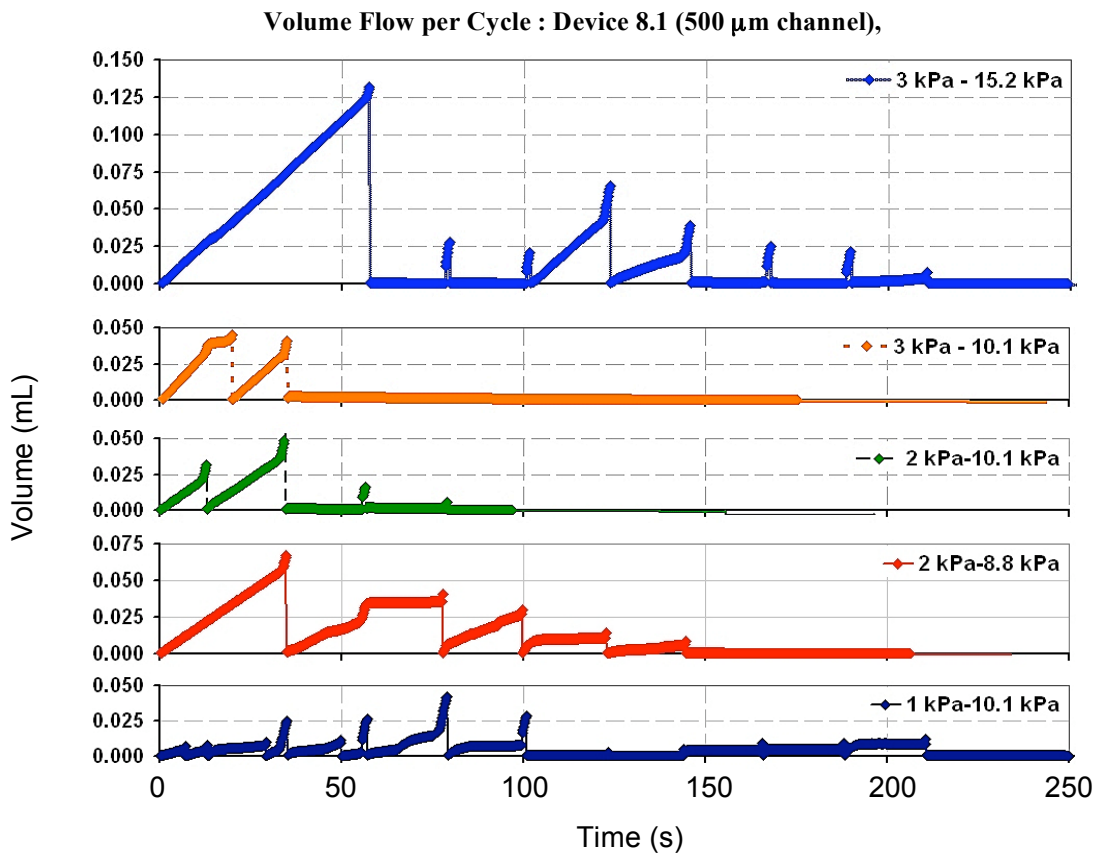


Figure 3.14 : The first pressure shown on each plot is the closing pressure, while the second pressure shown is the opening pressure.

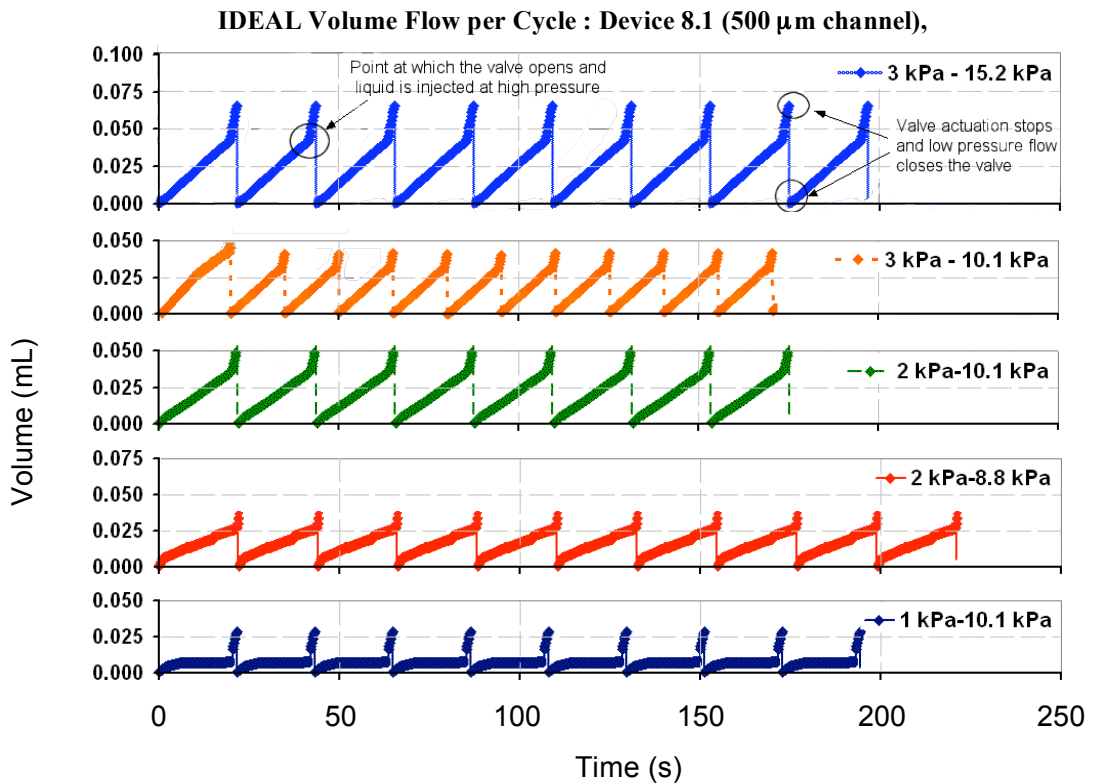


Figure 3.15 : Ideal plot of volume flow per cycle for each of the above plots. Created using manufactured data to allow comparison to the plots of experimental data shown in Figure 3.14. Designed to accommodate not only the ideal plot shape, but also the change due to changing pressures.

Several test system conditions were proposed to characterise the behaviour of the Check valve. Two major problems, other than the lack of a closing, or opening for that matter, pressure trend being exhibited are observed.

Valve 2 - Cycle	Open	2 s
"	Closed	20 s
Valve 3	Open	
Closing Pressure	Opening Pressure	
1 kPa	5148 Pa	
"	7623 Pa	
"	10138 Pa	
2 kPa	8788 Pa	
"	10138 Pa	
3 kPa	10138 Pa	
"	15207 Pa	

Table 3.3 : Check Valve 8.1 'Open' test experimental conditions.

The Check valve did not always open when the actuating pressure was applied, although as expected the valve did close quickly when NR valve 1 closed.

The liquid flow through the secondary channel did not recommence in all cases when the Check valve closed. Unlike the 'basic' test condition, the 'advanced' tests result in a series of gas bubbles and liquid droplets being present in the waste tube.

As detailed in Section 5.2.1, even microscopic irregularities in the channel or tube walls can lead to pressure differences between the leading and trailing menisci of each droplet. The pressure differences are additive and the resulting back pressure is believed to be sufficient to prevent fluid flow through either the Check valve or secondary channel. The irregularity in valve behaviour can therefore be explained by the variability in back pressure. Further detail on the effects of multiple menisci, back pressure and the 'spring constant' effect of having many bubbles in a single channel are examined in greater detail in Chapter 5.

From this work we concluded that the variable back pressure, produced within the waste tube, always induces irregular behaviour in passive valves. Given that potentially integratable active valves were available (within the group), further development of, or investigation into, Check valves was therefore stopped pending investigation of active valves. Whilst Check valve research consumed considerable time, substantial insight into testing and fabrication was nonetheless gained.

Addendum : As previously noted, passive valves operating under the same principles as the Check valves developed here are demonstrated in an article by Jeon, Chiu, et al [117]. Despite their acknowledged success in developing passive valves that operate reproducibly, several observations regarding the article must be made. The most obvious issue is the lack of any masking or anti-bonding treatment to the valve membrane to prevent it bonding to the valve seat. This was the most problematic aspect of developing the Check valves described in this thesis and it is not discussed by the authors. Their passive valves are also only operating with a contiguous liquid supply running throughout the device. This prevents the back pressure problems encountered when attempting to test the valves with gas and liquid as would have been required for future devices in this project. It is therefore felt that the reported valves would show no greater capability under the conditions required for a microfluidic device containing gas and liquid than the Check valves developed and tested above.

3.4. Seal Valves

Actuation methods, in active microvalves, range from pneumatic [116], piezoelectric [118] and electromechanical to the more esoteric laser activated hydrogel [119], magnetohydrodynamic and ferrofluidic [120] approaches. Passive valves, being categorised instead by the basic design, comprise flap [114], check [117] and piston valves [115]. The majority of active and passive microvalves were originally produced using silicon and glass as substrates. Silicon or glass microvalves are not able to be integrated as readily and of the remaining valves, described in the literature, few are able to block gas as well as liquid flow or provide the reproducibility of action necessary to yield regular gas/liquid segments. As a result polymer based systems are becoming more common.

An active, gas impermeable, Seal valve integrated within a PDMS microfluidic structure has been recently developed by the University of Hertfordshire (UH) [118] group. However modification of the original design was necessary to demonstrate the possibility of reducing the dimensions of the fluid flow path from the valve seal to the gas/liquid junction. The original rationale behind developing integrated valves were to remove the original NR valve from directly controlling the fluid flow into the gas/liquid junction and to reduce the compressible volume of gas between the gas/liquid junction and the gas control valve. Reducing the volume between the gas valve and the gas/liquid junction increases the rate of pressure rise against which liquid, flowing into the gas supply channel from the junction, must push (see Section 5.2). A unidirectional passive valve does so by preventing the gas on the reverse side of the valve being compressed, however an active valve is capable of acting as the gas control valve. *Therefore reducing the compressible volume of gas requires the channel connecting the valve and the gas/liquid junction to be as short and narrow as possible.*

The original valves developed by Tan, Tracey, et al [118, 121] were constructed with a PDMS body and a glass microscope slide base. This restricted the channel diameter to a minimum of 750 μm (the minimum diameter hole drillable in glass using readily available technology). Modelling of the valve sealing behaviour (unpublished data provided by J. B. Davis (2005)) indicated that the PDMS walls of the Seal valve's through via required support from the base to operate at full potential. Therefore reduction of the via diameter (see Figure 3.16) and subsequently the compressible volume of gas, required a different base substrate. An advantageous consequence of reducing the via diameter is the potential to reduce the total internal volume of the valve. The original Seal valve design demonstrated by Tan, Tracey, et al [118] was therefore further developed and tested.

3.4.1. Experimental, Results and Discussion

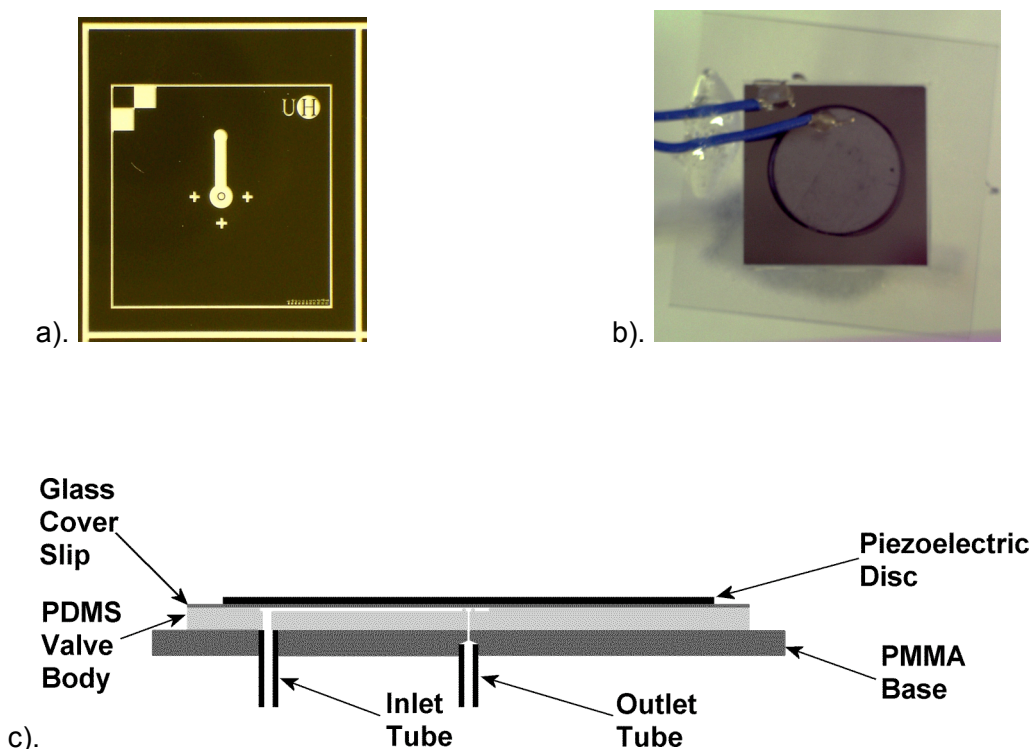


Figure 3.16 : a). Photomask used to produce the microstructured PDMS seal valve, b). Photograph, and c). schematic of the assembled Seal valve.

Seal valve assembly is described in detail in Appendix 1.4.4. However specific mention must be made of the use of SiO_2 coated PMMA as the Seal valve base.

PMMA was selected as an alternative to glass microscope slides for the base material of the Seal valves. Previous tests had indicated that $300\ \mu\text{m}$ holes could be drilled reproducibly in PMMA, compared to about $900\ \mu\text{m}$ for holes drilled in glass. This combined with the ready availability of flat pieces, the ability to accurately cut uniform sized pieces and its relative durability made it a promising choice. A company (Spectrum Coatings Ltd, Manchester, UK) with the ability to evaporatively coat PMMA with a $100\ \text{nm}$ SiO_2 layer was identified. Given that PDMS irreversibly bonds to the SiO_2 coating following UV/O_3 treatment, this opened the way to the adoption of PMMA as an alternative base substrate for PDMS devices.

Initial assembly of the Seal valves did not include placing a water soluble spacer over the valve seat. No flow was recorded through the first Seal valve despite pressures of up to $150\ \text{kPa}$ being applied. Following a method adopted for the same problem in the assembly of Check valves, introducing a water soluble spacer during manufacture, fluid flow was possible without pressure being applied. This (pleasingly) justifies the previous experiments with soluble spacers.

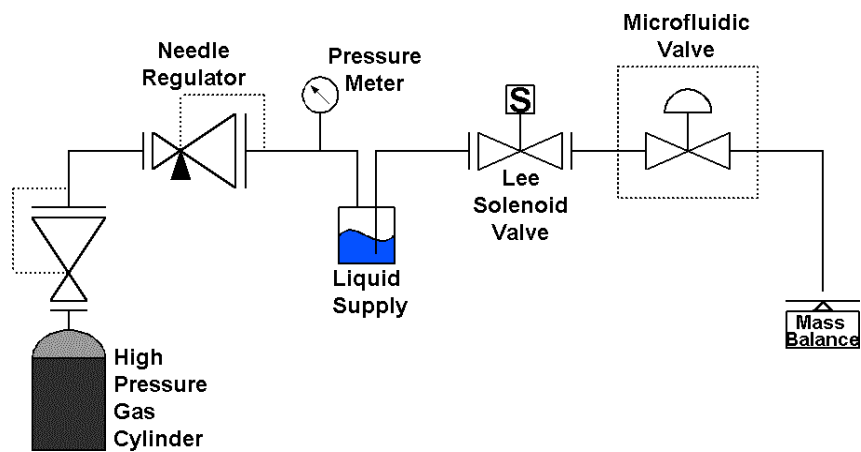


Figure 3.17 : Schematic of Seal valve test set-up.

Tests of the flow rate of water through the Seal valve as a function of the voltage applied to the piezoelectric bimorph and the observation of complete sealing of the valve against gas were made. However following the sealing of the valve membrane against the valve seat a concerted effort was required to achieve fluid flow again. It was necessary to apply a reverse pressure to force the valve open. Adhesion via stiction of the valve seat to the glass cover slip forming the valve membrane is believed to occur when the valve is closed. The diameter of the valve chamber prevents the piezoelectric bimorph from generating sufficient flexure to overcome the adhesive forces of the valve seat to the valve membrane.

Given sufficient time a number of methods of patterning the top surface of the valve seat were proposed that would have prevented the valve seat sealing to the membrane without compromising the sealing ability of the Seal valve. Unfortunately it was judged that further protracted development of integrated valving would adversely affect the research into developing an efficient vapour collection method which was seen as the heart of this work.

Additional research into the Seal valves was therefore halted and the decision made to continue using external active valves to control the gas and liquid flow into the gas collection devices. Lee valves (The Lee Company, CT, USA) were believed to be sufficiently small and the fluid path connecting the valve seat to the microfluidic device short enough to allow them to operate as effectively as Seal valves may have with further development.

4. INTRODUCTION TO VAPOUR COLLECTION

As discussed in Section 1.3.1, efficient collection of vapour and representative sampling of a carrier gas flow are fundamental problems for analytical chemists. Low concentration vapour collection using sorbents is efficient and, in the case of VOCs, has been found to be more reproducible than the primary alternative, the canister method [122]. Solid sorbent methods are reviewed first, followed by liquid sorbent in which the vapour and liquid are in direct contact.

4.1. Diffusion

Whilst a microfluidic vapour analysis system does not necessarily require a *microfluidic* vapour collection module, there are solid grounds for its development and inclusion. Efficient and rapid collection of vapour molecules requires fast diffusion of vapour molecules to the surface of and subsequent rapid diffusion into and through the sorbent. The small channel sizes found in microfluidic devices intrinsically implies that diffusion distances are small and therefore diffusion to the sorbent surface is rapid. Short diffusion times through the full thickness of the sorbent are best achieved again by either decreasing the physical depth of the sorbent or the type of sorbent used. Thin membranes, either coated onto the surface of channels or acting as a barrier through which molecules must pass, are common within microfluidics. Finally, as vapour phase diffusion is much more rapid than liquid or solid phase diffusion, the rate of diffusion into the sorbent is determined by the speed of diffusion of the vapour through the sorbent.

Harper [123] reviews 11 representative solid sorbents used in active VOC samplers. Many of the sorbents were originally used in gas-solid chromatography. While gas-liquid chromatography (GC) is more common, Harper states that the solid coatings used in gas-solid chromatography “showed greater adsorptive capacity.” The majority of the substrates are micro-porous and function by trapping vapour molecules within the pores. Many of the vapours exhibit rapid diffusion into, and subsequent removal from, sorbents. However if the chemical or physical properties of the sampled VOC change markedly, the sorbent must be changed due to the fixed size of the micropores for a specific sorbent. Therefore the use of such solid sorbents restricts the use of a vapour collection module to the collection of a limited range of vapours.

Current GC stationary phases are excellent replacements, for the solid sorbents mentioned by Harper [123] and Wang and Austin [122], for use in collecting low concentration VOCs in air. They are able to dissolve a wide range of VOCs and, as the VOC concentration is low, adsorptive capacity is invalidated as an argument against their use. Gas-liquid

chromatography stationary phases are frequently, despite what the name implies, solid polymers and are therefore capable of being formed into thin membranes.

GC stationary phases exhibit liquid like behaviour and can therefore be described using diffusion and equilibrium equations for gasses and liquid. The movement of vapour molecules within and between the carrier gas and sorbent are difficult to explain using the basic diffusion theory covered in Chapter 1. Fick's First Law of Diffusion (Equation 6, Section 1.2.1), previously stated to define diffusion through a carrier gas, only does so, if the *average* concentration of the diffusing species is time invariant.

As the vapour is diffusing into the sorbent, Fick's First Law is applicable only once equilibrium has been reached between the vapour concentration in the gas phase and that dissolved within the sorbent. The equilibrium ratio between the concentration of vapour dissolved in the sorbent and the gas phase concentration is known as Henry's constant. As defined by Henry's Law (Equation 8) :

$$K_H = C_a / p_a \quad \text{Equation 8}$$

where K_H is Henry's constant (M/atm), C_a and p_a are the aqueous concentration (mol/L or M) and partial pressure in air (atm) respectively of the VOC, applies equally to liquids and the solids in question.

Diffusion of vapour molecules through the carrier gas and through the sorbent are governed by Fick's Second Law (Equation 7, Section 1.2.1). Whilst the vapour concentration is initially assumed to be constant throughout the carrier gas, as the vapour diffuses into the sorbent the concentration decreases in the region of the sorbent surface. A local concentration gradient is therefore formed, 'down' which the vapour molecules diffuse. The concentration difference is initiated in the sorbent as the vapour molecules diffuse into the exposed sorbent surface and again 'down' the concentration gradient towards the other sorbent surface. The integrated solution to Fick's second law is shown (Equation 9), assuming the physical model of a channel surface coated with a sorbent (Figure 4.1) [124].

$$\frac{C}{C_0} = 1 - \frac{4}{\pi} \cdot \sum_{n=0}^{\infty} \left(\frac{(-1)^n}{2n+1} \cdot \cos\left(\frac{(2n+1)\pi}{2} \cdot \frac{x}{d}\right) \cdot \exp\left(-\frac{(2n+1)^2 \pi^2}{4} \cdot \frac{Dt}{d^2}\right) \right) \quad \text{Equation 9}$$

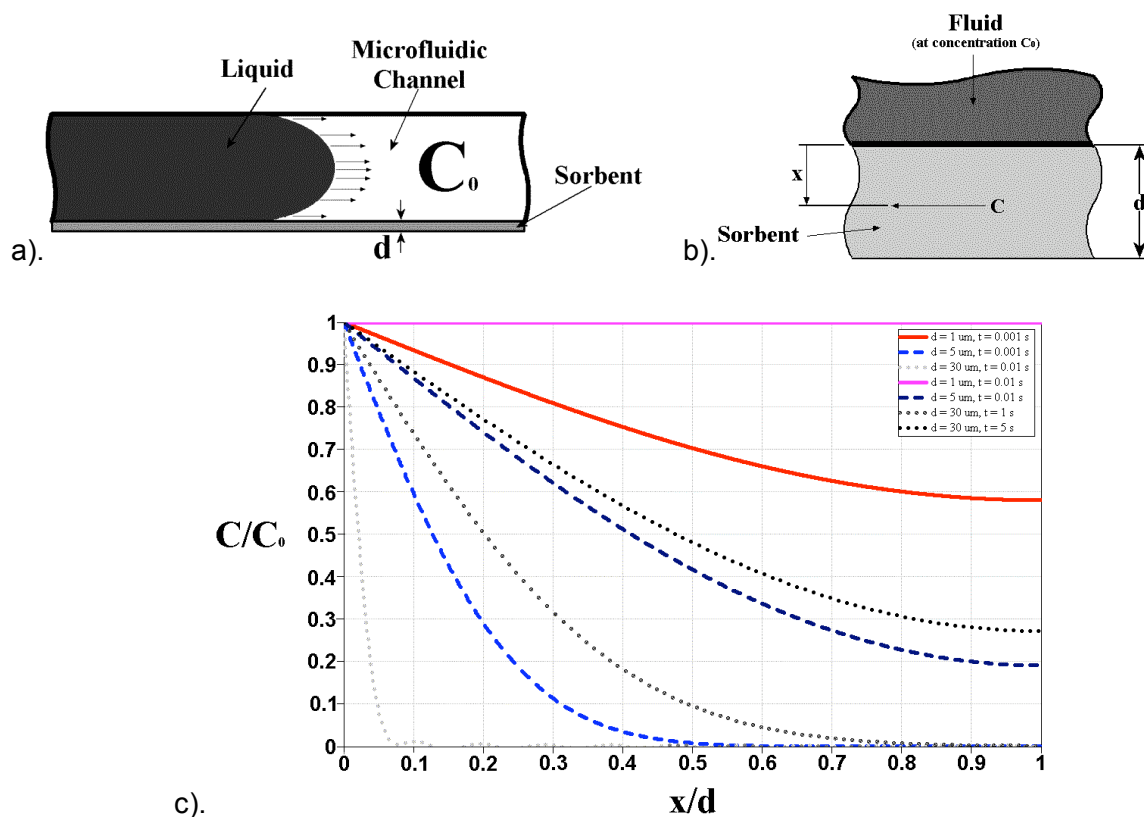


Figure 4.1 : a). and b). Physical model for the system upon which c). the plot of Equation 9 is based. The diffusion constant of the vapour/sorbent system, in this case ethanol / PDMS, is $4.5 \times 10^{-10} \text{ m}^2 \text{ s}^{-1}$.

Equation 9 relates the concentration of vapour, relative to the gas stream concentration, in the sorbent to each relative depth within the sorbent [124]. As shown by plotting Equation 9 (Figure 4.1 c), increasing the sorbent thickness from $5 \mu\text{m}$ to $30 \mu\text{m}$ increases the time for the relative vapour concentration to reach about 45 % at half the sorbent thickness, from 10 ms to 5 s.

Using microfluidic vapour collection devices with a sorbent having liquid-like adsorbing properties increases the rate of vapour collection and the collection efficiency. The following introductory sections introduce various microfluidic vapour collection methods, focussing on the use of direct gas/liquid contact and specifically segmented flow, and the experimental requirements introduced by the chosen analysis system. A logical progression from the experimental requirements and the properties of both membrane permeation and direct gas/liquid contact, vapour collection modules demonstrates the reasoning leading to the selection of the chosen vapour collection method.

4.2. Microfluidics

Several methods have been developed for collecting vapours and gases into liquids microfluidically (for example falling drop [125], segmented flow [126], counter current flow [127]). While all of the methods stated are not defined in the articles as being microfluidic, the volumes and channel dimensions used still permit the modules designed to be classified as microfluidic. Not all vapour collection methods used commercially or in standard vapour analysis instruments have microfluidic equivalents. However some methods have been developed specifically to take advantage of the flow regimes found in microfluidic devices. Microfluidic modules for the collection of gases or vapours have been developed for applications as diverse as gas analysis, organic and particle synthesis, and gas separation. Methods used for the collection of vapours are frequently used for the collection of gases as well, and vice versa, hence in this section no distinction is made between them.

4.2.1. Solid Sorbent Vapour Collection

Membrane permeation and direct gas to liquid contact have both been comprehensively investigated in two phase or multiphase microfluidic devices. Kovvali, Vemury, et al [128] classify membrane based extraction of vapour molecules into four different flow patterns, mixed, cross, cocurrent and countercurrent (Figure 4.2). Each of the patterns shown in Figure 4.2 is applicable to both micro- and meso-fluidic channel sizes. Direct gas/liquid contact vapour collection in contrast has frequently been developed to operate under the flow conditions found at microfluidic dimensions.

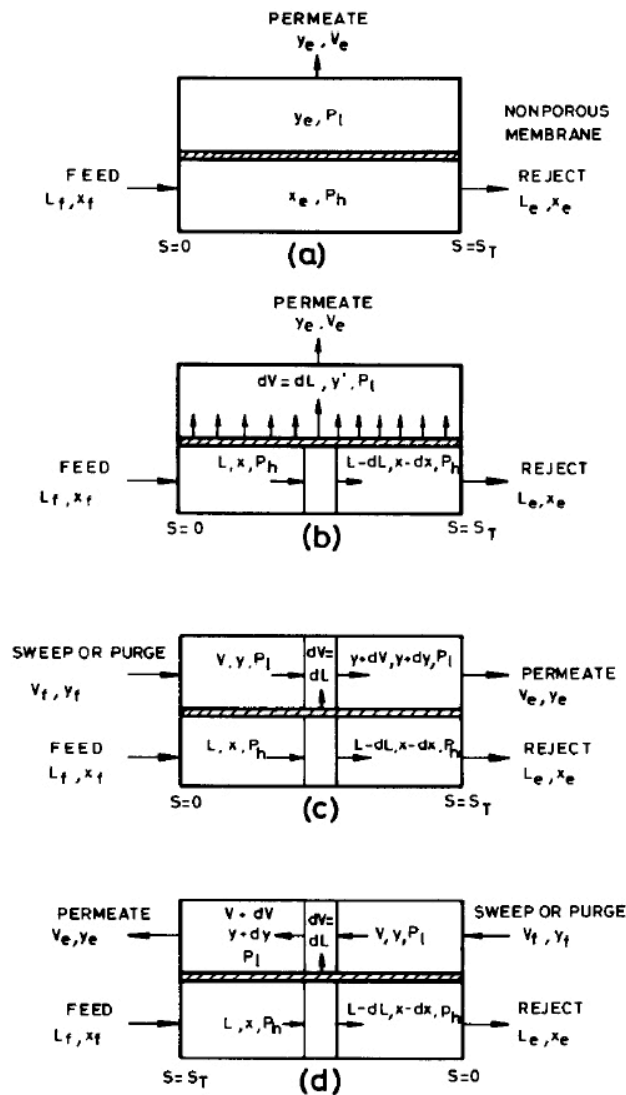


Figure 4.2 : Membrane permeation flow patterns as given in Kovvali, Vemury, et al [128]. a). Permeation through a non-porous membrane with equal pressure on both sides of the membrane, b). Permeation through a membrane where an over-pressure is applied, c). co-current flows of feed and capture mixtures with an over-pressure being applied to the feed side, and d). counter-current flows of the feed and capture mixture again with an over-pressure applied to the feed side.

While the membrane gas permeation behaviour investigated by Kovvali, Vemury, et al [128] is not specifically applied to microfluidic devices, many examples of each variant exist. Frenzel [127] and Timmer, van Delft, et al [75] provide examples of annular and planar co-current membrane permeation for the detection of sulphur dioxide and ammonia respectively. Counter-current flow examples of annular and planar membrane permeation are provided by Vollmer, Probst, et al [129] for the case of oxygen and Toda, Dasgupta, et al [130] for the case of hydrogen. Finally Toda, Ohira et al [131] use a reverse form of the cross flow pattern, in which air containing H_2S is fed vertically onto a membrane and diffuses into fluid flowing across the opposite surface of the membrane. While the mixed flow pattern described by Kovvali, Vemury, et al [128] is the only one of the four patterns

shown in which a non-porous membrane is actually shown, all of the examples above use non-porous membranes. Strathmann [132] provides a comprehensive review of membrane technology in the context of chemical separation processes. The use of porous or microporous membranes has previously been elucidated as having limitations associated with the variation in response to analyte collection as a function of pore size as well as membrane material.

4.2.2. Liquid Sorbent Vapour Collection

A more interesting development in the field of gas or vapour accumulation in liquid exploits direct contact between the two phases. Multiphase flow in microfluidic devices has been recently reviewed in detail by Gunther and Jensen [3]. As the review covers not only gas and liquid, but also oil and water flows, a brief summary of the various modes given is presented here along with a number of techniques covered elsewhere.

A number of methods of forming stable contiguous gas and liquid flow in microchannels have been investigated. Patterning channels to create hydrophobic and hydrophilic regions [133-135] is the most commonly utilised method. While it is possible to have laminar flow without patterning specific hydrophilic regions within a channel, the surface tension effects created by the patterning increase the stability of the fluid flows. Despite a number of groups being involved in research into laminar gas and liquid flow and the obvious potential, no evidence of true applications involving the absorption of gas or vapour into the liquid has been found in the literature. This may be due to the consequent limitation in time that the gas and liquid flows are in contact and therefore the limited extraction time [134].

Vapour and gas accumulation in falling droplets has been presented in numerous papers. Cardoso and Dasgupta [136] determine the atmospheric nitrogen dioxide (NO₂) concentration to <10 ppb by accumulation into a dynamically forming, falling, and then reforming, droplet composed of a chromophore producing reagent. Kumemura and Korenaga [125] likewise analyse for the presence of atmospheric NO₂, to a limit of 2 ppb, with a device they define as microfluidic. Although the former journal article does not define the device as microfluidic, the dimensions of the supply channels are smaller than the latter journal article (300 μm and 375 μm – 5,000 μm respectively). Gas dissolving in the forming droplet is transported by a combination of diffusion and internal convection and hence dissolves rapidly. The low detection limits are achieved by integrating the gas accumulation into the droplet over an extended period of time, 5 minutes and about 7.5 minutes respectively. Several other examples of similar devices exist [137, 138].

In the same vein as the falling drop microreactor, Jahnich, Baerns, et al [139] introduce the concept of the falling film microreactor (FFMR). While similar to the falling droplet, the falling film increases the surface area to volume ratio of the liquid exposed to the gas flow [140]. As the FFMR has only been investigated for use as a microreactor for the investigation of dangerous synthetic organic reactions, requiring fine control of experimental conditions, no direct comparison is available for its use as an analytical tool. A single channel, non-gravity controlled, version of the FFMR is created by controlling the flow rates of gas and liquid feeds to produce a stable liquid/gas interface.

Finally, direct gas/liquid contact has been realised by interspersing gas bubbles within a liquid flow. Much research, typically at millifluidic dimensions, has been performed on this technique for industrial processes where mixing of, or reaction between liquids, or gas and liquid, is necessary. Recent focus on multiphase flow in microfluidic devices has led to similar research, as that performed on industrial processes, being undertaken over the past 6 or 7 years. Much of the research, in both milli and microfluidics, has focussed on the flow patterns, the forces that affect them and, particularly in microfluidics, the effect of channel geometry.

Detailed research into multiphase flow and gas bubble and liquid slug movement was first covered in the 1961 seminal paper by G.I. Taylor [141]. Several other groups publishing that year also covered the movement of bubbles and liquid slugs through fine bore tubing, also under conditions at which viscosity and surface tension overcame inertial forces. Suo and Griffith [142] first investigated experimental gas/liquid flow patterns and the difference between theoretical and experimental results. The development of monolithic honeycomb catalysts of several centimetres span, containing channels up to several millimetres diameter [143-145], increased the interest in small channel gas/liquid flow. As a result much research was conducted into characterising boundaries in flow/phase space showing the range of conditions under which different regions of gas/liquid flow patterns formed. This research has since been continued by several groups making microfluidic devices for multiphase flow.

Much of the published microfluidic multiphase research has to date been a practical examination of the various possibilities inherent within the flow regimes offered by the fluid flow at microfluidic channel dimensions. Baroud and Willaime [146] and Doku, Verboom, et al [147] both provide comprehensive reviews of microfluidic gas and liquid flows within general reviews of multiphase microfluidic devices and chemistry respectively. A range of research extending from the formation of individual streams of small bubbles by shearing sheath flow [148] (Figure 4.3) through to the development of the previously discussed

boundaries in flow/phase space [149, 150] (Figure 4.4) have all been investigated in the decade since multiphase flow in microfluidics became an important research topic.

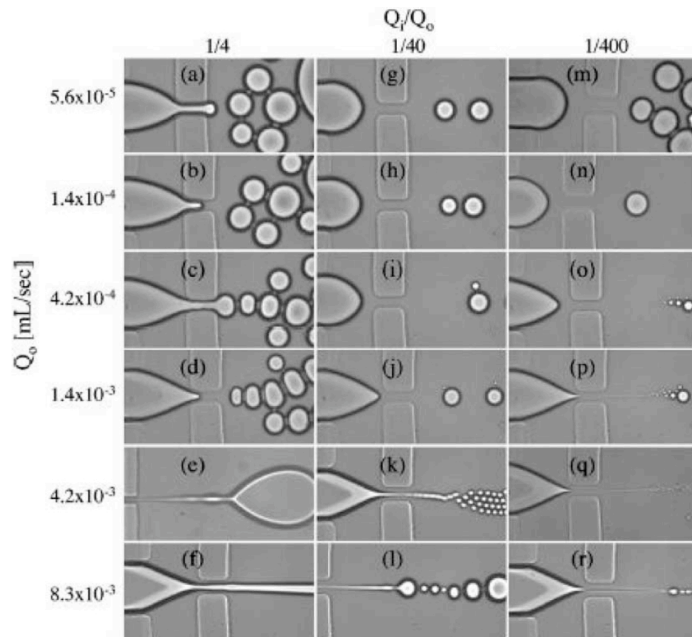


Figure 4.3 : Bubble formation by shearing sheath flow (taken from Anna, Bontoux, et al [151]).

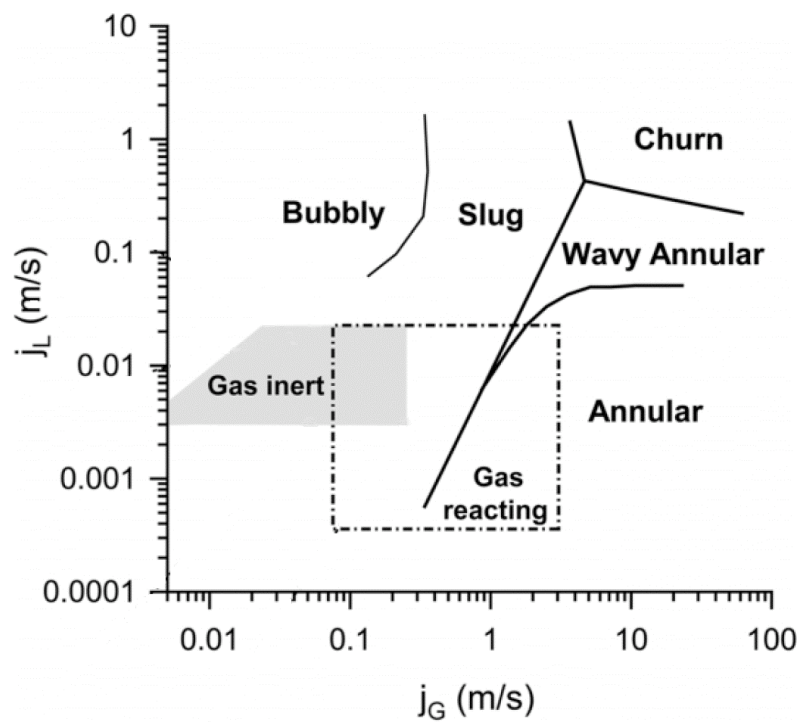


Figure 4.4 : Gas – liquid flow regime diagram developed by Gunther, Khan, et al [150].

4.3. Microfluidics for Vapour Analysis

Analytical systems for the analysis of gas using fluid absorption require stable gas and liquid flow, a constant gas/liquid ratio and, for a low detection limit, a high gas/liquid volume flow ratio. Few of the multiphase microfluidic devices developed to-date fulfil these criteria. Several, such as the microbubbling unit produced by Ganan-Calvo and Gordillo [148] while producing regular bubble sizes within a constant liquid flow rate, do not have a gas/liquid volume flow ratio high enough to make them efficient analytical tools. However a number of research groups have manufactured microfluidic devices with the potential to act as low detection limit, gas collection modules for analytical systems.

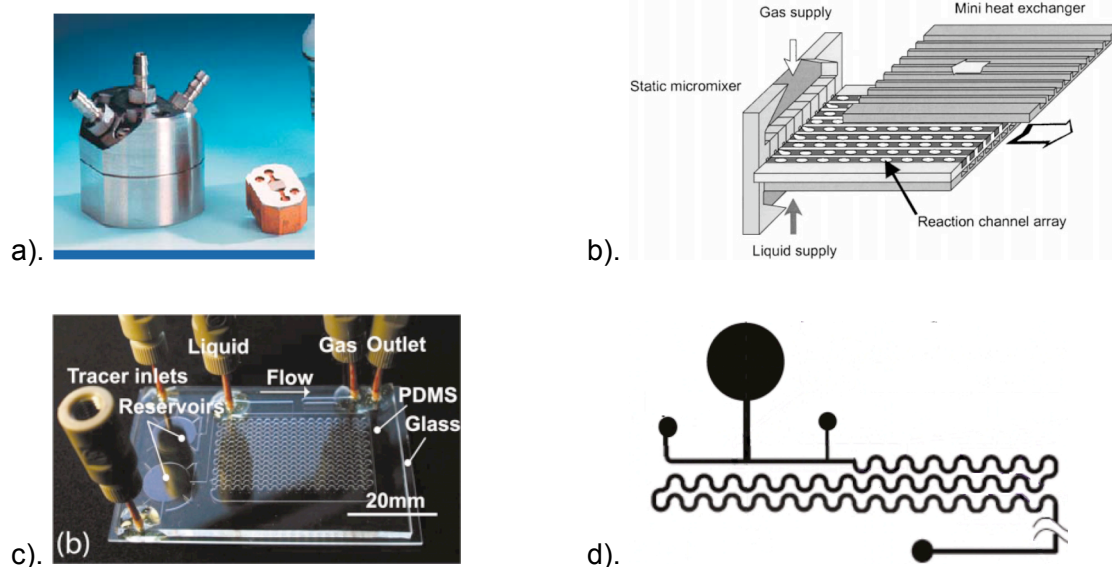


Figure 4.5 : a). Stainless steel MBC reactor (from [147]) ,b). Schematic of MBC (from [139]) ,c). PDMS device for production of segmented flow & d). Schematic of same (both from [150])

Jensen's research group, at the Massachusetts Institute of Technology (MIT) [126, 150, 152], and a group at the Institut für Mikrotechnik Mainz GmbH [139] have both produced devices in which stable, regular, segmented flow has been produced. Gunther, Khan, et al [150], from the former group, demonstrate a PDMS microfluidic device (as shown in Figure 4.5 c.) for the efficient mixing and reaction of two liquids using recirculating flows found in segmented gas and liquid flow (discussed in more detail below). Stable segmented flow is produced over a range of gas and liquid flow rates using syringe pumps to control both gas and liquid flows. Gunther, Jhunjhunwala, et al [152] examine the recirculating flow streams formed within the liquid droplets in greater detail using similarly designed devices to those manufactured by Gunther, Khan, et al [150]. Jahnisch, Baerns, et al [139] constructed the Microbubble Column (MBC) microfluidic device. The MBC, manufactured in stainless steel (as shown in Figure 4.5 a.), operates at higher pressure and therefore flow rates than the

PDMS devices manufactured at MIT. Liquid flow is established by an HPLC pump while gas flow is set by a mass flow controller.

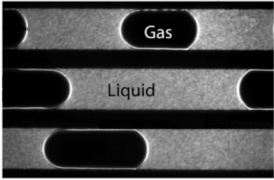
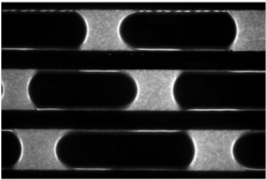
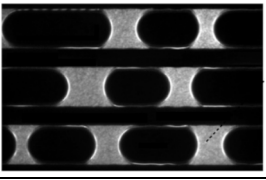
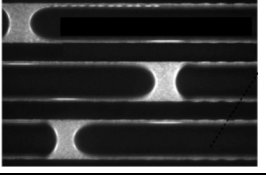
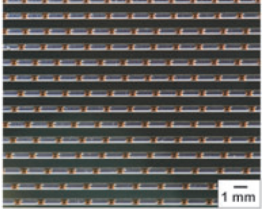
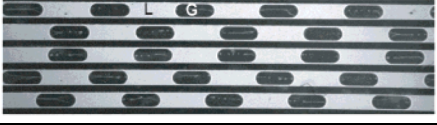
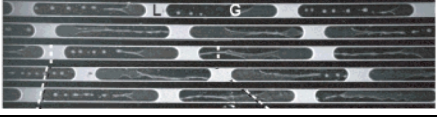
Reference	Gas Flow Rate ($\mu\text{L}/\text{min}$)	Liquid Flow Rate ($\mu\text{L}/\text{min}$)	Relative Flow Rates	Image (where available)
[139]	12 100	216	56	
300 x 100 μm	24 200	216	112	
	32 700	216	151	
	50 000	216	231	
[150]	68.4	10.8	6.3	
400 x 150 μm	108	68.4	1.6	
	288	68.4	4.2	
	864	10.8	80	
[126]	60	30	2	
[152]	4	4	1	
400 x 150 μm	16	4	4	

Table 4.1 : Segmented flow conditions for references [126, 139, 150, 152]. All flow rates in $\mu\text{L}/\text{min}$

Segmented flow produced in the PDMS devices manufactured at MIT does not exhibit many of the problems exhibited by membrane or polymer sorbent multiphase microfluidic gas collection modules. As previously demonstrated, solid sorbents require significant diffusion time to allow for the absorption of gas into or through the sorbent. Liquid droplets separated by gas bubbles display recirculating flow streams as shown originally by Taylor in 1961 [141] and recently by Gunther, Jhunjhunwala, et al in 2005 [152] as shown in Figure 4.6. The recirculation flow was characterised by Taylor as occurring for $m < 0.5$ (calculated using Equation 10), that is for low bubble slip through liquid droplets.

$$m = \frac{(U_b - U_{bulk})}{U_b} \quad \text{Equation 10}$$

where U_b and U_{bulk} are the bubble and liquid velocities respectively.

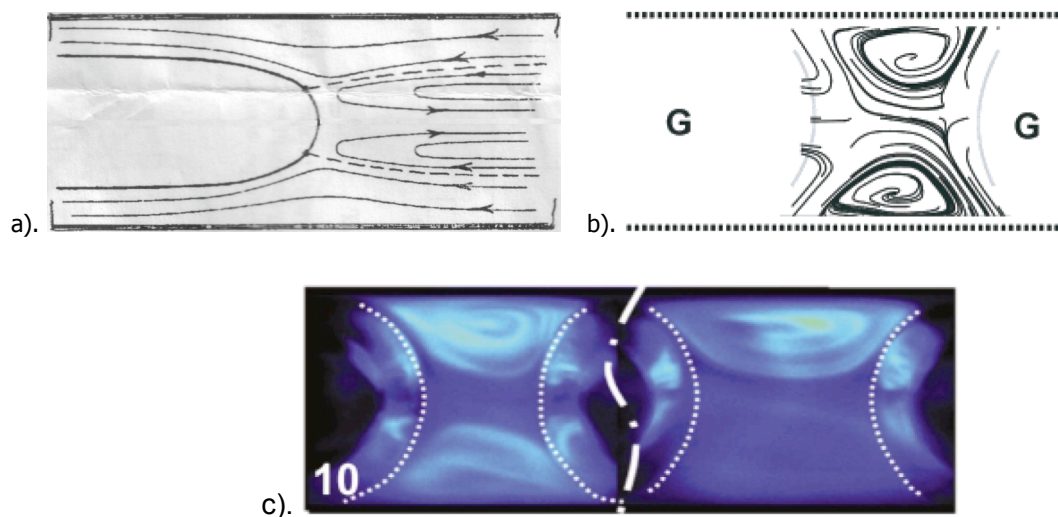


Figure 4.6 : Recirculating flow patterns as shown by a). Taylor (from [141]) and b). Gunther, Jhunjhunwala, et al (from [152]) and c). fluorescent tracer image of same (from [150])

Gunther, Khan, et al [150] further clarify the effect of the recirculation patterns with respect to the mixing efficiency. The channel length, relative to the hydraulic diameter so as to account for the lower efficiency of larger diameter channels, required (so as to achieve 90% homogeneity) is shown as a function of the Peclet number (Equation 5, Section 1.2.1). Comparison (see Figure 4.7) with other efficient methods of mixing in microfluidic channels demonstrated that the liquid/gas segmented flow device had comparable efficiency with the water/oil segmented mixer [153] while operating at higher flow rates, hydraulic diameter and greater efficiency than the staggered herringbone mixer (SHM) [154] or three dimensional serpentine [155].

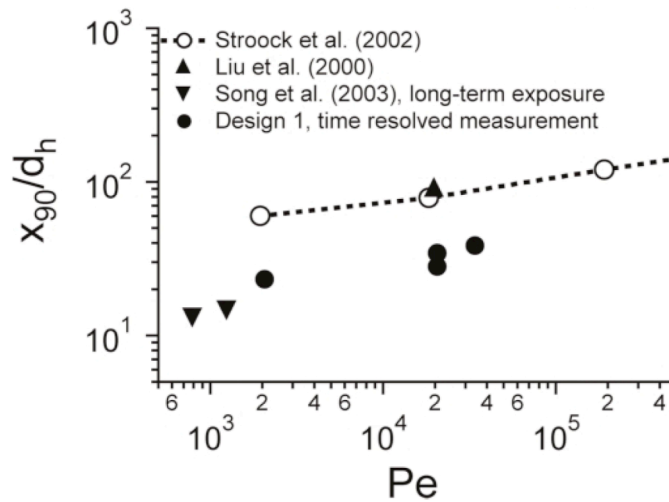


Figure 4.7 : Comparison of the mixing efficiency of liquid/gas segmented flow vs Stroock, et al's SHM [154], Liu, et al's three dimensional serpentine [155] and Song, et al's water/oil segmented flow mixer [153]. Taken from Gunther, Khan, et al [150].

Finally quantification of the recirculating flow and the uniformity of the gas/liquid segmentation was also performed. Gunther, Khan et al [150] observed a maximum velocity component, normal to the main fluid flow, of 25% the bulk velocity. By plotting the vorticity, Gunther, Jhunjhunwala, et al [152], enable the mixing potential to be quantified rapidly for each droplet as a function of the gas and liquid flow rates (see Equation 11). This method of determining the mixing efficiency is more accurate and faster than measuring the channel distance required to achieve 90% mixing as done by Gunther, Khan, et al [150]. Lastly, a plot of the liquid slug length distribution indicates that, while the images demonstrate regular gas/liquid segmentation, the variation in slug length is relatively large ($1.3 \pm 0.2 \times$ channel width).

$$Vorticity = \frac{\partial U}{\partial y} + \frac{\partial V}{\partial x} \quad \text{Equation 11}$$

With V being the liquid velocity in the direction of the channel and U being the liquid velocity normal to the channel.

4.4. Experimental Parameters

Diffusion of gas molecules through membranes into a capture solution displays many advantages over most of the multiphase flow methods presented. Membrane-based multiphase systems generally exhibit more stable gas and liquid flow over widely varying flow rates, easier fluid handling and simpler complete systems. However as previously stated, the major problem demonstrated by membrane multiphase devices is the delay in response due to the increased diffusion times through the membrane. The recirculating flow streams observed in segmented gas/liquid flow overcame this problem and also exhibit many of the advantages stated above of membrane based systems.

However all segmented flow multiphase microfluidic systems observed are more complex than membrane based systems. The injection of gas and liquid into a microfluidic channel without any deterministic control over the segmentation implies fine control over the flow rates. This is necessary to maintain stable segmented flow against the increasing back pressures (explained in Section 5.1) encountered as the number of menisci increase. Jensen's research group at MIT utilise syringe pumps to ensure constant gas and liquid flow rates. Despite the low pulsatility found in the syringe pumps used by Gunther, Khan, et al [150], *two hours was still required to pressurise the microfluidic system and develop stable segmented flow*. In contrast, the liquid and gas flow within the MBC, developed at the Institut für Mikrotechnik Mainz GmbH, were controlled by an HPLC pump and a mass flow controller attached to a pressurised gas source. While the system requirements are less complex than operating two syringe pumps, the system only operates effectively, because the high pressures, created by the syringe pumps in trying to maintain a set flow rate, exceeded meniscus derived forces in the microfluid structures.

Further development of a gas analysis system, in which a gas collection device produced segmented gas and liquid flow, was judged to be possible. However several conditions are necessary to take full advantage of both the microfluidic platform, the gas/liquid segmentation and to fulfil requirements created by other sections of the analysis system.

Minimising the size of the gas collection module to take advantage of the miniaturisation possible with microfluidics requires small gas and liquid supply units. The decision was therefore made to use pressure driven gas and liquid supplies. As discussed in Sections 6.1 and 6.3.1, vapour analysis was initially designed for a chemiluminescent reaction system. Following testing of the initial reaction scheme, a new vapour analysis method utilising absorbance was selected. The long reaction time for analyte vapour captured by the solution was the major limitation of the chosen vapour analysis system. Material considerations limited the maximum device size. To achieve the long reaction times

necessary low flow rates and therefore pressures were necessary. Device design and experimentation were therefore constrained by these requirements.

5. VAPOUR COLLECTION

The following chapter is of a significant length. Hence it has been subdivided into six sections. Brief summaries of each section follow.

Section 5.1 details the experimental methodology used to test the devices discussed in Sections 5.2 – 5.6 and described in Appendix 1.

Section 5.2 summarises the major stages of microfluidic device development and the primary rationale upon which major design modifications were made. The dominant fluid flow effects dominating device behaviour throughout the course of research into segmented flow for vapour capture and analysis are also discussed briefly.

Sections 5.3 to 5.6 document the results of experiments performed using the microfluidic devices manufactured to produce segmented flow. Each section relates to a series of photomask designs, grouped according to the major fluid control devices therein and the substrate in which the microfluidic devices are manufactured. The experiments are presented chronologically. However any periods in which research into segmented flow vapour collection was halted, so as to investigate other areas, are not discussed.

Section 5.3 examines briefly the initial devices manufactured to provide a preliminary understanding of segmented fluid flow production. The devices were all manufactured in PDMS with gas and liquid injection controlled with NR valves. Serious problems with gas and liquid flow break-up were observed immediately. Methods were implemented to prevent this, however further problems caused by gas compressibility and multiple menisci passing over uneven channel walls caused research to be temporarily directed towards integrated valving. Little detail is provided about the individual experiments and minor modifications between devices, manufactured from each photomask design, as this information has no long term significance in the development of this thesis.

Section 5.4 presents the results and their discussion for two distinct devices. The first, 'Modular' device was manufactured from discrete, commercially available components. This Modular device confirmed that the interaction between the menisci and the channel walls was important to pressure driven flow. The second device was actually a series of devices manufactured, using PMMA, solely to provide information about fluid flow at the gas and liquid junction. The micro-junctions manufactured in PMMA, while individually providing no long term information, demonstrated a method by which devices could be tested quickly while still giving sufficient results for device evolution to continue.

Section 5.5 groups the devices manufactured, in PDMS and using Lee valves to control the gas and liquid injection, to establish the best micro-junction design for manipulating the direction of fluid flow directly at the intersection of the two phases. Static passive valves, acting to enhance the meniscus back-pressure, were included to reduce the effect of gas compressibility within the gas supply channel. High resolution photomasks were also used for the first time to provide better defined features (determined to be absolutely necessary for the successful operation of the passive valves).

Finally, in Section 5.6, the designs observed to best manage the fluid injection, at the micro-junction, were included within a series of devices in which different channel designs were evaluated. The effect of the high resolution photomask, providing smaller incidental surface roughness, on the flow of the gas and liquid segments as they pass through a long channel is observed for the first time. Well defined, effective, passive valve designs combined with triple depth devices and modifications to the standard manufacturing method resulted in a device in which controlled, regular, segmented flow was first observed over a series of pressures and valve timings.

5.1. Experimental

All devices manufactured for the production of segmented flow were tested in the same manner. Differences originate in the manner in which the devices were manufactured and therefore set-up for testing or how data was acquired made.

Devices are named based on the photomask number, the wafer number and then finally the design within that wafer if more than one exists. For instance Device 2.b.2 is from photomask **2**, wafer **b** and design **2** within that wafer. Due to the manner in which the device designs evolved, the photomask number is also an indicator of the particular *type* of design, while the wafer and design numbers indicate specific variations within that design. The wafer number and design number within each wafer were assigned pragmatically with dimensions, calculated flow resistances and details of each design being maintained within a Microsoft Excel spreadsheet.

Photomask	Design #	Application	Major Modifications
1	.1 - .3	Segmented flow	
2	.2.a - .3.b	Segmented flow	w/ flow restrictors
3	.2.a - .3.b	Segmented flow	w/ curved supply channels
4	.1.a - .4.b	Segmented flow	Injectors
5a	.1 - .5	Segmented flow	1 st double depth
6	.1.a - .1.c	Burst valves	Gas/Liquid & single phase flow
7	.1.a - .1.d	Burst valves	Single phase flow
8	.1.a - .2.b	Check valves	
	.3.a - .3.c	Piezo foamer	Not examined
9	.1.1 - .2.4	Check valves	Full device design
----	Modular	Segmented flow	-Upchurch T-junction & connectors. -FEP tubing for supply/reaction channel.
----	PMMA junctions	Segmented flow	
10	.1.a - .2.d	Segmented flow	Microjunctions
	.3.1 - .3.2	Piezo foaming mixer	
11	.1.a - .2.d	Segmented flow	Microjunctions
	.3.1 - .4.3	Seal valve	
	.8.1 - .8.4	Flap valve	
12	.1.a - .1.b	Segmented flow	Diagonal
	.2.a - .2.b	Segmented flow	Serpentine
	.3.a - .3.b	Segmented flow	Spiral

Table 5.1 : List of photomasks and intended application of devices produced from each design.

5.1.1. NR Valve Controlled Devices

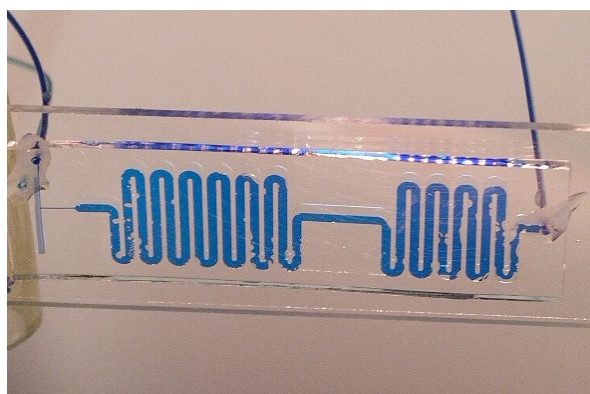


Figure 5.1 : Representative examples of device manufactured from photomask of Design 1 – 5. The nylon tubing fluid inputs and output can be seen at the top, with the epoxy adhesive surrounding the fluid connection points.

Devices manufactured from designs on photomasks 1 to 5, for the production of segmented flow, were manufactured with nylon tubing fluid connections (Figure 5.1). Normally open 2 port solenoid valves manufactured by Neptune Research (NR) were used to control the fluid supply to all devices from photomasks 1 to 5. Fluoroethylene polymer (FEP) tubing (5 cm of approximately 750 μm internal diameter, ID) attached to the nylon tubing fluid supply by PEEK Unions (Upchurch Scientific, Oak Harbor, USA) was used to connect the NR valves to the microfluidic devices. FEP tubing (30 cm) connected the NR valve controlling the liquid supply to the liquid source, a pressurisable HPLC bottle (250 mL) (Figure 5.2).

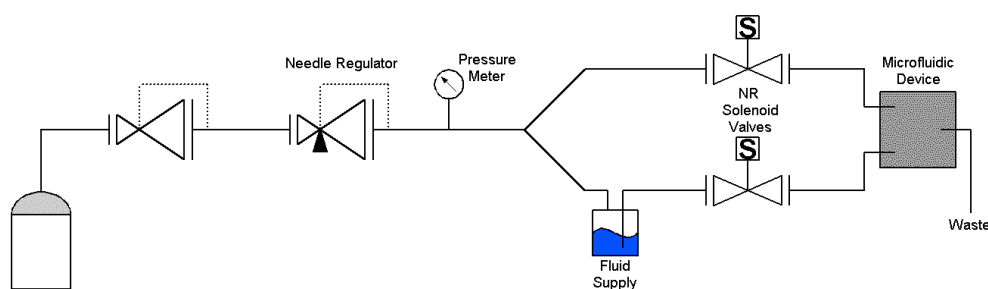


Figure 5.2 : Fluid schematic of segmented flow device testing set-up for devices produced using designs from photomasks 1 – 5.

5.1.2. Non-PDMS Devices

Modular Device

FEP tubing (750 μm ID, 50 cm long) was connected to a precision, 100 μm ID, T-junction (Upchurch Scientific) to form a modular device for the production of segmented flow (Figure 5.3 a). VHS Microdispensing valves (The Lee Company Ltd.) attached to the T-junction by

FEP tubing inserted into a Lee 062 Minstac Fitting System. FEP tubing (20 cm long) connected the liquid source to the associated Lee valve while flexible PVC tubing (3 mm ID, 10 cm long) was used to connect the Lee valve to the gas supply.

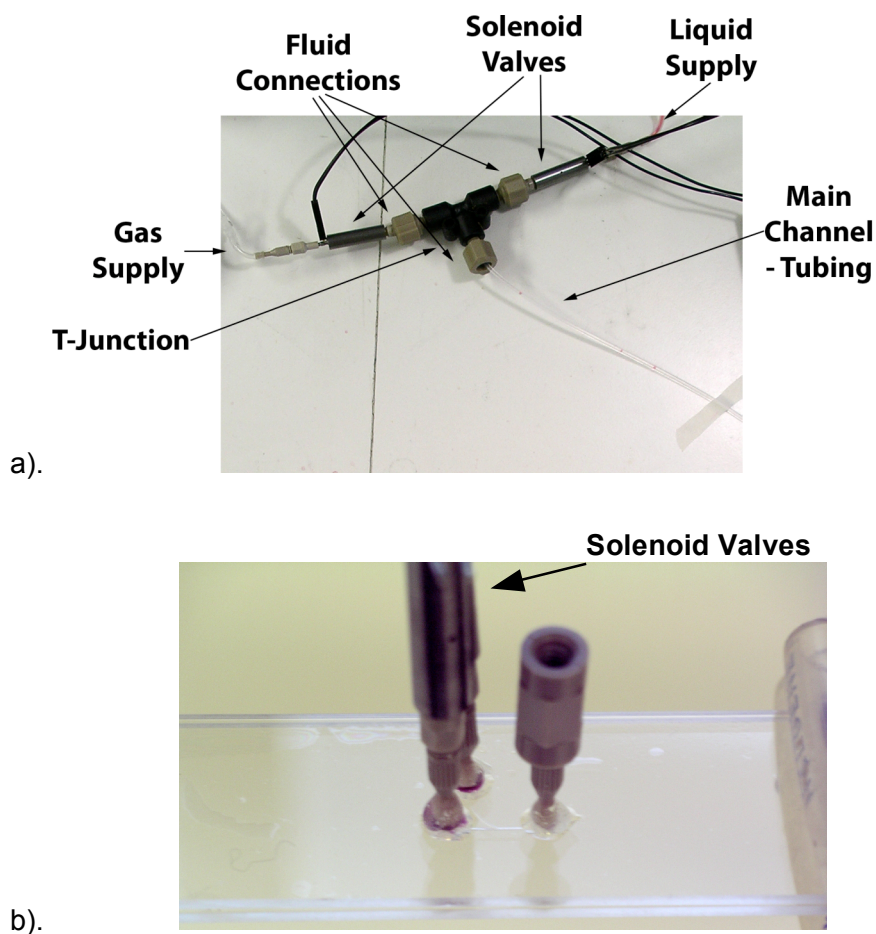


Figure 5.3 : Representative examples of a).a modular device and b). a micro-junction realised in PMMA.

PMMA Junctions

Fluid supplied to PMMA devices incorporating milled microjunctions was controlled by Lee valves. Minstac nozzles (0.005 inch ID) were glued with fast curing Araldite™ (Huntsman Advanced Materials, Duxford, UK) epoxy adhesive into the three fluid connection holes of the PMMA junction (Figure 5.3 b).). Lee valves were screwed directly on to the connectors for the fluid supplies while the main channel, formed initially of flexible PVC tubing (3 mm ID, 10 cm long) and later of FEP tubing (50 cm long), was forced over the end of the Minstac nozzle to ensure a gas tight fit. Fluid connections from the gas and liquid sources were made as per the above method.

5.1.3. Lee Valve Controlled PDMS Devices

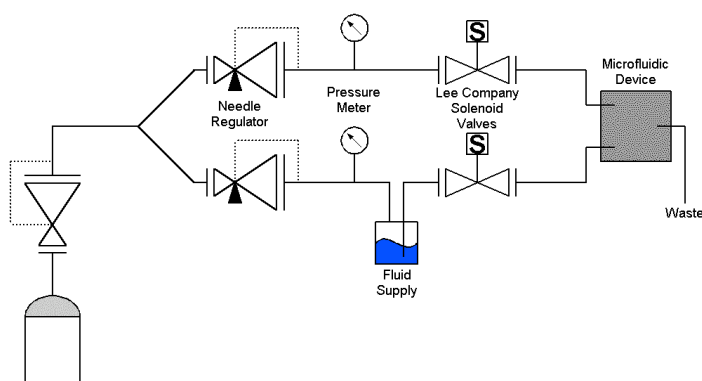


Figure 5.4 : Schematic of set-up for testing segmented flow devices from photomasks 10 – 12.

The above arrangement (Figure 5.4), with minor changes, was used for supplying fluid to the push-fit microfluidic devices (from photomask designs 10 to 12). Minstac nozzles, rather than being glued, were pushed directly into the pre-drilled 1.1 mm diameter holes in the PDMS (see Figure 5.5 a.). The PDMS formed a gas tight seal around the nozzles. Two different arrangements were used to attach tubing to the main channel leading to the container for waste solution. Initially the waste tube was formed of a Minstac nozzle, push-fitted into the device, with flexible PVC tubing (5 mm ID, 10 cm long) attached. Finally, the end of the main channel was opened directly by cutting diagonally across the device (as per Figure 5.5 c). & d.). The end of the channel was widened by drilling into it with a 700 μm drill bit. Nylon tubing (750 μm OD, 250 μm ID, 30 cm long) was then push-fitted into the end, forming a gas tight seal (Figure 5.5 b.).

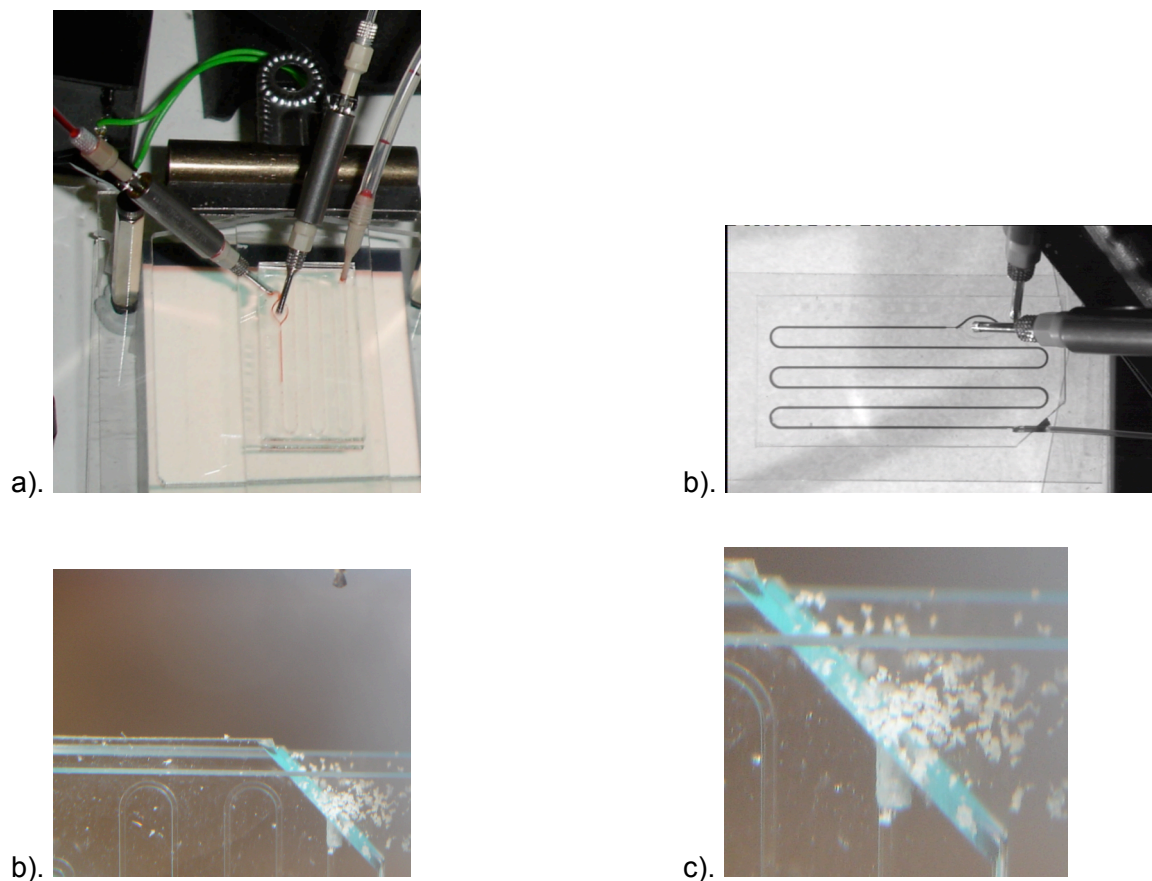


Figure 5.5 : a) Representative example of PDMS device assembled with 'push-fit' fluid connections as per devices manufactured from Designs 10 – 12, b). Device 12.1 with push-fit nylon tubing inserted, c). Widening of end of main channel on microfluidic device from design 12 and d). Close-up of end drilled channel.

5.1.4. Generic Set-up Detail

Valve timings were set by a custom made electronic control board, designed for other purposes, by the group and assembled by the author (Figure 5.6). A BX-24 computer, driven by an Atmel AT90S8535 processor loaded with the BasicX compiler, was pre-programmed by the group. The program provided the ability to open and close valves by modifying a text file (script), that was then loaded onto the BX-24 computer (an example script is shown in Appendix 2). Several text files were written by the author for each experiment to allow for the testing over a range of gas and liquid volume ratios. Priming, filling the connective tubing with fluid prior to the main sequence of valve openings and closings, was also provided for in the program.

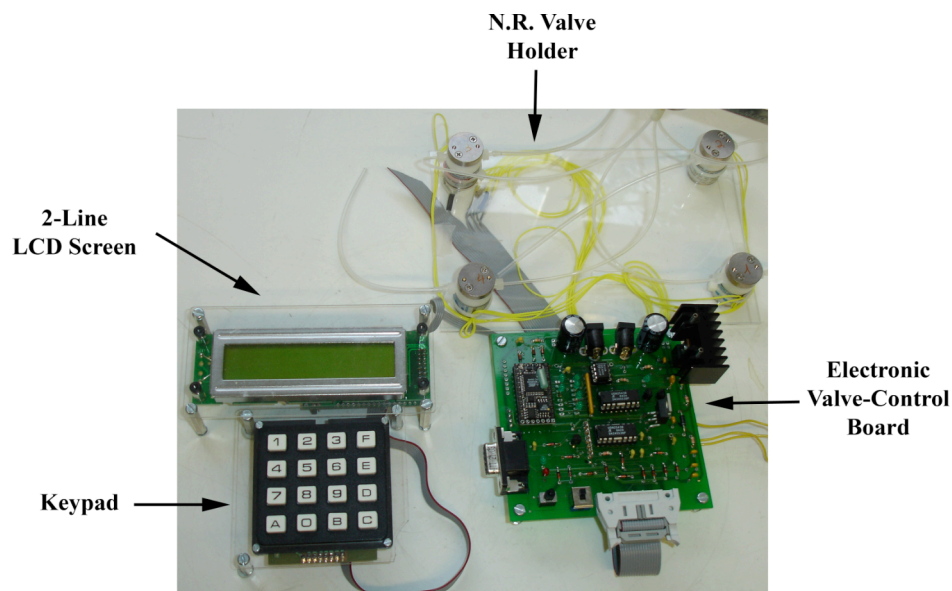


Figure 5.6 : Photograph of valve microcontroller with the keypad, screen and valves attached via ribbon cable. During the experiments conducted into vapour collection, only two of the four valves shown were used.

Lee valves are capable of operating at up to 1000 Hz, compared to NR valves which are realistically limited to 10 Hz (despite the manual stating a capability of 20 Hz). The program, into which the text file was loaded, was initially written to accept times as steps of one second. After the introduction of Lee valves it was modified to reduce this to steps of one millisecond. The majority of the text files were written with a maximum of 400 sequential time steps. Following further software development it became possible to use timing loops and therefore extend the period over which devices from photomask 12 were able to be tested. The number of each valve is defined by the connection point on the microcontroller board. This information is then used to specify the gas and liquid valve opening and closing times or whether a rest period (where both valves are closed) is incorporated. These times are alternated as appropriate, for example: *Gas, Liquid, Rest or Gas, Rest, Liquid* (see the following example or Appendix 2).

A fragment of an example valve control script follows : Valve 1 controls the liquid flow and valve 2 the gas flow. The example script was repeated 80 times in the actual script used experimentally.

on:1;	valve 1 is opened and valve 2 closed for 1 s.
off:2;	
time:1;	
on:0;	both valves are closed for 1 s.
off:1;	
time:1;	
on:2;	valve 2 is opened for 3 s.
off:0;	
time:3;	
on:0;	both valves are closed for 1 s.
off:2;	
time:1;	

Both NR and Lee valves, used to control separate microfluidic systems, are operated by applying a 'spike' voltage (9 volts for the NR valves and 9.5 volts for the Lee valves) to initially open them. The 'spike' voltage is then decreased to a 'hold' voltage (4.5 volts for both makes of valve). NR valves are capable of being directly powered from the electronic control board. Lee valves require separate, grounded, power supplies to the electronic control board and the length of the opening 'spike' is also controlled separately by a 'Spike and Hold Driver' (The Lee Company Ltd.).

Prior to testing, all devices were primed with carbon dioxide (CO₂). This prevents the formation of stable gas bubbles that remain within the tubing and microfluidic channels subsequent to priming with aqueous solution. All devices were tested using nitrogen (BOC gases) and filtered (to 0.2 µm), *degassed* water or aqueous dye solutions.

During testing a number of conditions, other than the valve opening and closing times and applied pressures, were observed. Priming of the microfluidic device fully with either gas or liquid affected the back pressure and could therefore be important to the initial operation of the device. Whether the liquid or gas valve was the first to open was also recorded.

Observation of the devices in operation and associated recordings were made in several different ways. A fluorescence microscope operating in transmission mode was used to view the active area of interest of the microfluidic devices in greater detail. Entire microfluidic devices were viewed by eye, attached to a purpose built PMMA frame with a white electroluminescent sheet (RS components) as the light source. Initial visual recordings were made using a digital camera (Pentax Optio 550) either handheld or mounted on a stand. Video recordings were made with a compact, high sensitivity, industrial monochrome video camera (576x768 pixels, CV-A50C, JAI UK Ltd.) either attached directly to the fluorescence microscope or to a Computar 18 – 108/f2.5 zoom lens (Computar, NY, USA) to view the entire device¹. The video feed from the camera was directed simultaneously into a DVD recorder and a frame grabber (Imagination PXC-200A, CyberOptics Semiconductor) operating within a Pentium™ 4 PC (Dell)². This allowed simultaneous recording, in high quality mode, and viewing of the video feed. Monochrome stills presented here are single frame images taken from video recordings of the devices in operation³.

1 The Zoom lens was unavailable for the majority of the original video recordings. Visual records therefore tend to be either photographic or taken through a microscope with associated loss of general flow information.

2 The original DVD recorder (Eurotech DVR-4001) was less reliable (and ultimately failed completely) than the replacement (LiteOn LVW-5026). Approximately half of the recordings were unreadable after review. Despite being able to record from design 5 onwards little visual information remained. Fortunately text descriptions of the results sufficed.

3 The video camera outputs in PAL format. At 25 frames per second the stills obtained from the video camera are sometimes indistinct. A high-speed video camera would have provided clearer images, but it was unnecessary in view of the high cost, limited period of use and possibility of obtaining clear images if an experiment is performed for a sufficient period of time.

Addendum :

Video and photographic evidence of experiments performed using devices 1 – 4 could not be obtained as the frame grabber had not been obtained at this point . No other method of taking clear photographs or video was easily available. Initial observations are therefore taken from experimental notes.

5.2. Summary

The results and their discussion presented here are extremely detailed in order to allow a full explanation of the developments from device to device. While minor effects frequently affected the design of individual devices, consistent patterns in the fluid flow behaviour were responsible for the majority of the changes. The discussion is presented to emphasise these patterns. However a brief review of these observed patterns and the major changes in the development of a segmented flow gas collection module are presented below for the lay reader.

Throughout the discussion observations of minor changes to fluid flow behaviour are made, but not necessarily in the section in which the experiments are discussed. This, seemingly delayed, narrative is due to the understanding of fluid behaviour, specifically multi-phase fluid behaviour, developing over the course of device development. Therefore the consequences of knowledge gained from observations made in one experiment may not have become apparent, used and hence discussed here until several subsequent experiments had been performed.

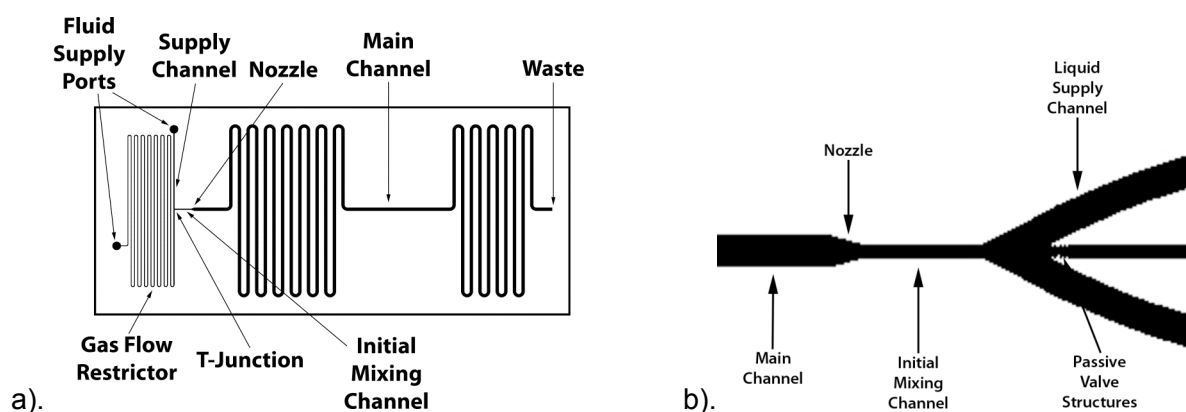


Figure 5.7 : Device structure designation of a). one of the original NR valve controlled devices, b). a high resolution device controlled by Lee valves.

Discussion of research into segmented flow microfluidic vapour collection devices is divided into a number of developmental stages. The stages are defined either by the substrate used or the valves that control the supplied fluid flow. A brief review of the divisions and the devices included are presented here before a more detailed discussion of each developmental stage during the body of the results and discussion. Initial devices were developed, in PDMS, to operate using NR solenoid valves to control the fluid flow. Following the observation that reducing the volume of gas between the valve and the gas/liquid junction was essential to regular segmented flow, research into developing valves to integrate into the vapour collection device was commenced (as discussed in Chapter 3).

During the period of integrated valve development, devices manufactured from alternative substrates and incorporating Lee micro-dispensing valves (in future referred to simply as Lee valves) were researched. Following the decision to halt research into integrated valves due to time restrictions, research into PDMS based devices was recommenced, but utilising Lee valves rather than NR valves. Finally, incorporation of passive valve structures, a triple depth structure and a novel extension to the cast channel to allow full fluid flow to develop resulted in regular segmented flow being observed.

A tabulated summary of the changes in design from device to device is provided within each numbered section. Each device's designation is taken from these tables. As discussed in Section 5.1, the photomask number is used to originally specify which evolutionary stage a device belongs to. Photomasks 7 to 9 concern the development of integrated valves and are therefore not discussed here.

5.2.1. Major Fluid Flow Artefacts

Pressure driven segmented gas and liquid flow within microfluidic devices was consistently affected by the properties of the device fabrication method, fluid properties and the supporting fluid control devices. The design of the microfluidic devices was gradually modified so as to manage these effects and allow the controlled manipulation of both phases.

Two recurring effects were observed during testing of the majority of segmented flow microfluidic devices. *Firstly, liquid being pushed into the gas supply channel and secondly, the stop/start nature, and occasionally complete stopping, of fluid flow were determined to be THE major effects to be controlled before segmented flow could be realised.*

The liquid being pushed into the gas supply channel was believed to result from the compressibility of gas and was the principal reason behind the change in research direction to development of integrated valving. The rationalization being that reducing the compressible volume of gas, between the gas/liquid junction and the control valve, would reduce either the volume of liquid that would penetrate the gas supply channel or prevent it occurring altogether.

Changing the substrate and, later, the photomask supplier were both found to prevent the stop-start nature of the fluid flow, which was determined to result from the surface roughness of the channel walls. As observed in Section 3.3.1, as the number of menisci increase the back pressure tends to increase. This is related, as discussed in Section 5.3.1, to the constantly varying contact angle, between the gas/liquid meniscus and the channel wall¹. The contact angle of segmented, two-phase flow constantly changes as it moves over the channel wall.

The changing contact angle is caused by both the flow variation, as the phase being injected changes, and the channel wall roughness resulting from the spot size of the photomask printers (which causes the scalloped effect noted in Figure 5.21 a). As the experimental contact angle approaches the theoretical contact angle, the surface energy across a meniscus approaches the minimum. If a meniscus possesses close to the minimum surface energy, then the pressure required to impel the fluids increases.

Each of the gas bubbles can be considered to be equivalent to a spring due to its potential for positive and negative volume change. Each of the gas/liquid menisci are believed to adjust their position slightly to achieve the lowest possible energy given that the volume of the droplet does not change. Therefore, as the number of menisci increases, the number existing at close to the minimum surface energy increases and therefore the back pressure increases.

The replacement of NR valves with Lee valves was intended to overcome two effects: firstly an asymmetric pumping effect as the NR valve opened and closed and a slow state change time. NR valves, possessing a large internal volume, produced a forward and reverse pumping effect as the valve closed and opened respectively (as discussed previously in Section 3.1). Lee Valves, operating under different operating principles, did not produce this action and therefore the start and end period of fluid flow during each injection was smoothed. A by-product of this effect was the production of short periods of time when the flow of fluids in the main channel stopped briefly. This is believed to aggravate the effect of channel surface roughness on the menisci by providing time for stable menisci positions to develop. This effect was not exhibited by Lee valves. As discussed in Section 5.1.4, NR valves possessed a state change frequency of 10 Hz, whereas Lee valves provided greater control over the production of gas and liquid segment volume as a result of the higher state change frequency (1000 Hz).

¹ This is not immediately obvious as the leading and trailing menisci of a droplet theoretically possess equal surface energies and therefore any back pressure should be cancelled by an equal and opposite forward pressure from the other meniscus.

5.2.2. NR Valve Controlled PDMS Devices

NR valves were used to control the devices manufactured using photomasks 1 to 5a. All photomasks incorporated fluid supply channels that merged at a T shaped junction which then expanded into a serpentine main channel via a nozzle. Major changes to the designs between photomask 1 and photomask 5a included the addition of a flow restrictor to the gas supply channel, narrowing of the main channel from 1 mm to 300 μm , the use of all PDMS channels and a number of different modifications to the T-junction. A number of minor changes were tried in an attempt to either determine the most effective way of changing the fluid flow in a pre-defined manner or the best fabrication method. For example, the use of a 50 μm and a 20 μm gas flow restrictor in Device 2.2 a and b respectively and simple passive valves in Device 4.2 and 4.4. The minor changes were only used in one photomask before being abandoned as ineffective, whereas the major changes were incorporated into several photomasks.

Photomask Number	Tested Permutations	Changes from Previous Segmented Flow Designs
1	.1 Full serpentine .2 Two joined serpentines .3 Externally joined serpentines	
2	.2 - .3 as above .a 50 μm wide flow restrictor .b 20 μm wide flow restrictor	- Introduction of gas flow restrictor
3	.2 - .3 as for design 1	- All PDMS channels - Narrowing of channel (1 mm to 300 μm) - Square main channel (300 μm) - Nozzle angle increased from 45° to 70°
4	.1 Simple junction .2 Toothed structure .3 As for .2 with flap valve .4 Toothed structure	- Redesign of gas/liquid junction a. Gas injected into liquid flow b. Liquid injected into gas flow - Narrowing tooth structure at end of flow restrictor. - Reduction of flow restrictor length - Attempted flap valve on liquid supply
5a	.1 Liquid injected .3 Gas injected .5 Liquid sheath flow	- Double depth manufacture - Liquid flow full depth, flow restrictor half depth - Injection of gas into liquid sheath flow

Table 5.2 : Summary of the evolution of the microfluidic devices from photomask 1 to 5a.

5.2.3. Non-PDMS Devices

Two non-PDMS devices were tested during the period of research into integrated valving. The first (Modular device) consisted of individual, readily available and connectable components, while the second consisted of a fine gas/liquid junction milled into PMMA using a PCB prototyping machine (LPKF Protomat 91s/vs). Fluids supplied to both devices were controlled by Lee valves as at that time research into integrated valving was ongoing and Lee valves were capable of being attached easily. Components were chosen for both devices with the aim of reducing the surface roughness of the gas/liquid junction and the main channel. The Modular device proved more effective, than the previous NR controlled PDMS devices, at producing segmented flow, however the junction component's design prevented further research. In contrast, research into the PMMA junctions, while not continued in PMMA, was used as the basis for the development of the next generation of PDMS segmented flow devices.

Design	Tested Permutations	Changes from Previous Segmented Flow Designs
Modular Device	Direct gas/liquid T-Junction Gas injection T-Junction Liquid injection T-Junction	<ul style="list-style-type: none"> - PEEK moulded (250 μm diameter channels) junction. - Extruded FEP tubing (750 μm) operating as fluid supply and main channels. - Lee valves controlling the fluid supplied to the device. - Independent gas and liquid pressure control.
PMMA Junctions	.2 [250 x 200] μm channels Angled gas supply into liquid. .3 [150 x 30] μm channels .4 [150 x 30] μm gas supply Other channels [250 x 200] μm .5 [250 x 200] μm channels	<ul style="list-style-type: none"> - PMMA milled channels - Finer liquid and gas junctions. - Separate design and testing of gas/liquid junction from complete device.

Table 5.3 : Summary of the non-PDMS devices developed and the evolving testing conditions.

5.2.4. Lee Valve Controlled PDMS Devices

Following suspension of the investigation into integrated valves, all further microfluidic research was conducted into segmented flow vapour collection. The PMMA fabrication method did not provide the scope to manufacture certain desired features, therefore subsequent devices were manufactured in PDMS. However the results of the previous experiments conducted on the PMMA junctions and the effectiveness of the Lee valves were used to develop this generation of devices.

Continuing from the previous experiments, the focus of research remained the fluid flow behaviour at the junction. The effectiveness of a series of test junctions was compared and the results of the experiments used to design the next generation of devices. These devices, manufactured using high resolution photomasks to decrease the channel wall 'roughness' and the precision of individual features, were also test junctions. However the test junctions incorporated similar designs for passive valves exploiting deliberate microsurface patterning to stop the movement of the gas/liquid meniscus into the gas supply channel. Experimental testing again involved observing the behaviour of the fluid flow at the junctions.

Photomask Number	Tested Permutations	Changes from Previous Segmented Flow Designs
10	.1.a - .2.d See Figure 2.57	-Return to PDMS devices -Test of different junction designs
11	.1.a - .2.d	-High resolution photomasks -Test of variety of contact angle based passive valves for different junctions

Table 5.4 : Summary of research into Lee valve controlled PDMS devices.

5.2.5. Segmented Flow Device

The last and most effective devices for producing segmented flow were manufactured using the results from the previous design and incorporating them, along with several other major modifications. Two of the previous design's test junctions were used in separate devices. However to increase their effectiveness, the devices were manufactured in a *triple depth structure*. This maintained the small dimensions of the gas supply channel (thereby increasing the efficacy of the passive valve structures) while simultaneously retaining a square section main channel (thus keeping the meniscus surface energy in the horizontal and vertical plane equal). A method was also developed to allow the *extension of the main channel without a sudden change in direction* as previously required. This allowed the full development of segmented fluid flow. It is believed that all modifications contributed to the observation of regular gas and liquid segmented flow.

Photomask Number	Tested Permutations	Changes from Previous Segmented Flow Designs
12	.1.a - .3.b	- Incorporation of junctions in device. - Triple depth structure. - Direct extension of main channel.

Table 5.5 : Final device characteristics

5.3. NR Valve Controlled PDMS Devices

5.3.1. Design 1

Devices 1.1 - 1.3 (Figure 5.8) and later similar designs, 2.2 - 2.3 and 3.2 – 3.3, were attempts to determine whether segmented flow could be achieved. Physically separating gas collection and analysis modules could be performed without any connecting tubing if Devices 1.2 and 1.3 operated correctly. The first devices produced were based on a previous mixing device developed by my colleague, Dr Tan. No examples of segmented flow microfluidic devices were published prior to the commencement of initial device design (Gunther, Khan, et al's first journal article on multiphase flow was published in mid-2004). Segmented, two phase flow had been achieved using similar designs, albeit using two liquids. Therefore the decision was made to utilise the direct T-junction used by Tan initially.

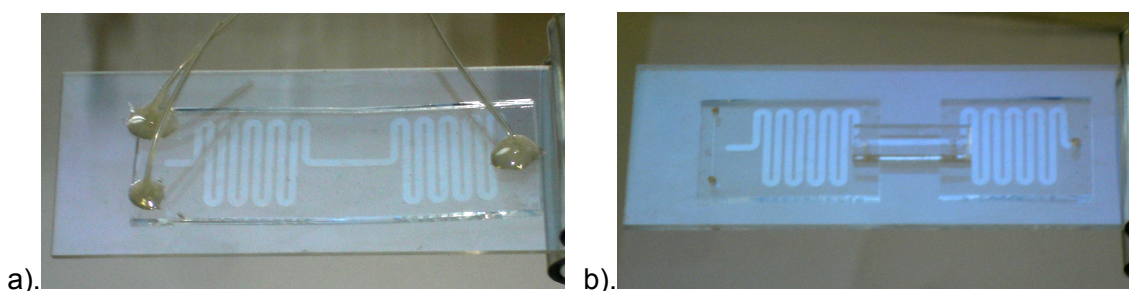


Figure 5.8 : Photographs of devices 1.2 and 1.3.

All tests were performed using the set-up shown in Figure 5.1 and commenced with the device being primed with degassed, deionised water. The valve controlling the flow of liquid into the device (henceforth known as the liquid valve) and the valve controlling the flow of gas into the device (henceforth known as the gas valve) were alternately opened and closed to inject fluid. Following each injection of gas or liquid a large proportion of each phase was not removed by the subsequent injection of the alternate phase. It was hypothesised that either a fine liquid layer remained on the channel wall or bubbles formed at the point of intersection of the PDMS wall and the trailing edge of the liquid on the wall.

The driving equation for the stability, and therefore the probability of break-up, of a meniscus is the Young-Laplace equation. Equation 12 is a version applicable to meniscus in closed channels [156].

$$\Delta P = -2\gamma \cdot \cos\theta \cdot \left(\frac{1}{w} + \frac{1}{h} \right)$$

Equation 12

Where

ΔP is the pressure differential at the meniscus between two phases,

w and h refer to the channel cross-sectional dimensions (m),

θ to the contact angle between the liquid surface and the channel wall (degrees) and

γ to the surface tension ($\text{N}\cdot\text{m}^{-1}$).

Increasing the pressure differential increases the force required to break the liquid menisci. Importantly, the Young-Laplace equation relates more to the geometry of the interface between the two fluids as both the channel dimensions and the contact angle affect the diameter of the arc formed by the curvature of the interface. Therefore while the channel dimensions alone were believed to be primarily responsible for the formation of the bubbles, the stability of the bubbles is attributable to both the dimensions and the hydrophobicity of PDMS.

The Young-Laplace equation does not allow *accurate* calculation of the minimum channel dimensions or desired liquid/solid contact angle for the segmented flow desired. Primarily this results from pressure driven flow distorting the shape of the fluid front (see Figure 5.9). The degree of distortion, of the menisci, from the theoretical curvature, increases as the pressure increases. However the Young-Laplace equation does serve as a guide to the effects of changing channel size and surface properties.

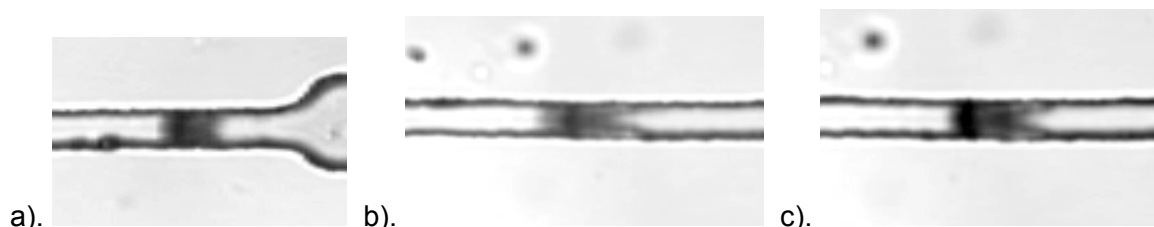


Figure 5.9 : Fluid front distortion resulting from pressure driven flow. a). The fluid at rest, b). demonstrating distortion at the rear menisci as the droplet moves and c). distorted even further as the pressure induced flow increases.

5.3.2. Design 2

Modifying design 1 by adding a flow restrictor to the gas supply channel resulted in design 2. Initial pressure control was limited to a gas regulator directly attached to the pressurised gas cylinder. The flow restrictor increased the fluidic resistance, for gas flow, by a factor of 10 and concomitantly decreased the velocity of gas entering the main channel by the same factor (Table 5.6). Thereby the pressure exerted on the meniscus and the likelihood of breaking the meniscus were reduced. The stability of the droplets *was increased*, however the bubbles continued to split into separate bubbles, with the majority of the bubble break-

up occurring at the T-junction and at the nozzle widening from the initial mixing channel to the main channel.

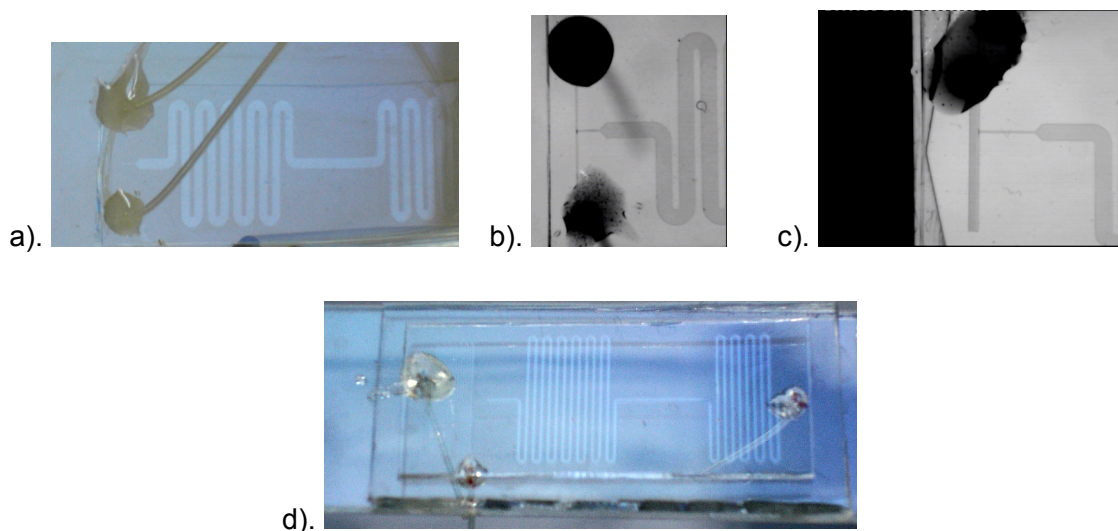


Figure 5.10 : a). and b). Device 1.2 (1 mm wide main channel and directly opposing T-junction), c). Device 2.2.1 (1 mm wide main channel and directly opposing T-Junction with gas flow restrictor) and d). Device 3.2.1 (300 μm wide main channel and directly opposing T-junction with gas flow restrictor).

	Devices		
	1.b	2.b.1	3.b.1
R_{total} (liquid)	1.051×10^{13}	1.051×10^{13}	6.910×10^{12}
Q	1.903	1.903	2.894
R_{total} (gas)	1.513×10^{11}	6.784×10^{13}	8.360×10^{11}
Q	132.19	0.295	23.92
R_{condition1}	4.78×10^{12}	7.25×10^{13}	3.639×10^{12}
Q = $v/10$	4.18	0.276	5.496

Table 5.6 : Flow resistances ($\text{kg/m}^4 \cdot \text{s}^2$), volume flow rates (Q in $\mu\text{L}/\text{min}$) and associated fluid velocities (v in m/s), at the end of the primary mixing channel, for devices 1 – 3 including fluid supply tubing. Flow rates calculated based on applied pressure of 20 kPa.

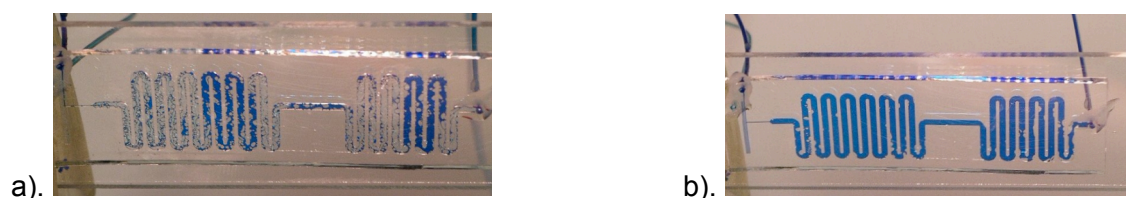


Figure 5.11 : Device 2.2.a with bubbles adhering to the side wall a). during experiment & b). following the experiment and flushing with degassed liquid. These images indicate how severely flow is restricted by the bubbles & how solidly they adhere to the channel walls.

5.3.3. Design 3

Further modifications were incorporated into design 3 to overcome the bubble break-up. The nozzle angle was increased, the flow restrictor was lengthened and the channel width was reduced from 1 mm to 300 μm . Design 3, and all subsequent gas collection PDMS devices, were further modified by bonding the structured PDMS to a blank piece of PDMS to create channels with uniform surface properties and hence contact angles.

Liquid apparently flowing into the gas supply channel was first observed in Design 3. This effect was observed many times during subsequent experiments with all segmented flow devices. *Preventing this effect was later determined to be VITAL to the success of developing a segmented flow vapour collection module for low concentration vapour analysis*¹. Therefore further evaluation of this effect appears throughout this discussion. No satisfactory hypothesis was determined for this behaviour and theoretically there should have been little flow of liquid into the gas supply channel. The back-pressure down-stream of the gas/liquid junction should have been much lower than that of the flow restrictor. Therefore, despite the high proportion of the total gas flow resistance exhibited by the flow restrictor (see Table 5.7), the liquid should not have completely filled the flow restrictor as was observed on numerous occasions during experiments from design 3 onwards.

Device Structure	Flow Resistance ($\text{kg/m}^4 \cdot \text{s}^2$)		Proportion of Total Resistance		Pressure Drop (kPa)	
	Liquid	Gas	Liquid	Gas	Liquid	Gas
Liquid bottle - Input	2.1×10^{12}	-----	30.2	-----	14.0	-----
Chip Input	1.6×10^{12}	2.8×10^{10}	22.7	3	9.4	19.3
Flow Restrictor	-----	7.5×10^{11}	-----	90	-----	1.4
Supply channels	3.1×10^{11}	5.5×10^9	4.4	0.7	8.5	1.3
Initial Mixing Channel	9.3×10^{10}	1.4×10^9	1.3	0.2	8.3	1.2
Main Channel	1.3×10^{12}	2.3×10^{10}	18.6	2.8	4.5	0.7
Waste Channel	1.6×10^{12}	2.8×10^{10}	22.7	3.4	0	0

Table 5.7 : Device 3.2.a – The calculated flow resistance and proportion of the total flow resistance of each flow structure of the device, including the supply and waste tubing. Also shown are the pressure applied to each fluid at the end of the respective flow structure. Calculation of the flow resistances are made by assuming a device depth of 100 μm and of the pressures by assuming an applied pressure of 20 kPa and a single fluid within the flow path.

1 It was so vital that the research into integrated valves was eventually begun to aid in preventing it.

5.3.4. Device 4

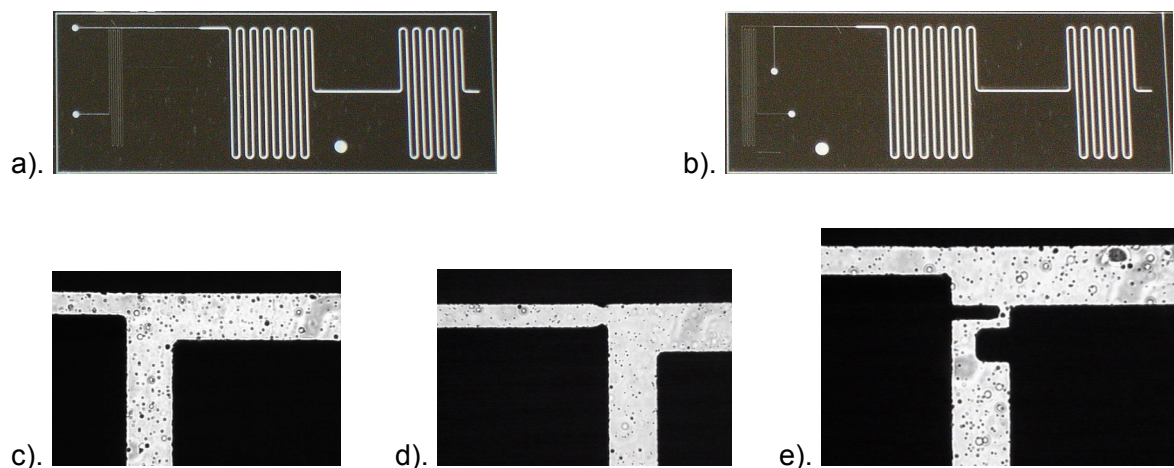


Figure 5.12 : The photomasks for design 4 intended to operate as a) a gas injector to a liquid stream and b) a liquid injector. c) to e) show representative junction designs for the gas injector.

Four new junction designs were developed for Device 4 based on a redesign of the original T-junction (three are shown in Figure 5.12 c). – e).). The various junctions were all tests to determine the most effective method of using microfluidic structures to passively control fluid flow.

The refinements to the junction and the flow restrictor did not prevent liquid flowing into the gas supply channel. The fine structures had insufficient detail to offer any resistance to the liquid flow. As shown by comparing Figure 5.13 a) and b), photomask resolution was the limiting factor in the device detail. Low resolution resulted in insufficient definition of the fine structural features used to specify the meniscus hold point. However comparison of equivalent devices manufactured from design 4 did prove that liquid injecting into a gas stream produced better flow characteristics at the liquid/gas junction than gas injecting into a liquid stream. Despite this, liquid was observed to flow into the gas stream in both cases.

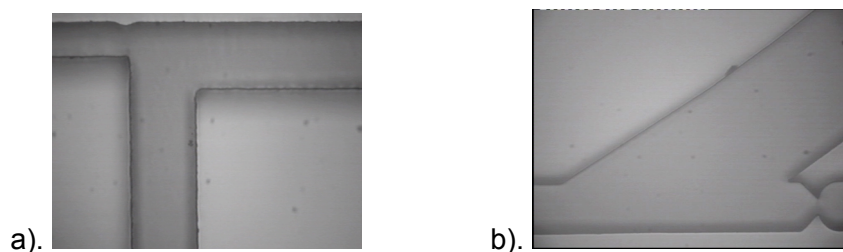


Figure 5.13 : Photographs of SU-8 moulds of a) Device 4.2.b (the photomask is shown in Figure 5.12 d) and b) Device 11.1.a. Illustrating the difference in the resolution of fine structures found in design 4 and design 11.

Break-up of gas and liquid segments was prevented for the first time by the use of lower pressures. A pressure meter (Druck, Linc., UK) allowed finer measurement of the gas pressure, while a hydrostatic head was used to provide low liquid pressures. Therefore

segmented liquid and gas flow was improved compared to previous devices, but was limited to a maximum of 10 cycles before both liquid and gas flow stopped altogether.

5.3.5. Design 5

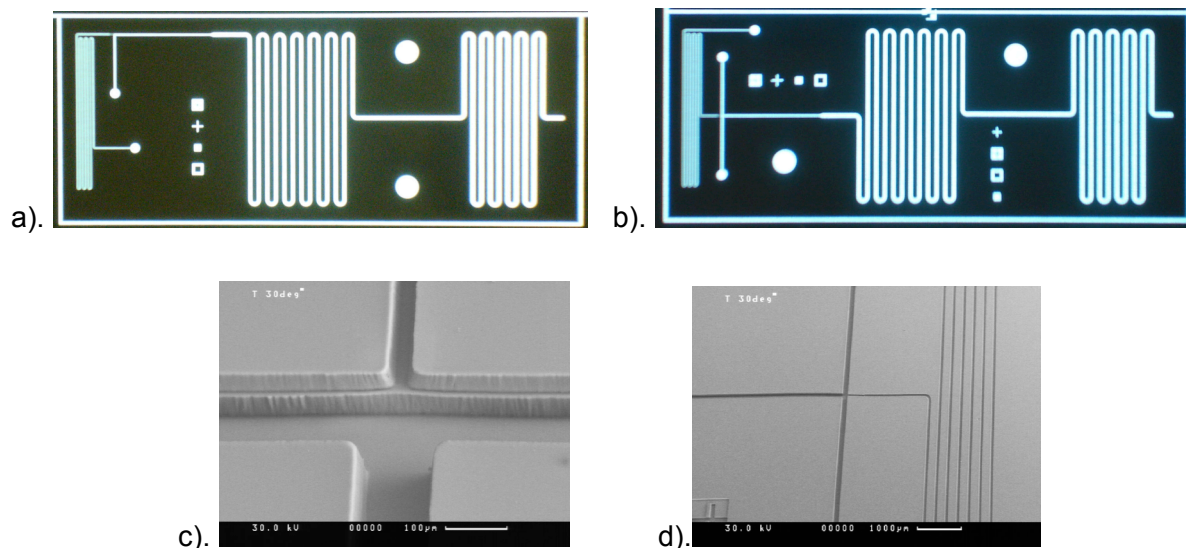


Figure 5.14 : Photographs of photomask 5a. a) and b). Full design for Devices 5a.1 and 5a.5 respectively. Scanning electron microscope (SEM) images of c). the junction and d). the supply channels and flow restrictor of the PDMS casting for Device 5a.5. The SEM images show the double depth nature of Device 5a.1, 5a.3 and 5a.5.

Design 5a (the 'a' being used to differentiate this photomask from a previous, unused photomask) was an attempt to utilise different methods to produce the effect for which Design 4 was designed, but failed to achieve: the prevention of liquid flow into the gas supply channel. Using double depth mould manufacture and a slightly changed gas supply channel exit design (as shown in Figure 5.14) overcame the limitations to feature definition observed in Design 4. Similar designs to 5a.5 (Figure 5.14 b.) had previously been noted in microfluidic multiphase flow devices [146]. However the majority had been used to create monodisperse droplets within a gas flow.

Pressure control was achieved as for Device 4 and video recordings of experiments undertaken using Device 5a.1 allowed results to be reviewed *in detail* for the first time. Accordingly discussion of the results will henceforth be more detailed.

Irregular, but frequent gas/liquid segmentation occurred under almost all experimental conditions. Liquid was observed to flow into the gas supply channel despite the severe flow restriction created by the reduced depth (Figure 5.15 a).). Device 5a.1 (liquid injector) was more effective than Device 5a.3 (gas injector) at achieving regular gas flow into the liquid flow. Small imbalances in flow resulted in Device 5a.5 (opposing liquid injectors) being difficult to set-up without bubbles remaining in one of the liquid supply channels.

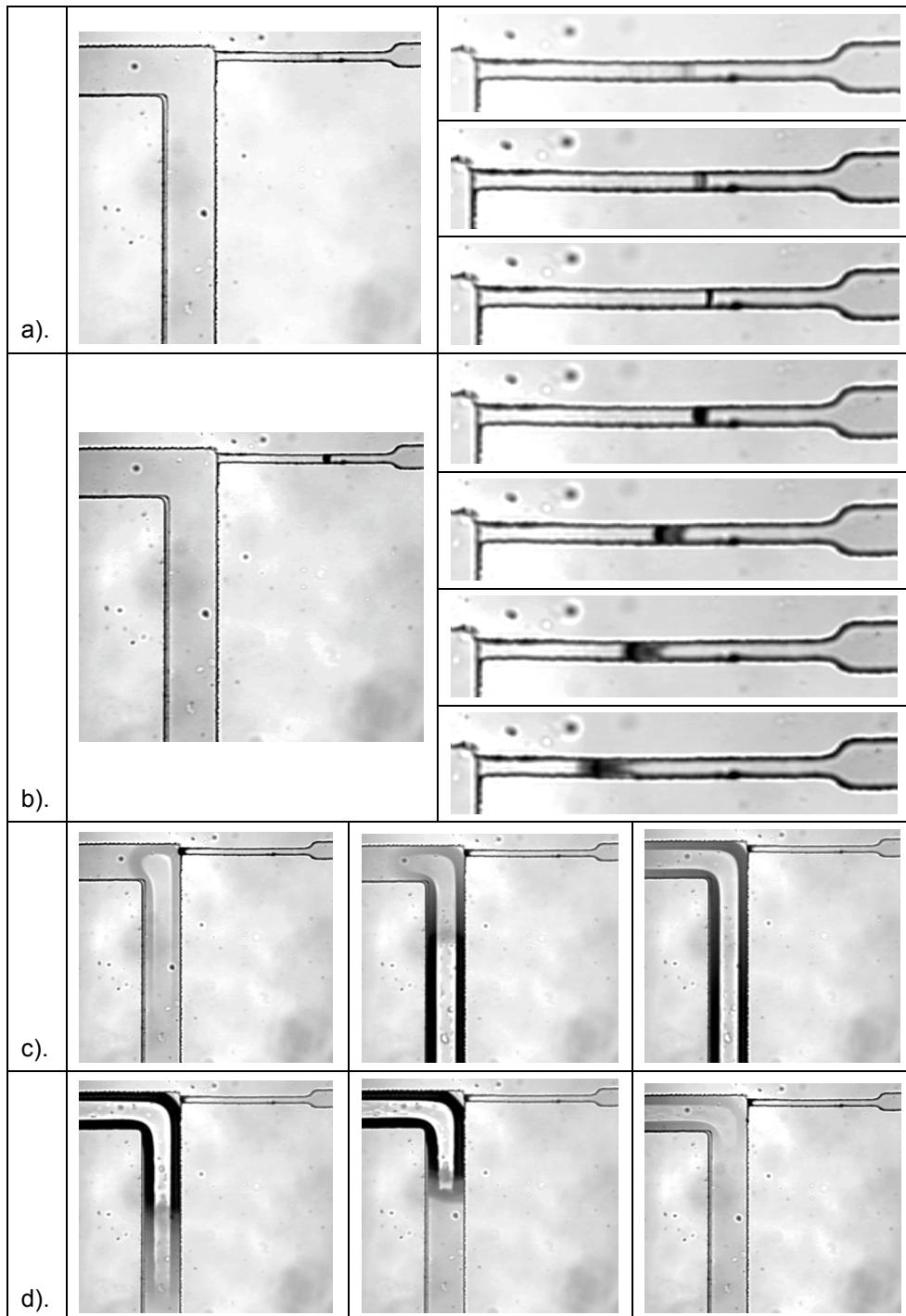


Figure 5.15 : Stills from video recording of experiments performed on Device 5a.1. a). Liquid flowing into the gas channel, b). Gas pushing the liquid out of the gas supply channel, c). Gas injection into the gas/liquid junction and initially flowing into the liquid supply channel before flowing into the main channel and d). liquid pushing gas out of the liquid supply channel and then flowing down the main channel before repeating the cycle.

The gas injection timing and meniscus movement at the gas and liquid junction indicates that the microfluidic structures and pressure ratio were not responsible for the gas/liquid segmented flow. It is believed that the liquid valve opening created a low pressure zone into which gas was drawn (Figure 5.15 c).). The gas was then pushed down the main channel, simulating gas/liquid segmentation (Figure 5.15 d).). Separating the gas supply

channel from the liquid flow at the gas/liquid junction allows any pressure variations resulting from external valving to be isolated to the phase in which they occur. Development of valves that could be integrated into microfluidic devices at the gas/liquid junction, as stated at the beginning of Section 3.1, resulted from this requirement.

5.4. Non-PDMS Devices

5.4.1. Modular Device

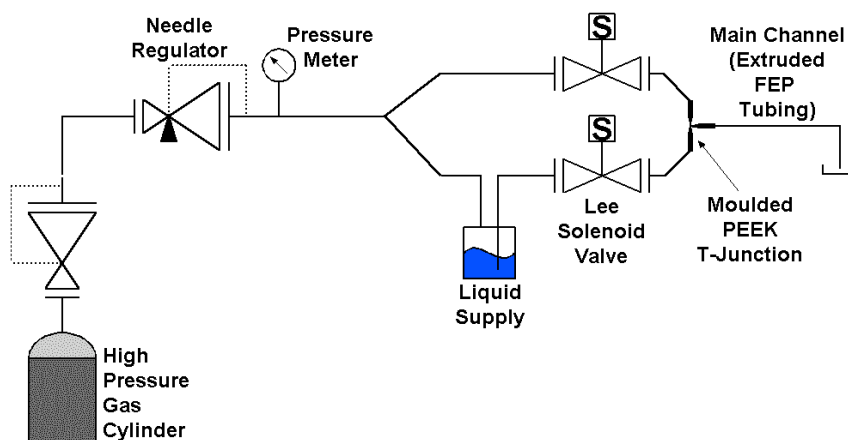


Figure 5.16 : Modular Device Set-up.

During the development and testing of integrated valves a number of gas collection designs were attempted¹. The majority were unsuccessful. A modular device for producing segmented flow was assembled and tested. The device (Figure 5.3 a.) was intended to utilise the smooth sidewalls of the FEP tubing and precision engineered PEEK T-junction to effect a basic microfluidic device without SU-8 processing or PDMS assembly.

Further consideration of the Young-Laplace law (Equation 12, Section 5.3.1) and possible influences on gas and liquid flow led to a desire for smoother channel walls than were available using current microfluidic gas collection manufacturing methods. The 4040 dots/inch photomasks provided a spot size of about 10 μm (see Figure 5.21 a.). As we have discussed, observation of gas/liquid menisci had previously displayed a low pressure start/stop behaviour that could not be explained by valve opening and closing. Menisci form to reduce the surface energy of liquid in droplets or surrounding gas bubbles. Changing the contact angle changes the pressure difference between the inside and outside of the droplet and therefore also changes the surface energy of the liquid. The start/stop behaviour exhibited was understood to result from the additive resistance of multiple individual menisci reaching positions at which the contact angle resulted in a surface energy minimum.

¹ Most of the devices tried were from ideas or designs for microfluidic gas collection modules that were unrelated to the original segmented flow proposal. For instance a PDMS/PZT device for foam generation or a miniaturised venturi gas scrubber manufactured from tubing and joined syringes were two of approximately five devices or ideas that were attempted.

Several components became available for use during the period of valve development: micro-dispensing Lee valves; miniature gas regulators (Type 91, Marsh Bellofram Corp, WV, USA) and another digital pressure meter. The FEP tubing (750 μm ID) and PEEK T-junction had much smoother sidewalls than were provided by previously cast PDMS devices. They were therefore ideal for testing the new components and the hypothesis regarding the effect of surface smoothness on segmented gas and liquid flow.

The Lee valves and the Marsh Bellofram miniature gas regulator were better able to finely control the flow of fluid. Lee valves did not exhibit the pumping effect that Neptune Research valves demonstrated due to the low fluid volume moved by the piston during opening and closing (Figure 5.17). The miniature gas regulator also demonstrated finer control and was more stable at low pressures. Finally, the digital pressure meter allowed accurate and continuous measurements to be made throughout an experiment, ensuring the stability of the pressure applied to the gas and liquid flow.

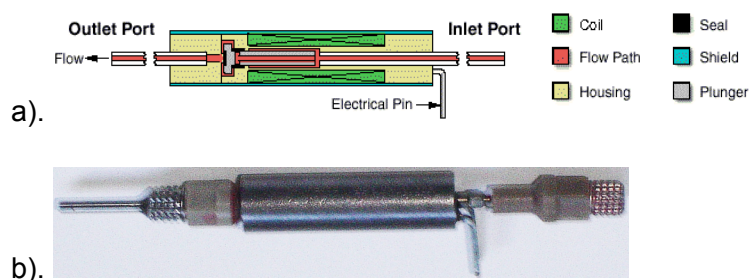


Figure 5.17 : a). Schematic of Lee valve internals and b). photograph of Lee valve with Nozzle attached to fluid outlet.

All experiments were conducted with the PEEK T-junction arranged with the gas and liquid supply tubes directly opposed. Initial experiments with the junction arranged to operate as a gas or liquid injector were determined to provide no difference in performance. Some start/stop behaviour was exhibited, especially when the applied pressure decreased below a critical limit. The critical pressure depended upon the opening times of the gas and liquid valves.

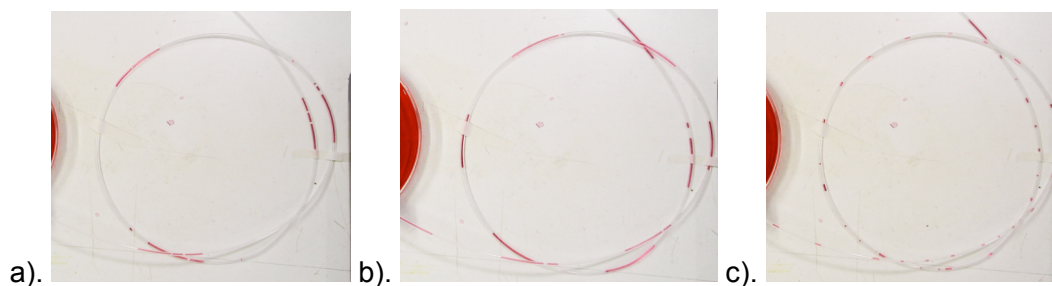


Figure 5.18 : Photographs of experiments performed, using the Modular design, showing the change as the valve opening times were varied. All photographs were from experiments performed at 15 kPa with the liquid, then gas being injected followed by a rest period. All times shown are in milliseconds. a). 500, 200, 1000; b). 500, 100, 1000; c). 50, 20, 1000.

Despite the start/stop behaviour, the experiments generally showed that the smoothness of the channels did allow more continuous flow. Several trends in the degree of both gas and liquid segment stability (Figure 5.18) and length variation (Figure 5.19) were observed as the valve timing was changed (Figure 5.18) or the pressure was increased (Figures 5.18 and 5.19). However the results of these experiments were specific to the modular device as later devices (design 12) using smaller internal diameter main channels were found not to exhibit similar behaviour.

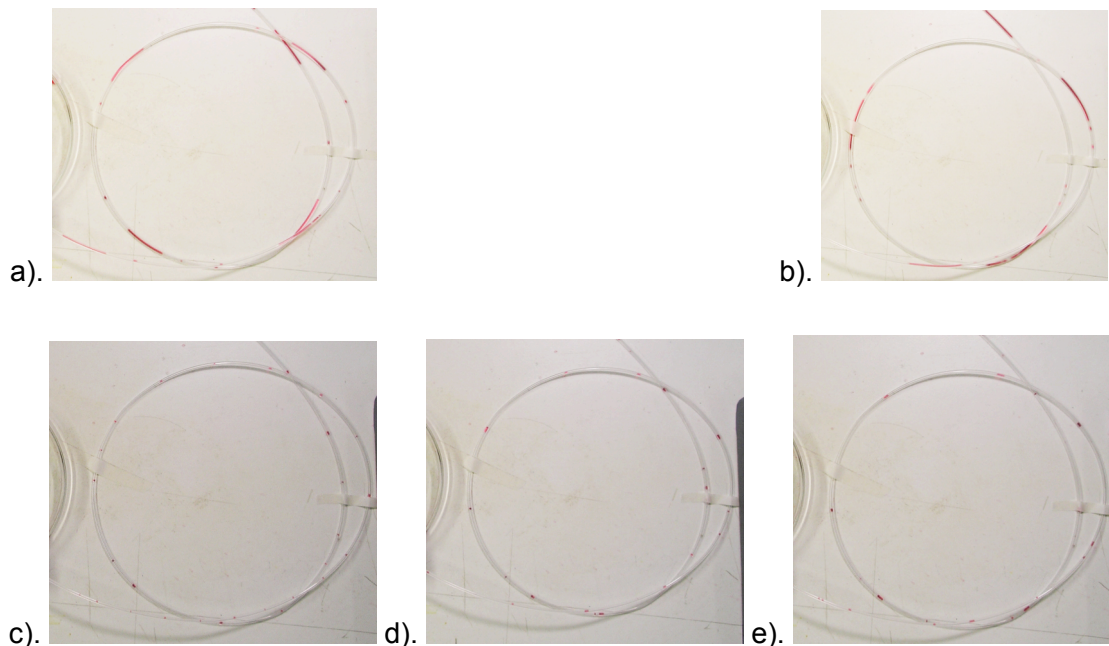


Figure 5.19 : Photographs of experiments performed, using the Modular design, showing the change as the injection pressure was varied. a). and b). were from experiments with injection timings of 200 ms (gas) and 500 ms (liquid) and applied pressures of 15 kPa and 20 kPa respectively. c), d). and e). were taken from experiments performed with timings of 200 ms (gas), 500 ms (liquid) and 1000 ms (rest) in that order and with applied pressures of 10 kPa, 15 kPa and 20 kPa respectively.

Following the discontinuation of integrated or microengineered valves, work continued on the modular design concept. However a transparent material, able to be rapidly prototyped was required for the junctions, as monitoring of the interaction between gas and liquid was essential for the production of new junction designs. Still deemed to be essential for the production of regular gas/liquid segmented flow, the design of the junction was the main focus of the all the following work on producing stable and regular gas and liquid segmented flow.

5.4.2. PMMA Micro-junctions

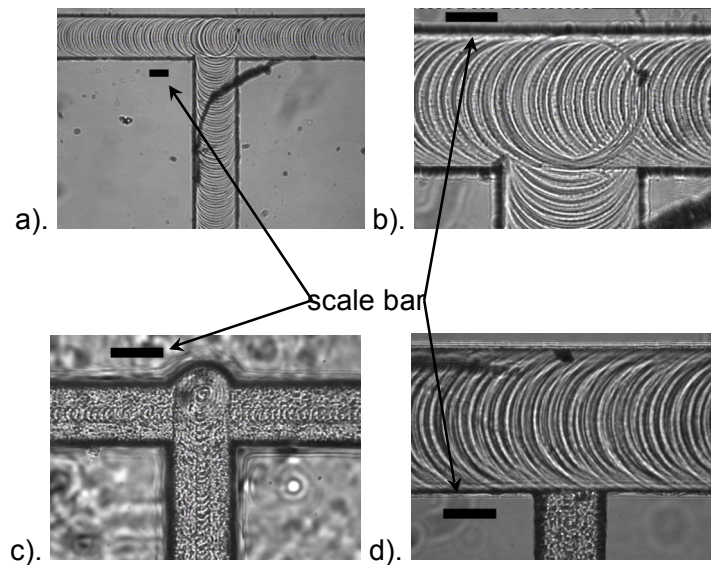


Figure 5.20 : Images of selected micro-junctions milled into PMMA. a). and b). Design 2, c). Design 3, d). Design 4. The scale bar = 100 μ m. Image a). was taken using a x3.2 objective while subsequent images were through a x10 objective. All dimensions can be found in Table 5.3. The faint lines between each channel result from milling one channel over the end of the preceding channel.

The next generation of devices were manufactured in PMMA (Figure 5.20). PMMA could be milled to produce smoother channel side walls (although the base of the channel was more uneven), than those of basic, soft lithographically patterned, PDMS devices (Figure 5.21). Casting of PDMS was unnecessary as PMMA devices were much less complex than previous PDMS devices so as to focus investigation on the flow of liquid and gas into the junction as the liquid valve opened and gas valve closed and vice versa. For instance: the main channel was removed, to prevent interference from back pressure, resulting from multiple menisci; and the flow restrictor was eliminated, as fine pressure control had become possible; and fine structures present at the junction were not included.

Valve attachment to the devices was one of the most important aspects of the PMMA junction designs. Reducing the length of the supply channels was used to decrease the volume of gas, between the gas/liquid junction and the valve seat, and therefore the amount of gas that could be compressed. Movement of liquid into the gas supply channel should thus be decreased.

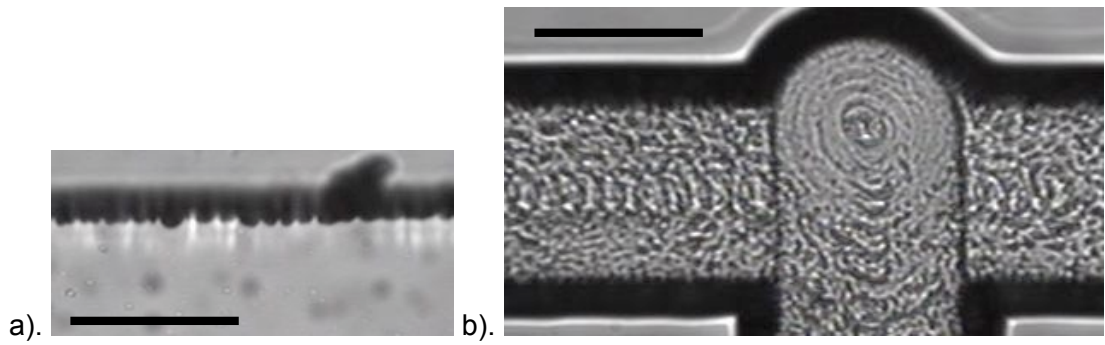


Figure 5.21 : a). PDMS channel wall (using low resolution photomask) and b). PMMA channel wall (scale bar = 100 μ m).

Two different junction designs were tried, a direct T-junction and an angled injector to examine the hypothesis that injecting fluid in the direction of flow would produce more regular fluid flow behaviour. Three variants of the T-junction (Figure 5.20) and one of the angled injector junction were manufactured to test the effect of changing the channel width and depth. After brief testing of all four devices the angled injector was determined to provide the most regular behaviour. No visual evidence of the comparative tests was obtained. Although all T-Junctions were tested in all system arrangements, liquid injector, gas injector and directly opposing, the liquid injector arrangement of the angled injection junction gave the best flow characteristics.

The angled injector design in most cases produced regular injection times and always demonstrated recurring fluid flow patterns, while fluid flow into the T-Junction was irregular in all system arrangements. Angled low pressure (below about 5 kPa) injection of liquid into a gas stream was reliable (although still dependant upon the timing used) while at low pressures the angled gas injector did not operate. Both the gas and liquid injector arrangement, of the T-junction, produced small droplets and bubbles within the alternate fluid's supply channel. While generally expelled, the extra menisci resulting would, in a device containing a main channel, have resulted in massively increased flow resistance.

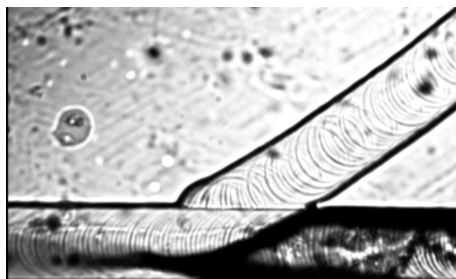


Figure 5.22 : Gas streaming effect as exhibited with fast gas and liquid flow rates.

Experiments were performed, on both the angled and T-junctions, examining the effect of utilising the fast switching times of Lee valves (to obtain short valve opening times) and the independent fluid pressure control (to monitor the effect of changing gas and liquid pressure separately). The investigation into short (less than 100 ms) valve opening times found that they provided insufficient time for stable flow to develop. In contrast, changing the pressure to each fluid independently, while useful for broad experimentation, did not demonstrate any major changes in flow pattern as the pressures were changed. A gas 'streaming' effect (Figure 5.22) was observed in the angled injector design when operating in gas injection mode. However only the degree of the gas 'streaming' effect varied.

From the results of experiments performed on the angled injector and T-junctions, a number of conclusions were drawn that led to device and experimental design changes. A narrower channel (channels in the angled injector device were 250 μm in diameter) was proposed so that the liquid being injected would contact the opposite wall and break the flow of gas faster, ensuring a cleaner slug formation. The narrow channel for the junction therefore required a nozzle for expansion to a wider channel to allow a longer observation period of the droplets and bubbles¹. Although a number of alternatives were considered (discussed further in the next section), PDMS was the only clear alternative substrate in which a smooth nozzle could be engineered. Liquid flow into the gas supply channel was also more limited than had been observed in previous devices. Structures such as those investigated previously (for examples, see Figure 5.12) were therefore potentially effective enough at this point to prevent liquid flow into the gas channel.

Experimental methodology was modified by imposing minimum and maximum testable valve timings and pressures. The PMMA devices were compared briefly by testing each device. After determining which produced the most reliable gas and liquid injection over a combination of valve times and pressures, that device was examined thoroughly to establish operating limits. Device 10 was compared briefly, as for the PMMA device, to determine the most consistent gas and liquid injection times *and volumes*. Understanding that better resolution and structural definition was necessary, the results of that comparison led directly to the development of Device 11.

¹ Purely because the volume of the bubbles and droplets will not change that much despite using narrower channels. A narrower channel just means that the fluid spends less time within the viewable region of the microscope.

5.5. Lee Valve Controlled PDMS Devices

As all devices presented in the figures and text for photomask designs 10 to 12 are presented in separate sections, the designation for each device is abbreviated to aid the reader. Thus a device labelled 'Device 1.c' in Section 5.5.1 below, actually refers to Device 10.1.c. However the original designation, '10', is removed as it is self-evident, being in the section for devices manufactured from Design 10. Where a device is referred to in a section other than that in which its design is presented, the full designation is provided.

5.5.1. Design 10

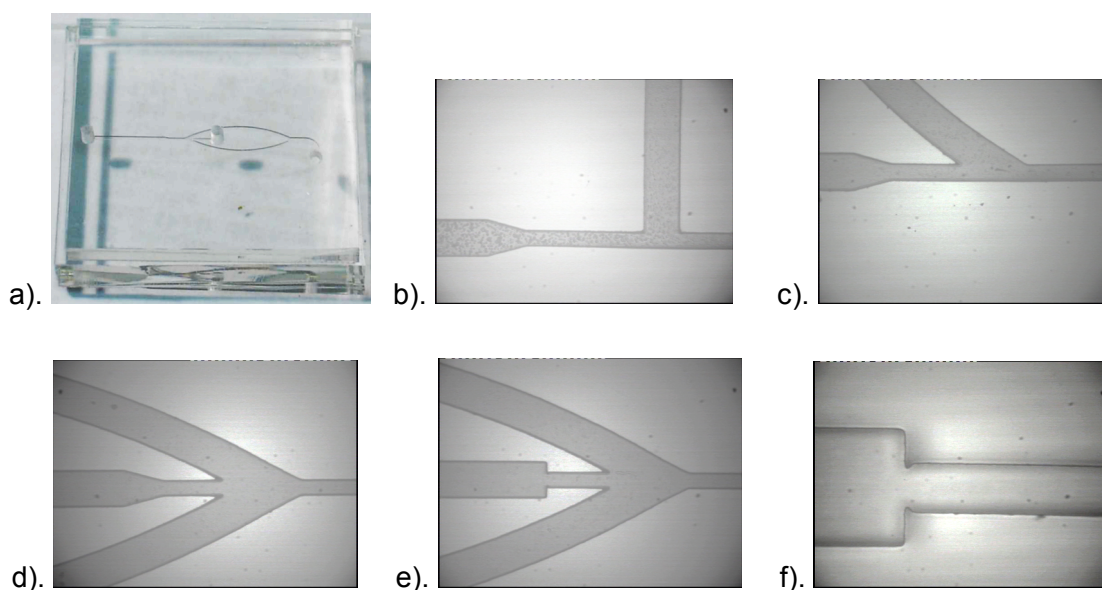


Figure 5.23 : a). Photograph of Device 2.c indicating the general design of the devices following manufacture, that is with the push-fitted fluid connections, the fluid supply and the micro-junction designs only included. The total dimensions of the device were 18 mm x 18 mm. Photographs exhibiting the variety of fluid supply designs investigated with b). Device 1.a, c). Device 1.c and d). Device 2.c shown. d). and e). Photographs of the two main junction designs produced and f). A close-up of the second junction design (Device 2.d shown).

Design 10 was a hybrid series of devices in which concessions between the ease of rapid prototyping and the low resolution of the photomasks were necessary. As stated in Section 5.4.2, the nozzle expanding the junction channel into the mixer channel required smooth sidewalls. Several alternatives, including hot-embossing, milling parallel stripes (Figure 5.24) and using UV photopatternable PMMA were all considered. PDMS was eventually settled on as the best substrate. The limitations of the photomask resolution were recognised and devices designed to include structures only requiring low resolution. In designs incorporating fine structures (1.b and 2.d. See Figure 5.23 f.) the detail necessary to prove the operating principle was low and in both cases was sufficient.

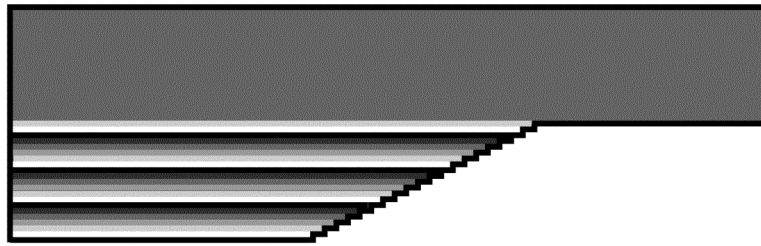


Figure 5.24 : Planned design for the manufacture of a PMMA nozzle using parallel milled stripes. The image demonstrates the manner in which the initial channel would then be widened, with the striped effect indicating a 4 μm lateral shift in the position of the milling tool, before travelling parallel to the original channel (thereby widening it).

As we have discussed, the results of the experiments performed on the PMMA junctions determined the best experimental conditions for the Device 10 junctions. A preliminary test was undertaken to confirm that the short valve opening times were also unsuitable for the PDMS junctions. As before, the short valve opening times led to droplet break-up while the long valve opening times produces more consistent droplet production. At very low pressure (≈ 2 kPa), for both short and long valve opening times, the droplets that formed at the junction were not cleared from the device fast enough to prevent the build up of back-pressure. The ‘pinning’ (brief immobilisation) of menisci to the channel wall was clearly observed, indicating that the surface roughness significantly influences the fluid flow (Figure 5.25).

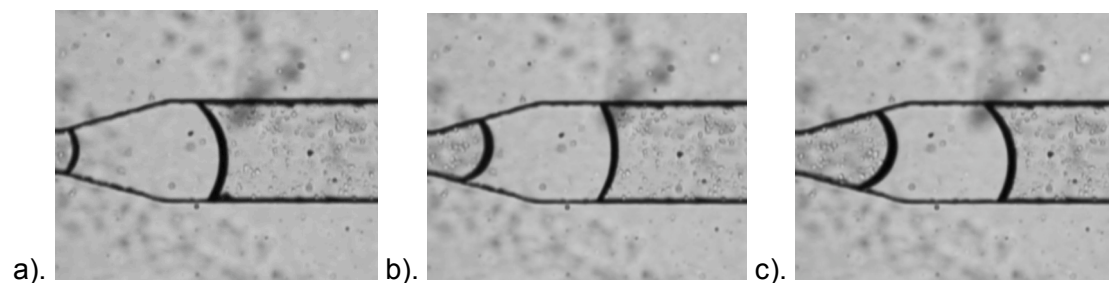


Figure 5.25 : Meniscus ‘pinned’ to the channel wall by the roughened surface. a). Initial image of moving droplet, b). Start of pinning of the trailing meniscus, and c). the trailing bottom edge of the meniscus still remaining stationary as the droplet continues moving to the right (with the meniscus changing shape to accommodate the ‘pinned’ edge).

Tests on Device 1.a at low (4 kPa) and mid (8 kPa) pressures led to all following devices being tested at 4 kPa. As the experiments were conducted as a comparative test the absolute effectiveness of each device and effectiveness at producing regular gas and liquid flow and preventing liquid from flowing into the gas supply channel are not initially detailed. All experiments were conducted under the pressures and timings shown in Table 5.8.

Device	Pressure	Comparative Rating
1.a	4 kPa, 8 kPa	8
1.b	4 kPa,	3
1.c	4 kPa	2
1.d	4 kPa	7
2.a	4 kPa	5
2.b	4 kPa, 6 kPa (necessary to actually achieve smooth flow)	5
2.c	4 kPa	3
2.d	4 kPa	1

Table 5.8 : Device 10 experiments. All valve times were Liquid = 500 ms, Gas = 200 ms, Rest = 1000 ms.

Decreasing comparative ratings indicate improving performance. Equal ratings denote no differentiable difference in performance, although this may be due to an improvement in one aspect with a simultaneous deterioration in another. For instance liquid flow into the gas supply channel is greater in Device 2.a than Device 2.b, but the gas flow in Device 2.b does not always start immediately when the valve is opened.

Both Device 1.c and Device 2.d, the two best performing devices of the eight designed, presented similar results. Despite the poor structural resolution, Device 2.d was judged to be the best device produced. The flow patterns of liquid injected into the junction were initially towards the main channel and only towards the end of the injection time, into the gas supply channel. The small structure acting as a contact angle based passive valve (more detail is provided in the description of Design 11) was gratifyingly effective at preventing the flow of liquid further into the gas supply channel. As both Device 1.c and Device 2.d were designed with similar structures, both were used as bases for the multiple variants of Design 11.

5.5.2. Design 11

All junctions in Design 11 were designed to utilise the principal of a sudden change in contact angle 'pinning' the meniscus and acting as a passive valve. Leu and Chang (2004) [157] characterise valves operating under the same principles, referred to by them as capillary stop valves, for use on a CD platform¹. The various devices are test structures, as were all devices manufactured from Design 10, developed to examine the effect of slight changes in the original basic structure.

¹ A CD microfluidic platform uses centripetal force as the pumping mechanism and passive, one shot valves with internal fluid reservoirs and external detection.

Design 11 utilised a high resolution (64,000 dots per inch) photomask to achieve better structural definition. The availability of reasonably priced, high resolution, acetate photomasks had only recently been discovered at this stage, hence the late inclusion of this very useful tool.

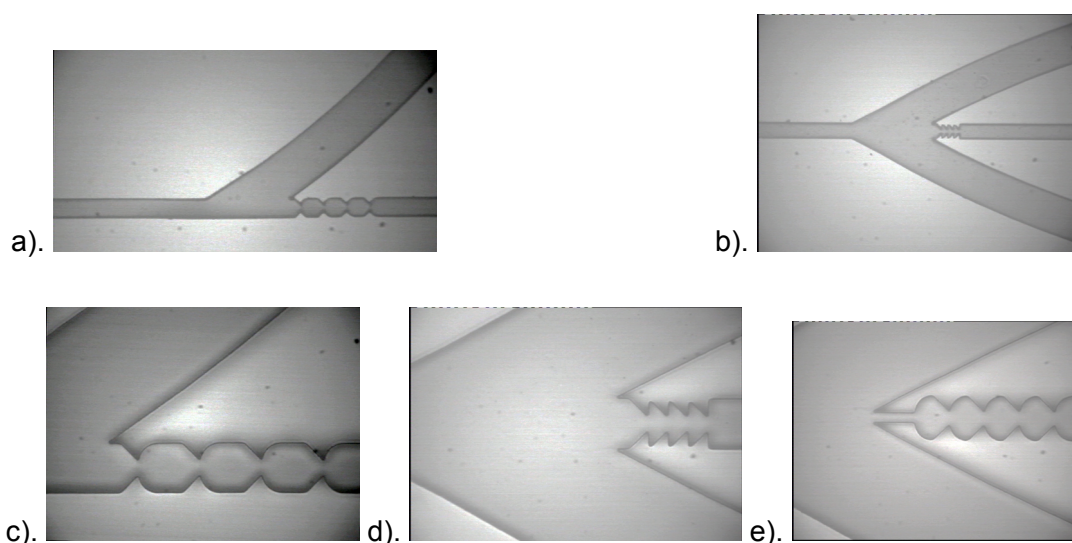


Figure 5.26 : Photographs of moulds for Design 11, a). General design of mould for devices of designation 11.1, b). General design of mould for devices of designation 11.2. c). to e). Representative moulds indicating the level of detail and slight structural variation in the toothed structures found in c). Device 1.c., d). Device 2.b and e). Device 2.c.

Device	Pressure	Comparative Rating
1.a	4 kPa, 8 kPa	2
1.b	4 kPa,	8
1.c	4 kPa, 8 kPa	3
1.d	4 kPa	5
2.a	3 kPa, 5 kPa, 8 kPa, 12 kPa	1
2.b	5 kPa, 6.5 kPa, 8.3 kPa	7
2.c	2 kPa, 5 kPa, 8 kPa, 12 kPa, 15 kPa	6
2.d	5 kPa, 8 kPa, 12 kPa	4

Table 5.9 : Device 11 experiments. All valve times were Liquid = 500 ms, Gas = 200 ms, Rest = 1000 ms.

A mixture of single and multiple passive valves, forming ‘jaw-like’ structures, were designed. Other modifications include the smooth curve at the fluid entrance side of the valve structure, to allow easier removal of solution if the valve does ‘burst’. For experiments in which the liquid penetrated the gas supply channel, meniscus movement was slowed slightly over the structures in Devices 10.1.c and 10.2.d. The movement of the meniscus is governed by pressure, rather than the speed of the liquid flow. Despite this, the introduction of a structure that created a back-pressure against the meniscus *did* slow the meniscus

movement, at least briefly. Therefore the use of multiple passive valves was investigated to gradually slow then stop the penetration of liquid into the gas supply.

The original aim of the research project was the development of an *analytical* instrument. An analytical instrument requires precise control over fluid volumes and solution concentrations. If the valves do stop liquid flowing into the gas supply channel (as shown in Figure 5.27), then designing junctions with the valve structures in close proximity, for examples see Devices 1.b, 2.c, reduces the difference in droplet volumes.

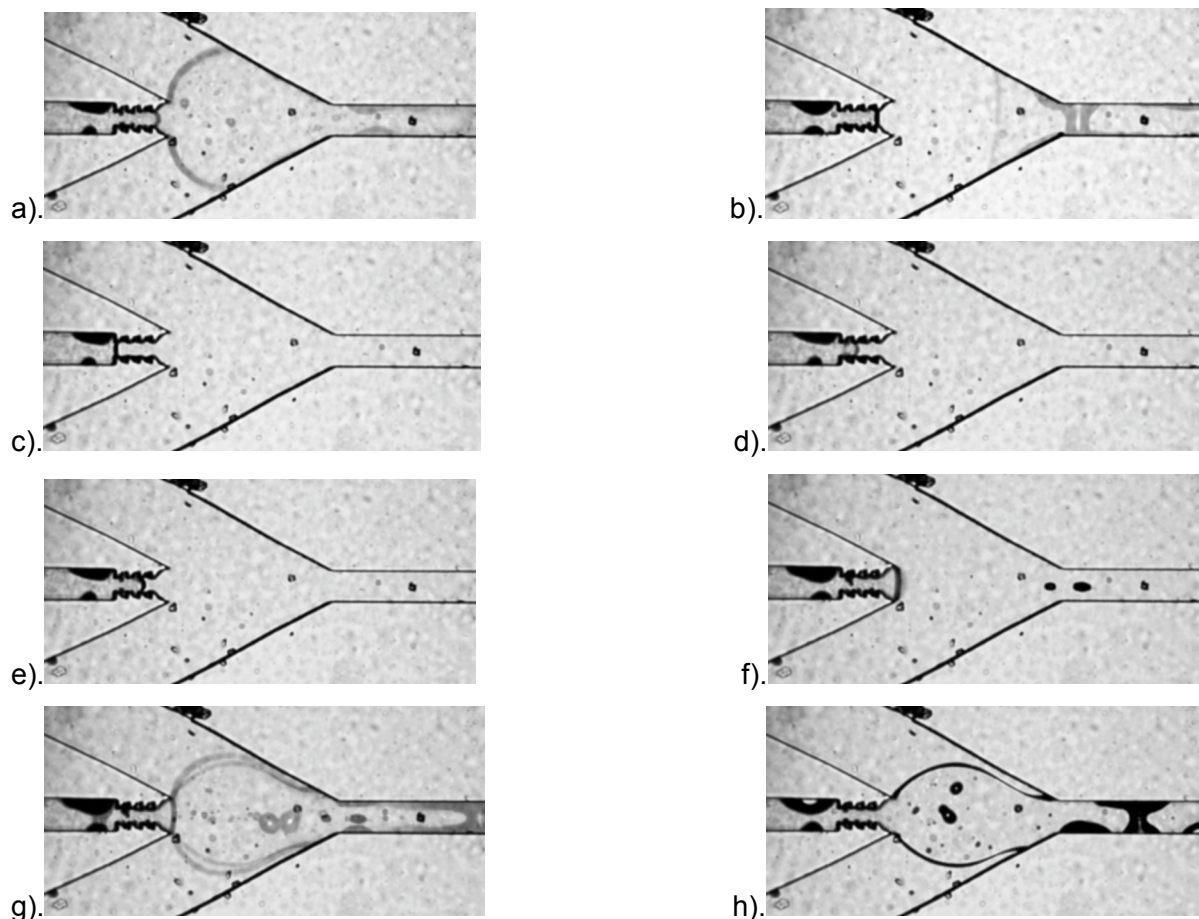


Figure 5.27 : Stills from experiments conducted on Device 2.b. The series of images comprise one cycle and, as shown by images b). and c). the passive valve structures do operate as designed. However if the valve structures are filled with liquid, then the liquid flow will bypass the valve.

Design 10 was used primarily to define the best flow structure and, partially, the best junction. In the same manner, design 11 uses the flow structures to allow refinement of the junction design. The junction designs Device 1.a to 1.d were replicated in Device 2.a to 2.d. In a comparative test of devices with equivalent junctions, that is Device 1.a with Device 2.a, Device 1.b with 2.b, etc, Device 11.2 performed better than the equivalent Device 11.1, in almost all (Table 5.9).

Two predominant features, in the junction designs, adversely affected the liquid flow patterns within the gas/liquid junction. Firstly, the placement of multiple valve structures very close together decreased the efficiency of the individual valve structures. Secondly, the difference in the entrance to the gas supply channel was the primary reason why Device 11.2 tended to be more efficient than Device 11.1.

Individual valve structures were capable of ‘pinning’ even a distended meniscus (Figure 5.28 a).). The removal of liquid from ‘burst’ valves was never completely effective and therefore placing two valve structures close together forced the liquid to be pushed closer to the top of the structures (compare Figure 5.28 b). and c).). A distended meniscus is more likely to contact this liquid and therefore more likely to merge, bursting the valve. Separating multiple valve structures increased their individual efficiency.

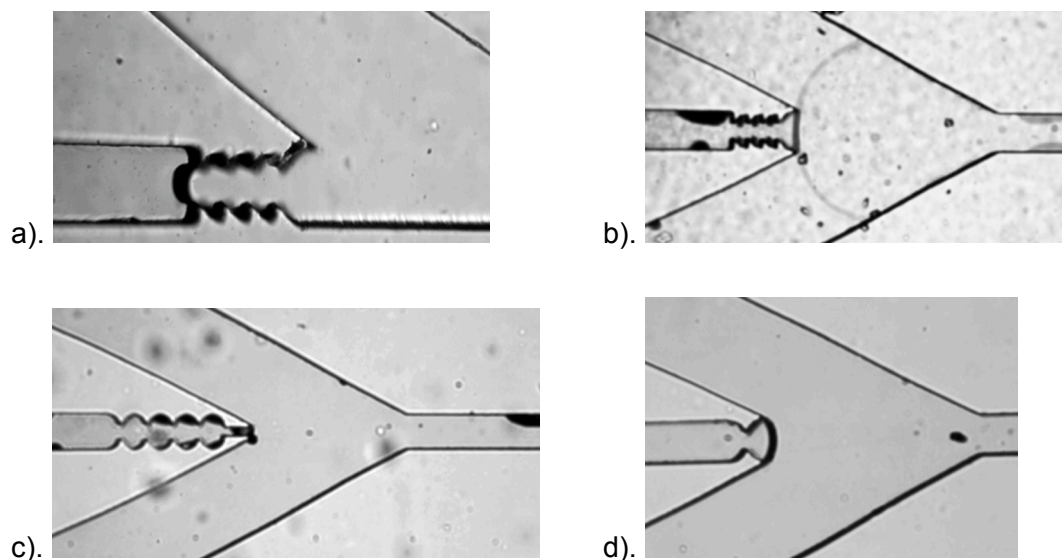


Figure 5.28 : a). Distended meniscus ‘pinned’ by a single valve structure, Liquid shown behind ‘burst’ passive valve with b). contiguous second valve structure (Device 2.b) and c). without (Device 2.c), d). gas supply channel entrance on Device 2.a acting as a passive valve.

Finally, the clearly defined gas supply channel entrance of Devices 2.a, 2.b and 2.d function as another, contact angle controlled, passive valve. Figure 5.28 b). clearly illustrates this effect. The influence of the gas supply entrance design is demonstrated by the fact that Device 2.c (Figure 5.28 c).) is the only device with dual liquid injection channels to be judged as performing less reliably than the equivalent single liquid injection channel device.

5.6. Segmented Flow Devices

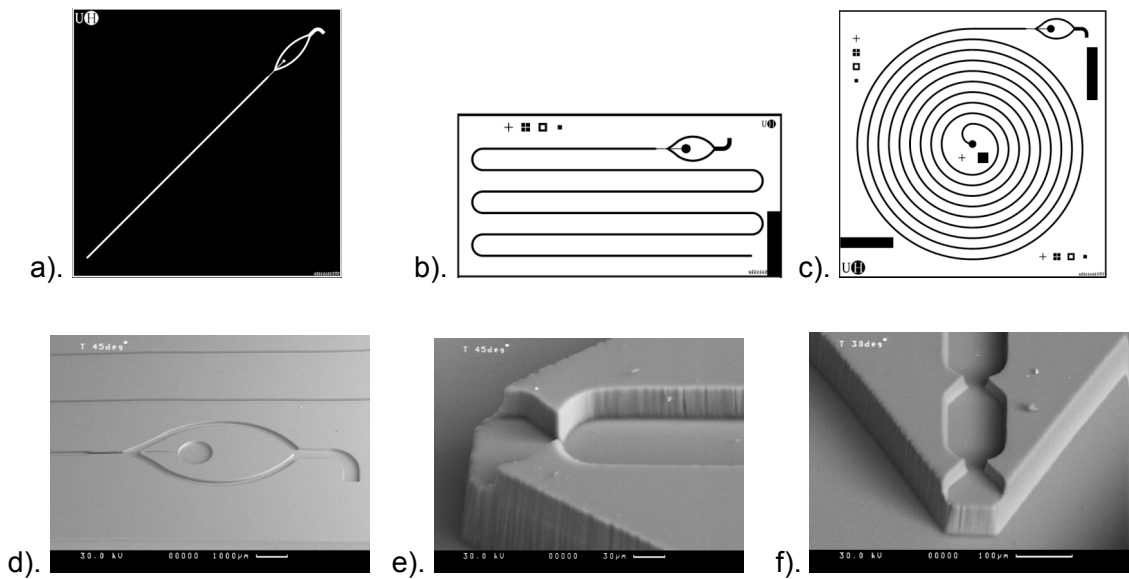


Figure 5.29 : General photomask design a). 1.x, b). 2.x and c). 3.x. d). SEM of the supply channels and micro-junction on Device 2.1. SEMs of e). the junction and passive valve structures of Device x.a and f). Device x.b.

Design 12, the final generation of microfluidic device designed for this project, finally incorporated the gas/liquid junctions within possible working structures. Curving the fluid entrance side of the valve structure was, as planned in Device 11, more effective at removing liquid if the valve burst. This was therefore included in the design of the valves in Device 12. The use of multiple valve structures was also effective, but including more than two was impractical due to the necessary separation between the structures (Figure 5.29 e). and f).). To allow testing of the junctions with increasing numbers of menisci, three different main channel designs were also proposed (Figure 5.29 a). to c).).

Finally, a triple depth structure was used in an attempt to keep the height to width ratio of both the gas supply channel and the main channel close to one. As both the top and bottom pieces of PDMS were structured, careful alignment over the entire device during the assembly process was necessary.

The ability of Device 12.1 to produce segmented flow was examined briefly. A design incorporating a junction attached to a 35.5 mm main channel running diagonally across a chip, it possessed the shortest channel of the three main designs. The behaviour was therefore expected to be similar to that of the test junctions. Even two liquid segments being present in the main channel at the same time was sufficient to slow the flow of liquid and gas drastically. Segmented flow only occurred when the liquid droplet was completely flushed from the short main channel before the next segment was injected. High pressures

were therefore necessary. Even increasing the gas injection time to 10 times the liquid injection time was unsuccessful.

Timing (ms)		Pressure		Segmented
Liquid	Gas	Liquid	Gas	
500	200	3.15	6	
"	"	3.29	5.11	
		5.81	10.86	
500	500	3.10	5.85	
"	"	"	8.40	√
		4.32	7.62	√
500	1000	2.23	4.7 – 4.95	+
		2.30	5.82	
		4.28	8.05	√
500	2000	4.34	7.37	√
		5.42	7.3 – 7.4	√
		6.66	7.36	
			7.90	+

Table 5.10 : Experimental conditions under which Device 2.a was tested, with the tests in which segmented flow was observed indicated by a √, and those in which stable, but irregular segmented flow occurred indicated by a +.

Device 12.2 was tested next, despite the results of tests on Device 12.1 indicating that it would require even higher pressures to produce segmented flow.

Tests of Device 2.a demonstrated successful production of segmented flow for the first time (Figure 5.30).

Table 5.10 indicates that valve timing is not a strong indicator of the pressures under which segmented flow can be generated in Device 12.2. However analysis of the photographs of successive tests in which segmented flow was observed, as shown in Table 5.11, show that the volume of the bubbles and droplets only varied by about 10 % over the length of the tubing. The Droplet and bubble sizes were calculated using the coordinate system assigned to each photograph by the processing software (Paintshop Pro, Corel, UK). As the actual droplet and bubble sizes vary slightly, the standard deviation and the ratio of bubble to droplet size are therefore more indicative of the stability of the fluid flow over a range of valve opening times and applied pressures.

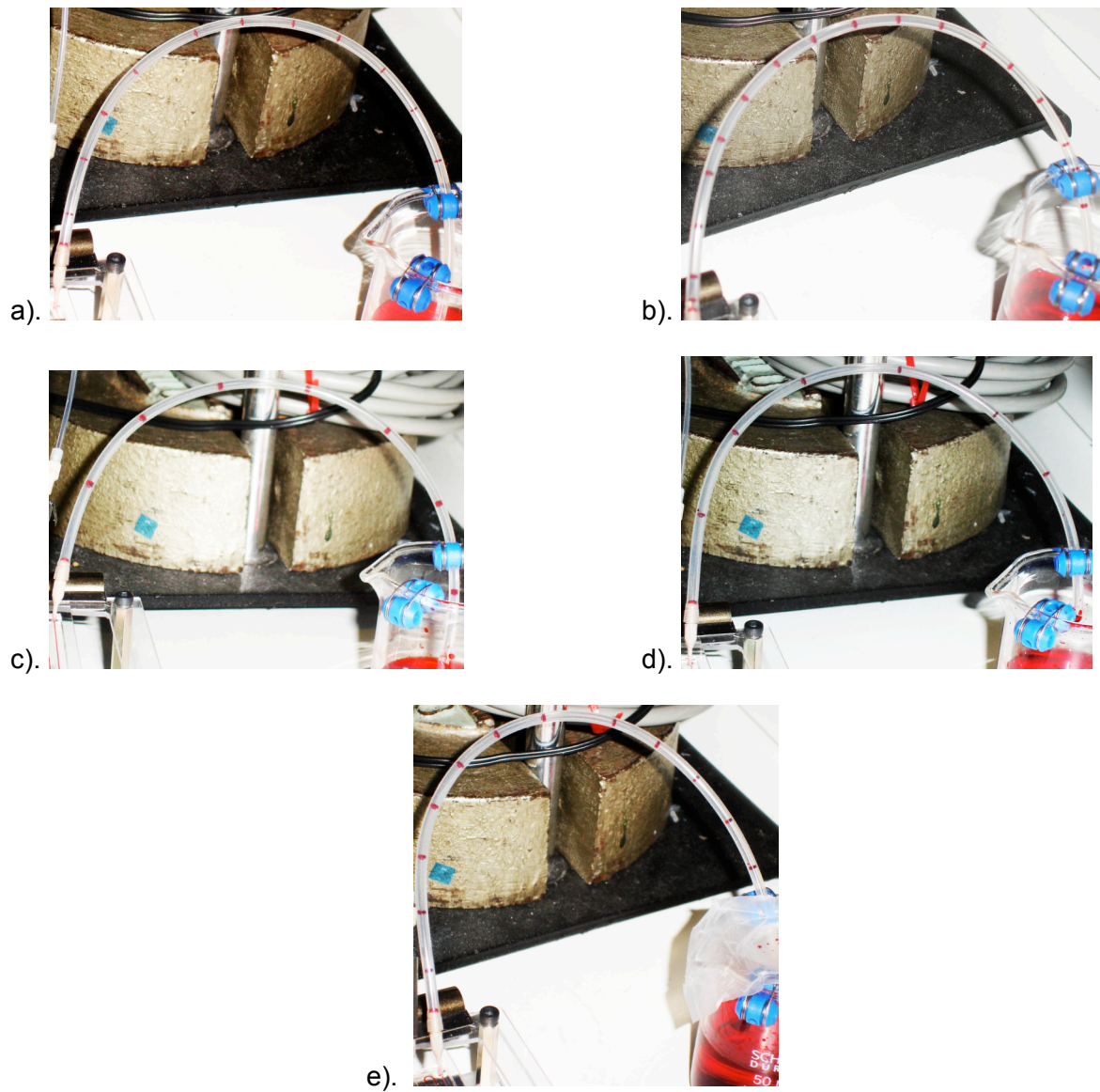


Figure 5.30 : Photographs of the waste tubing (leading from the main channel of Device 2.a) demonstrating segmented gas and liquid flow. Each photograph corresponds in turn to an experiment performed under the conditions shown in Table 5.11.

Timing (ms)		Pressure (kPa)		Drop Size (pixel)		Bubble Size (pixel)		Ratio
Liquid	Gas	Liquid	Gas	Average	σ	Average	σ	
500	500	3.10	8.40	6	2	213	29	34
500	500	4.32	7.62	12	2	161	18	14
500	1000	4.28	8.05	17	1	302	9	18
500	2000	4.34	7.37	8	1	305	37	37
500	2000	5.42	7.3 7.4	16	2	261	16	16

Table 5.11 : Experimental conditions under which Device 2.a was tested.

Each test was performed for a minimum of 15 minutes to ensure that the gas and liquid segmented flow was stable and not a temporary effect. Multiple repeats of each test were

also performed to ensure that the stable, regular segmented flow was not a chance occurrence.

Device 2.a was remade without a hole drilled into the PDMS for the waste channel. The end of the device was then cut diagonally, leaving the end of the main channel exposed. By drilling into the end of the channel (Figure 5.31), using the main channel as a guide, nylon tubing (250 μm ID) could be accurately inserted onto the end of the main channel, forming an hermetic seal with the surrounding PDMS. The flow of liquid and gas from the main channel into the nylon tubing was smoother than that previously occurring into the waste channel (Figure 5.32). *Initial tests on the device indicated that the modified Device 2.a was at least equally effective at producing segmented flow as the original Device 2.a was.*

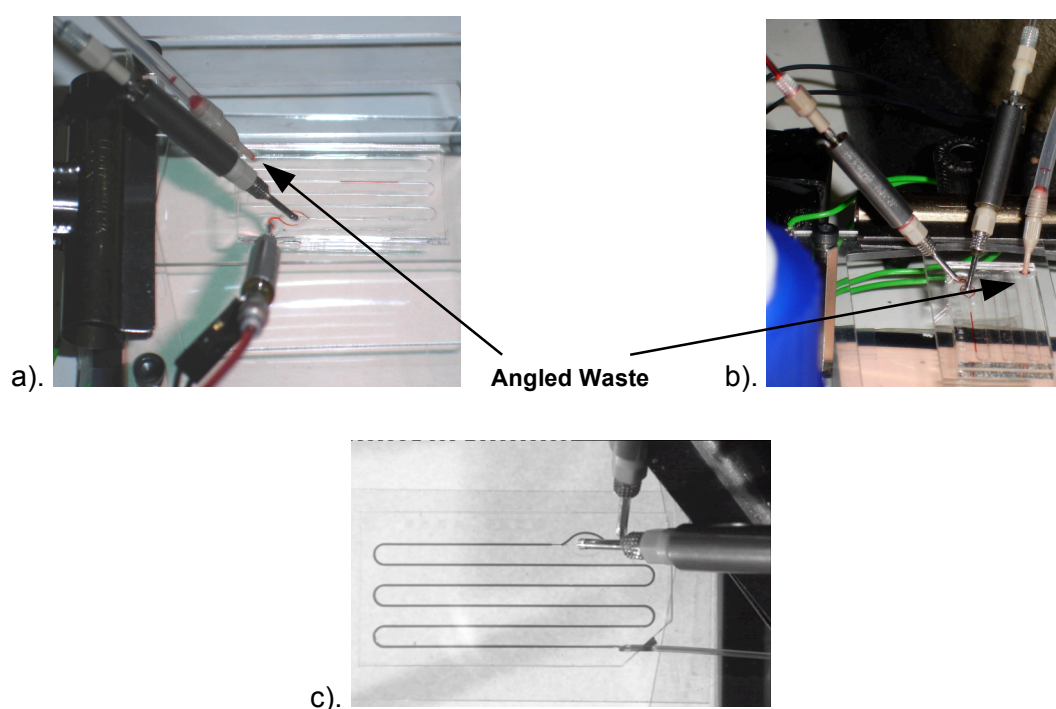


Figure 5.31 : The changing methods in which the tubing was connected to the end of the microengineered channel. Original fluid connection arrangement of Device 2.x a). Side view and b). Top view. c). Modification of the fluid connection for Device 2.a.

The modification to Device 2.a removed the possibility of the angled connection of the waste channel to the device being responsible for no consistent pattern, of either valve timing or applied pressure, producing segmented flow. Unfortunately a rapid, severe change in the direction of fluid flow caused the liquid to collect at the entrance to the waste channel. Limitations in the design of the connectors meant that the diameter of the waste channel was twice the width of main channel. The fluid collected at the entrance only moves into the waste channel once sufficient volume has collected to entirely block the entrance to the waste channel to a depth of at least 2 – 3 mm.

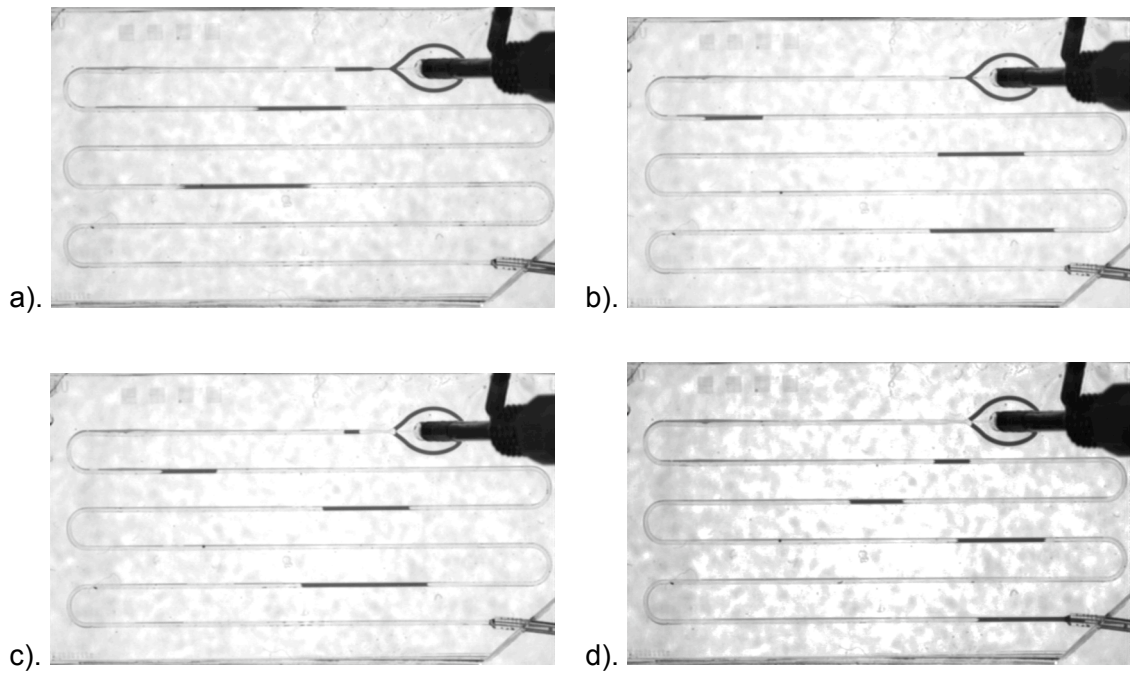


Figure 5.32 : Stills from video recording of the *modified Device 2.a* in operation. a). to c). Demonstrate the flow of three segments as a fourth is being injected from the liquid supply channels into the junction, whilst d). shows the effect of a liquid slug entering the extension to the main channel from the microengineered serpentine. The liquid slugs in images a). to c). decrease steadily in length as a result of a novel script being run just prior to Device 2.a failing. The effect was planned and the device operated entirely as intended.

Unfortunately the device was extremely fragile and eventually the PDMS to PDMS bond failed. Insufficient time remained for further device manufacture or development. Research into the production of segmented flow for the collection of gas for vapour analysis was therefore ceased at this point.

6. VAPOUR ANALYSIS

The original remit of this research project was the creation of a bio-inspired microfluidic device for the analysis of vapour. Initial communication with the industrial sponsor indicated a greater enthusiasm for an external detection module. Following discussion of the advantages, namely the requirement for a smaller sample size, smaller final system size and the potential to develop a more sensitive analysis module, the industrial sponsor was persuaded of the benefits of simultaneous development of a gas collection device, analytical method and detection module.

Additional discussion on an analyte for the determination of the efficiency of the system was then required. Original requests to the industrial sponsor for suggestions for an analyte representative of a compound they were specifically interested in detecting were not followed up. Further requests finally resulted in *ethanol* being suggested as a model analyte. Water solubility, availability, ease of handling, safety issues and volatility were all provided as motivation for ethanol being suggested.

A method of analysing for ethanol was developed. As discussed in section 6.1, ethanol is not a straightforward compound to detect in an aqueous solution. Section 6.1 therefore expands on the sensitive and easily integrated technique used and tested macroscopically. While, as detailed in section 5.2, the microfluidic gas collection system was never fully developed, the final technique employed is believed to be suitable for microfluidic application.

While not discussed in chapter 6 during the investigation of diffusion and the rules governing it, a method of decreasing the detection limit of diffusion based detection systems was conceived. It was observed that the limits to solubility inherent in Henry's Law could be overcome if an irreversible reaction consumed the analyte as it dissolved. No evidence of previous observation of this effect was found in the literature. Chapter 7 expounds on this idea, which we term Chemical Amplification and reports on the design of an experiment that was used to test the hypothesis.

6.1. Introduction

As previously stated in section 1.1.3 and 1.3.2, most VOC detection methods are designed for vapour phase operation.

Microfluidic analysis methods have advanced rapidly over the past 10 years. Much of the recent work has focused on biological materials, either as an aid to chemical detection [81, 158-161] or as the analyte [59, 83, 162-166]. Despite this, as has been shown previously in Chapters 3 and 5, the development of the fluid aspect of the microfluidic system is frequently more complex than that of the analysis.

Differentiation of quantification and qualification is necessary at this point. Many of the microfluidic devices developed to this point are *qualification* as supposed to *quantification* devices. Qualification involves the identification of a particular compound or material as being present, but is not required to make a distinction in the concentration (qualitative). Analysis however requires not only identification of the compound, but also determination of its concentration (that is qualitative and quantitative). The microfluidic device being developed was intended to act as an analytical tool. Requirements were therefore placed on specificity and the device's concentration-response relationship. This is discussed in further detail later.

The original remit of developing a single microfluidic device expanded to the development of vapour collection and analysis devices and testing of the chosen vapour analysis method. Greater complexity in the design and manufacture of the device led to a simple vapour detection method being chosen.

6.1.1. Microfluidic Methods

Many standard chemical analysis methods, including optical, thermal, electrochemical, gravimetric and mass spectrometric, have been integrated into microfluidic systems [167, 168]. Most analysis methods require integrated sensors either in contact with or slightly separated, yet still encapsulated within the bulk of the device, from the flow stream [169-171]. Mass spectroscopy and optical analysis methods on the other hand can be employed with multiple fluidic devices by a 'plug-and-play' set-up.

Integrating sensors within a microfluidic analysis module increases the complexity of manufacture and operation of the device. Electrochemical [169] or thermal [172] analysis are the most common techniques found in microfluidic devices after optical analysis. The incorporation of electrodes requires either the deposition and patterning of an electrically conductive layer or the fine placement of separate electrodes within or close to the

microchannel. Therefore, despite amperometric, potentiometric & conductimetric analysis all having been performed on a microfluidic platform, the added complexity of incorporating the electrodes led to solely optical methods being considered.

6.1.2. Ethanol Analysis

Several methods were examined as possible aqueous ethanol analysis methods. Low concentration aqueous ethanol solutions are difficult to differentiate from water by basic methods such as conductivity, pH or absorbance. As discussed by Azevedo, Prazeres, et al [173], most ethanol analysis methods used without first reacting the ethanol operate within the gas phase. Aqueous phase unreacted-ethanol analysis can be performed by photometric analysis, with high detection limits, or electrochemical analysis, with lower detection limits, but still high compared to some more sensitive ethanol analysis methods.

The least complicated method of detecting ethanol was determined to be by oxidation of ethanol with the concomitant reduction of the oxidising agent to form a more easily detectable compound.

Several of the methods discussed previously, including various electrochemical and optical techniques, have been used for ethanol detection. The Association of Analytical Chemists recommends a variety of methods from gas chromatography to the oxidation of ethanol with dichromate followed by determination of the unreacted dichromate by titration [174]. None of the methods proposed were capable of being easily converted for use in a microfluidic system. Techniques that had previously been used microfluidically were therefore investigated.

Ease of integration, sensitivity (single molecule detection is possible using confocal fluorescence microscopy [175]) and availability led to optical detection of ethanol being selected. Several methods, all based on the previously discussed formation of a detectable compound upon reaction of a substrate with ethanol, were therefore investigated including absorbance, fluorescence and chemiluminescence (the automatic emission of light by certain chemicals as they react).

Absorbance in microfluidic devices tends to be the least sensitive of the three optical detection methods mentioned above. The absorbance is defined by the Lambert-Beer equation (Equation 13) :

$$A = \epsilon l.C$$

Equation 13

in which

C (mol/L or M), is the concentration of the analyte,

l (cm), the length of solution through which the light being absorbed has passed and

ϵ ($M^{-1} \cdot cm^{-1}$), the extinction coefficient is used to calculate the absorbance.

Creating a microfluidic device with a light path travelling along the length of a channel is difficult to create due to reflections from channel walls and the changes in channel dimensions resulting from the malleability of PDMS. As microfluidic channels are shallow, compared to standard absorbance cells, and the path length is therefore short, the absorbance is low.

Fluorescence and chemiluminescence are potentially more sensitive than absorbance, due to the higher signal to noise ratio obtainable [78]. Detection methods utilising fluorescence or chemiluminescence were thus researched.

Initial investigation was undertaken into a two stage chemiluminescent reaction utilising ethanol oxidation with the production of chromium (III) (Cr^{3+}). The Cr^{3+} then acts as a catalyst for the oxidation of luminol to 3 – aminophthalate (see Section 6.3.1, Figure 6.5). The reduction of Cr^{6+} to Cr^{3+} was determined to occur only when ethanol was present despite the presence of hydrogen peroxide (H_2O_2). As the initial reaction was intended to take place under alkaline conditions the reduction of Cr^{6+} by H_2O_2 should not have occurred. The solution containing luminol and H_2O_2 was acidic however. When the two solutions were mixed, despite the presence of a buffer to maintain the alkaline conditions, Cr^{3+} was produced without the oxidation of ethanol taking place.

Following the discovery of the above chronic problem with the chromium based reactions, a two stage, enzyme catalysed reaction resulting in a fluorescent compound was investigated. The first reaction involves oxidation of ethanol by alcohol oxidase (AOD) produces hydrogen peroxide and acetaldehyde. Following this, the second horseradish peroxidase (HRP) catalysed reaction, between hydrogen peroxide and *p*-hydroxyphenylacetic acid (4-HPAA), produces a fluorescent dimer of 4-HPAA (see Section 6.3.2, Figure 6.6).

Difficulties in integrating a deep UV (315 nm) light source into a microfluidic device then led to the suggestion, from the industrial sponsor, of a method utilising absorbance being examined. The method chosen after investigation of several possible HRP substrates was a slight modification of the previous reaction. Replacement of 4-HPAA with *p* – aminoantipyrine (4-AAP) resulted in the production of an easily detectable chromophore. While not ideal, for the reasons presented above, the ease of analysis was judged to be worth the loss in sensitivity and it was clear that when better instrumentation was available a more sensitive method could be returned to.

6.2. Experimental

Chemical Name	Abbreviation	Supplier	Grade
Alcohol oxidase (from P.P.)	AOD	Sigma-Aldrich	
<i>p</i> – Aminoantipyrine	4-AAP	Sigma	ACS
Ammonium chloride	NH ₄ Cl	Sigma	“
Chromium sulphate	Cr ₂ (SO ₄) ₃	Sigma	“
Potassium dihydrogen phosphate	K ₂ HPO ₄	Sigma	“
Ethanol		Sigma	Absolute
Ethylene diamine tetraacetic acid	EDTA	Sigma	ACS
Guaiacol		Sigma	“
Horseradish peroxidase	HRP	Sigma	
Hydrogen peroxide	H ₂ O ₂	Sigma	ACS
<i>p</i> – Hydroxyphenylacetic acid	4-HPAA	Sigma	“
Luminol		Sigma	“
Potassium dichromate	K ₂ CrO ₇	Sigma	“
Silver nitrate	AgNO ₃	Sigma	“
Sodium carbonate	NaCO ₃	Sigma	“
Sodium hydroxide	NaOH	Sigma	“
Sulfuric acid	H ₂ SO ₄	Sigma	“
Tetramethyl benzidine hydrochloride	TMB	Sigma	“

f). Chemiluminescent reagent (40 mL) and Analyte solution (10 mL) were finally mixed and observations recorded.

Second Reaction Test

g). $\text{Cr}_2(\text{SO}_4)_3$ (0.02 M) was dissolved in Base Solution 1 to form Reaction Solution 3.

h). Chemiluminescent reagent (25 mL) and Reaction solution 3 (25 mL) were then mixed and observations recorded.

6.2.2. Fluorescence

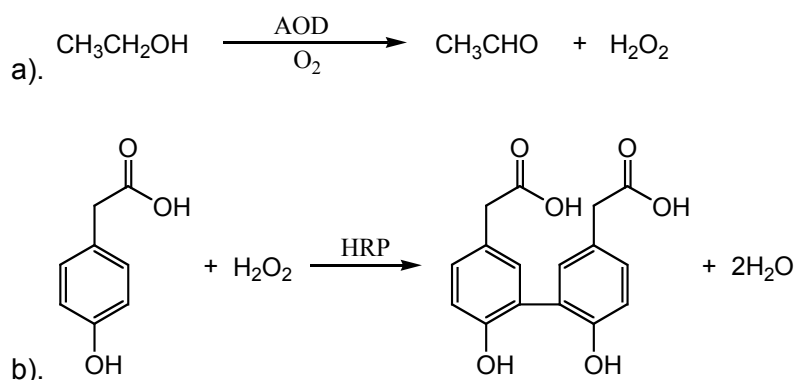


Figure 6.2 : The two stage fluorescence detection scheme. a). Alcohol oxidase catalyses the oxidation of ethanol to acetaldehyde producing hydrogen peroxide as a by-product followed by b). the horseradish peroxidase catalysed reaction of 4-hydroxyphenylacetic acid (4-HPAA) with hydrogen peroxide to produce the fluorescent dimer, 6,6'-dihydroxy-(1,1'-biphenyl)-3,3'-diacetic acid ((4-HPAA)₂).

Base Solution 1

0.1 M Phosphate solution (KH_2PO_4 / KOH) at pH 8.5.

Base Solution 2

4-HPAA (3.9 mM) dissolved in NH_4Cl solution (0.1 M) at pH 9.5.

Full Reaction Blank

a). AOD (8.9 μL) was added to Base Solution 1 (25.005 mL) then mixed and heated at 30°C for 30 minutes.

b). HRP (10 μL) was added to Base Solution 2 (25 mL) to form the Fluorescent reagent.

c). The AOD and Base Solution 1 mixture was mixed with the Fluorescent reagent (25.01 mL) and heated at 30°C for 30 minutes.

Full Reaction Test

- d). Base Solution 1 (500 μL) was mixed with ethanol (11.57 μL).
- e). Base Solution 1 and ethanol mixture (5 μL) was then mixed with Base Solution 1 (25 mL) and AOD (8.9 μL) and heated.
- f). The Base Solution 1, ethanol and AOD mixture (25.0139 mL) was mixed with the Fluorescent reagent (25.01 mL) and heated at 30°C for 30 minutes.

Reaction 2 Blank

- g). Base Solution 1 (25.005 mL) was mixed with Fluorescent reagent (25.01 mL) and heated at 30°C for 30 minutes.

Reaction 2 Test

- h). Base Solution 1 (300 μL) and H_2O_2 (10 μL) were mixed.
- i). Base Solution 1 and H_2O_2 (5 μL) was mixed with Base Solution 1 (25 mL).
- j). The Base Solution 1 and H_2O_2 mixture (25.005 mL) was mixed with Fluorescent Reagent (25.01 mL) and heated at 30°C for 30 minutes.

Analysis

Two spectra were obtained.

- k). Reaction 2 Test solution with Reaction 2 Blank solution as background.
- l). Full Reaction Test solution with Full Reaction Blank solution as background.

6.2.3. Absorbance - Tetramethylbenzidine

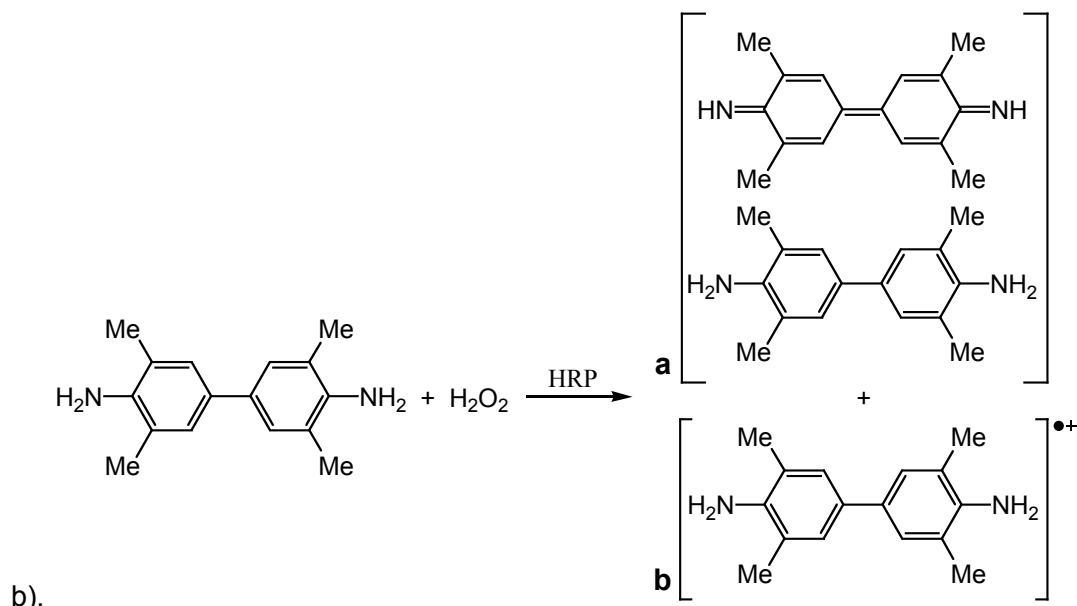
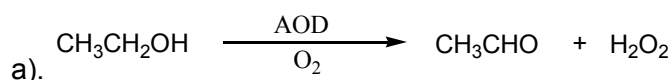


Figure 6.3 : Two stage absorbance detection scheme. a). As per the fluorescence detection scheme, alcohol oxidase catalyses the oxidation of ethanol to acetaldehyde producing hydrogen peroxide as a by-product followed by b). the horseradish peroxidase catalysed reaction of tetramethylbenzidine with hydrogen peroxide to produce the charge transfer and cation free radical products.

All absorbance measurements were made using a Jenway 6300 non-scanning UV/Vis. Spectrophotometer.

Dark and Light Stability

a). TMB (217 μM), was dissolved in potassium acetate buffer solution at (0.2 M) at pH 5.0.

b). To determine the stability of TMB in the dark, the absorbance of the solution was measured, at 652 nm, every minute.

The stability of TMB when exposed to light was determined by measuring the absorbance of the solution, at 652 nm, with one minute's exposure to the light from a fluorescent tube between each measurement.

Reaction Kinetics

- c). TMB (250 μ M) was dissolved in phosphate buffer solution (0.2 M) at pH 7.0 to form the chromophore reagent.
- d). HRP (10 units) was added to the chromophore reagent (3 mL).
- e). H₂O₂ was added to the solution to reach a concentration of 250 μ M.
- f). Steps c). and d). were repeated and then H₂O₂ was added to reach a concentration of 125 μ M.
- g). Steps c). and d). were repeated (however using 200 U of HRP) and then H₂O₂ was added to reach a concentration of 125 μ M.
- h). Step c). was repeated. HRP and AOD (100 U and 50 U respectively) were then added to the chromophore reagent.
- i). H₂O₂ was then added to reach a concentration of 125 μ M.
- j). Steps h). and i). were repeated. Ethanol was then added to reach a concentration of 250 μ M.
- k). Steps h). and i). were repeated, but with 1mM of TMB in step h).. Ethanol was then added to reach a concentration of 1 mM
- l). Step h)., i). and k). were repeated, but with 1 mM of TMB in h). and 500 μ M of ethanol in k).
- m). Step h)., i). and k). were repeated, but with 1 mM of TMB in h). and 250 μ M of ethanol in k)..
- n). All measurements of the solution absorbance were made at 652 nm.

Solubility Tests

- o). Repeat step c). and measure the absorbance.
- p). Repeat step c)., then add DMSO until a 1 % solution is reached. The final solution was placed in an ultrasonic bath for 5 minutes and then the absorbance measured.
- q). Repeat step o)., but add DMSO until a 10 % solution is reached.

Guaiacol was also investigated as a potential substrate. However it was observed to be only partially soluble in an aqueous solution.

6.2.4. Absorbance – 4-Aminoantipyrene

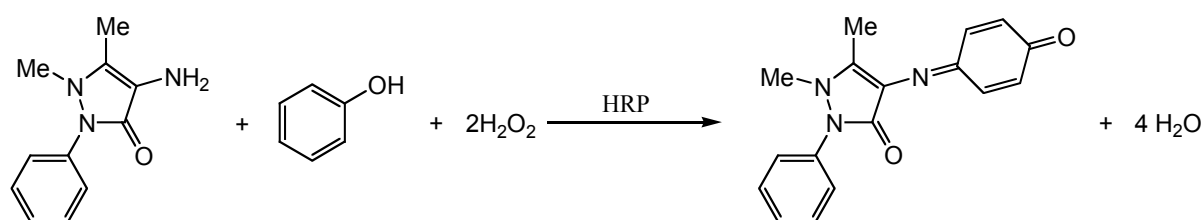


Figure 6.4 : The second reaction of the two stage absorbance detection scheme. Horseradish peroxidase catalyses the reaction between 4-aminoantipyrene (4-AAP), phenol and hydrogen peroxide to produce imino-p-benzoquinone-4-antipyrene (from Tang, Wang, et al [176]). The first reaction, i.e. the AOD catalysed oxidation of ethanol, is as per Figure 6.3 a). and is therefore not shown.

All absorbance measurements were made using a Jenway 6300 non-scanning UV/Vis. Spectrophotometer.

Buffer Solution

Phosphate solution (0.2 M) at pH 7.0 was formed by dissolving KH_2PO_4 and KOH in deionised water.

Stability of Reaction Product

- Phenol (0.171 M) and 4-AAP (2.6 mM) were dissolved in buffer solution (0.05 L) to form the chromophore reagent.
- Ethanol (1.954×10^{-4} M) was dissolved in buffer solution.
- Chromophore reagent (140 μL), ethanol (1.5 mL), buffer solution (1.36 mL), AOD (15 U), HRP (4 U) were mixed in a disposable cuvette which was then quickly placed in the spectrophotometer.
- Measurements of the absorbance, at 510 nm, were made every minute over a period of 10 hours.

Reaction Stoichiometry

1 : 1

- Phenol (0.1465 M) and 4-AAP (2.094 mM) were dissolved in buffer solution (0.05 L) to form the chromophore reagent.
- H_2O_2 (195.4 μM) was dissolved in buffer solution.

g). Chromophore reagent (140 μL), H_2O_2 solution (1.5 mL), buffer solution (1.36 mL) and HRP (1 U) were then mixed, left to react for 30 minutes and the absorbance measured.

2 : 1

h). Steps e). and f). were repeated. Step g). was repeated with chromophore reagent (140 μL), H_2O_2 solution (750 μL), buffer solution (2.11 mL) and HRP (1 U).

1 : 2

i). Steps e). and f). were repeated. Step g). was repeated with chromophore reagent (70 μL), H_2O_2 solution (1.5 mL), buffer solution (1.43 mL) and HRP (1 U).

j). Solutions were also made up for other ratios.

k). All measurements of the solution absorbance were made at 510 nm.

Reaction Kinetics

l). Step e). was repeated. Ethanol (586.2 μM) was dissolved in buffer solution.

m). Chromophore reagent (140 μL), ethanol solution (500 μL), buffer solution (2.34677 mL), HRP (5 U) and AOD (20 U) were mixed.

n). Steps l). and m). were repeated, however the buffer solution volume was reduced (2.3362 mL) and the AOD increased (40 U).

o). All measurements of the solution absorbance were made at 510 nm.

6.3. Results and Discussion

6.3.1. Chemiluminescence

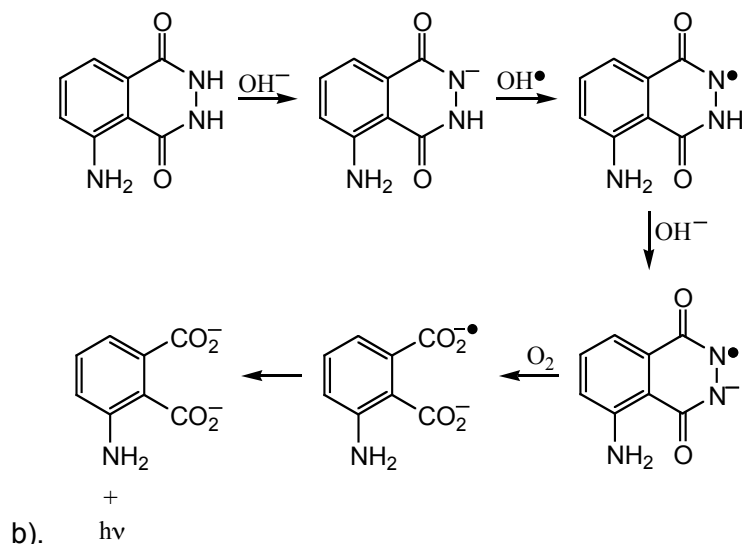
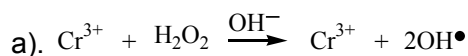


Figure 6.5 : a). The chromium (III) catalysed formation of hydroxyl radicals, in alkali solution [177], that then react, b). with luminol, under basic conditions, to form aminophthalate and light [178]. The oxidation of ethanol by potassium dichromate to acetic acid and chromium (III) is a purely redox reaction and is therefore not shown.

The chemiluminescence based ethanol detection method was derived by combining two separate chemical reactions. Oxidation of ethanol by $\text{K}_2\text{Cr}_2\text{O}_7$ to produce acetaldehyde was believed to result in the formation of Cr^{3+} ions from the reduction of Cr^{6+} . The oxidation of luminol by H_2O_2 is catalysed by Cr^{3+} . The intensity of the light produced by the oxidation of luminol has been proven to be linearly dependant upon the concentration of Cr^{3+} [179].

It was impressed upon the researcher by his colleagues that a simple microfluidic design was desired. Developing a chemical system in which all the reagents could be incorporated into one solution implied only a single liquid supply channel would be necessary. Several additional reagents, including EDTA (a complexing reagent), were added based on literature observation of their enhancement of reaction efficiency and specificity.

Three reactions were determined to be necessary to prove the method functioned as required. A test of the second reaction alone, to determine if the signal produced at the intended test concentration was observable, was intended as a validation step. A blank run of the entire reaction scheme in which the full reaction solution, without the ethanol, was

mixed to confirm that emitted light was a result of the oxidation of ethanol. Then finally the full reaction was performed.

The test of the second reaction alone was performed first. Dissolved $\text{Cr}_2(\text{SO}_4)_3$ acted as a source of Cr^{3+} ions. Upon mixing the chemiluminescent reagent and the reaction solution ($\text{Cr}_2(\text{SO}_4)_3$) a bright blue light was emitted. This proved that the second reaction performed as intended, at the concentrations desired.

Following this result, the blank reaction was executed next. Mixing the chemiluminescent reagent with the buffer in which the ethanol was normally dissolved, should not have resulted in light being emitted. However immediately upon mixing the H_2O_2 solution with the luminol, $\text{Cr}_2\text{O}_7^{2+}$, EDTA mixture, light was emitted. No immediate explanation was forthcoming. It had previously been suggested that H_2O_2 would be capable of reducing $\text{Cr}_2\text{O}_7^{2+}$ to Cr^{3+} . As the oxidation potential required to reduce $\text{Cr}_2\text{O}_7^{2+}$ was higher than the oxidation potential of H_2O_2 , this was thought highly unlikely.

Further literature search disclosed that H_2O_2 was capable of reducing $\text{Cr}_2\text{O}_7^{2+}$ in an acidic solution. Despite the luminol/ H_2O_2 solution being alkali, the $\text{Cr}_2\text{O}_7^{2+}$ /ethanol solution is acidic. Mixing of the two would produce localised areas of low pH and therefore production of excess Cr^{3+} .

The chemiluminescence method was therefore disregarded as a viable ethanol detection method.

6.3.2. Fluorescence

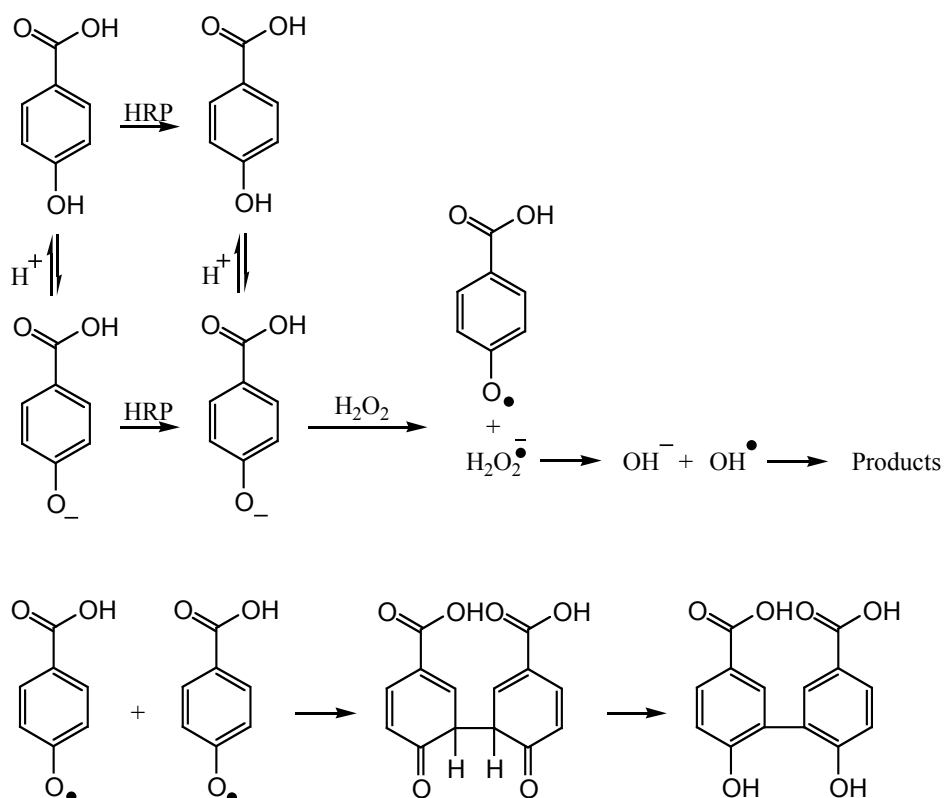


Figure 6.6 : The mechanism of the horseradish peroxidase catalysed dimerisation of 4-HPAA by H₂O₂ to form the fluorescent (4-HPAA)₂ [180].

Increasing the specificity, while maintaining the sensitivity inherent to light emitting versus light absorbing detection methods led to the investigation of an enzyme catalysed, fluorescence based ethanol detection method. Enzymes are catalysts, normally specific to a limited number of substrates. Several methods utilising either alcohol dehydrogenase (ADH) [181] or AOD [73, 173] had previously been developed. However ADH requires the expensive co-enzyme Nicotinamide Adenine Dinucleotide (NAD).

Alcohol oxidase has been thoroughly investigated as a catalyst for the reaction of ethanol and oxygen [158, 182-184]. In spite of methanol and *i*-propanol also being substrates [184], AOD offered the best possible reaction method and, apart from the two reported above, specificity. The AOD catalysed reaction between ethanol and oxygen produces acetaldehyde and H₂O₂ as bi-products. Neither product of the reaction is optically directly detectable.

A second reaction to produce a fluorescent compound was therefore introduced. H₂O₂ could have been directly reacted with, for instance luminol, with Cr³⁺ as a catalyst. However a method involving the horseradish peroxidase (HRP) catalysed reaction between H₂O₂ and 4-hydroxyphenylacetic acid (4-HPAA) was reported that provided a more sensitive detection

method [185, 186]. The production of H_2O_2 has an inhibitory effect on the catalytic ability of HRP [187]. However the rate of reaction of H_2O_2 with 4-HPAA was rapid in comparison to the rate of formation of H_2O_2 (based on the results of experiments conducted with TMB and 4-AAP). Therefore H_2O_2 reacts almost immediately upon its formation [173].

BRENDA (<http://www.brenda.uni-koeln.de/>), the database of enzymes and their properties, lists almost 80 HRP substrates. However many of the fluorescent substrates are differentiated by the quenching, rather than production, of a fluorescent compound. The Stokes shift, the difference between the excitation and emission wavelength, is small for many of the substrates, increasing the degree of filtering required.

The product of the HRP catalysed reaction between 4-HPAA and H_2O_2 exhibited none of these traits. 4-HPAA itself is non-fluorescent, leading to a low background. The Stokes shift, 97 nm, is also much larger than any other substrate observed (Excitation = 317 nm and Emission = 414 nm) [188]. While no absolute value for the efficiency of photon emission versus excitation was discovered, Guilbault, Brignac and Juneau [188] compare the fluorescence efficiency of several fluorophores. Their results indicate that the 4-HPAA product is relatively efficient.

As no fluorescence detector was available at the time that development of the method started, measurements of the viability of the method were to be taken using a scanning uv/vis. spectrophotometer. As a result any test spectrum obtained of the reactions required a blank solution. Hence the requirement for four solutions, that is the two test solutions with the associated blanks.

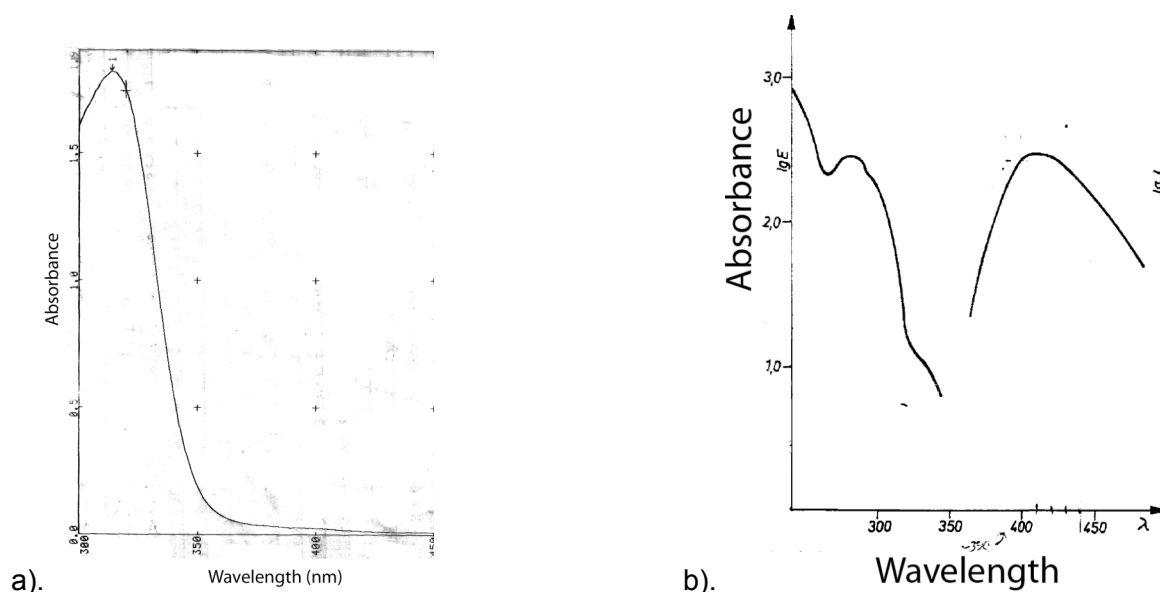


Figure 6.7 : a). The measured spectrum of the HRP catalysed 4-HPAA and H_2O_2 reaction mixture with the background subtracted. The absorbance peak occurs at 314 nm. b). The absorbance and emission spectra, plotted on the same axes, of the same reaction. The background is not subtracted and therefore the peak

observed at 314 nm in figure a). is here observed as a slight 'hump' on the side of another peak. Taken from Hofmann, Hofmann, et al .

The spectrum of the HRP catalysed reaction between 4-HPAA and H_2O_2 ((Figure 6.7 a).) exhibits an absorbance peak at the same wavelength as that shown in Hofmann, Hofmann, et al [189] (Figure 6.7 b).). While the spectrum taken of the full reaction exhibits a large amount of noise below about 300 nm (Figure 6.8), a faint peak does exist at about 314 nm. All spectra were taken with the solution contained within a 4cm path length quartz cuvette. Despite the spectra taken, without a measurement of the light emitted when the solution is excited, no definite proof existed of the production of the fluorophore.

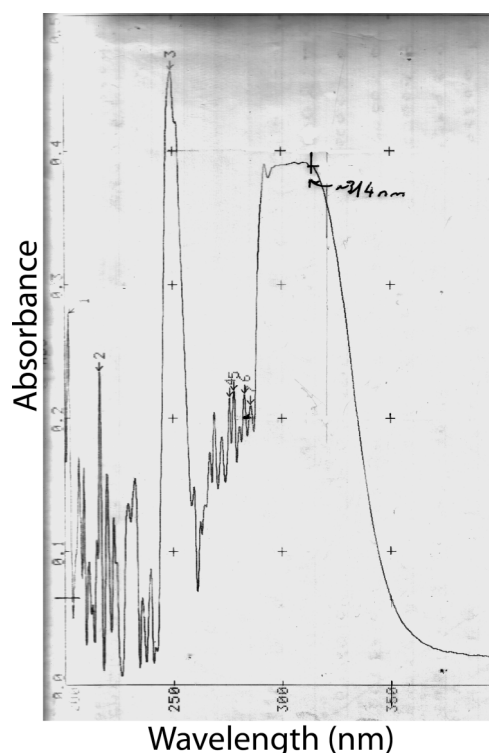


Figure 6.8 : The measured absorbance spectrum of the AOD catalysed oxidation of ethanol and the subsequent HRP catalysed reaction between H_2O_2 and 4-HPAA reaction mixture with the background subtracted. The edge of the main absorbance peak occurs at 314 nm.

6.3.3. Absorbance - Tetramethylbenzidine

Following a suggestion of the industrial sponsor, a more experimentally verifiable optical detection method. Despite the loss in sensitivity, absorbance based methods were therefore investigated. At this point the primary application of the detection method was also intended to be the experimental determination of the chemical amplification discussed in Chapter 7. At the time research into TMB as a substrate of HRP was initiated the primary

application of the ethanol and method, was testing the Chemical Amplification hypothesis discussed in Chapter 7.

Several suggestions, all based on the previous AOD/HRP catalysed two step reaction method, were made by the industrial sponsor. The literature investigation of all HRP substrates suggested, while time consuming, was necessary. ABTS (2,2' – azino-bis(3-ethylbenzothiazoline-6-sulfonate) and TMB were both proposed. As Figure 6.9 shows, both reactions produce radical cations as intermediates. A quenching step is required by both substrates to complete the reaction and produce a stable compound. As previously stated, the detection method was proposed to operate within a simple microfluidic device. As further steps would make a microfluidic device more convoluted, the quenching step was therefore disregarded.

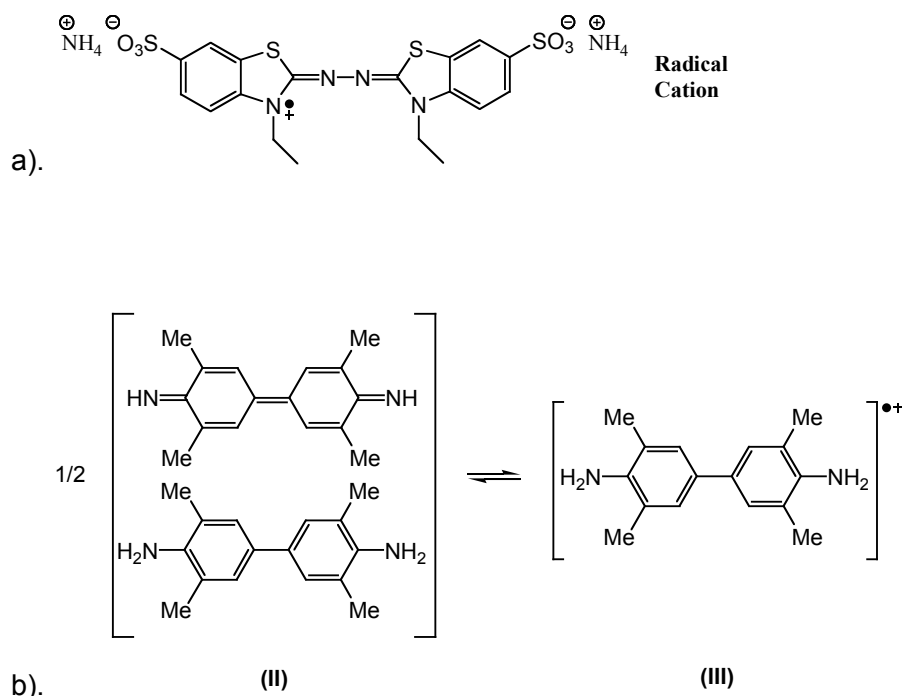
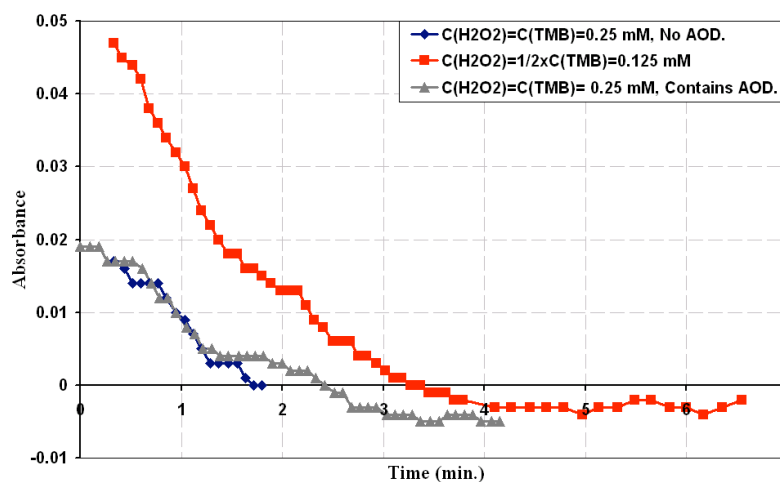


Figure 6.9 : The HRP catalysed products of the reaction between hydrogen peroxide and a). ABTS (unstable radical cation product) [190] and b). TMB (charge transfer complex (II) and cation free radical (III) products) [191].

The intermediates of both the reaction of TMB and ABTS were both believed to be unstable due to their free radical nature. The equilibrium between the charge transfer complex and the cation free radical (compound II and III of Figure 6.9) adds to the equilibrium conditions that lead to the idea behind chemical amplification [191]. While the overall equilibria between the ethanol vapour and solution phase can be summarised by Henry's law, the equilibrium between the charge transfer complex and the cation free radical is not so easily characterised. The proportion of compound II to compound III is changed by the dilution factor, however the magnitude of the change is not clearly defined [191]. Despite these reservations testing the utility of the TMB intermediate was possible by providing for the

While performing a full calculation of the reaction rate constants, was not deemed necessary, understanding the effect of changing the reagent concentration was appropriate. Measurement of the absorbance as a function of time as the initial ratio of H_2O_2 to TMB or ethanol to TMB ratio or AOD and HRP concentrations were varied, demonstrated the optimal reagent concentrations to achieve short reaction times.

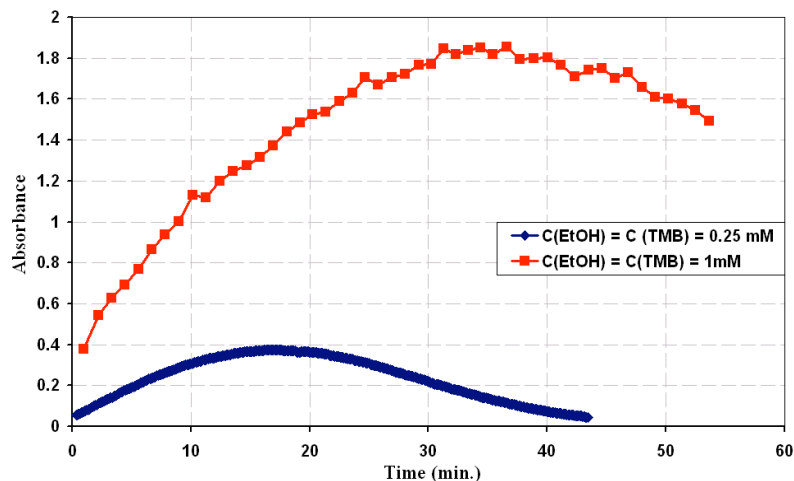
The Absorbance of the HRP Catalysed TMB Oxidation by H_2O_2



a).

The Absorbance of the HRP Catalysed Oxidation of TMB

Following the Oxidation of Ethanol by AOD to produce H_2O_2



b).

Figure 6.12 : a). Plots of the absorbance of the oxidation product of TMB. The plots relate solely to the HRP catalysed reaction between H_2O_2 and TMB despite the experiment 4 solution also containing AOD. All reactions had reached completion before placement of the cuvette within the spectrophotometer, hence the plots only showing the decline in absorbance. b). As per a)., however the reaction to produce the chromophore was reliant upon the initial, AOD catalysed reaction of ethanol to produce the H_2O_2 . The plots indicate that this initial reaction is the rate determining reaction.

Following the observation of a persistent precipitate in the TMB solution a new substrate was determined to be necessary.

6.3.4. Absorbance – 4-Aminoantipyrine

Despite the tests on the TMB solution indicating that the detected intermediate was sufficiently stable and responded linearly across a wide concentration range, only substrates producing non-radical analytes were examined. Guaiacol was examined first, but was almost immediately abandoned after it was found to be only partially soluble in aqueous solution.

Several conditions, some optional and some required, were then imposed upon the substrates examined: solubility in aqueous solution buffered at pH 7; time stable substrate and product; room temperature stable substrate and product; known chemistry (optional); and a single stage chemical reaction. Following more research and requests on professional fora, the HRP substrate system 4-aminoantipyrine / phenol was tested (basic reaction scheme shown in Figure 6.4, full reaction in Figure 6.13).

The 4-AAP/phenol HRP substrate system, originally developed by Trinder [192, 193], has recently been reexamined as a stable [194], effective, H₂O₂ specific [195], HRP substrate. Investigation of the inhibition of HRP by H₂O₂ using the 4-AAP/phenol system as the ideal substrates [187] provides a full reaction model (Figure 6.13).

As shown in Figure 6.13 [187], of which the first three reactions are from Chance [196], the full reaction (Figure 6.4) involves the formation of a series of radicals. Metelitzka, Litvinchuk, et al [197] concluded from their experiments that if the phenol concentration far exceeded that of the 4-AAP, then enzymatic oxidation of 4-AAP was unlikely. Provided sufficient 4-AAP was present (not mentioned, but in Nicell and Wright [187] the oxidation of 4-AAP was observed above 5 mM), dimerisation of the phenol radical was minimal. The resulting reaction is therefore a straightforward cascading electron exchange with the final product produced, provided the initial concentrations are within the correct range.

Based on the calculations of Nicell and Wright [187], the distribution of HRP into the three different species is rapid. While they derive the optimum H₂O₂ concentration for the optimum HRP activity, the calculations are effectively irrelevant for the full ethanol oxidation to chromophore formation reaction. It has previously been shown that the AOD catalysed oxidation of ethanol is the rate limiting reaction. This is confirmed later however to ensure that changing substrate does not radically change the order of rate limiting reaction.

While Metelitzka, Litvinchuk, et al and Nicell and Wright both provide reaction conditions, the initial testing conditions were taken from the Worthington Biochemical Manual (<http://www.worthington-biochem.com/HPO/default.html>) [187, 197]. The conditions provided were confirmed by the reference indicated on the webpage (Trinder [193]).

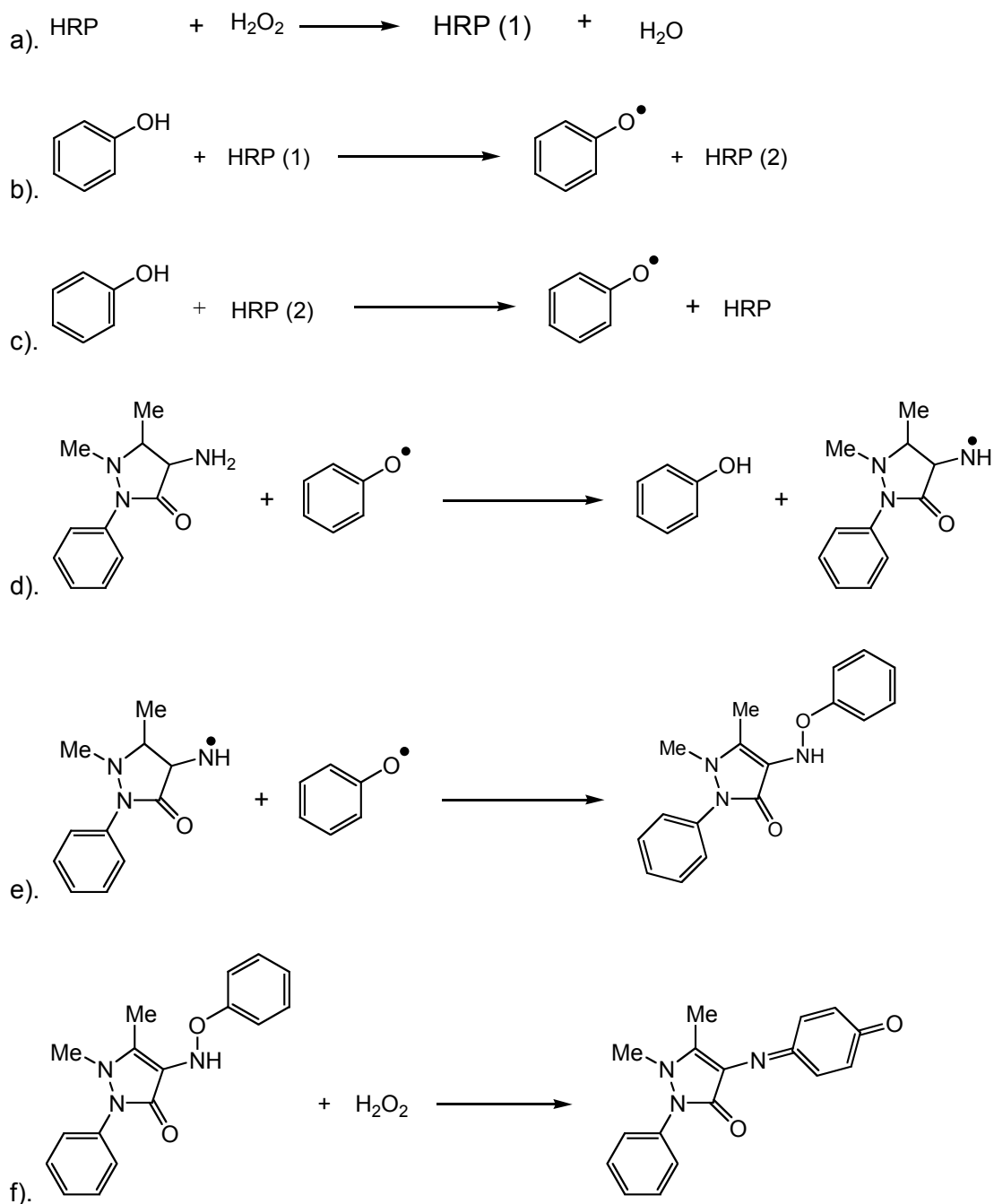


Figure 6.13 : Proposed reaction scheme for the HRP catalysed oxidation of the 4-AAP/ phenol substrate system by H_2O_2 (taken from Nicell and Wright [187]).

While the reaction was more complicated, in some respects, due to the presence of two substrates, the presence of stable reactants and product far outweighed these reservations.

While 4-AAP was believed to be light stable, the reaction product stability was unknown. While Tang, Wang, et al [176] previously used the 4-AAP/phenol substrate system to measure the formation of UV created superoxide anion radical ($\text{O}_2^{\bullet-}$), they do not overtly state that no product breakdown occurred. They merely state that the optimum UV exposure time of the solution was 15 minutes. The measurement of the reaction product stability was therefore still necessary. Following measurements performed as per the

method in Section 6.2.4, the reaction product was found to be stable when exposed to light for periods of up to 3 hours. However, as the final chemical amplification experiments were conducted over periods of up to 7 hours with further measurements being taken up to 12 hours later as confirmation, the experiments were still performed in a darkened room.

Reaction stoichiometry was also measured to determine the range of H_2O_2 / 4-AAP ratios over which the absorbance was linear. As expected the linear range terminated at a ratio of 1:1, however the absorbance was linear to a ratio of 1:16 (Figure 6.14). Above a ratio of 1 : 1 only a logarithmic trend line provided a close fit to the data (Figure 6.14). However as this is greater than the maximum ratio the experiment was to be performed over, the exact relationship was irrelevant.

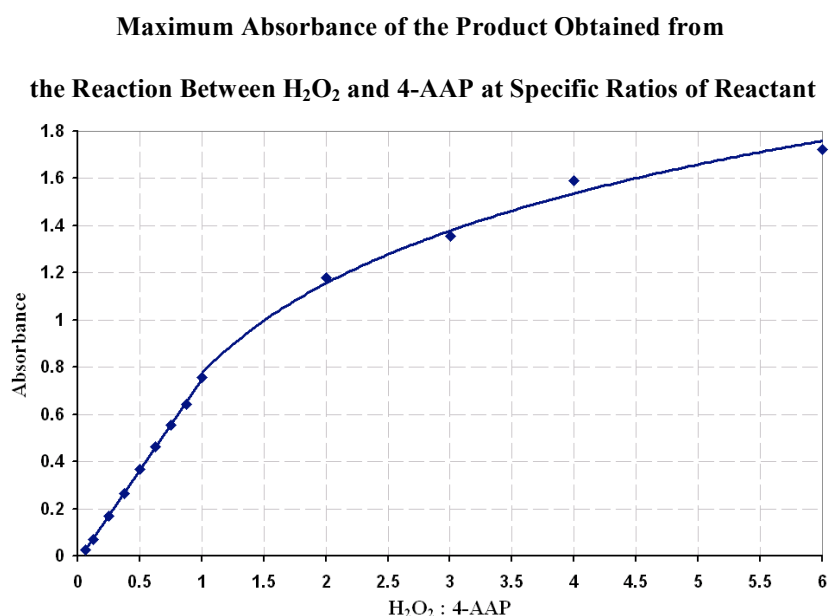


Figure 6.14 : Plot of the relationship between the ratio of H_2O_2 and 4-AAP and absorbance. Separate lines of best fit are shown for data points below and above a 1:1 ratio.

Finally the effect of changing the AOD concentration was determined. As AOD was by far the most expensive reagent used, yet the oxidation of ethanol the rate limiting reaction, a balance between speed and cost had to be obtained. Measuring the effect of doubling the AOD concentration indicated that the »reaction time was halved (Figure 6.15). Doubling the concentration of the AOD used in the chemical amplification experiments from 20 U to 40 U was judged to be an effective balance.

Effect of Doubling the AOD Concentration on the Rate of Reaction

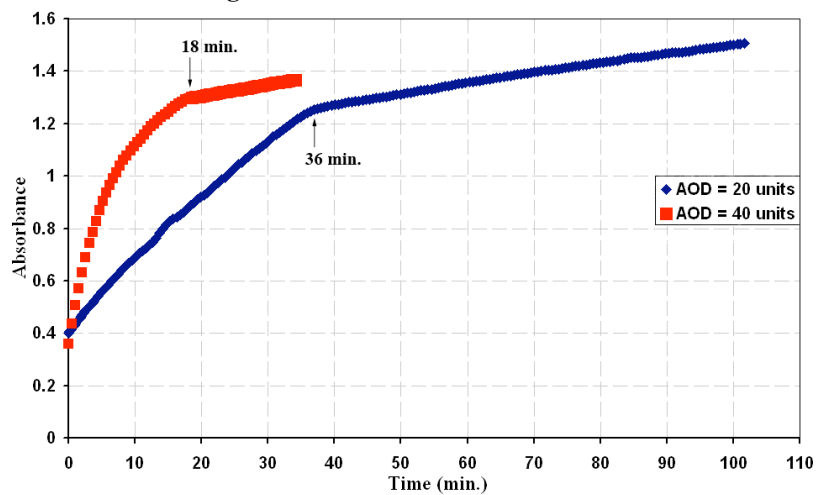


Figure 6.15 : Plot of the effect, on the rate of reaction, of doubling the AOD concentration.

7. PHASE-TO-PHASE EXTRACTION VIA A CHEMICAL REACTION TO GIVE LOWER LIMITS OF CHEMICAL DETECTION

7.1. Introduction

Phase-to-phase extraction via a chemical reaction to give lower limits of chemical detection is here-after referred to as 'Chemical Amplification' on the grounds of brevity. Though not strictly correct, the abbreviated form is the most appropriate, brief reference term.

Analyte preconcentration methods for both gas and liquid phase analysis involve the collection of molecules from within a confined space over a period of time. The molecules are then released within a much shorter period of time into a stream of fluid flowing into a detector. Gas phase detection generally involves the accumulation of molecules into a polymer or a ceramic [198]. Liquid phase preconcentration involves either an absorption/desorption method similar to the gas-phase method [199], liquid/liquid extraction [200] or one of the numerous electrokinetic methods [201]. Chemical amplification however, is a novel method that is unrecognised for its potential in microfluidics and its applicability solely to multiphase flow.

The distribution of a compound between two phases is determined by the partition coefficient [202], of which Henry's Law (Equation 8, Section 4.1) and the octanol-water partition are two specific examples. Partition coefficients are formulated by assuming that sufficient time is given for the compound to dissolve in the phase having a concentration lower than that defined by the coefficient. A plot of the average concentration, of a compound moving from phase 1 to 2, in phase 1 has the asymptotic form shown in Figure 7.1 a) and in phase 2 the inverse asymptote shown in 7.1 b). The partition coefficient is therefore actually the limit to the apportionment of a compound.

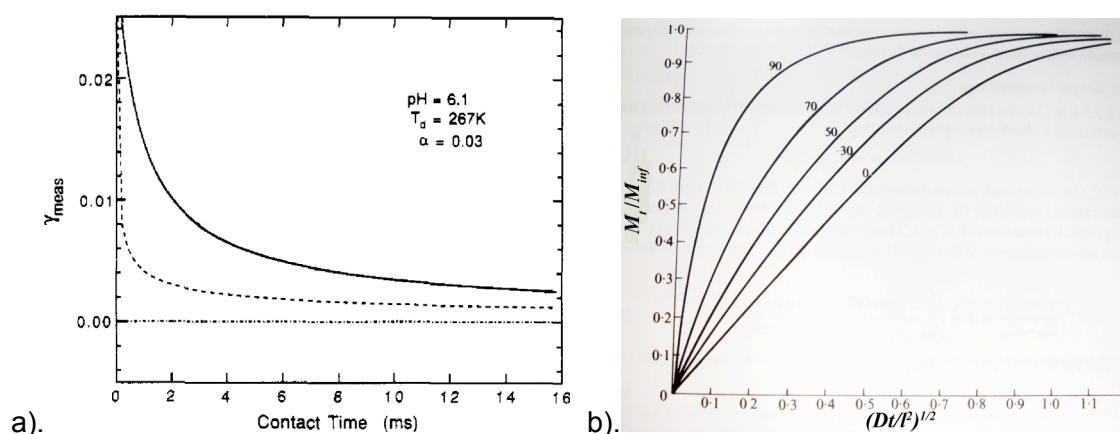


Figure 7.1 : General form of time vs concentration plot for a). Phase 1 and b). Phase 2. a). The plot, from Jayne, Duan, et al [203], is of the theoretical uptake coefficient (ratio of gas phase and liquid phase fluxes) for acetaldehyde based on the addition of contributing uptake coefficients, see Figure 7.3, (broken line) and the modified version of that equation (solid line). The plot relates the overall uptake coefficient to the time exposure of a droplet to acetaldehyde vapour. The dotted line at zero is the asymptote. The plot also assumes rapid diffusion through phase 1 ensuring equal concentration throughout. b). The uptake by a plane sheet from a stirred solution (analogous to the fast diffusion through a gas ensuring even concentration), of limited volume. The multiple lines show the developing concentration gradient through the sheet as a function of time. Taken from Crank [124].

Equations for calculating the partition coefficient vary depending on both the analyte molecule and the solvent system. Despite this, a basic equation, such as Equation 14 can be written.

$$K = \frac{f_1(C(A)_{phase2})}{f_2(C(A)_{phase1})} \quad \text{Equation 14}$$

K is the partition coefficient,

f_1 and f_2 are functions and

$C(A)$ is the concentration of A in phase 1 or 2 as indicated.

Therefore to achieve the greatest preconcentration effect for an analyte being extracted from phase 1 into phase 2 is achieved when the partition coefficient is as high as possible.

Reaction of the analyte in phase 2 reduces the concentration of the analyte within that phase and therefore induces more of the analyte to dissolve in phase 2.

Assuming an appropriate reaction, that does not form an equilibrium, can be found, the system equilibria take the form:

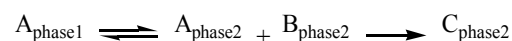


Figure 7.2 : Expression of Chemical Amplification in terms of chemical equilibria and irreversible reactions.

If the reaction between A and B to form C occurs in conditions conducive to the dissolution of A into phase 2 then after an infinite length of time all of A will have been extracted from phase 1. Realistically, due to application requirements, the system will only be able to operate for a limited period of time. Therefore the advantage of chemical preconcentration over standard solvent/solvent preconcentration only applies if the concentration occurs over a shorter time period or is significantly higher.

There are therefore a number of caveats to the applicability of Chemical Amplification. The first is that the reaction should, preferably, be a non-equilibrium reaction or that the rate of the reverse reaction is several orders of magnitude less than the forward reaction. This ensures that any product (C) that is formed will not spontaneously reform large quantities of A and B over a brief period of exposure to the original solvent. The reaction conditions may also introduce antagonistic effects, such as affecting the initial solubility of A in phase 2 (A will still dissolve, but more slowly), these will be discussed in greater detail later. The last caveat is that the time consumed and thought required to implement Chemical Amplification may be better spent elsewhere if the proportional decrease in A_{phase1} is low.

A prime example of this is the current system. Despite the initial idea of Chemical Amplification being developed for use with a vapour that is highly soluble in the liquid phase, the largest relative increases in concentration will result if chemical preconcentration is used to dissolve a gas that is almost insoluble in the liquid phase.

The hypothesis of Chemical Amplification has been examined before [203-207]. *However these previous investigations did not consider the use of Chemical Amplification for the detection of ultra low concentration analytes.* Danckwerts [205] appears to have been one of the first to examine the effect on dissolution of having a reactive solute. Although the effect on the rate of absorption of a compound into separate media when a first-order or pseudo first-order reaction of the compound occurs was examined, the overall solubility was not investigated.

In contrast Jayne, Davidovits, et al [204] study the total solubility of a solute in aqueous solution as a function of the pH. The solute, SO₂, is normally found in a gaseous state, but dissolves in and reacts with water at the interface to form an HSO₃⁻H⁺ complex. This then reacts further to form HSO₃⁻ as it penetrates into the body of the solution. The reaction was found to be closely dependant upon the pH of the solution. Equation 15, showing the dependency of Henry's constant (K_H^*) upon the various reaction constants (K_1 and K_2) and the hydrogen ion concentration [H^+], was derived:

$$K_H^* = K_H \left(1 + \frac{K_1}{[H^+]} + \frac{K_1 K_2}{[H^+]^2} \right) \quad \text{Equation 15}$$

For the system studied, changing the pH from 3 to 5 increases Henry's constant from 44 to 4400. That is, SO_2 becomes 100 times more soluble.

In a later paper, Jayne, Duan, et al [203] examine the effect on relative solubility of acetaldehyde, which reacts with water in their model, and formaldehyde, which doesn't. They develop an electrical circuit analogue for the acetaldehyde dissolution (Figure 7.3) which is basically equivalent to the chemical amplification experiment discussed later. The reaction studied is however reversible and as such is not directly equivalent to that investigated here.

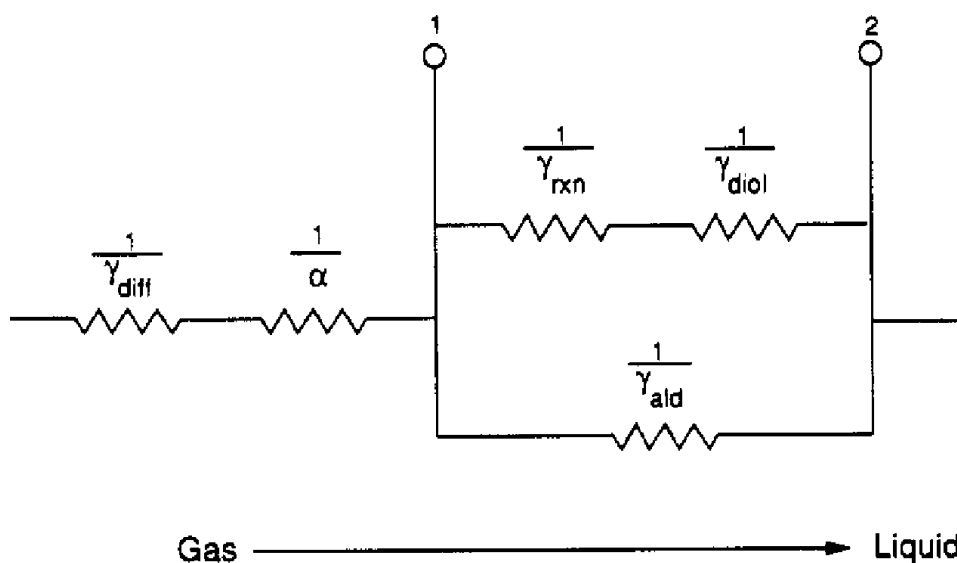


Figure 7.3 : Electrical circuit analogue, developed by Jayne, Duan, et al [203], for the dissolution of acetaldehyde. The uptake coefficient described in Figure 7.1 is the total resistance resulting from the combination of the inverse gas diffusion uptake ($1/\gamma_{diff}$), mass accommodation coefficient ($1/\alpha$), reactive process uptake ($1/\gamma_{rxn}$), saturation of liquid by diol ($1/\gamma_{diol}$) and saturation of liquid by aldehyde ($1/\gamma_{ald}$).

Finally, another journal article by Naik and Doraiswamy examines the dissolution of compounds within solution using phase transfer catalysts (PTC) to artificially boost the solubility [206]. Naik and Doraiswamy [206] review the state of research into the use of PTC to dissolve partially soluble or insoluble compounds. PTC are a generic term for a broad range of compounds that operate via a wide variety of mechanisms. Some, such as certain clathrates, form stable complexes that transport compounds within the insoluble phase.

There are PTCs however that are involved in catalysing the reaction between the insoluble compound and another molecule. This is directly equivalent to the ethanol analysis system discussed here. Although the mechanisms presented are not equivalent as the reactions considered are not related to the oxidation of ethanol.

As previously stated, no literature was discovered that discusses the enhancement of dissolution of compounds via reaction for low concentration analysis. As such, no reference

is made in the observed literature of the need for an irreversible reaction. However logic dictates that an irreversible reaction will enhance the dissolution more than a reversible reaction, assuming that the rate of reaction is not taken into consideration. An irreversible reaction also provides for the later analysis of the analyte without concern for its evaporation during transfer or storage, provided the correct reaction is utilised.

The AOD catalysed oxidation of ethanol, without a subsequent reaction, is not an appropriate reaction for analysis via the stated phase-to-phase extraction enhancement. Acetaldehyde and H_2O_2 are irreversibly formed during the reaction, but as both acetaldehyde and H_2O_2 can evaporate and H_2O_2 dissociates, another, immediate, reaction is necessary. The HRP catalysed reaction of H_2O_2 with the substrates TMB and later 4-AAP accomplishes this. As the preliminary tests of these reactions have been discussed in Chapter 6, the following sections examine the investigation specifically for the purposes of testing the hypothesis of chemical amplification.

7.2. Experimental

Chemical amplification experiments carried out with both TMB and 4-AAP were performed at night, in a curtained off section of the laboratory with all lights switched off to ensure that no light affected the reaction products of either method.

7.2.1. Tetramethylbenzidine

All absorbance measurements were made using a Jenway 6300 non-scanning UV/Vis. Spectrophotometer, at 652 nm.

Buffer Solution

Phosphate solution (0.2 M) at pH 7.0 was formed by dissolving KH_2PO_4 and KOH in deionised water.

Two Bottle Method

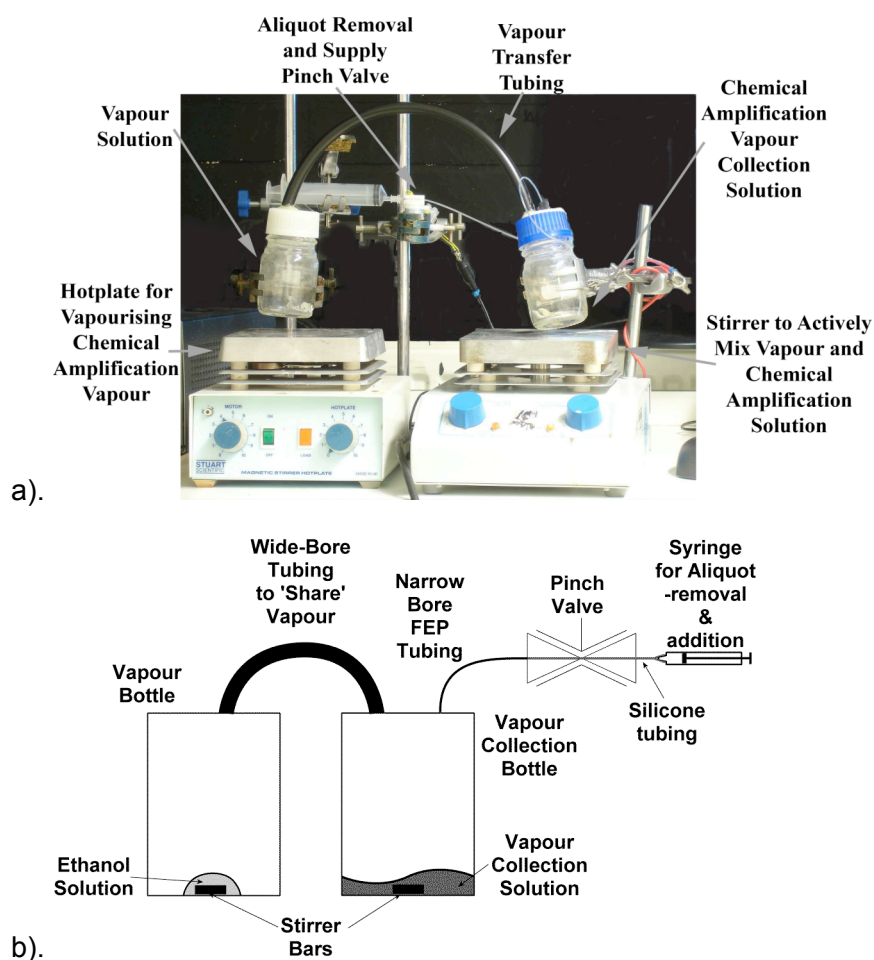
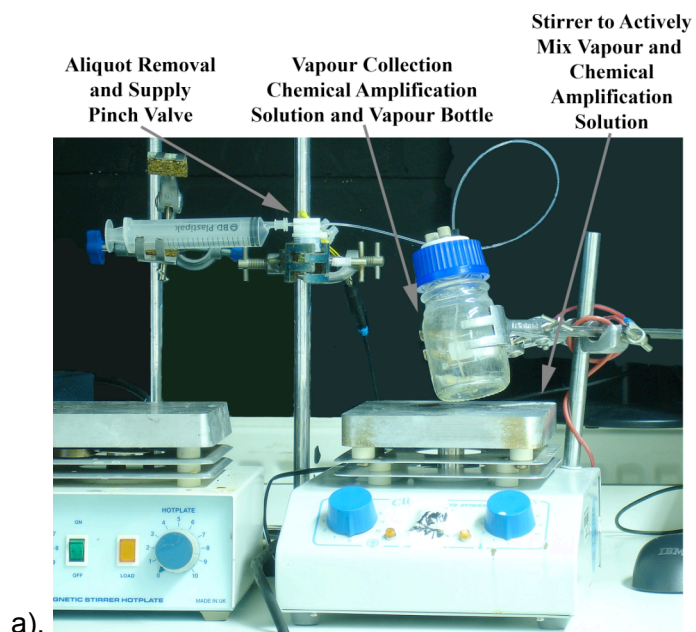


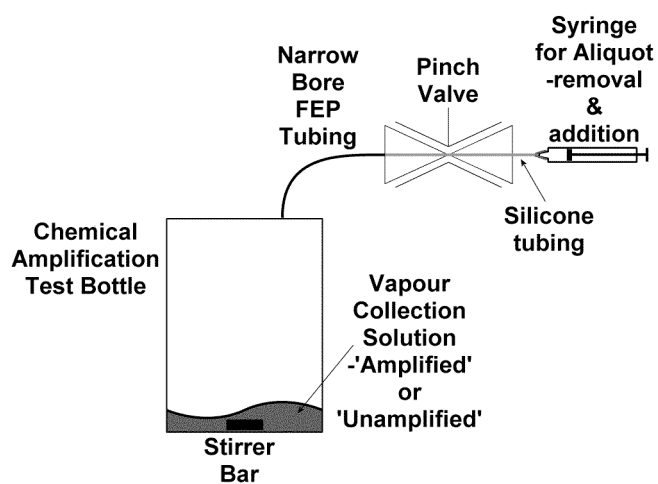
Figure 7.4 : a). Photograph of two bottle chemical amplification set-up and b). schematic of same.

- a). The two bottle chemical amplification determination system was assembled as shown in Figure 7.4. HPLC bottles (100 mL) were used as the main containers, rubber o-rings were used to seal the lids to the bottles and an NR pinch valve was used to control the flow of liquid into or out of the withdrawal tubing. PVC tubing connected the two bottles, FEP tubing (760 μm ID) led from the bottle containing the chromophore solution to the NR pinch valve, with the pinch being silicone tubing. Withdrawals of chromophore solution were made using disposable syringes (20 mL).
- b). TMB (0.5 mM), HRP (100 U) and AOD (50 U) were dissolved in buffer solution (100 mL) and mixed to form the chromophore solution.
- c). Chromophore solution (50 mL) was added to the solution bottle, the lid screwed on and stirring started.
- d). Ethanol (42.8 mM) dissolved in buffer solution (291.9 μL) was added to the vapour flask, the lid attached and stirring and heating (50°C) started.
- e). The base absorbance of the chromophore solution was measured.
- f). The mass of an empty syringe was measured (Syringe 1w).
- g). Buffer solution (approx. 15 mL) with TMB, HRP and AOD added to achieve the same concentration as the chromophore solution was drawn into a second syringe (Syringe 1a).
- h). The mass of syringe 1a was measured.
- i). After 40 minutes, both stirrer bars were stopped.
- j). Syringe 1w was attached to the silicone tubing, the valve opened and chromophore solution (approx. 15 mL) withdrawn. The valve was closed and syringe 1w was then detached and placed to the side.
- k). Syringe 1a was attached in its place, the valve opened and the contents pushed into the solution bottle, taking care to ensure no bubbles were pushed into the system. The valve was then closed and the syringe detached.
- l). The mass of both syringe 1w and syringe 1a were then measured.
- m). The absorbance of the chromophore solution in syringe 1w was then measured.
- n). The experiment was halted at this point as the second absorbance measurement was lower than the original base absorbance measurement.

One Bottle Method – Run 1



a).



b).

Figure 7.5 : a). Photograph of one bottle chemical amplification set-up and b). schematic of same.

Note : The pH of the buffer solution for this method was increased to 7.5 to increase the Henry's constant of ethanol.

o). The one bottle chemical amplification determination system was assembled as shown in Figure 7.5. All equipment was as per the Two Bottle Chemical Amplification System.

p). TMB (1 mM) was dissolved in a $\frac{2}{3}$ acetic acid/ $\frac{1}{3}$ buffer solution (100 mL) and mixed to form the chromophore solution.

q). Ethanol (17.13 mM) was dissolved in buffer solution (100 mL).

- r). Chromophore solution (10 mL), HRP (10 U), AOD (5 U) and ethanol (291.94 μ L) was added to the bottle, the lid screwed on and heating (40°C) and stirring started.
- s). The base absorbance of the chromophore solution was measured.
- t). The mass of an empty syringe was measured (Syringe 1w).
- u). Buffer solution (approx. 8 mL) with TMB, HRP and AOD added to achieve the same concentration as the solution in the bottle was drawn into a second syringe (Syringe 1a).
- v). The mass of syringe 1a was measured.
- w). Syringe 1w was attached to the silicone tubing 40 minutes after the ethanol was added. The valve was then opened and solution (approx. 8 mL) withdrawn. The valve was closed and syringe 1w was then detached and placed to the side.
- x). Syringe 1a was attached in its place, the valve opened and the contents pushed into the solution bottle, taking care to ensure no bubbles were pushed into the system. The valve was then closed and the syringe detached.
- y). The mass of both syringe 1w and syringe 1a were then measured.
- z). The absorbance of the solution in syringe 1w was then measured. Excess solution was stored separately.
- aa). Steps f). to l). were repeated four more times. The numbered label was incremented on each subsequent set of syringes and withdrawn solution. The time between each withdrawal was approximately 30 minutes.
- ab). Steps a). to m). were repeated the following evening, although without any AOD added. The measured absorbances from this series provided the blank measurements to the previous night's experiment.

Note : Two variants of the above experiment were tried or planned. However as the basic steps and the concentrations are the same, the basic changes to the original experiment only are noted. Explanations for each experiment are provided in Section 7.3.

1. Repeating the above experiment, however with the chemically amplified and unamplified runs performed at the same time.
2. Sequential and gradually smaller withdrawals of reaction solution without the addition of any replacement chromophore reagent.

Following the final experiment, examination of the flask containing the chromophore solution led to the observation of a very fine precipitate. Solubility tests using DMSO on the precipitate, identified as TMB, were unsuccessful. This led to the conclusion that TMB was unsuitable for this application.

7.2.2. 4 – Aminoantipyrine

All absorbance measurements were made, using a Jenway 6300 non-scanning UV/Vis. Spectrophotometer, at 510 nm.

The test of chemical amplification, performed using 4-aminoantipyrine and phenol as the HRP substrate, followed a modified version of the single bottle method shown above. Despite the similarities the full methodology is presented to avoid confusion.

Apart from the preparation of the buffer solution and the equipment, all experimental steps were performed at night time, in a darkened room, using the light from a single computer monitor to provide illumination.

Buffer Solution

Phosphate solution (0.2 M) at pH 7.0 was formed by dissolving KH_2PO_4 and KOH in deionised water.

Chemical Amplification Experiment 1						
	Blank	Abs_{max}	Amplified		Unamplified	
			Initial	Aliquots	Initial	Aliquots
Buffer Solution	2.847	2.347	7.824	7.593	7.860	7.621
Ethanol	-----	0.5	1.667	-----	1.667	-----
Chromophore Sol ⁿ	0.140	0.14	0.467	0.373	0.467	0.373
AOD	20 U	20 U	66 ² / ₃ U	53 ¹ / ₃ U	-----	-----
HRP	5 U	3 U	13 ¹ / ₃ U	10 ² / ₃ U	13 ¹ / ₃ U	10 ² / ₃ U
Total Volume	3.000	3.000	10.000	8.000	10.000	8.000

Chemical Amplification Experiment 2							
	Blank		Abs _{max}	Amplified		Unamplified	
				Initial	Aliquots	Initial	Aliquots
Buffer Solution	2.847		2.347	7.824	7.593	7.860	7.621
Ethanol	-----		0.5	1.667	-----	1.667	-----
Chromophore Sol ⁿ	0.140		0.14	0.467	0.373	0.467	0.373
AOD	20 U		20 U	66 ² / ₃ U	53 ¹ / ₃ U	-----	-----
HRP	5 U		3 U	13 ¹ / ₃ U	10 ² / ₃ U	13 ¹ / ₃ U	10 ² / ₃ U
Total Volume	3.000		3.000	10.000	8.000	10.000	8.000
Chemical Amplification Experiment 3							
	Blank		Abs _{max}	Amplified		Unamplified	
				Initial	Aliquots	Initial	Aliquots
Buffer Solution	8.473		3.473	3.473	4.237	3.579	4.289
Ethanol	-----		5.000	5.000	-----	5.000	-----
Chromophore Sol ⁿ	1.400		1.400	1.400	0.7	1.4	0.7
AOD	200 U		200 U	200 U	100 U	-----	-----
HRP	40 U		40 U	40 U	20 U	40 U	20 U
Total Volume	10.000		10.000	10.000	5.000	10.000	5.000
Chemical Amplification Experiment 4							
	Blank		Abs _{max}	Amplified		Unamplified	
	1	2		Initial	Aliquots	Initial	Aliquots
Buffer Solution	1.479	6.373	1.373	1.373	3.187	1.479	3.239
Ethanol	5.000	-----	5.000	5.000	-----	5.000	-----
Chromophore Sol ⁿ	3.500	3.500	3.500	3.500	1.750	3.500	1.750
AOD	-----	200 U	200 U	200 U	100 U	-----	-----
HRP	40 U	40 U	40 U	40 U	20 U	40 U	20 U
Total Volume	10.000	10.000	10.000	10.000	5.000	10.000	5.000

Table 7.1 : Volumes of reagent used for blank and maximum absorbance solutions and for the Amplified and Unamplified (full experimental) solutions for all 4-AAP chemical amplification experiments.

- a). The chemical amplification experiments were performed using the same equipment set-up as defined in the One Bottle Method described above.
- b). 4-AAP (2.065 mM) and phenol (0.147 M) were dissolved in buffer solution (50 mL) to form the chromophore solution.
- c). Ethanol (1.465 mM) was dissolved in buffer solution (100 mL).

- d). AOD (1 U \equiv 0.5291 μ L) was used as provided by the supplier, while HRP (1 U \equiv 0.5291 μ L) was dissolved in buffer solution to achieve the same concentration as the AOD solution.
- e). Blank solutions 1 and 2 and the solution used to determine the maximum absorbance possible with the amplified solution (Abs_{max}) were prepared by mixing the appropriate reagents (shown in Table 7.1) in clear glass bottles (30 mL).
- f). The absorbance of the Abs_{max} solution was measured every 30 s initially, then every 2 minutes and finally every 5 minutes until the maximum absorbance was reached.
- g). The absorbance of both Blank 1 and Blank 2 were measured at the start and finish of the experiment.
- h). While the Abs_{max} solution reaction continued, the initial Unamplified and Amplified solutions were mixed, separately, as per the volumes shown in Table 7.1. They were each mixed in one of the HPLC bottles. Ethanol solution was added last in both cases, with the bottle lids being attached immediately following it's addition.
- i). The mass of an empty syringe was measured (Syringe U1-w, ie Unamplified solution – aliquot 1 – withdrawal).
- j). Secondary Unamplified solution was mixed, as per the volumes shown in Table 7.1, in a syringe.
- k). The mass of the syringe (Syringe U1-a) containing the solution was measured.
- l). Syringe U1-w was attached to the silicone tubing 40 minutes after the ethanol was added. The valve was then opened and solution (approx. 5 mL) withdrawn. The valve was closed and Syringe U1-w was then detached and placed to the side.
- m). Syringe U1-a was attached in its place, the valve opened and the contents pushed into the solution bottle, taking care to ensure no bubbles were pushed into the system. The valve was then closed and the syringe detached.
- n). The mass of both Syringe U1-w and Syringe U1-a were then measured.
- o). Solution in Syringe U1-w was ejected into a glass bottle and AOD (100 U) added. The bottle was labelled and stored away from any light source.
- p). Steps i). to l). were repeated seven more times. The numbered label was incremented on each subsequent set of syringes and withdrawn solution. The time between each withdrawal was approximately 20 minutes.

q). Steps i). to l). were repeated for the amplified solution with the following changes

- Each syringe and associated solution was labelled Syringe A# -a or -w.

- The first aliquot was taken from the Amplified Solution bottle after approximately the same length of time that the Abs_{max} solution took to reach the maximum absorbance (signalling reaction completion).

- Following measurement of the mass of both syringes, after the aliquot addition, the withdrawn solution was ejected into a glass bottle. However no AOD was added and the absorbance was measured immediately before the bottle was stored.

7.3. Results and Discussion

All chemical amplification methods were intended to prove that the concentration of ethanol remaining in the air of a *closed system*, containing a solution in which an irreversible reaction with ethanol took place, was lower than that in which the reaction did not take place.

As stated above, the set-up containing the ethanol/reaction solution must be a closed system. Composition of the reaction reagent and associated solutions must be almost identical, with only a single carefully chosen component removed. Several other important factors also became apparent during the development of the final methodology, however these will be discussed later.

The total volume of ethanol vapour capture solution and the volume and number of aliquots taken was based on calculations of the efficiency. Comparison was made of the analyte present in the Unamplified and Amplified aliquots. The Amplified solution was assumed to absorb 100% of the ethanol vapour for simplicities sake. Each aliquot would remove analyte from the solution and each subsequent addition of solution dilute the remaining analyte. The calculations accounted for the dilution of the dissolved analyte and any analyte present as vapour. Then, based on Henry's Constant, the new concentration of analyte in the capture solution was determined. This was repeated for several aliquots. The difference between the Unamplified and Amplified aliquots was then compared.

Table 7.2 presents a summary of the results, from the theoretical calculations of the Unamplified and Amplified solution analyte concentrations, for a 10 mL and an 8 mL aliquot capture solution and aliquot volume respectively. Also shown is the equation used for the calculation of the number of moles of gas. The calculations present the proportionate effect of the Amplified versus the Unamplified solutions. For the Amplified solution calculations, all vapour is assumed to have been absorbed and reacted by the vapour collection solution.

All calculations for the Unamplified solution are based on a rearranged form of Equation 16 (used for the calculation of Henry's constant). Equation 16 is rearranged so that the number of moles of vapour (n_g) present in the experiment container is presented in terms of the container and solution volumes, the total number of moles of analyte present in the system (n_T), the gas constant (R) and the temperature (T).

$$K_H = \frac{\frac{n_l / V_l}{n_g \times R \times T}}{V_g} \quad \text{Equation 16}$$

Aliquot		Unamplified		Amplified	Percentage Difference
		n (moles)	Conc.	Conc.	
1	Gas	9.2×10^{-9}			
	Liquid	5.0×10^{-6}	5.0×10^{-4}	5.0×10^{-4}	0.2
2	Gas	1.9×10^{-9}			
	Liquid	1.0×10^{-6}	1.0×10^{-4}	2.0×10^{-4}	50
3	Gas	3.7×10^{-10}			
	Liquid	2.0×10^{-7}	2.0×10^{-5}	8.0×10^{-5}	75
4	Gas	7.5×10^{-11}			
	Liquid	4.1×10^{-8}	4.1×10^{-6}	3.2×10^{-5}	87

Table 7.2 : Subscript *l* refers to liquid, *g* to gas, A to the Amplified solution and U to the Unamplified solution. 5.00×10^{-6} moles of ethanol are added to the capture solution originally.

7.3.1. Tetramethylbenzidine

2 Bottle Method

Physically separating the ethanol solution from the reaction reagent was originally believed necessary. To this end an experimental set-up in which two bottles, one for the ethanol solution and one for the reaction reagent. The bottles were connected by drilling holes into the lids of both bottles to accommodate the largest bore tubing available. Holes were sealed using a two-part epoxy adhesive (Araldite™). To prevent the possibility of absorption of the ethanol by a rubber o-ring, the sealing ability of the lids alone were tested. Neither provided an air-tight seal and therefore the o-ring was used.

The contents of both the Vapour and the Collection/Amplification solution bottles were stirred. The Collection/Amplification solution was stirred to ensure fresh solution was always in contact with the air and vapour mix. Heating the ethanol solution until completely evaporated and stirring the contents of both bottles continually was intended to increase the speed of mixing of the ethanol vapour and air in the Vapour bottle and then throughout the system..

Notes on methodology :

The reaction reagent volume (50 mL) and aliquot size (15 mL) were chosen based on calculations made using Table 7.2 combined with the perceived ease of operating with a larger volume. Measuring the mass of solution withdrawn and added allowed more accurate calculation of the volume of solution remaining within the bottle. A pinch valve was used to close the system as the internal volume moved is low. The small amount of light provided by a computer monitor was sufficient to see the movement of the meniscus as gas was pushed into the tubing leading to the Reaction reagent bottle. Closing the valve before the meniscus reached the solution, and therefore increased the volume of gas in the system, was possible.

A lower absorbance in the first aliquot (0.27) than in the base solution (0.31) indicated a higher concentration of TMB product in the base solution. This was illogical and therefore indicated something was wrong with the methodology.

It was subsequently noted that the epoxy seal, between the tubing connecting the two bottles and the lids, was broken. No further attempt to seal the tubing and the lids was successful.

1 Bottle Method

Consideration of the mechanics of the equipment set-up and vapour movement to and from solution led to the abbreviated equipment set-up shown in Figure 7.5. The reaction time of the AOD catalysed reaction was believed to be much longer than the desorption time of ethanol from solution. Injecting the ethanol directly into the reaction reagent solution while stirring did not affect the proportion of ethanol dissolved in the solution. The one bottle system is therefore effectively a compressed Two Bottle system. Compressing the system decreased the complexity of the set-up and therefore any chance for gas leaks to occur.

The reaction reagent and aliquot volumes (10 mL and 8 mL respectively) were adopted after it was found practicable to operate with lower volumes and to decrease the amount of AOD and HRP used.

Amplified solution aliquots and the associated unamplified solution differed only in that the blank solutions lacked AOD. Possible production of H_2O_2 by the UV steriliser module, in reverse osmosis water purification systems, led to the possibility of the TMB reacting with H_2O_2 in the buffer, rather than from the reaction reagent. The omission of AOD therefore allowed the measurement of the H_2O_2 already present without creating any extra H_2O_2 .

To account for the absorbance of the base solution, without any reacted TMB present, a blank solution was prepared and the absorbance of that solution measured. The solution contained all components, apart from ethanol. Therefore the background H_2O_2 concentration and AOD and HRP absorbance would all be accounted for. Blank solution was prepared and the absorbance measured separately at the time the Amplified and Unamplified experiments were performed. The absorbance of unreacted TMB solution had previously been observed to change slightly over time. Measurement of the blank absorbance, as with the aliquot absorbances, was performed for a period of approximately 30 minutes and the absorbance change as a function of time determined. This was then used to calculate the actual aliquot absorbances.

The aliquot absorbance for each subsequent aliquot should decrease in both the Amplified and Unamplified experiments. Subtracting the absorbance of the Unamplified solutions (measured to provide a blank absorbance) from the Amplified absorbances for each aliquot should have provided the actual effect of the Amplified solution. That is, the absorbance reading for the Unamplified aliquot 1 solution was subtracted from the Amplified aliquot 1 solution. No such pattern was observed for either the Amplified or the Unamplified experimental runs. Again, as shown in Figure 7.6, no such pattern was shown when the Unamplified absorbances are subtracted from the Amplified absorbances.

Plot of the Amplified–Unamplified Solution Absorbances for the

Unsuccessful Experimental Test of Chemical Amplification Using TMB

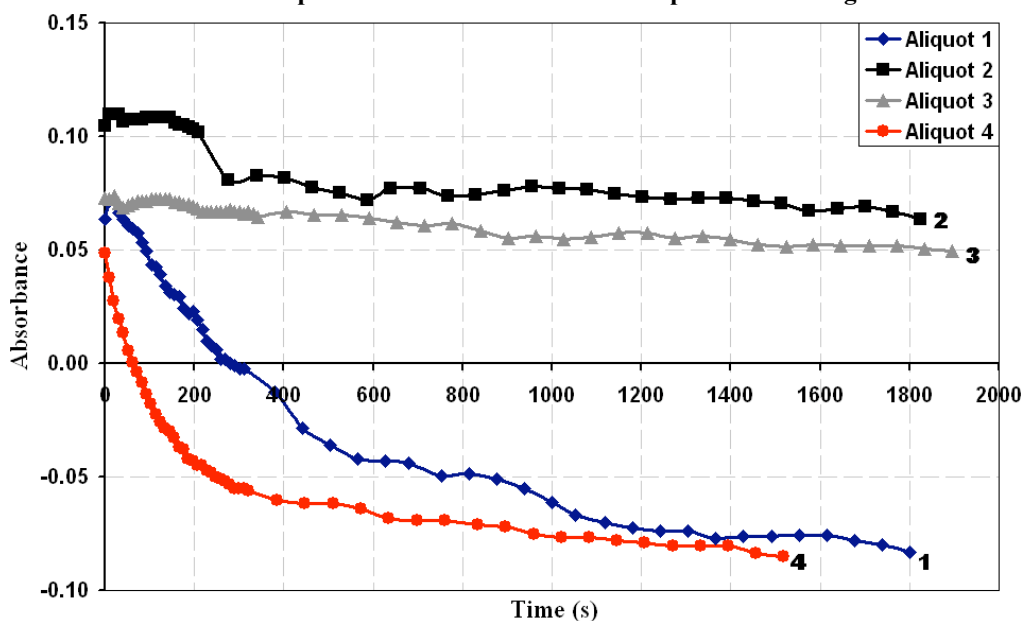


Figure 7.6 : Temporal change in the relative absorbance of the Amplified and Unamplified TMB, ethanol reaction solutions used to test the chemical amplification hypothesis.

This experimental method was therefore modified.

1 Bottle Method - modification 1

The first modification to the 1 Bottle Method was planned, but never executed. By performing the Amplified and Unamplified experiments simultaneously the experimental conditions of all solutions would be identical. While not assuring that the results would follow the expected pattern, fewer variables would have been present.

1 Bottle Method – modification 2

Aliquot			Unamplified		Amplified	Percentage Difference
Number	Volume		n	C	C	
1		Gas	2.0×10^{-8}			
	25 mL	Liquid	1.0×10^{-4}	2.0×10^{-3}	2.0×10^{-3}	0.02
2		Gas	3.1×10^{-8}			
	15 mL	Liquid	5.0×10^{-5}	2.0×10^{-3}	2.0×10^{-3}	0.04
3		Gas	3.7×10^{-8}			
	8 mL	Liquid	2.0×10^{-5}	1.3×10^{-3}	2.0×10^{-3}	3.3
4		Gas	2.5×10^{-8}			
	5 mL	Liquid	9.3×10^{-6}	1.2×10^{-3}	2.0×10^{-3}	41.6
5		Gas	2.3×10^{-8}			
	2 mL	Liquid	3.5×10^{-6}	7.0×10^{-4}	2.0×10^{-3}	65.0

Table 7.3 : Solutions to the Equations presented in Table 7.2 based on gradually decreasing aliquot volumes.

The second modification utilised the solutions to the calculations from Table 7.2 yielding Table 7.3. By starting with a large solution volume and taking gradually smaller aliquots, the experimental methodology was simplified. No solution was added to the closed system and therefore no further mixing of Amplified or Unamplified solution was necessary.

The modified 1 Bottle Method was executed. However a fine green precipitate was observed in all the aliquots after several hours had passed. The precipitate invalidates the experimental results as it may have been present before the reaction started without being observed. Uneven distribution of precipitate between aliquots could have affected the absorbances to differing degrees.

As the precipitate was believed to be unreacted TMB, its dissolution was vital to ensuring the applicability of the TMB method to such a sensitive experiment. As previously mentioned, several tests using DMSO as a dissolution aid were performed (Section 6.2.3). None of the tests were successful and therefore no further chemical amplification tests could be performed.

Following enquiries on professional fora, two replacement substrates were suggested. Guaiacol was proposed first, but as previously stated at the end of Section 6.2.3, it was found to be only partially soluble in aqueous solution. Finally, a submission from the Methods and Reagents forum on bio.net (<http://www.bio.net/bionet/mm/methods/>) recommended the 4-Aminoantipyrine /phenol two substrate system. Examination of this system and indicated that it fulfilled many of the required characteristics. Subsequent tests on the 4-AAP/Phenol/H₂O₂, HRP catalysed reaction, as detailed in Section 6.2.4, proved that it was an ideal replacement for TMB.

7.3.2. 4-Aminoantipyrine

Three different methodologies, using the 4-AAP/phenol substrate system, were tried over the course of four repeat experiments. All were based on the first modification of the “1 Bottle Method”. The first two followed the methodology of the first modification of the “1 Bottle Method”, but using the substrate concentrations of the 4-AAP chemical amplification method.

The first and second attempts to experimentally prove chemical amplification using the 4-AAP/phenol substrate system were performed using the experimental methodology of the first modification of the “1 Bottle Method”. Volumes of the two experiments were as shown in Table 7.1.

Plot of the Amplified–Unamplified Solution Absorbances for the

First Experimental Test, of the Chemical Amplification Hypothesis, Using 4-AAP.

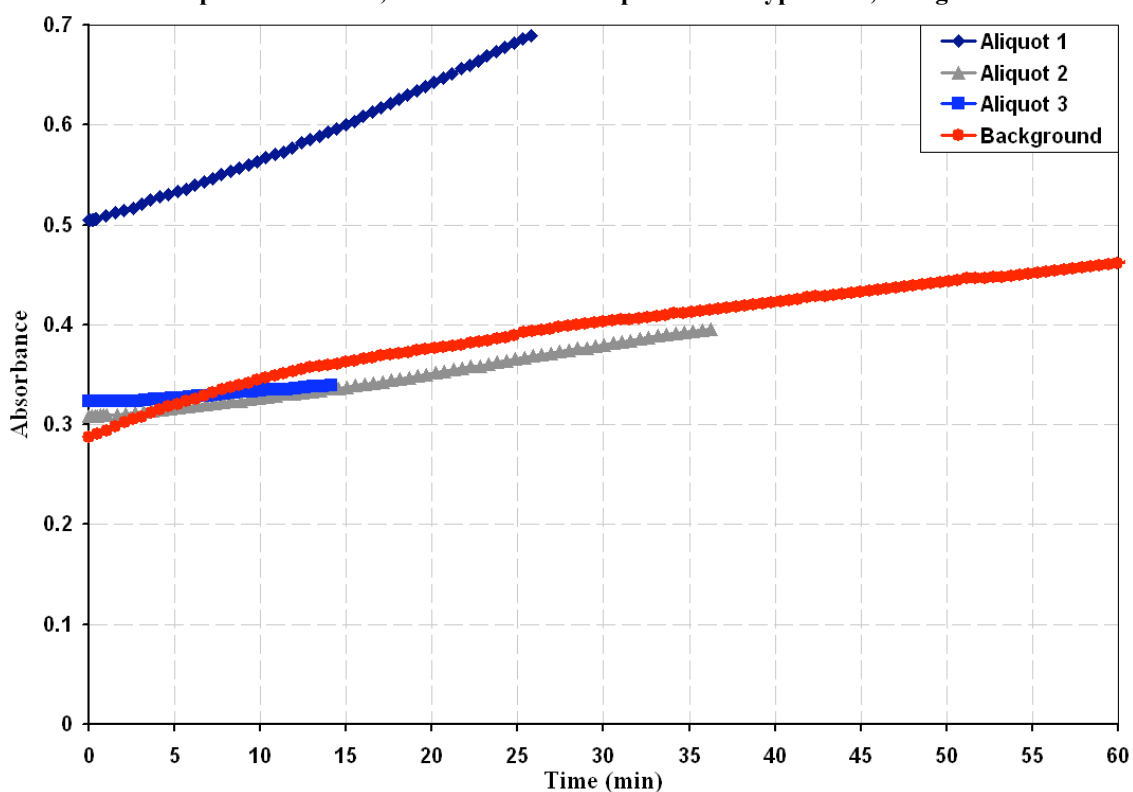


Figure 7.7 : The differential absorbance resulting from measurements of the amplified and unamplified solutions, for each aliquot. This is the plot from the first experimental test of chemical amplification using 4-aminoantipyrine and was found to be irregular as a result of contamination.

Experiment 1 was halted after only three aliquots (Figure 7.7). The suspect high background absorbance of the Blank solution decreased the signal to noise ratio at relatively high absorbances. Contamination was suspected, so a thorough investigation was executed using variants of the Amplified solutions. Finally the cause of the high background absorbance was attributed to contamination. It was believed that the contamination was methanol from cleaning solution. All further experiments were conducted with direct extraction of the atmosphere surrounding the working area so as to ensure complete removal of methanol vapour.

**Experimental Test 2 Using 4-AAP : Comparison of the Maximum Absorbance
of Each Aliquot Taken from the Amplified and Unamplified Solutions.**

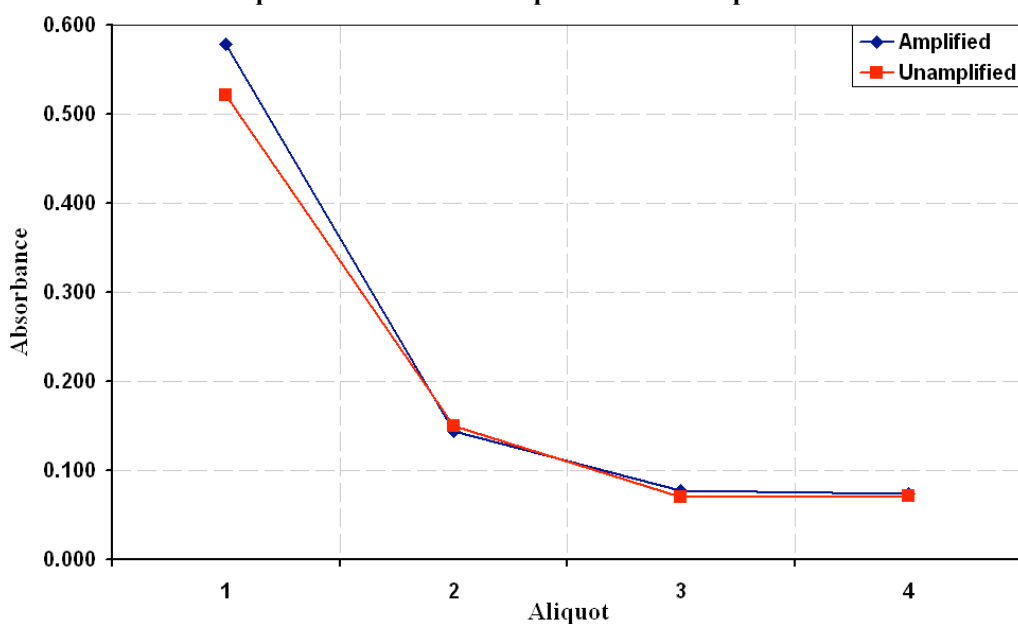


Figure 7.8 : Plot of absorbance of the Amplified versus Unamplified solutions used to test the chemical amplification hypothesis. The plot is taken from the results of the second experiment, testing this, conducted using 4-AAP.

Experiment 2 was a direct repeat of experiment 1. The absorbance of the aliquots of the Amplified and the Unamplified solutions, after the blank had been subtracted from both, was plotted (Figure 7.8). Unamplified solution theoretically has a lower absorbance than the Amplified solution. The plot indicates that either better measurements or more sensitive solutions were required.

The “1 Bottle Method” was modified again for the last two experiments conducted using the 4-AAP/Phenol reaction scheme. The second modification to this method was deemed to be less effective than the first modification. Returning to the calculations performed using Table 7.2 and the plots obtained from previous experiments, the number of aliquots taken was found to be important to effectively observing chemical amplification. While the volume of the aliquots was also important, taking more aliquots allowed a definite trend to be observed. Modification 2 would eventually limit the number of aliquots, while the first modified “1 Bottle Method” could be expanded further.

Following recalculation of Table 7.2 an initial solution volume of 10 mL and aliquot volume of 5 mL were determined to be the most effective volume for the experimental methodology. The need to operate in darkness limited the time length of the experiment and therefore the number of aliquots that could be taken. Higher aliquot volumes would have resulted in absorbances, of the final aliquots, being indistinguishable from the solution background

absorbance. Lower aliquot volumes would have led to lower relative difference between the Unamplified and Amplified solutions' absorbance.

Experimental Test 3 Using 4-AAP : Comparison of the Maximum Absorbance of Each Aliquot Taken from the Amplified and Unamplified Solutions.

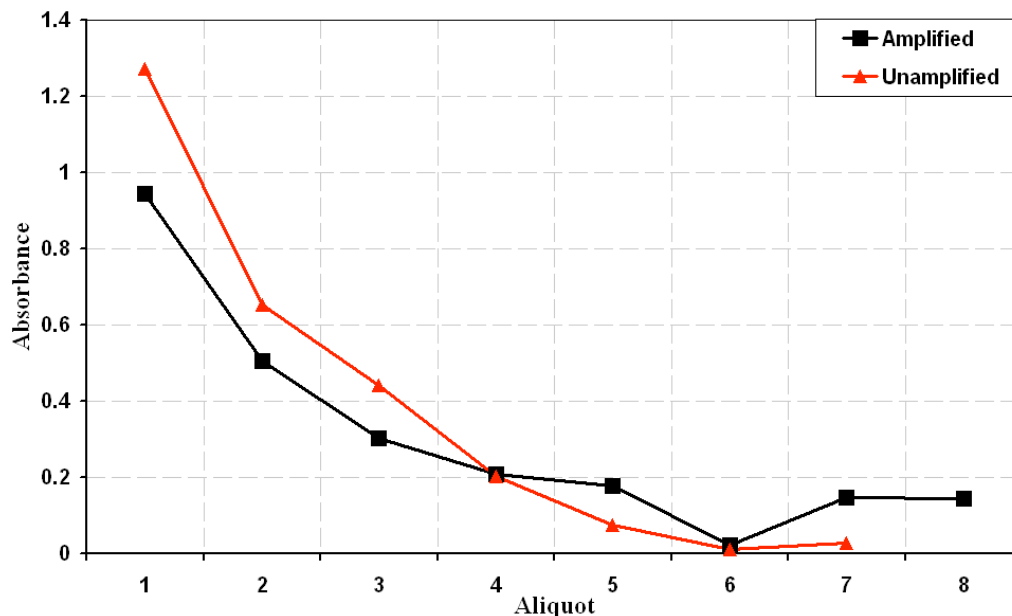


Figure 7.9 : As per Figure 7.8, but the plot describes the results from the third experiment into chemical amplification performed using 4-AAP as an HRP substrate.

No pattern emerged from the plot of the adjusted Amplified versus adjusted Unamplified solutions in Experiment 3 (Figure 7.9).

The timing and aliquot sequence and solution concentration were the two major changes between Experiment 3 and Experiment 4. Both the Amplified and Unamplified aliquots from Experiment 3 were taken in sequence. That is, the first Amplified solution aliquot (A1) was taken, then the first Unamplified aliquot (U1), then A2, U2, and so on. The addition of AOD to the freshly withdrawn Unamplified solution aliquot required that measurement of the absorbance was delayed for 7 hours while the reaction proceeded to completion.

Previous tests had determined the extent of the linearity of the absorbance as a function of 4-AAP/phenol concentration. Increasing the concentration of 4-AAP/phenol and ethanol solution in the final experiment was deemed possible without exceeding the linear range. Disposable cuvettes had been purchased in which all four sides could provide optical paths. By using the shorter path length, the absorbance stayed within the measurement range of the spectrophotometer. The concentration of 4-AAP/phenol solution and ethanol solution was therefore increased by a factor of 2.5 for the final experiment.

Chemical Amplification Experiment

Experimental Test 4 Using 4-AAP : Comparison of the Maximum Absorbance
of Each Aliquot Taken from the Amplified and Unamplified Solutions.

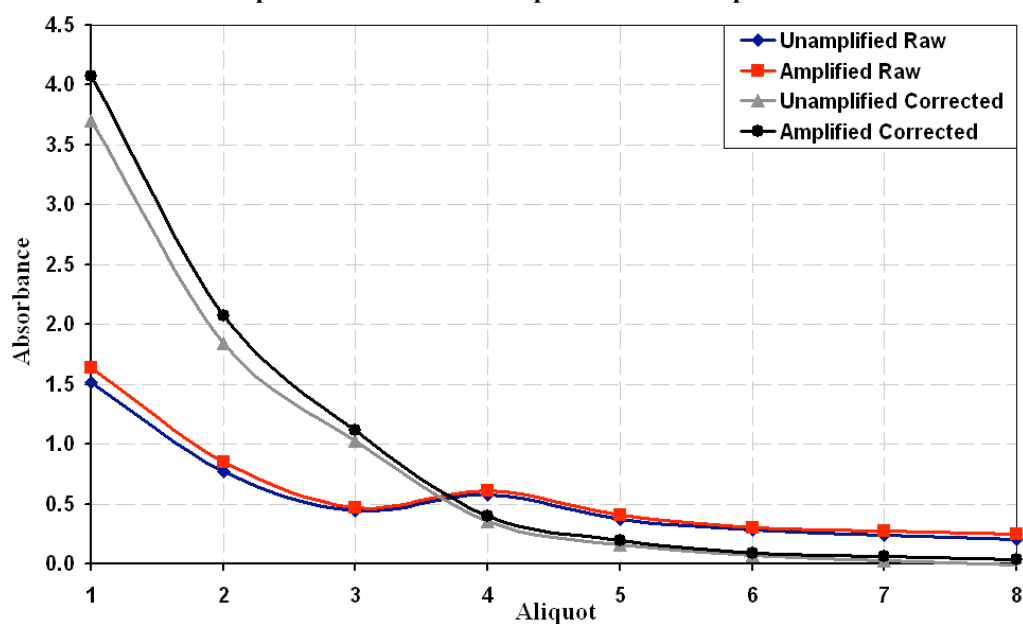


Figure 7.10 : As per Figures 7.8 and 7.9. However the plot relates to the results from Experiment 4, the final experiment. The data treatment used to adjust the raw data is described below.

The fourth experiment provided data that resulted in the best practicable proof of the chemical amplification hypothesis given the historic, but in this context, unfortunate, choice of ethanol as a test analyte. The raw experimental data was processed before calculations to determine the degree of amplification were performed. Figure 7.10 presents the raw and processed data. Data was processed to remove the background absorbance and the effects of using a shorter path length, for the first three aliquots, and dilution, of the unamplified aliquots with AOD. The first three raw data points were obtained using the short path length of the cuvette to enable a higher initial chromophore concentration to be used. This initial high concentration enabled eight aliquots to be taken and therefore a high amplified response relative to the unamplified absorbance to be achieved.

Calculation of the degree of amplification was based on three initial equations. The assumption that the Abs_{max} solution actually gave the absorbance resulting from complete conversion of ethanol was determined to be false. Performing the calculations in this manner, rather than using the Abs_{max} , was therefore necessary. Following Equation 3.6, all variables and coefficients are defined.

Equation 13, the previously discussed Lambert-Beer Equation for the calculation of absorbance.

$$A = \varepsilon \times C \times \ell \quad \text{Equation 13}$$

which can be abbreviated to :

$$C_n \propto A_n \quad \text{Simplified Equation 13}$$

Equation 16, a modified version of Henry's law (Equation 8), is then applied.

$$K_H = \frac{\frac{n_l / V_l}{n_g \times R \times T}}{V_g} \quad \text{Equation 16}$$

The equivalence of the Henry's constant for each aliquot (Equation 17).

$$K_{Hn} = K_{Hn+1} \quad \text{Equation 17}$$

Solving the Equations simultaneously Equation 18 is calculated :

$$K_{Hn+1} = \frac{\left(\frac{A_n}{A_{n+1}} \times V_{gn} - V_{gn+1} \right)}{\left(V_{ln+1} - \frac{A_n}{A_{n+1}} \times (V_{ln} - V_{ln}) \right)} \times R \times T \quad \text{Equation 18}$$

C_n	Concentration of dye in aliquot n . Equivalent to the concentration of dissolved ethanol.
A_n	Absorbance of aliquot n .
K_{Hn}	Henry's constant of aliquot n .
n_l	Number of moles of ethanol in solution.
V_l	Volume of the solution.
n_g	Number of moles of ethanol present as vapour.
R	Gas constant
T	Temperature in Kelvin.
V_{ln}	Volume of aliquot n .
$K_{Hn}(\text{Amplified}_n)$	Henry's constant of the Amplified aliquot n .
$K_{Hn}(\text{Unamplified}_n)$	Henry's constant of the Unamplified aliquot n .

Table 7.4 : List and definition of variables found in Equations 16 – 18.

Using Equation 19 :

$$\text{Degree of Amplification} = \frac{K_{Hn}(\text{Amplified}_n)}{K_{Hn}(\text{Unamplified}_n)} \quad \text{Equation 19}$$

the degree of amplification was calculated. The final results are shown in Table 7.5. Results are shown for each aliquot, as all external factors, such as reaction time, aliquot or solution volume, background absorbance and the lack of a known maximum absorbance are accounted for either by experimental design or in the calculation.

Aliquot number	Degree of Amplification	σ_{abs}
2	-1.1	4
3	1.4	0.8
4	-1.1	0.4
5	6.2	0.7
6	2.9	0.2
7	2.7	0.2
8	0.2	0.02

Table 7.5 : Calculated Degree of Amplification with associated absolute error for each aliquot.

Of the calculated Degree of Amplification, it was determined that only the results for aliquots 6 and 7 were reliable. The measured absorbance of aliquot 8 was above the background absorbance and the measured error in absorbance was about 0.002. Despite this, in previous experiments it had been noted that as the measured absorbance approached the background absorbance, the measurements drifted from the expected value. This rendered the measured absorbance for aliquot 8 unreliable. Experimental error rendered the measured absorbance for the Unamplified aliquot 4 invalid. Finally, the measured absorbances for aliquots 1 to 3, while probably being correct, were inaccurate once processed. The validity of the factor used to convert the absorbance when measured on the short cuvette path length to an equivalent normal path length absorbance was doubtful. The value used was an average of the ratio measured using other solutions. Despite a higher relative error than other measurements the error was judged to be low enough for the results to be valid. However measurements of the ratio, of the long path length absorbance to the short path length absorbance, taken at other times resulted in different averages. As a result, only the processed absorbances for aliquots 5, 6 and 7 are known to be correct.

Performing the calculations for the Amplified and Unamplified aliquots 5, 6 and 7 leads to the Degree of Amplification of aliquots 6 and 7 being legitimate.

Therefore :

Degree of Amplification = 2.8 ± 0.3

While the results upon which this value is calculated are limited by experimental uncertainty. The results are believed to be the best that it is possible to collect given the analyte and the limitations of the instrumentation and the equipment available.

Limitations to the experimental time available, which had already been exceeded, imposed by the PhD program, prevented further corroboration of the result.

8. CONCLUSION

8.1. Vapour Collection

Research into and eventual manufacture of a pressure driven, segmented flow, microfluidic device for vapour collection was conducted. Following the microfabrication and testing of preliminary low resolution devices, greater understanding of the major processes governing two phase fluid flow was achieved.

The establishment of stable segmented flow required finer control than that provided by external pressure sources and valves. Several integrated fluid regulating methods were investigated as the desired properties of the control methodologies were determined. Integrated or integratable Burst, Check and Seal Valves were researched. Burst valves could not be reliably manufactured. Check valves' response times prevented them from being applicable within segmented flow devices, however further development might result in viable unidirectional flow valves. Seal valves were not able to produce regular opening and closing times, as required for a segmented flow, vapour analysis device and were therefore rejected. However further development of the Seal valve's design might result in operational Seal valves.

The evolution of the design of a microfluidic device for the production of stable, pressure driven, segmented gas/liquid flow resulted in a device in which such flow was observed. Such evolution occurred as a consequence of the observed changes to the segmented flow pattern resulting in modifications to the subsequent device design. Fast response time and low volume, external valves combined with high resolution, passive valve structures were both necessary to increase the degree of fluid flow control. *The final device tested exhibited uniform, pressure driven, segmented flow. However the conditions under which it was tested are insufficient to state categorically that the device would have operated under all conditions.* Slight changes to the manufacturing techniques are believed to be necessary before a completely operational device could be presented.

8.2. Chemical Amplification

Following development of the vapour collection system, literature and experimental investigations of analytical methodologies were undertaken. Ethanol was selected for use as a convenient analyte to measure the effectiveness of the vapour collection system. Wet chemical, including standard and biochemical, reactions were investigated following a literature review. A detailed study of each of the analytical methods tested was performed to account for sensitivities to external physical and chemical effects. This study was also extended to an investigation of the modifications to the vapour collection device and the fluid flow regimes required for the chosen method to be most effective.

Ethanol, whilst non-toxic and commonly available was observed to be much more difficult to detect in aqueous solution than expected. Several methods were fully tested before the correct methodology was recognised. *Chemical Amplification*, a two phase method for the augmentation of a detection method in which the analyte is present in one phase, but the assay is performed in the other, was introduced.

Measurement of the Chemical Amplification of ethanol (with a Henry's constant of 200 M/atm) dissolution was always going to be difficult compared to notable examples of low solubility compounds such as 2,4,6-TNT or 2,4-DNT. This was exacerbated by the basic nature of the available spectrophotometer. Modifying the original experiment by performing parallel and simultaneous amplified and unamplified experiments removed temporal and base solution differences. The final selection of the aliquot and original solution volumes provided for multiple aliquots to be taken. *The final experiment proved the hypothesis of Chemical Amplification increasing the proportion of analyte dissolving from one phase into another.*

If this hypothesis had been extended to a more appropriate compound, whether taken from those of interest to anti-terrorist organisations or, just as relevant, environmental groups, then evidence and justification for this hypothesis being of further interest in an analytical context would have been stronger. It would have been less complex to develop a method for an analyte in which the amplified and unamplified response were greater. The care required to try and prevent the slightest physical difference between the two solutions impacting upon the chemical result was *significant*.

8.3. Microfabrication Experiments

The development of methods by which multi-layered structures could be constructed was of major importance for the prevention of differing menisci contact angles (as discussed in Chapter 5). Triple layer structures were designed and manufactured so as to achieve the segmented flow reported in Chapter 5. However further improvement of the alignment method is necessary for the triple depth structures to be completely contiguous throughout the length of the device.

As reported in Chapter 3, masking PDMS to prevent bonding of small regions was unsuccessful. Theoretically once masked by a confluent, UV-resistant (at one or both frequencies) and impermeable membrane, PDMS under the mask should not subsequently bond to another piece of PDMS despite being treated with UV/ozone. Several different masking materials were used, but PDMS continued to bond in all cases. No definite conclusion can be drawn, however it is currently sufficient that an alternative method for masking a section of liquid flow path has been developed. However solution of this problem would allow several of the previously researched valves to be reinvestigated.

A series of experiments were also performed to develop a method by which the surface of PMMA could be chemically modified to provide moieties reactive to UV/ozone treated PDMS. As discussed briefly in Chapter 3, Seal valves were placed onto a PMMA substrate. To bond the PDMS casts to the PMMA it was necessary to coat the PMMA with an SiO₂ coating. While not discussed in detail during within this thesis a serious effort was made to hydrolyse the surface of PMMA using a range of concentrations and temperatures of sodium hydroxide (NaOH). Partial success was achieved. However full bonding only occurred on samples warped (and hence rendered useless) by temperature. Partial bonding did occur on physically unchanged (to the naked eye) samples. However the results were insufficient to justify continuing this line of research.

9. FUTURE WORK

Of the techniques encapsulated within this programme of work, in the authors opinion Chemical Amplification demonstrates the greatest potential and requirement for further investigation. Research performed during the course of this project was limited to investigation of chemical amplification as an aqueous solution based analytical method for ethanol vapour. As ethanol is highly soluble in water the use of chemical amplification to increase the sensitivity of the analysis method would in reality be unnecessary. However, the greatest potential for using chemical amplification in an analytical context is for the determination of a compound that is *almost insoluble* in the phase in which the reaction is taking place. Future applications have been suggested in fields as varied as cell biology and explosives detection. As each analyte/phase system requires a different reaction scheme for chemical amplification to proceed, it is not possible to propose details of potential specific research here.

However a basic indication of an area of possible interest is that of detection of 2,4,6-TNT. Remote chemical detection of mines (in which the most common explosive remains 2,4,6-TNT) is predicated by absorption of TNT present at the parts per trillion level in the air over the soil covering a mine [42]. A constantly regenerating liquid surface (possible even with a limited liquid supply by recirculation) in which the TNT is almost completely soluble, due to an irreversible reaction, should be able to absorb more of the TNT. The normal, localised, dissolution/evaporation equilibria that occur, as analyte concentration increases at the surface and then diffuses into the sorbent, are diminished. Using chemical amplification to overcome the insolubility of TNT in an aqueous solution would remove the need to use organic solvents or polymers as sorbents and allow enzyme based reactions to be used to increase the specificity, as occurred within this programme of work.

The majority of microfluidic devices investigated during the course of this program of research are believed to show little evidence of the potential to progress to a stage whereby they are completely competitive to existing devices, Seal valves are believed to show promise as future microfluidic components. Further developments of these integratable piezoelectric driven valves could include: surface modification of the valve seat to prevent stiction to the valve membrane; an alternative substrate to the SiO₂ coated PMMA currently used; and preferably a different, more flexible, method of bonding the piezoelectric disc to the patterned PDMS. However it is acknowledged that Dr Tan was responsible for their initial, and ultimately future, development.

10. REFERENCES

- [1] *Collins English Dictionary*, 8, Collins, UK, 2006.
- [2] M. Michulec, W. Wardencki, M. Partyka and J. Namiesnik, 2005, Analytical Techniques used in Monitoring of Atmospheric Air Pollutants, *Critical Reviews in Analytical Chemistry*, 35, 2, 117-133.
- [3] A. Gunther and K. F. Jensen, 2006, Multiphase microfluidics: from flow characteristics to chemical and materials synthesis, *Lab On A Chip*, 6, 1487-1503.
- [4] W. Gopel, 2000, From electronic to bioelectronic olfaction, or: from artificial "moses" to real noses, *Sensors and Actuators, B: Chemical Sensors and Materials*, 65, 70-72.
- [5] B. J. Doleman and N. S. Lewis, 2001, Comparison of odor detection thresholds and odor discriminabilities of a conducting polymer composite electronic nose versus mammalian olfaction, *Sensors and Actuators B: Chemical*, 72, 1, 41-50.
- [6] J. W. Gardner and P. N. Bartlett, *Electronic Noses: Principles and Applications*, First, Oxford University Press, Midsomer Norton, 1999.
- [7] R. A. Steinbrecht, 1997, Pore Structures in Insect Olfactory Sensilla: A review of data & concepts, *International Journal of Insect Morphology and Embryology*, 26, 3/4, 229-245.
- [8] B. S. Hansson, 2002, A bug's smell - research into insect olfaction, *Trends in Neurosciences*, 25, 5, 270-274.
- [9] C. Murphy 1987, 'Olfactory psychophysics', in T. E. Finger and W. L. Silver (eds.), *Neurobiology of Taste and Smell*, Wiley, New York, pp. 251-273.
- [10] N. Jones, 2001, The nose and paranasal sinuses physiology and anatomy, *Advanced Drug Delivery Reviews*, 51, 5-19.
- [11] S. Dey, R. N. K. Hooroo and D. Wankhar, 1995, Scanning electron microscopic studies of the external morphology of sensilla on the legs of a butterfly, *Graphium sarpedon* (Lepidoptera--Papilionidae), *Micron*, 26, 5, 367-376.
- [12] J. Krieger and H. Breer, 1999, Olfactory Reception in Invertebrates, *Science*, 286, 720-723.
- [13] T. A. Keil 1999, 'Morphology and Development of the Peripheral Olfactory Organs', in B. S. Hansson (ed.), *Insect Olfaction*, Springer-Verlag, p. 457.
- [14] R. W. S. Schneider, B. A. Price and P. A. Moore, 1998, Antennal morphology as a physical filter of olfaction: temporal tuning of the antennae of the honeybee, *Apis mellifera*, *Journal of Insect Physiology*, 44, 677-684.
- [15] M.-S. Kim and D. P. Smith, 2001, The Invertebrate Odorant-Binding Protein LUSH is required for Normal Olfactory Behaviour in *Drosophila*, *Chemical Senses*, 26, 195-199.
- [16] Z. Deyu and W. S. Leal, 2002, Conformational Isomers of Insect Odorant-Binding Proteins, *Archives of Biochemistry and Biophysics*, 397, 1, 99-105.
- [17] M. J. Huotari, 2000, Biosensing by Insect Olfactory Receptor Neurons, *Sensors and Actuators B: Chemical*, 71, 212 - 222.

- [18] P. Pelosi, 1996, Perireceptor Events in Olfaction, *Journal of Neurobiology*, 30, 1, 3-19.
- [19] H. Gray, '*Anatomy of the Human Body*', ed. W. H. Lewis. Bartleby.com, p. <http://www.bartleby.com/107/>, 2000.
- [20] M. A. Craven, J. W. Gardner and P. N. Bartlett, 2000, Electronic Noses - Development and Future Prospects, *Trends in Analytical Chemistry*, 15, 9, 486-493.
- [21] W. Gopel, C. Ziegler, H. Breer, D. Schild, R. Apfelbach, J. Joerges and R. Malaka, 1998, Bioelectronic noses: a status report Part I, *Biosensors & Bioelectronics*, 13, 3 - 4, 479-493.
- [22] D. Tucker, 1963, Physical Variables in the Olfactory Stimulation Process, *Journal of General Physiology*, 46, 453-489.
- [23] S. Lovett, 'Explosives Search Dogs', in *Proceedings of the First International Symposium on Explosive Detection Technology*, ed. S. M. Khan. NSTI, FAA Technical Center, Atlantic City International Airport, NJ, USA., pp. 774 - 775, 1991.
- [24] D. A. Marshall and D. G. d. Moulton, 1981, Olfactory sensitivity to α -ionone in humans and dogs, *Chem. Senses*, 6, 1, 53-61.
- [25] J. Yinon, 2003, Detection of explosives by electronic noses, *Analytical Chemistry*, March 1, 2003, 99A - 105A.
- [26] J. Goddard 1997, 'A History of Gas Analysis', in J. D. Hogan (ed.), *Specialty Gas Analysis: A Practical Guidebook*, John Wiley & Sons Canada Ltd, Canada, p. 200.
- [27] P. M. Chu, 2003, Advances in optical methods for trace gas analysis, *Analytical and Bioanalytical Chemistry*, 376, 3, 305-307.
- [28] P. Aragón, J. Atienza and M. D. Climent, 2000, Analysis of Organic Compounds in Air: A Review, *Critical Reviews in Analytical Chemistry*, 30, 2-3, 121-151.
- [29] W. Gopel, 1998, Chemical imaging: I. Concepts and visions for electronic and bioelectronic noses, *Sensors and Actuators, B: Chemical Sensors and Materials*, 52, 125-142.
- [30] D. James, S. M. Scott, Z. Ali and W. T. O'Hare, 2005, Chemical sensors for electronic nose systems, *Microchimica Acta*, 149, 1-2, 1-17.
- [31] Y. Okahata, 'A Lipid-coated Quartz crystal Microbalance as an Olfaction Sensor', in *Olfaction and Taste IV*, eds. K. Kurihara, N. Suzuki and H. Ogawa. Springer-Verlag, Tokyo, pp. 703-707, 1994.
- [32] E. Tamiya and I. Karube, 1991, Chemical Vapour Sensing Using a Lipid-Coated SAW Resonator Oscillator, *Biosensors & Bioelectronics*, 6, 9-14.
- [33] J. White, J. S. Kauer, T. A. Dickinson and D. R. Walt, 1996, Rapid Analyte Recognition in a Device Based On Optical Sensors and the Olfactory System, *Analytical Chemistry*, 68, 13, 2191-2202.
- [34] D. D. Stubbs, S.-H. Lee and W. D. Hunt, 2003, Investigation of Cocaine Plumes Using Surface Acoustic Wave Immunoassay Sensors, *Analytical Chemistry*, 75, 6231-6235.

- [35] L. Marques, U. Nunes and A. T. d. Almeida, 2002, Olfaction-based Mobile Robot Navigation, *Thin Solid Films*, 418, 51-58.
- [36] E. J. Houser, T. E. Mlsna, V. K. Nguyen, R. Chung, R. L. Mowery and R. Andrew McGill, 2001, Rational materials design of sorbent coatings for explosives: applications with chemical sensors, *Talanta*, 54, 3, 469-485.
- [37] T. Frisk, D. Ronnholm, W. Van Der Wijngaart and G. Stemme, 2006, A micromachined interface for airborne sample-to-liquid transfer and its application in a biosensor system, *Lab on a Chip - Miniaturisation for Chemistry and Biology*, 6, 12, 1504-1509.
- [38] A. Heilig, N. Barsan, U. Weimar, M. Schweizer-Berberich, J. W. Gardner and W. Gopel, 1997, Gas identification by modulating temperatures of SnO₂-based thick film sensors, *Sensors and Actuators, B: Chemical*, 43, 1-3, 45-51.
- [39] K. J. Albert, M. L. Myrick, S. B. Brown, D. L. James, F. P. Milanovich and D. R. Walt, 2001, Field-deployable sniffer for 2,4-dinitrotoluene detection, *Environmental Science & Technology*, 35, 15, 3193-3200.
- [40] K. J. Albert and D. R. Walt, 2000, High-Speed Fluorescence Detection of Explosives-like Vapors, *Analytical Chemistry*, 72, 9, 1947-1955.
- [41] T. M. Swager and J. H. Wosnick, 2002, Self-amplifying semiconducting polymers for chemical sensors, *Mrs Bulletin*, 27, 6, 446-450.
- [42] M. Fisher, M. laGrone, C. Cumming and E. Towers, 'Utilization of Chemical Vapor Detection of Explosives as a Means of Rapid Minefield Area Reduction', in *Fifth International Symposium on Technology and the Mine Problem*, vol. 2 Society for Counter Ordnance Technology, Naval Postgraduate School, Monterey, USA, 2002.
- [43] A. D'Amico, C. Di Natale, A. Macagnano, F. Davide, A. Mantini, E. Tarizzo, R. Paolesse and T. Boschi, 1998, Technologies and tools for mimicking olfaction: status of the Rome "Tor Vergata" electronic nose, *Biosensors and Bioelectronics*, 13, 6, 711-721.
- [44] D. J. Butcher, 2000, The real-time analysis of gases by direct sampling-mass spectrometry: elemental and molecular applications, *Micromechanical Journal*, 66, 55 - 72.
- [45] R. G. Ewing, D. A. Atkinson, G. A. Eiceman and G. J. Ewing, 2001, A critical review of ion mobility spectrometry for the detection of explosives and explosive related compounds, *Talanta*, 54, 3, 515-529.
- [46] D. L. Garcia-Gonzalez and R. Aparicio, 2002, Sensors: From biosensors to the electronic nose, *Grasas y Aceites*, 53, 1, 96-114.
- [47] K. E. Peterson, 1982, Silicon as a Mechanical Material, *Proceedings of the IEEE*, 70, 5, 420-457.
- [48] O. Geschke, H. Klank and P. Telleman, *Microsystem Engineering of Lab-on-a-Chip Devices*, Wiley-VCH Verlag GmbH, Morlenbach, 2004.
- [49] F. M. White, *Viscous Fluid Flow*, 2nd, McGraw-Hill International Editions, Singapore, 1991.
- [50] F. M. White, *Fluid Mechanics*, 3rd, McGraw-Hill International Editions, USA, 1994.

- [51] P. J. A. Kenis, R. F. Ismagilov and G. M. Whitesides, 1999, Microfabrication Inside Capillaries Using Multiphase Laminar Flow Patterning, *Science*, 285, 5424, 83-85.
- [52] K. A. Triplett, S. M. Ghiaasiaan, S. I. Abdel-Khalik and D. L. Sadowski, 1999, Gas-liquid two-phase flow in microchannels Part I: two-phase flow patterns, *International Journal of Multiphase Flow*, 25, 3, 377-394.
- [53] P. A. Greenwood and G. M. Greenway, 2002, Sample manipulation in micro total analytical systems, *TrAC Trends in Analytical Chemistry*, 21, 11, 726-740.
- [54] J. Eijkel, 2007, Liquid Slip in Micro- and NanoFluidics: Recent Research and its Possible Implications, *Lab On A Chip*, 7, 299 - 301.
- [55] S. Prabhakara and M. D. Deshpande, 2004, The No-Slip Boundary Condition in Fluid Mechanics, *Resonance*, 9, 4, 50 - 60.
- [56] P. Tabeling, 'Some Basic Problems in Microfluidics', in *14th Australasian Fluid Mechanics Conference*, Adelaide University, Adelaide, Australia, p. 6, 2001.
- [57] H. J. V. Tyrrell, 1964, The Origin and Present Status of Fick's Diffusion Law, *Journal of Chemical Education*, 41, 7, 397-400.
- [58] W.-J. Chang, D. Akin, M. Sedlak, M. R. Ladisch and R. Bashir, 2003, Poly(dimethylsiloxane) (PDMS) and Silicon Hybrid Biochip for Bacterial Culture, *Biomedical Microdevices*, 5, 4, 281-290.
- [59] C. H. Ahn, J. W. Choi, G. Beaucage, J. H. Nevin, J. B. Lee, A. Puntambekar and J. Y. Lee, 2004, Disposable smart lab on a chip for point-of-care clinical diagnostics, *Proceedings of the IEEE*, 92, 1, 154-173.
- [60] D. J. Laser and J. G. Santiago, 2004, A review of micropumps, *Journal of Micromechanics and Microengineering*, 14, 6, R35-R64.
- [61] P. Woias, 2005, Micropumps - Past, progress and future prospects, *Sensors and Actuators, B: Chemical*, 105, 1, 28-38.
- [62] V. Hessel, H. Löwe and F. Schönfeld, 2005, Micromixers—a review on passive and active mixing principles, *Chemical Engineering Science*, ?, ?, ?
- [63] P. Wang, G. Xu, L. Qin, Y. Xu, Y. Li and R. Li, 2005, Cell-based biosensors and its application in biomedicine, *Sensors and Actuators B: Chemical*, 108, 1-2, 576-584.
- [64] P. J. Viskari and J. P. Landers, 2006, Unconventional detection methods for microfluidic devices, *ELECTROPHORESIS*, 27, 9, 1797-1810.
- [65] E. J. Staples and G. Watson, 1999, *Method and Apparatus for Identifying and Analysing Vapor Elements*, Amerasia Technology Inc., (patent).
- [66] M. W. Geis and R. R. Kunz, 'Chemical concentrator for rapid vapor detection', in *Detection and Remediation Technologies for Mines and Minelike Targets IV*, vol. 3710. SPIE, Orlando, FL, USA, pp. 421-432, 1999.
- [67] D. A. M. Mackay and M. M. Hussein, 1979, Large Bore Coated Columns for Sampling and Concentration of Organic Volatiles in Air, Headspace and Water Analysis, *Journal of Chromatography*, 176, 291 - 303.

- [68] K. L. Hambacker, S. Kapila, P. K. Nam, M. Gehrke and V. I. Flanigan, 'Rapid vapor concentrator and detection system for nitroaromatics', in *Detection and Remediation Technologies for Mines and Minelike Targets VI*, vol. 4394. SPIE, Orlando, FL, USA, pp. 899-911, 2001.
- [69] J. I. Baumbach, 2006, Process analysis using ion mobility spectrometry, *Analytical and Bioanalytical Chemistry*, 384, 5, 1059-1070.
- [70] D. D. Parrish and F. C. Fehsenfeld, 2000, Methods for gas-phase measurements of ozone, ozone precursors and aerosol precursors, *Atmospheric Environment*, 34, 12-14, 1921-1957.
- [71] I. Sanz-Vicente, S. Cabredo and J. Galban, 1998, Gas chromatography with UV-vis molecular absorption spectrometry detection: Increasing sensitivity of the determination of alcohols and phenols by derivatization, *Chromatographia*, V48, 7, 542-547.
- [72] Y. Takabayashi, M. Uemoto, K. Aoki, T. Odake and T. Korenaga, 2006, Development and optimization of a lab-on-a-chip device for the measurement of trace nitrogen dioxide gas in the atmosphere, *The Analyst*, 131, 573-578.
- [73] X. Xie, A. A. Suleiman, G. G. Guilbault, Z. Yang and Z.-a. Sun, 1992, Flow-injection determination of ethanol by fiber-optic chemiluminescence measurement, *Analytica Chimica Acta*, 266, 2, 325-329.
- [74] C. B. Boring and P. K. Dasgupta, 1997, An affordable high-performance optical absorbance detector for capillary systems, *Analytica Chimica Acta*, 342, 2-3, 123-132.
- [75] B. H. Timmer, K. M. van Delft, R. P. Otjes, W. Olthuis and A. v. d. Berg, 2004, Miniaturized measurement system for ammonia in air, *Analytica Chimica Acta*, 507, 1, 137-143.
- [76] C. E. W. Hahn, 1998, Electrochemical analysis of clinical blood-gases, gases and vapours, *Analyst*, 123, 6, 57R-86R.
- [77] W. E. Steiner, B. H. Clowers, P. E. Haigh and H. H. Hill, 2003, Secondary Ionization of Chemical Warfare Agent Simulants: Atmospheric Pressure Ion Mobility Time-of-Flight Mass Spectrometry, *Analytical Chemistry*, 75, 6068 - 6076.
- [78] D. A. Skoog, F. J. Holler and T. A. Nieman, *Principles of Instrumental Analysis*, 5th, Thomson Learnign Inc., USA, 1998.
- [79] R. B. Silverman, *The Organic Chemistry of Enzyme-Catalysed Reactions*, 1st, Academic Press, USA, 2000.
- [80] F. Jameison, R. I. Sanchez, L. Dong, J. K. Leland, D. Yost and M. T. Martin, 1996, Electrochemiluminescence-Based Quantitation of Classical Clinical Chemistry Analytes, *Analytical Chemistry*, 68, 8, 1298 - 1302.
- [81] A. Roda, M. Guardigli, E. Michelini, M. Mirasoli and P. Pasini, 2003, Analytical Bioluminescence and Chemiluminescence, *Analytical Chemistry*, 75, 21, 462A - 470A.
- [82] D. Figeys and D. Pinto, 2000, Lab-on-a-Chip: A Revolution in Biological and Medical Sciences - A look at some of the basic concepts and novel components used to construct prototype devices., *Analytical Chemistry*, 72, 9, 330A - 335A.

- [83] P. S. Dittrich and P. Schuille, 2003, An Integrated Microfluidic System for Reaction, High-Sensitivity Detection, and Sorting of Fluorescent Cells and Particles, *ANALYTICAL CHEMISTRY*, 75, 21, 5767 - 5774.
- [84] K. Huikko, R. Kostianen and T. Kotiaho, 2003, Introduction to micro-analytical systems: bioanalytical and pharmaceutical applications, *European Journal of Pharmaceutical Sciences*, 20, 149 - 171.
- [85] P. Gravesen, J. Branebjerg and O. S. Jensen, 1993, Microfluidics - a review, *Journal of Micromechanics and Microengineering*, 3, 4, 168-182.
- [86] N. Rott, 1990, Note on the History of the Reynolds Number, *Annual Review of Fluid Mechanics*, 22, 1, 1-12.
- [87] N.-T. Nguyen and S. T. Wereley, *Fundamentals and Applications of Microfluidics*, Artech House Inc., USA, 2002.
- [88] K. Fateh-Alavi, 'The Effect of Stabilizers on the Discharge-Induced Oxidation of Crosslinked Polydimethylsiloxane'. KTH Fiber-och Polymerteknologi, Stockholm, p. 67, 2004.
- [89] W. L. Robb, 1968, Thin silicone membranes--their permeation properties and some applications, *Ann N Y Acad Sci*, 146, 1, 119-37.
- [90] I. De Bo, H. Van Langenhove, P. Pruuost, J. De Neve, J. Pieters, I. F. J. Vankelecom and E. Dick, 2003, Investigation of the permeability and selectivity of gases and volatile organic compounds for polydimethylsiloxane membranes, *Journal of Membrane Science*, 215, 1-2, 303-319.
- [91] J. C. Lotters, W. Olthuis, P. H. Veltink and P. Bergveld, 1997, The mechanical properties of the rubber elastic polymer polydimethylsiloxane for sensor applications, *Journal of Micromechanics and Microengineering*, 7, 3, 145-147.
- [92] J. H. Chan and S. T. Balke, 1997, The thermal degradation kinetics of polypropylene: Part III. Thermogravimetric analyses, *Polymer Degradation and Stability*, 57, 2, 135-149.
- [93] G. Camino, S. M. Lomakin and M. Lazzari, 2001, Polydimethylsiloxane thermal degradation Part 1. Kinetic aspects, *Polymer*, 42, 6, 2395-2402.
- [94] L. Fritz and D. Hofmann, 1997, Molecular dynamics simulations of the transport of water-ethanol mixtures through polydimethylsiloxane membranes, *Polymer*, 38, 5, 1035-1045.
- [95] J. N. Lee, C. Park and G. M. Whitesides, 2003, Solvent compatibility of poly(dimethylsiloxane)-based microfluidic devices, *Analytical Chemistry*, 75, 23, 6544-6554.
- [96] R. Feng and R. J. Farris, 2003, Influence of Processing Conditions on the Thermal and Mechanical Properties of SU8 Negative Photoresist Coating., *Journal of Micromechanics and Microengineering*, 13, 80-88.
- [97] J. M. Shaw, J. D. Gelorme, N. C. LaBianca, W. E. Conley and S. J. Holmes, 1997, Negative Photoresists for Optical Lithography, *IBM Journal of Research and Development*, 41, 1/2, 81 - 94.
- [98] H. Lorenz, M. Despont, N. Fahrni, N. LaBianca, P. Renaud and P. Vettiger, 1997, SU-8: a low-cost negative resist for MEMS, *Journal of Micromechanics and Microengineering*, 7, 3, 121-124.

- [99] <http://www.geocities.com/guerini/>,
- [100] J. Brandrup and E. H. Immergut, 'Polymer Handbook'. Wiley Interscience, USA, 1989.
- [101] D. Armani, C. Liu and N. Aluru, 'Re-Configurable Fluid Circuits by PDMS Elastomer Micromachining', in *12th International Conference on MEMS, MEMS 99*, Orlando, USA, 1998.
- [102] D. C. Duffy, J. C. McDonald, O. J. A. Schueller and G. M. Whitesides, 1998, Rapid Prototyping of Microfluidic Systems in Poly(dimethylsiloxane), *Analytical Chemistry*, 70, 23, 4974 - 4984.
- [103] K. Efimenko, W. E. Wallace and J. Genzer, 2002, Surface Modification of Sylgard-184 Poly(dimethyl siloxane) Networks by Ultraviolet and Ultraviolet/Ozone Treatment, *Journal of Colloid and Interface Science*, 254, 2, 306-315.
- [104] Y. Berdichevsky, J. Khandurina, A. Guttman and Y.-H. Lo, 2004, UV/ozone modification of poly(dimethylsiloxane) microfluidic channels, *Sensors and Actuators B: Chemical*, 97, 2-3, 402-408.
- [105] A. de Mello, 2002, Plastic fantastic?, *Lab on a Chip*, 2, 2, 31N-36N.
- [106] J. B. Davis, Personal Communication, 2007.
- [107] G. A. C. M. Spierings, J. Haisma and F. J. H. M. van der Kruis, 1995, Direct bonding of organic polymeric materials, *Philips Journal of Research*, 49, 1-2, 139-149.
- [108] H. Becker and U. Heim, 2000, Hot embossing as a method for the fabrication of polymer high aspect ratio structures, *Sensors and Actuators a-Physical*, 83, 1-3, 130-135.
- [109] L. Martynova, L. E. Locascio, M. Gaitan, G. W. Kramer, R. G. Christensen and W. A. MacCrehan, 1997, Fabrication of plastic microfluid channels by imprinting methods, *Analytical Chemistry*, 69, 23, 4783-4789.
- [110] K. W. Oh and C. H. Ahn, 2006, A review of microvalves, *Journal of Micromechanics and Microengineering*, 16, 5, R13-R39.
- [111] C. Feldt and L. Chew, 2002, Geometry-based macro-tool evaluation of non-moving-part valvular microchannels, *Journal of Micromechanics and Microengineering*, 12, 5, 662.
- [112] J. E. Rehm, T. J. Shepodd and E. F. Hasselbrink, 'Mobile Flow Control Elements for High-Pressure Micro-Analytical Systems Fabricated Using In-Situ Polymerization', in *Micro Total Analysis Systems 2001*, vol. 1, eds. J. M. Ramsay and A. v. d. Berg. Kluwer Academic Publishers, pp. 227 - 229, 2001.
- [113] E. Stemme and G. Stemme, 1993, A valveless diffuser/nozzle-based fluid pump, *Sensors and Actuators A: Physical*, 39, 2, 159-167.
- [114] M. L. Adams, M. L. Johnston, A. Scherer and S. R. Quake, 2005, Polydimethylsiloxane Based Microfluidic Diode, *Journal of Micromechanics and Microengineering*, 15, 1517 - 1521.
- [115] E. F. Hasselbrink Jr, T. J. Shepodd and J. E. Rehm, 2002, High-pressure microfluidic control in lab-on-a-chip devices using mobile polymer monoliths, *Analytical Chemistry*, 74, 19, 4913-4918.

- [116] M. A. Unger, H. P. Chou, T. Thorsen, A. Scherer and S. R. Quake, 2000, Monolithic microfabricated valves and pumps by multilayer soft lithography, *Science*, 288, 5463, 113-116.
- [117] N. L. Jeon, D. T. Chiu, C. J. Wargo, H. Wu, I. S. Choi, J. R. Anderson and G. M. Whitesides, 2002, Design and Fabrication of Integrated Passive Valves and Pumps for Flexible Polymer 3-Dimensional Microfluidic Systems, *Biomedical Microdevices*, 4, 2, 117 - 121.
- [118] C. K. L. Tan, M. C. Tracey, J. B. Davis and I. D. Johnston, 2005, Continuously Variable Mixing-ratio, Micromixer with Elastomer Valves, *Journal of Micromechanics and Microengineering*, 15, 1 - 9.
- [119] D. T. Eddington and D. J. Beebe, 2004, Flow control with hydrogels, *Advanced Drug Delivery Reviews*, 56, 2, 199-210.
- [120] N. Pamme, 2006, Magnetism and microfluidics, *Lab on a Chip - Miniaturisation for Chemistry and Biology*, 6, 1, 24-38.
- [121] C. K. L. Tan, 'The Development of a Variable Mixing-Ratio Alternate-Flow Injection Micromixer with Elastomer Valves', in *STRI*, vol. Doctor of Philosophy. University of Hertfordshire, Hatfield, 2006.
- [122] D. K. W. Wang and C. C. Austin, 2006, Determination of complex mixtures of volatile organic compounds in ambient air: an overview, *Analytical and Bioanalytical Chemistry*, 386, 4, 1089-1098.
- [123] M. Harper, 2000, Sorbent trapping of volatile organic compounds from air, *Journal of Chromatography A*, 885, 1-2, 129-151.
- [124] J. Crank, *The Mathematics of Diffusion*, 2nd, Oxford University Press, Oxford, 1975.
- [125] M. Kumemura and T. Korenaga, 2003, Droplets formation from microfluidic device for sampling and measurement of atmospheric nitrogen dioxide, *The Analyst*, 129, 105 - 106.
- [126] B. K. H. Yen, A. Günther, M. A. Schmidt, K. F. Jensen and M. G. Bawendi, 2005, A Microfabricated Gas-Liquid Segmented Flow Reactor for High Temperature Synthesis: The Case of CdSe Quantum Dots, *Angewandte Chemie*, 117, 2 - 6.
- [127] W. Frenzel, 1994, Permeation denuder for sampling and continuous analysis of gases Part 1. System configuration, basic studies and application to atmospheric ammonia and sulfur dioxide, *Analytica Chimica Acta*, 291, 3, 305-320.
- [128] A. S. Kovvali, S. Vemury, K. R. Krovvidi and A. A. Khan, 1992, Models and analyses of membrane gas permeators, *Journal of Membrane Science*, 73, 1, 1-23.
- [129] A. P. Vollmer, R. F. Probst, R. Gilbert and T. Thorsen, 2005, Development of an integrated microfluidic platform for dynamic oxygen sensing and delivery in a flowing medium, *Lab On A Chip*, 5, 1059 - 1066.
- [130] K. Toda, P. K. Dasgupta, J. Li, G. A. Tarver and G. M. Zarus, 2001, Fluorometric Field Instrument for Continuous Measurement of Atmospheric Hydrogen Sulfide, *Analytical Chemistry*, 73, 23, 5716 - 5724.

- [131] K. Toda, S.-I. Ohira and M. Ikeda, 2004, Micro-gas analysis system [μ]GAS comprising a microchannel scrubber and a micro-fluorescence detector for measurement of hydrogen sulfide, *Analytica Chimica Acta*, 511, 1, 3-10.
- [132] H. Strathmann, 1981, Membrane separation processes, *Journal of Membrane Science*, 9, 1-2, 121-189.
- [133] B. Zhao, J. S. Moore and D. J. Beebe, 2001, Surface-Directed Liquid Flow Inside Microchannels, *Science*, 291, 5506, 1023-1026.
- [134] A. Hibara, S. Iwayama, S. Matsuoka, M. Ueno, Y. Kikutani, M. Tokeshi and T. Kitamori, 2005, Surface Modification Method of Microchannels for Gas-Liquid Two-Phase Flow in Microchips, *Analytical Chemistry*, 77, 3, 943 - 947.
- [135] J. M. Bauer and D. J. Beebe, 'Microscale Measurements of Flow Bounded by Air-Water Interface', in *Micro Total Analysis Systems 2002*, vol. 1, ed. Y. Baba. Kluwer Academic Publishers, pp. 100 - 102, 2002.
- [136] A. A. Cardoso and P. K. Dasgupta, 1995, Analytical Chemistry in a Liquid Film/Droplet, *Analytical Chemistry*, 67, 15, 2562 - 2566.
- [137] S. R. Liu and P. K. Dasgupta, 1995, Liquid Droplet - A Renewable Gas Sampling Interface, *Analytical Chemistry*, 67, 13, 2042 - 2049.
- [138] Z. Genfa and P. K. Dasgupta, 2000, A Continuous Film-Recirculable Drop Gas-Liquid Equilibration Device. Measurement of Trace Gaseous Ammonia, *Analytical Chemistry*, 72, 14, 3165 - 3170.
- [139] K. Jahnisch, M. Baerns, V. Hessel, W. Ehrfeld, V. Haverkamp, H. Lowe, C. Wille and A. Guber, 2000, Direct fluorination of toluene using elemental fluorine in gas/liquid microreactors, *Journal of Fluorine Chemistry*, 105, 1, 117-128.
- [140] J. M. Commenge, T. Obein, G. Genin, X. Framboisier, S. Rode, V. Schanen, P. Pitiot and M. Matlosz, 2006, Gas-phase residence time distribution in a falling-film microreactor, *Chemical Engineering Science*, 61, 2, 597-604.
- [141] G. I. Taylor, 1961, Deposition of a viscous fluid on the wall of a tube, *Journal of Fluid Mechanics*, 10, 161 - 165.
- [142] M. Suo and P. Griffith, 1964, Two-Phase Flow in Capillary Tubes, *Transactions of the ASME: Journal of Basic Engineering*, September 1964, 576 - 582.
- [143] V. Hatziantoniou and B. Andersson, 1984, The segmented two-phase flow monolithic catalyst reactor. An alternative for liquid-phase hydrogenations, *Industrial and Engineering Chemistry Fundamentals*, 23, 1, 82-88.
- [144] T. A. Nijhuis, M. T. Kreutzer, A. C. J. Romijn, F. Kapteijn and J. A. Moulijn, 2001, Monolithic catalysts as efficient three-phase reactors, *Chemical Engineering Science*, 56, 3, 823-829.
- [145] M. J. Simmons, D. C. Y. Wong, P. J. Travers and J. S. Rothwell, 2003, Bubble Behaviour in Three Phase Capillary Microreactors, *International Journal of Chemical Reactor Engineering*, 1, A30 - A45.
- [146] C. N. Baroud and H. Willaime, 2004, Multiphase flows in microfluidics, *Comptes Rendus Physique*, 5, 5, 547-555.

- [147] G. N. Doku, W. Verboom, D. N. Reinhoudt and A. v. d. Berg, 2005, On-microchip multiphase chemistry—a review of microreactor design principles and reagent contacting modes, *Tetrahedron*, 61, 2733 - 2742.
- [148] A. M. Ganan-Calvo and J. M. Gordillo, 2001, Perfectly Monodisperse Microbubbling by Capillary Flow Focusing, *Physical Review Letters*, 87, 27, 1 - 4.
- [149] T. Cubaud, U. Ulmanella and C.-M. Ho, 'Two-Phase Flow in Microchannels with Surface Modifications', in *International Conference on Multiphase Flow*, Yokohama, pp. 1 - 11, 2004.
- [150] A. Günther, S. A. Khan, M. Thalmann, F. Trachsel and K. F. Jensen, 2004, Transport and reaction in microscale segmented Gas-liquid flow., *Lab on a Chip*, 4, 278 - 286.
- [151] S. L. Anna, N. Bontoux and H. A. Stone, 2003, Formation of dispersions using "flow focusing" in microchannels, *Applied Physics Letters*, 82, 3, 364-366.
- [152] A. Gunther, M. Jhunjhunwala, M. Thalmann, M. A. Schmidt and K. F. Jensen, 2005, Micromixing of Miscible Liquids in Segmented Gas-Liquid Flow, *Langmuir*, 21, 4, 1547 - 1555.
- [153] H. Song, J. D. Tice and R. F. Ismagilov, 2003, A microfluidic system for controlling reaction networks in time, *Angewandte Chemie - International Edition*, 42, 7, 768-772.
- [154] A. D. Stroock, S. K. W. Dertinger, A. Ajdari, I. Mezic, H. A. Stone and G. M. Whitesides, 2002, Chaotic mixer for microchannels, *Science*, 295, 5555, 647-651.
- [155] R. H. Liu, M. A. Stremler, K. V. Sharp, M. G. Olsen, J. G. Santiago, R. J. Adrian, H. Aref and D. J. Beebe, 2000, Passive mixing in a three-dimensional serpentine microchannel, *Journal of Microelectromechanical Systems*, 9, 2, 190-197.
- [156] M. J. Jensen, G. Goranovic and H. Bruus, 2004, The clogging pressure of bubbles in hydrophilic microchannel contractions, *Journal of Micromechanics and Microengineering*, 14, 7, 876-883.
- [157] T.-S. Leu and P.-Y. Chang, 2004, Pressure barrier of capillary stop valves in micro sample separators, *Sensors and Actuators A: Physical*, 115, 2-3, 508-515.
- [158] A. R. Vijayakumar, E. Csoregi, A. Heller and L. Gorton, 1996, Alcohol biosensors based on coupled oxidase-peroxidase systems, *Analytica Chimica Acta*, 327, 3, 223-234.
- [159] R. Davidsson, F. Genin, M. Bengtsson, T. Laurell and J. Emneus, 2004, Microfluidic Biosensing Systems: Part 1. Development and Optimisation of Enzymatic Chemiluminescent u-Biosensors Based on Silicon Microchips, *Lab On A Chip*, 4, 481 - 487.
- [160] R. Davidsson, B. Johansson, V. Passoth, M. Bengtsson, T. Laurell and J. Emneus, 2004, Microfluidic Biosensing Systems: Part 2. Monitoring the Dynamic Production of Glucose and Ethanol from Microchip-Immobilised Yeast Cells Using Enzymatic Chemiluminescent u-Biosensors, *Lab on a Chip*, 4, 488 - 494.
- [161] R. Schulte-Ladbeck, P. Kolla and U. Karst, 2003, Trace analysis of peroxide-based explosives, *Analytical Chemistry*, 75, 4, 731-735.
- [162] S. Gawad, L. Schild and P. Renaud, 2001, Micromachined impedance spectroscopy flow cytometer for cell analysis and particle sizing, *Lab on a Chip*, 1, 1, 76 - 82.

- [163] I. Braslavsky, B. Hebert, E. Kartalov and S. R. Quake, 2003, Sequence information can be obtained from single DNA molecules, *Proceedings of the National Academy of Sciences*, 100, 7, 3960 - 3964.
- [164] M. A. McClain, C. T. Culbertson, S. C. Jacobson, N. L. Allbritton, C. E. Sims and J. M. Ramsey, 2003, Microfluidic Devices for the High-Throughput Chemical Analysis of Cells, *Analytical Chemistry*, 75, 21, 5646 - 5655.
- [165] H.-P. Chou, C. Spence, A. Scherer and S. Quake, 1999, A microfabricated device for sizing and sorting DNA molecules, *Proceedings of the National Academy of Sciences*, 96, 11 - 13.
- [166] P. S. Dittrich and A. Manz, 2006, Lab-on-a-chip: microfluidics in drug discovery, *Nature Reviews: Drug Discovery*, 5, 210 - 218.
- [167] M. A. Schwarz and P. C. Hauser, 2001, Recent developments in detection methods for microfabricated analytical devices, *Lab on a Chip*, 1, 1, 1-6.
- [168] J. H. Chan, A. T. Timperman, D. Qin and R. Aebersold, 1999, Microfabricated Polymer Devices for Automated Sample Delivery of Peptides for Analysis by Electrospray Ionization Tandem Mass Spectrometry, *Analytical Chemistry*, 71, 4437 - 4444.
- [169] G. J. M. Bruin, 2000, Recent Developments in Electrokinetically Driven Analysis on Microfabricated Devices, *Electrophoresis*, 21, 3931 - 3951.
- [170] J. P. Kutter, 2000, Current developments in electrophoretic and chromatographic separation methods on microfabricated devices, *Trac-Trends in Analytical Chemistry*, 19, 6, 352-363.
- [171] R. D. Oleschuk and D. J. Harrison, 2000, Analytical microdevices for mass spectrometry, *Trac-Trends in Analytical Chemistry*, 19, 6, 379-388.
- [172] Y. Weiping, L. Chong, L. Jianhua, M. Lingzhi and N. Defang, 2005, Thermal distribution microfluidic sensor based on silicon, *Sensors and Actuators, B: Chemical*, 108, 1-2 SPEC. ISS., 943-946.
- [173] A. M. Azevedo, D. M. F. Prazeres, J. M. S. Cabral and L. P. Fonseca, 2005, Ethanol biosensors based on alcohol oxidase, *Biosensors and Bioelectronics*, 21, 2, 235-247.
- [174] A. Caputi Jr, 'Official Methods of Analysis'. Association Of Analytical Chemists, Washington DC, 1990.
- [175] M. Unger, E. Kartalov, C.-S. Chiu, H. A. Lester and S. R. Quake, 1999, Single Molecule Fluorescence Observed with Mercury Lamp Illumination, *BioTechniques*, 27, 5, 1008 - 1014.
- [176] B. Tang, Y. Wang and L. Ma, 2004, Simple and rapid catalytic spectrophotometric determination of superoxide anion radical and superoxide dismutase activity in natural medical vegetables using phenol as the substrate for horseradish peroxidase, *Analytical and Bioanalytical Chemistry*, 378, 2, 523-528.
- [177] X. L. Shi, N. S. Dalal and K. S. Kasprzak, 1993, Generation of Free Radicals from Hydrogen Peroxide and Lipid Hydroperoxides in the Presence of Cr(III), *Archives of Biochemistry and Biophysics*, 302, 1, 294-299.
- [178] E. H. WHITE and D. F. ROSWELL, 1970, The Chemiluminescence of Organic Hydrazides, *Chemiluminescence*, 3, 54 - 62.

- [179] W. R. Seitz, W. W. Suydam and D. M. Hercules, 1972, Determination of Trace Amounts of Chromium(III) Using Chemiluminescence Analysis, *Analytical Chemistry*, 44, 6, 957 - 963.
- [180] Z. Genfa, P. K. Dasgupta, W. S. Edgmond and J. N. Marx, 1991, Determination of hydrogen peroxide by photoinduced fluorogenic reactions, *Analytica Chimica Acta*, 243, 207-216.
- [181] B. S. Walters, T. J. Nielsen and M. A. Arnold, 1988, Fiber-optic biosensor for ethanol, based on an internal enzyme concept, *Talanta*, 35, 2, 151-155.
- [182] V. Menon, C. T. Hsieh and P. F. Fitzpatrick, 1995, Substituted alcohols as mechanistic probes of alcohol oxidase, *Bioorganic Chemistry*, 23, 1, 42-53.
- [183] I. J. Van Der Kleij, W. Harder and M. Veenhuis, 1991, Biosynthesis and assembly of alcohol oxidase, a peroxisomal matrix protein in methylotrophic yeasts: A review, *Yeast*, 7, 3, 195-209.
- [184] R. Couderc and J. Baratti, 1980, Oxidation of Methanol by the Yeast, *Pichia-Pastoris* - Purification and Properties of the Alcohol Oxidase, *Agricultural and Biological Chemistry*, 44, 10, 2279-2289.
- [185] F. Delgado-Reyes, I. Papaefstathiou, J. M. F. Romero and M. D. L. d. Castro, 1998, Monitoring ethanol production during wine fermentation processes by a pervaporation-enzymic derivatisation approach, *The Analyst*, 123, 2367 - 2372.
- [186] A. L. Lazrus, G. L. Kok, S. N. Gitlin, J. A. Lind and S. E. McLaren, 1985, Automated Fluorometric Method for Hydrogen Peroxide in Atmospheric Precipitation, *Analytical Chemistry*, 57, 917 - 922.
- [187] J. A. Nicell and H. Wright, 1997, A model of peroxidase activity with inhibition by hydrogen peroxide, *Enzyme and Microbial Technology*, 21, 4, 302-310.
- [188] G. G. Guilbault, P. J. Brignac and M. Juneau, 1968, New Substrates for the Fluorometric Determination of Oxidative Enzymes, *Analytical Chemistry*, 40, 8, 1256 - 1263.
- [189] V. F. Hofmann, L. Hofmann, W. Hubl and D. Meissner, 1984, Die Aktivitätsbestimmung der Meerrettich-Peroxidase (HRP) mit den Substraten H₂O₂ und *p*-Hydroxyphenyllessignature (HPA) im Fluoreszenz-Enzym-Immunoassay, *Zeitschrift für Medizinisches El Laboratorium Diagnostik*, 25, 1, 14 - 21.
- [190] R. E. Childs and W. G. Bardsley, 1975, The Steady-State Kinetics of Peroxidase with 2,2'-Azino-di-(3-ethylbenzthiazoline-6-sulphonic acid) as Chromogen, *Journal of Biochemistry*, 145, 93 - 103.
- [191] P. D. Josephy, T. Eling and R. P. Mason, 1982, The horseradish peroxidase-catalyzed oxidation of 3,5,3',5'- tetramethylbenzidine. Free radical and charge-transfer complex intermediates, *J. Biol. Chem.*, 257, 7, 3669-3675.
- [192] P. Trinder, 1969, Determination of blood glucose using an oxidase-peroxidase system with a non-carcinogenic chromogen, *Journal of clinical pathology*, 22, 2, 158-161.
- [193] P. Trinder, 1969, Determination of Glucose in Blood using Glucose Oxidase with an Alternative Oxygen Acceptor, *Annals of Clinical Biochemistry*, 6, 24-27.

- [194] D. A. Blake and N. V. McLean, 1989, A colorimetric assay for the measurement of glucose consumption by cultured cells, *Analytical Biochemistry*, 177, 1, 156-160.
- [195] J. E. Frew, P. Jones and G. Scholes, 1983, Spectrophotometric determination of hydrogen peroxide and organic hydroperoxides at low concentrations in aqueous solution, *Analytica Chimica Acta*, 155, 139-150.
- [196] B. Chance, 1952, The kinetics and stoichiometry of the transition from the primary to the secondary peroxidase peroxide complexes, *Archives of Biochemistry and Biophysics*, 41, 2, 416-424.
- [197] D. I. Metelitzka, A. V. Litvinchuk and M. I. Savenkova, 1991, Peroxidase-catalyzed co-oxidation of halogen-substituted phenols and 4-aminoantipyrine, *Journal of molecular catalysis*, 67, 3, 401-411.
- [198] M. F. Sipin, S. A. Guazzotti and K. A. Prather, 2003, Recent Advances and Some Remaining Challenges in Analytical Chemistry of the Atmosphere, *Analytical Chemistry*, 75, 2929 - 2940.
- [199] J. P. Quirino, M. T. Dulay, B. D. Bennett and R. N. Zare, 2001, Strategy for On-Line Preconcentration in Chromatographic Separations, *Analytical Chemistry*, 73, 22, 5539 - 5543.
- [200] X. Guo and S. Mitra, 2000, On-line membrane extraction liquid chromatography for monitoring semi-volatile organics in aqueous matrices, *Journal of Chromatography A*, 904, 2, 189-196.
- [201] R.-L. Chien, 2003, Sample Stacking Revisited: A Personal Perspective, *Electrophoresis*, 24, 486 - 497.
- [202] A. Leo, C. Hansch and D. Elkins, 1971, Partition Coefficients and Their Uses, *Chemical Reviews*, 71, 6, 525 - 616.
- [203] J. T. Jayne, S. X. Duan, P. Davidovits, D. R. Worsnop, M. S. Zahniser and C. E. Kolb, 1992, Uptake of Gas-Phase Aldehydes by Water Surfaces, *Journal of Physical Chemistry*, 96, 13, 5452 - 5460.
- [204] J. T. Jayne, P. Davidovits, D. R. Worsnop, M. S. Zahniser and C. E. Kolb, 1990, Uptake of SO₂(g) by Aqueous Surfaces as a Function of pH: The Effect of Chemical Reaction at the Interface, *Journal of Physical Chemistry*, 94, 15, 6041 - 6048.
- [205] P. V. Danckwerts, 1950, Absorption by Simultaneous Diffusion and Chemical Reaction, *Transactions of the Faraday Society*, 46, 300 - 304.
- [206] S. D. Naik and L. K. Doraiswamy, 1998, Phase transfer catalysis: Chemistry and engineering, *AIChE Journal*, 44, 3, 612-646.
- [207] P. Davidovits, J. H. Hu, D. R. Worsnop, M. S. Zahniser and C. E. Kolb, 1995, Entry of gas molecules into liquids, *Faraday Discussions*, 100, 65-81.

1. APPENDIX : Rapid Prototyping - Manufacture

1.1. Computer Aided Design (CAD)

Device designs were produced using L-Edit (Tanner EDA, California, USA). Standard resolution, 4040 dpi (6.24 $\mu\text{m}/\text{dot}$, minimum feature size 20 μm), photomasks were printed by Phillips Digital Services (Letchworth, UK). The L-Edit output file (.cif) was converted using LinkCAD (CA, USA) to a postscript file (.ps) before sending to Philips Digital Services. High resolution, 64 000 dpi (0.394 $\mu\text{m}/\text{dot}$, minimum feature size 4 μm), photomasks were printed by JD Phototools (Oldham, UK). Gerber (.gbr) files, again produced by converting the L-Edit output file using LinkCAD, were switched to the negative view, checked with GerbView (Software Companions, Oslo, Norway) before sending to JD Phototools. All photomasks were printed on overhead projector film (biaxially orientated polyethylene terephthalate sheets).

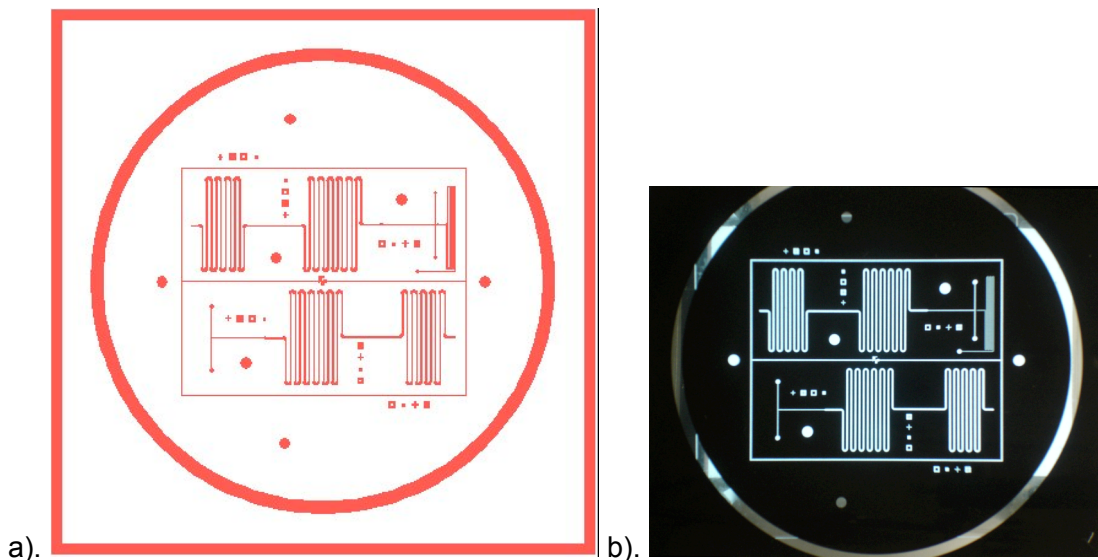


Figure A1.1 : a). Photomask Design 5a (as produced by L-Edit), b). Photograph of photomask (same design).

1.2. SU-8 Processing

3" Silicon wafers (Compart Technology, Peterborough, UK) were used normally without cleaning. SU-8 20** (Microchem Corp., MA, USA) was spun to the depth desired following the manufacturers' instructions using a Gyrset Resist Spinner. After resting for 30 minutes the SU-8 was soft-baked on a temperature controlled hotplate using the conditions shown in Table A1.1. Once cool the wafer and photomask were aligned using a Suss MJB Contact Aligner. The SU-8 was then exposed to ultraviolet light, normally following the manufacturers instructions (maximum single exposure 9s, for high resolution photomasks

single exposure times of 2s used). From previous measurements the lamp was shown to provide 350 mJ/cm².

	SU-8 thickness	d < 10 μm	10 μm < d < 50 μm	d > 50 μm
Soft-Bake	Condition 1	95°C, 20 min.	65°C, 5 min	45°C, 5 min
	Condition 2		95°C, 20 min	65°C, 5 min
	Condition 3			95°C, 20 min
Post-Exposure Bake	Condition 1	95°C, 5 min	65°C, 1 min	45°C, 1 min
	Condition 2		95°C, 7 min	65°C, 2 min
	Condition 3			95°C, 12 min

Table A1.1 : SU-8 20** processing conditions

The wafer was then post-baked using conditions shown on Table A1.1. Once cool the wafer, if single depth, was developed using SU-8 developer (Microchem Corp., MA, USA) following the manufacturers instructions. Once the wafer had been rinsed with *i*-Propanol and blown dry, ensuring that no drying marks remained, the height of the structures was measured with a precision digital dial gauge (Starrett, MA, USA).

If a mould with structures at 2 different depths (a double depth mould) was manufactured then rather than developing the wafer after the post-exposure bake, another layer of SU-8 was spun on top of the first layer. The depth required was slightly overestimated for the second layer as it tended to be thinner than the manufacturers specifications. As before, the wafer rested after spinning and was then soft-baked, using the temperature ramp times relating to the total thickness. The exposed sections of the first layer of SU-8 were aligned, using the alignment marks, carefully with the second photomask. The exposure dose was calculated purely for the second layer. The wafer was then post-exposure baked, using the total thickness ramp times as for the soft-bake and then developed.

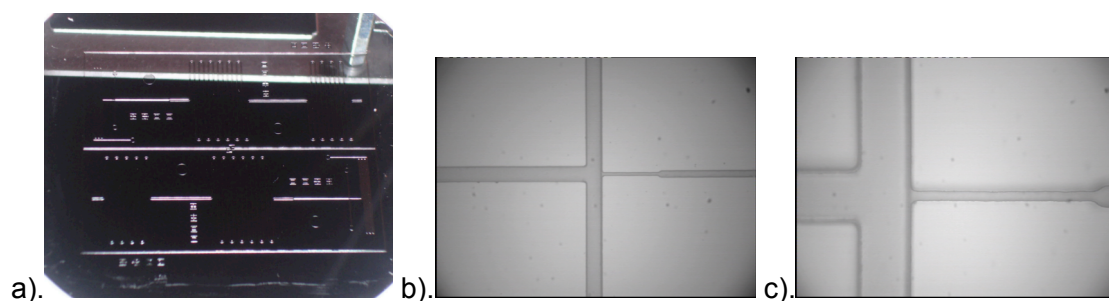


Figure A1.2 : a). Photograph of wafer with SU-8 mould (Design 5a), b). Close-up (x3.2) of same mould, c). same section of mould at x10.

1.3. Soft Lithography

Sylgard 184 (Dow Corning, MI, USA) Polydimethylsiloxane (PDMS) was then mixed at a ratio of 10:1 prepolymer/catalyst as per the manufacturers specifications. After mixing thoroughly and degassing in a desiccator connected to a vacuum pump the mixture was poured into a 1.5 mm thick (unless stated otherwise) PMMA frame placed over the wafer and around the structures. A lid flat optical glass if top planarity was important, PMMA otherwise, was placed over the frame and wafer, clipped on three sides with bulldog clips and placed on one side. After a resting period, to allow any gas bubbles to rise to the top edge of the frame, the last clip was attached and the wafer placed into a convection oven for 4 hours at 65°C. Standard instructions required 2 hours at 90°C, but the lower curing temperature warped the PMMA lid less.

After baking the wafer was removed and left to cool. The lid, frame, wafer and PDMS casting were then carefully disassembled. A plastic bag was sliced open to provide a clean surface and the casting laid onto this. The casting was then cut into separate devices using a razor blade and each device placed into closed plastic petri dishes for storage.

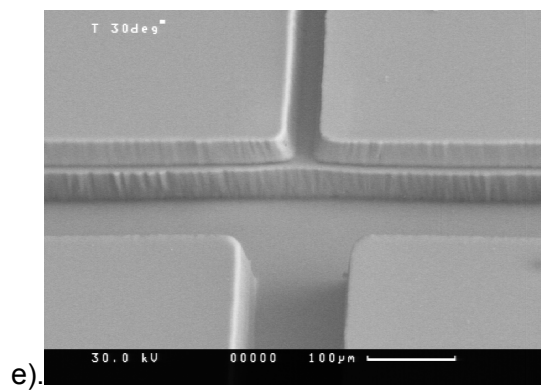
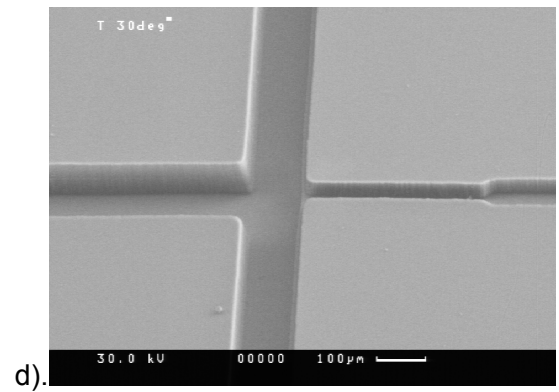
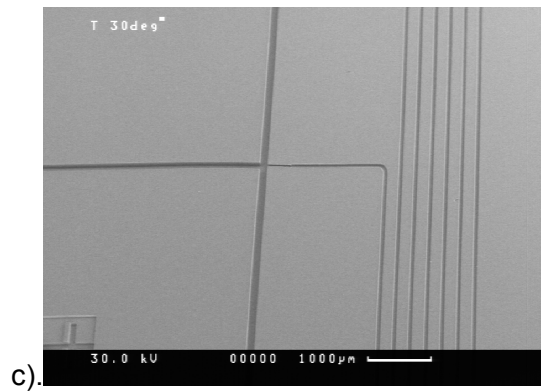
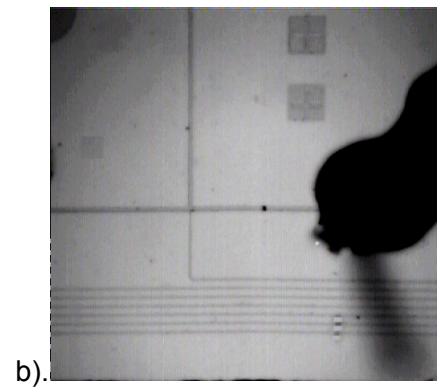
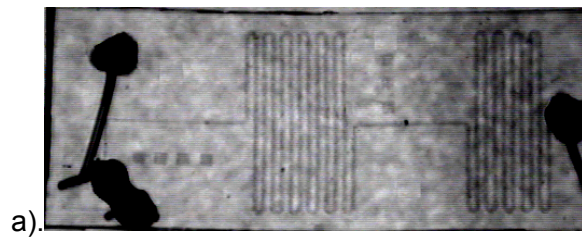


Figure A1.3 : a). Photograph of fully assembled PDMS device (5a.5), b). photograph of same device at slightly higher magnification, c). SEM image of PDMS casting (Device 5a.5), d). and e). Higher magnification SEM image of same PDMS casting (Device 5a.5).

1.4. Device Assembly

PDMS devices were assembled following a series of standard assembly procedures. However which assembly procedures and the particular sequence followed are dependant on the device being assembled. All devices requiring unique assembly methods will be described separately.

1.4.1. Standard Assembly

- a). The PDMS casting was placed onto a 1.2 mm thick borosilicate glass microscope slide. The positions of holes to be drilled were marked using a superfine permanent marker pen. After covering the markings with clear nail polish and allowing it to dry, the holes were drilled using a bench hand drill (Fortex, Leicester, UK) with a 0.8 mm diamond drill (Crystalite Corp., Ohio, USA).
- b). A flat piece of PDMS (cast as per the structured PDMS, but using a bare wafer) was cut to the same size as the structured PDMS and holes cored to align with the holes drilled in the microscope slide.
- c). The drilled microscope slide, PDMS casting and the PDMS flat were cleaned with Neutracon (Decon Ltd, East Sussex, UK), rinsed with D.I. water, blow-dried with filtered, compressed air and then placed into a desiccator for a further 30 minutes.
- d). After desiccation the slide and PDMS flat were placed into a UV/O₃ PSD-UVT system (Novoscan Technologies Inc., USA) bonding faces upright and treated using ambient air for 3 minutes at room temperature. The PDMS and glass microscope slide were then aligned and bonded.
- e). The composite was then placed (PDMS face upright), with the structured PDMS, into the UV/O₃ system for a further 3 minutes. The composite and the structured PDMS were then aligned, bonded and placed into a convection oven at 90°C for 3 hours.
- f). Fifteen cm lengths of 0.25 mm ID/ 0.75 mm OD nylon tubing (Fisher Scientific UK, UK) were then prepared. This involved cutting the ends at an angle of 45°. After the bonded device was removed from the oven and cooled, the tubing was carefully placed into the drilled holes angled side first.

g). Tubing was glued to the holes in the microscope slide using fast curing araldite™ (Huntsman Advanced Materials, Duxford, UK) epoxy adhesive. A 24 hour curing period was necessary before the device was able to be tested.

1.4.2. Push-fit Fluid Connection Devices

h). Holes were drilled into the structured PDMS using a 1.1 mm drill bit (LPKF Laser and Electronics, Wokingham, UK) from a bench hand drill. Drilling the PDMS at an incline produced holes angled to have liquid flowing as smoothly as possible into the PDMS channels. Drilled PDMS was cleaned before bonding to remove any swarf.

i). A flat piece of PDMS was cut to the same size as the structured PDMS.

Steps c. – e. were followed next, although the glass microscope slide was not drilled.

1.4.3. Check Valve

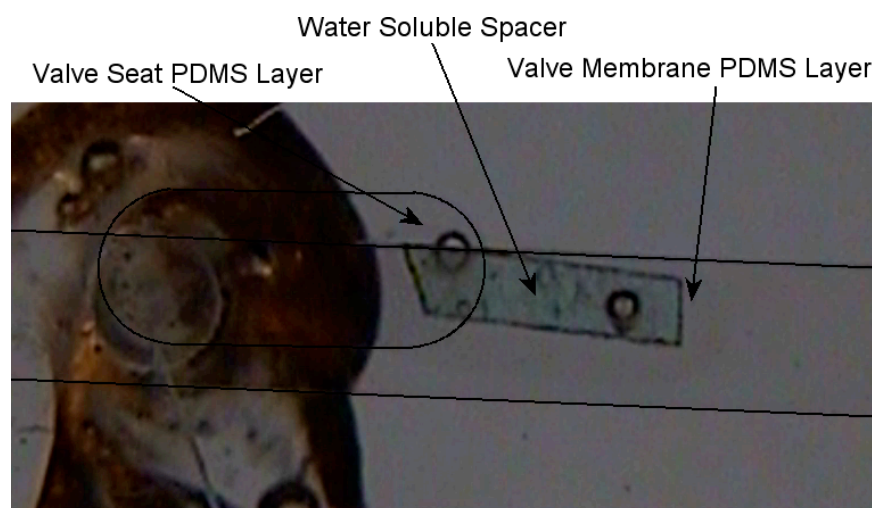


Figure A1.4 : Photograph of Check valve (Design 8.1) with water soluble spacer inserted between the valve seat and valve membrane. The channel walls are outlined artificially. The left hand drill hole is the valve input and the right hand drill hole is the valve output. At the centre of the large circular feature to the right of the image is the fluid input to the valve seat PDMS layer.

As per steps a. – d. with modifications as listed.

1. PDMS moulded to contain the valve membrane was cured in a frame manufactured from multiple pieces of acetate film (75 μm) cut to shape and layered to the required depth. This was dependant upon the thickness of membrane desired.
2. Before cleaning, carefully positioned 300 μm vertical holes were drilled in both structured PDMS components.

Subsequent assembly steps followed were :

j). 1. Polyurethane (PU) backed polyethylene (PE) tape was cut, to a desired size, to form a masking membrane.

2. Polyvinyl pyrrolidone was dissolved in water and later (step l.) a droplet of the aqueous solution applied to the PDMS and allowed to dry, forming a water soluble polymer spacer.

3. A 10 μm thick membrane (Wrigley's Ultra Thin Ice™, Wrigley's, USA) was cut with a razor blade to form a water soluble spacer. The spacer was cut to the desired length (1 – 3 mm) and thickness (250 μm – 1.2 mm) as required.

k). After bonding the two sections of the check valve, that is two different microscope slide, PDMS flat and structured PDMS composites, a spacer was carefully positioned on the top surface of one composite. It was positioned to prevent bonding of the PDMS between the holes drilled in the two pieces of structured PDMS. The PDMS surface of the composite was treated in the UV/O₃ system.

l). If the spacer was either PE tape or PDMS, it was removed before the next step. If not, then the spacer remained in place.

m). The two composites were next bonded, PDMS to PDMS, with the spacer between them.

Steps f. - g. were subsequently followed. Tubes were glued in both microscope slides.

1.4.4. Seal Valve

n). A flat (100 μm variation over 50 cm) 1.5 mm thick, 2.5 x 2.5 cm piece of polymethyl methacrylate, PMMA, (Clarex™, Nitto Jushi Kogyo Ltd, Japan) was milled for use as a device base. Markings were made on the base, in the centre and 1 cm, towards one side, from the centre.

o). The PMMA base was drilled (1.5 mm diameter hole) through at the off-centre mark followed by a 1.5 mm hole, drilled to a depth of about 1 mm, into the centre of the PMMA. The bottom of the PMMA base contains the two holes.

p). After thorough cleaning with deionised H₂O and *i*-propanol, the PMMA was coated with SiO₂ (Spectrum Coatings Ltd, Manchester, UK).

q). The flat side of the structured PDMS, cored at the inlet hole, was treated and then bonded to the top of the PMMA base. The cored hole and the through hole and the centre of the seal valve and the centre hole in the PMMA base were aligned before bonding.

r). Next, a 300 μm hole was drilled through the centre of the PDMS/PMMA composite. The hole connected the centre of the seal valve with the 1 mm deep hole in the bottom of the PMMA base. The PDMS/PMMA composite was then carefully cleaned.

s). A 10 μm thick water soluble spacer (Wrigley's Ultra Thin Ice™, Wrigley's, USA) was placed over the valve seat. The structured PDMS and an 18 x 18 x 0.11 mm glass cover slip (Menzel-Glaser, Braunschweig, Germany), one side pre-coated with chromium using a vacuum deposition system, were treated and bonded as per step e.

t). A 12.7 mm PZT bimorph disc (Piezo Systems, T216-A4NO-273X) was glued using conductive epoxy adhesive (Chemtronics, GA, USA) to the glass cover slip. Fine connecting wires were then attached with conductive epoxy to the top of the PZT and the edge of the cover slip.

u). Fluidic connections, 1.5 mm diameter PEEK tubing (Upchurch Scientific, Oak Harbour, USA), were finally glued with epoxy adhesive to the holes in the bottom of the PMMA base.

Addendum

Initial devices (designs 1 and 2) did not include a flat Section of PDMS sandwiched between the microscope slide and the structured PDMS. Once the liquid to channel wall contact angle was determined to be significant, a uniform channel wall was necessary. The glass/PDMS channel was therefore changed to an all PDMS channel.

1.4.5. PMMA

PMMA based devices were designed with AutoCAD LT (Autodesk Inc, Farnborough, UK). Channel widths, hole diameters and device boundaries were set during the AutoCAD design phase. Export files (.dxf) were opened in Circuit CAM (LPKF Laser and Electronics, Garbsen, Germany) and appropriate tool selections made for the channels, holes and device perimeter. The Circuit CAM output file (.lmd) was imported into Boardmaster (LPKF

Laser and Electronics, Garbsen, Germany). Associated data was then transmitted directly from the computer to the milling machine (LPKF ProtoMat 91s/vs).

Flat sheets of 1.5 mm thick PMMA, were snapped in half. One piece was placed on top of the other on the milling machine base. The protective cover plastic was not removed from the side, of the sheet of PMMA, to be milled. After securing both pieces in place the material area was selected.

The first milling tool was selected, the depth set, and then all channels using that tool were cut. This was followed by all the other channel cutting tools. Once all the channels had been milled, the holes were drilled in a similar manner and then finally the device was cut out of the surrounding substrate using a 2 mm contour router (a milling tool). All tools were supplied by LPKF Laser & Electronics Ltd.

After removing the swarf using a soft brush the last piece of protective plastic was removed from the PMMA. The milled PMMA base and lid were polished with a colloidal silica suspension (Mastermet 2, Buehler, Coventry, UK) then cleaned, followed by blow and desiccator drying. The two pieces of plastic that formed the device were then carefully positioned together and baked at 108°C for 2 hours between 2 large pieces of flat glass with a five kilogram weight placed on top. Finally PEEK, 1.06 mm internal diameter, Minstac connectors (The Lee Company, Connecticut, USA) were attached with epoxy adhesive.

2. APPENDIX 2 : Electronic Control

Shown below are abbreviated versions of two representative scripts written to control the valve timing and sequence for the valves controlling fluid flow into the segmented flow, vapour collection device and the integrated valve test circuits. The first is from the first generation of scripts, in which time is in seconds, and the second is from the final (third) generation of script, written to allow multiple timing loops.

2.1. Example Script 1 – Sequential

```
comm:    UH Undergraduate Microfluidics, Lab2 - Flow resistance & Flow control;
comm:+++++;
comm: time is in 1 second units, maximum time = 32k seconds;
comm:;
comm: pressurise....;
comm: now prime input with dye;
comm: gas is valve 2, water is valve 1;
comm: *****inject liquid bollus through line 2*****;
on:2;
off:0;
time:5;
comm: *****start mixing*****;
on:1;
off:2;
time:1;
on:0;
off:1;
time:1;
on:2;
off:0;
time:3;
on:0;
off:2;
time:1;
comm.: *****1 cycle*****;
on:1;
off:2;
time:1;
on:0;
off:1;
```

```

time:1;
on:2;
off:0;
time:3;
on:0;
off:2;
time:1;
comm.: *****2 cycles*****;
-----
-----
comm: completed 80 mixing runs (thats 160 s) & 321 time instructions;
on:2;
off:1;
time:20;
comm: now, turn all explicitly off for safety;
on:0;
off:1,2,3,4,5;
time:0;
comm: total is 323 time instructions;
comm:finished!;

```

2.2. Example Script 2 – Loop

```

comm: Flow resistance & Flow control;
comm:;
comm: time is in 1 millisecond units, maximum time = 32k seconds;
comm:;
comm: pressurise....;
comm: now prime input with dye;
comm: Segmented flow with short gas priming time;
comm: LIQUID = VALVE 6, GAS = VALVE 5;
on:5;
off:6;
time:50;
comm: LOOP - Gas filling channel;
jumpto:1;
time:0;
on:5;
off:6;
time:20;
on:0;

```

```
off:5;
time:100;
on:6;
off:5;
time:50;
comm: LOOP = Liquid - 50, Gas - 20;
-----
-----
comm: LOOP = Liquid - 50, Gas - 200;
jumpto:21;
time:0;
on:5;
off:6;
time:50;
comm: LOOP - Gas filling channel;
jumpto:25;
time:0;
comm: only stop once 'F' key on keypad pressed;
comm: completed experiment, clear all;
on:5;
off:6;
time:20000;
comm: now, turn all explicitly off for safety;
on:0;
off:1,2,3,4,5,6,7,8;
time:0;
comm:finished!;
```

3. APPENDIX 3 : Detail of Selected Microfluidic Experimental Conditions.

3.1. Design 2

Script	Pressure	Result
Gas (1 s) Liquid (1 s)	5 kPa	Initially stable. Length of liquid slugs \approx 3 x length of gas slugs. After about 20 cycles liquid filled the flow restrictor.
“	10 kPa	Unstable flow. Bubble break-up, although constant flow.
“	20 kPa	Highly unstable flow. Bubble to about the 6 th meander of the main channel.

Table 1 : Experimental observations for a representative subset (chosen from all gas/liquid timings) of experiments performed on devices from photomask 2.

3.2. Device 4

Cycle	Pressure		Result
	Gas	Liquid	
Gas (1 s)	2.88 kPa	6.6 kPa	No segmented flow -
Liquid (1 s)	4.22 kPa	“	No segmented flow -
	6.71 kPa	“	No segmented flow -

Table 2 : Experiments (Device 4.1.b). An initial 3 s gas flow was used before the main gas/liquid cycles in order to ensure that the device was completely free of liquid before the start of each experiment.

Increasing the ratio of the liquid to gas pressure above about 2:1 resulted in complete flow of liquid into the gas flow restrictor. No effect from using different structures at the entrance to the gas/liquid junction was observed. Likewise decreasing the ratio of the liquid to gas pressure below about 1:1 led to gas flowing into the liquid supply channel. While gas was more easily displaced from the liquid supply channel than vice versa, a long delay on the injection of liquid into the main channel resulted. This affected the gas/liquid segmentation.

3.3. Design 5a

Cycle	Pressure		Result
	Gas	Liquid	
Gas (1 s) Rest (3 s) Liquid (1 s)	3.85 kPa	4.9 kPa	After initial injections of gas, liquid was pushed into the flow restrictor.
	5.0 kPa	4.9 kPa	As above
	6.5 kPa	4.9 kPa	As above, however the gas occasionally expelled the liquid, but infrequently, until liquid completely filled the flow restrictor
	7.5 kPa	4.9 kPa	Gas initially injected, then liquid filled the flow restrictor
	8.5 kPa	4.9 kPa	Gas streamed through, then segmented for a short period, then gas streamed again.

Table 3 : Experiments (Device 5).

Several features of specific note, in experiments conducted on devices manufactured from design 5a, were the low pressures at which they initially appeared able to operate (liquid - 4.9 kPa, gas - 3.9 kPa minimum). Although further testing with longer experiment times exposed that this was incorrect. The ratio between the liquid and gas pressures was important in so far as the liquid was pushed from the flow restrictor faster if the ratio was higher. No other effect of increasing the gas to liquid pressure ratio was observed as there was no correlation between the pressure ratio and apparent volume injected or time injected for. Finally, the gas valve is open for 1 s, yet in all cases gas is injected for a maximum time of 750 ms, despite the liquid front being positioned directly at the junction for roughly 1.3 s.

The gas injection timing indicates that the microfluidic structures and pressure ratio are not responsible for the gas/liquid segmented flow. A gas valve opening time of 1 s followed by a 3 s rest period should result in a 1 s gas injection followed by a period of bubble expansion as the pressure downstream of the junction decreases. As the gas is injected for less than 1 s, following a period of gas movement towards the junction, and is followed immediately by liquid injection it is believed that the liquid valve opening created a low pressure zone into which gas is drawn. The gas is then pushed down the main channel, simulating gas/liquid segmentation.

3.4. Modular Device

Cycle (ms)	Pressure (kPa)
Gas (500), Liquid (1500) Rest (2000)	5.0, 5.5, 6.4, 8.0, 10.2
Gas (200), Liquid (500) Rest (1000)	10.3, 15.2, 20.0, 30.3
Gas (100), Liquid (500) Rest (1000)	12.5, 15.1, 20.0, 30.3
Gas (20), Liquid (50), Rest (1000)	13.1, 15.0, 20.1, 25
Gas (200), Liquid (500)	10.0, 15.3, 20.0
Gas (20), Liquid (50)	15.0, 18.0, 20.0, 30.4

Table 4 : List of representative experiments performed on the Modular Device demonstrating the range of pressures and valve timings used.

3.5. PMMA Micro-junctions

CYCLE (ms)			PRESSURE (kPa)
Gas	Liquid	Rest	
2000	1000	----	3.6 – 4.85 ,4.85, 15.0
500	1500	3000	15.0
400	500	----	≈ 4.0, 9.5 increased to 14.0
200	500	----	4.5 increased to 18.0 over the experiment.
10	2000		4.7, 17.2, 34.5

Table 5 : PMMA device representative experiments

Fluid flow into PMMA micro-junctions was irregular in all system arrangements. The gas injector produced small droplets and bubbles in the liquid supply channel. They were expelled when the liquid valve was next opened, however the extra menisci and slug break-up caused would have increased flow resistance massively in a device with a lengthy channel attached. Injecting liquid also resulted in droplet and bubble formation, although in the gas supply channel this time. The bubbles were smaller and were not always removed from the gas supply channel by the flow of gas. Directly opposing gas and liquid supply channels did not cause droplet break-up, but liquid flowed further into the gas supply channel and vice versa. At low pressures (below about 5 kPa) the flow of gas into the junction was intermittent and of irregular length due to the need to expel the liquid from the gas channel before gas could flow. This was more noticeable in the junction with 150 μm x 150 μm channels and the junction with different dimension channels.

The angled injector PMMA micro-junction design in most cases produced regular injection times and always demonstrated recurring fluid flow patterns. At low pressures (below about

5 kPa) the gas injector did not operate, with the liquid flowing into the gas supply and in subsequent cycles pushing the gas further up to the supply tubing. Low pressure injection of liquid into a gas stream was more reliable, although was still dependant upon the timing used. Short (200 ms to 500 ms) liquid injections, even at high pressure (>12 kPa), produced regular gas and liquid injections. Longer liquid injection times (1 s) resulted in a high flow resistance for both the liquid and the gas and therefore was only effective at very high pressures (>18 kPa).

3.6. Design 10

Valve Timing (ms) Liquid, Gas, Rest	Pressure (kPa)	Results
50, 100, 0	2	Pressure too low, timing of segments irregular as liquid enters gas channel and is then expelled.
	4	As above, but the timing is slightly improved.
	8	Much better, but still quite irregular.
500, 2000, 0	2	Drops held together, but insufficient pressure to force them through.
	4	Droplets break-up and pressure definitely insufficient.
	8	Droplets completely breaking up. Needs a fresh de-gas and flush with CO ₂ .

Table 6 : Device 10 preliminary tests. All tests were performed using Device 10.1.a.

3.7. Design 12

Timing (ms)		Pressure (kPa)
Liquid	Gas	
500	200	10
"	"	15
2000	200	11
"	"	13
20	200	15
50	500	13
"	"	15
20	500	12
		15
L ₁ – G ₁ – L ₂ – G ₂		13
50–500–20–500		15

Table 7 : Experimental conditions under which segmented flow was observed in Device 12.1.